



Norwegian University of
Science and Technology

Shear Capacity Assessment of an Existing Prestressed Concrete Bridge with Corrosion Damage

Carmen Elise Dybsjord

Civil and Environmental Engineering

Submission date: June 2017

Supervisor: Terje Kanstad, KT

Norwegian University of Science and Technology
Department of Structural Engineering



MASTER THESIS 2017

SUBJECT AREA: Concrete Structures	DATE: June 11 th 2017	NO. OF PAGES: 230
--------------------------------------	-------------------------------------	----------------------

TITLE:

Shear Capacity Assessment of an Existing Prestressed Concrete Bridge with Corrosion Damage

Skjærkapasitetskontroll av en eksisterende føreropspennet betongbru med korrosjonsskade

BY:

Carmen Elise Dybsjord



SUMMARY:

The thesis contains shear capacity calculations of the structural beams in The Hulvågen Bridge, a concrete element bridge consisting of prefabricated and pre-tensioned beams with a continuous cast-in-place bridge deck. The calculations have been performed using both NS 3473:1977 (valid when the bridge was designed) and Eurocode 2 (valid today). It is found that the capacity is more than sufficient for the three main shear failure mechanisms (diagonal tension, compressive shear and anchorage failure). The shear resistance in the interface between the beams and bridge deck is almost entirely utilized.

Due to its location at the Norwegian coastline, the bridge is exposed to extremely aggressive marine environment. Low requirements to concrete cover when the bridge was designed in 1987 makes it prone to chloride induced reinforcement corrosion. Observations from an excursion to the bridge in May 2017 indicates leakage of sea water through the bridge deck, while no visual signs of corrosion in the NIB beams have been found.

The effect that the various consequences of reinforcement corrosion can have on the shear capacity of the beam has been investigated. Based on the lack of observed corrosion damage, it can be concluded that neither of the three main shear failure mechanisms are likely to occur at this time. However, the prestressing steel in particular may corrode without visible signs at the concrete surface, and further examinations of chloride content in relevant parts of the bridge should therefore be performed. Leakage of sea water through the bridge deck may result in corrosion of the reinforcement crossing the interface, which may reduce the shear resistance at the interface. It is recommended to further examine the damages to the bridge deck and interface, and perform repairs where necessary.

RESPONSIBLE TEACHER: Professor Terje Kanstad

SUPERVISOR(S): Terje Kanstad, NTNU, and Håvard Johansen, Statens vegvesen

CARRIED OUT AT: Department of Structural Engineering, NTNU Trondheim

Abstract

The Hulvågen Bridge is a concrete element bridge, consisting of prefabricated and pre-tensioned beams with a continuous cast-in-place bridge deck. The bridge is a part of the Atlantic Ocean Road, opened in 1989. In this master's thesis the shear capacity of the composite structural beam, consisting of a NIB 1435/500 beam and the bridge deck, is in focus.

Shear capacity calculations of the bridge have been performed using both NS 3473:1977 (valid when the bridge was designed) and Eurocode 2 (valid today). The utilization ratios are well below 1.0 for all the three main failure mechanisms, i.e. diagonal tension failure, compressive shear failure and anchorage failure. Furthermore, it is found that the shear resistance in the interface between the beams and bridge deck is utilized to a degree of $\eta = 0.96$.

Due to its location along the Norwegian coastline, the bridge is exposed to extremely aggressive marine environment. Low requirements to concrete cover when the bridge was designed makes it highly prone to chloride induced reinforcement corrosion. Examinations of the bridge indicate leakage of sea water through the bridge deck, while no visual signs of corrosion in the NIB beams have been found.

The effect that the various consequences of reinforcement corrosion can have on the shear capacity of the beam has been investigated. Based on the capacity in the uncorroded state and the lack of observed damage in the beams, it can be concluded that neither of the three main shear failure mechanisms are likely to occur at this time. However, the prestressing reinforcement in particular may corrode without visible signs at the concrete surface, and the amount of corrosion damage in the beams may have been underestimated. Further examinations of chloride content in relevant parts of the bridge should therefore be performed.

Leakage of sea water through the bridge deck may result in corrosion of the reinforcement crossing the interface. This may reduce the shear capacity at the interface. Exceeding this capacity will not necessarily cause failure of the beam, but will require that the NIB beams must carry all design loads in the section without contribution from the bridge deck. The consequences of this must be further examined. In addition, it is recommended to further examine the damages to the bridge deck and interface, and perform repairs where necessary.

Sammendrag

Hulvågbrua er en betongelementbru bestående av prefabrikkerte før oppspente betongbjelker og et kontinuerlig plasstøpt dekke. Brua utgjør en del av Atlanterhavsveien, som ble åpnet i 1989. I denne masteroppgaven vurderes skjærkapasiteten av samvirkebjelken bestående av NIB 1435/500-bjelker og brudekket.

Skjærkapasitetsberegningene har blitt utført ved å benytte både NS 3473:1977, som var den gjeldende standarden da bruene ble dimensjonert, og Eurokode 2, som er i bruk i dag. Beregningene viser at bjelkene har rikelig kapasitet for de tre hovedtypene av skjærbrudd, nemlig strekkbrudd, trykkbrudd og forankringsbrudd. Videre er det funnet at den dimensjonerende skjærkapasiteten i støpeskjøten mellom NIB-bjelken og dekket er 96 % utnyttet.

Hulvågbrua er utsatt for ekstremt aggressivt marint miljø med sin plassering langs kysten. Lave krav til overdekning da bruene ble dimensjonert gjør den svært utsatt for kloridinitiert armeringskorrosjon. Undersøkelser av brua tyder på lekkasje av sjøvann gjennom brudekket, mens ingen synlige tegn på korrosjon i NIB-bjelkene har blitt funnet.

Effekten som de ulike konsekvensene av armeringskorrosjon kan ha på skjærkapasiteten av samvirkebjelken har blitt studert. Etersom få eller ingen skader i NIB-bjelkene har blitt funnet, samt at det er etablert at bjelkene har rikelig kapasitet i ukorroderet tilstand, kan det konkluderes med at det er lite sannsynlig at noen av de tre hovedtypene av brudd vil inntreffe på nåværende tidspunkt. Likevel bør videre undersøkelser av kloridinnhold utføres, da særlig spennarmering kan korrodere uten synlige tegn på betongoverflaten.

Lekkasje av sjøvann gjennom dekket indikerer at armeringen som krysser støpeskjøten mellom bjelken og dekket kan være svært utsatt for korrosjon. Korrosjon i denne armeringen kan redusere skjærkapasiteten til støpeskjøten. Dersom denne kapasiteten overskrides vil ikke nødvendigvis brudd i bjelken oppstå, men bjelken vil være nødt til å bære alle dimensjonerende laster i det aktuelle snittet uten bidrag fra brudekket. Videre undersøkelser av konsekvensene av dette er nødvendig. I tillegg er det anbefalt å gjøre videre undersøkelser av omfanget av skader på brudekket og i støpeskjøten, samt å utbedre skadene der det er nødvendig.

Preface

This master's thesis is the final part of a 5-year master's degree in Civil and Environmental Engineering at The Norwegian University of Science and Technology. The thesis is produced over 20 weeks during the spring of 2017.

The thesis regards shear capacity control of The Hulvågen Bridge at the Atlantic Ocean Road. Design loads are established using the analytical program `fap2D`, while the capacity calculations are performed using hand calculations. The bridge is controlled using standards and regulations that were valid when the bridge was designed, as well as standards and regulations valid today.

Through the work I have laid into this thesis, I have gained valuable insight into the process of establishing design loads and performing capacity calculations on existing concrete bridges. The study of the shear phenomenon, as well as the mechanism behind reinforcement corrosion and its consequences on the capacity of a structure, has been very interesting and informative. The fact that the calculations have been performed in connection with real challenges regarding capacity and deterioration in an existing bridge has been very motivating.

I would like to thank my supervisor Terje Kanstad for giving me the chance to switch to the field of concrete structures for my master's thesis. Furthermore I am grateful for excellent guidance throughout this semester. I would also like to thank Magda Paciorek for contributing with relevant studies for my literature research.

Trondheim, June 11th 2017

Carmen Dybsjord

Contents

1	Introduction	1
2	Standards and regulations	3
2.1	Standards	3
2.2	Regulations	4
3	Durability	5
3.1	Concrete	5
3.1.1	Porosity and permeability	6
3.2	Reinforcement deterioration mechanisms	9
3.2.1	Corrosion mechanism	10
3.2.2	Carbonation	11
3.2.3	Chloride induced corrosion	11
3.2.4	Corrosion of prestressed reinforcement	14
3.3	Concrete deterioration mechanisms	15
3.3.1	Chemical deterioration mechanisms	15
3.3.2	Physical deterioration mechanisms	17
3.4	Measures to increase concrete durability	19
3.4.1	Concrete cover	20
3.4.2	Concrete quality	21
3.4.3	Cracking	22
4	The Hulvågen Bridge	25
4.1	Presentation of The Hulvågen Bridge	25
4.1.1	The continuity of The Hulvågen Bridge	26
4.1.2	Drawings	28
4.1.3	NIB beams	28
4.1.4	Composite beams	30
4.2	Current state	30
4.2.1	Inspections and maintenance	30
4.2.2	Damages on the NIB beams	31
4.2.3	Damages on the bridge deck	33

5	Basis for design	35
5.1	Materials and cross sectional properties	35
5.1.1	Concrete	36
5.1.2	Regular reinforcement	39
5.1.3	Prestressed reinforcement	42
5.2	Simplifications and assumptions	45
6	Loads and load combinations	47
6.1	Classification of actions	48
6.2	Permanent action	48
6.2.1	Self weight	48
6.3	Variable action	49
6.3.1	Traffic loads	50
6.4	Deformation loads	52
6.4.1	Prestressing loads	52
6.5	Accidental action	57
6.6	Time related load effects	57
6.6.1	Redistribution of self weights	57
6.6.2	Secondary moments from prestressing	60
6.7	Limit states and load combinations	61
6.7.1	Ultimate Limit State	61
6.7.2	Serviceability Limit State	62
7	Design loads	65
7.1	Fap2D: Longitudinal direction	66
7.1.1	Assembling the model	66
7.1.2	Self weights	68
7.1.3	Traffic loads	70
7.2	Fap2D: Transversal direction	72
7.2.1	Assembling the model	72
7.2.2	Self weights	73
7.2.3	Traffic loads	74
7.3	Prestressing loads	76
7.4	Load combinations and design load on critical beam	77
7.5	Design loads on a simply supported bridge system	80
7.5.1	Fap2D: Modelling self weights and traffic loads	80
7.5.2	Prestressing loads	81
7.5.3	Load combinations and design load on critical beam	82
7.5.4	Comparing the two bridge systems	82
8	Shear	85
8.1	Shear force and its effect	85
8.2	Shear failure mechanisms	86
8.2.1	Diagonal tension failure	87
8.2.2	Compressive shear failure	88
8.2.3	Anchorage failure	88

8.3	Shear calculations in NS 3473	88
8.3.1	NS 3473:1973, 1st edition	89
8.3.2	NS 3473:1977, 2nd edition	93
8.3.3	NS 3473:1989, 3rd edition	93
8.3.4	NS 3473:1992, 4th edition	97
8.3.5	NS 3474:1998, 5th edition	97
8.3.6	NS 3473:2003, 6th edition	98
8.4	Shear calculations in EC2	98
8.4.1	Members not requiring design shear reinforcement	98
8.4.2	Members requiring design shear reinforcement	101
8.5	Anchorage capacity	102
8.6	Shear stresses at interface between concretes	105
8.6.1	Shear stresses induced by shear loads	105
8.6.2	Shear stresses at the interface	106
8.6.3	Shear resistance at the interface	107
9	Shear capacity control	109
9.1	Basis for the capacity calculations	109
9.2	NS 3473:1977	111
9.2.1	Compressive shear capacity	112
9.2.2	Diagonal tension capacity	115
9.3	EC2	120
9.3.1	Members not requiring design shear reinforcement	121
9.3.2	Members requiring design shear reinforcement	123
9.4	Anchorage capacity	124
9.5	Shear stresses at interface between beam and deck	125
9.5.1	Shear stresses at the interface	126
9.5.2	Shear resistance at the interface	126
9.6	Concluding remarks regarding the shear capacity	128
10	Consequences of reinforcement corrosion	133
10.1	Mechanical properties of corroded reinforcement bars	133
10.1.1	Reduction of reinforcement cross section	134
10.1.2	Ductility	134
10.1.3	Prestressed reinforcement	136
10.2	Bond between corroded reinforcement and concrete	137
10.3	Mechanical behaviour of corroded reinforced concrete structures	138
10.4	Effect of reinforcement corrosion on shear capacity	139
11	Shear capacity control of the corroded structure	147
11.1	Capacity calculations	147
11.1.1	Reduction in shear reinforcement area	148
11.1.2	Reduction in tensile reinforcement area	150
11.1.3	Reduction in beam web concrete cover	151
11.1.4	Anchorage capacity	153
11.1.5	Resistance at the interface between the beam and deck	153

11.1.6	Concluding remarks	154
11.2	Evaluation of corrosion in The Hulvågen Bridge	155
11.2.1	Observed damages from inspection in May 2017	155
11.2.2	Damages in connection with shear capacity	156
11.3	Similar bridge with extensive corrosion damage	159
12	Future work	163
13	Conclusion	165
	Bibliography	166
	Appendix A Drawings of The Hulvågen Bridge	171
	Appendix B Effective beam stiffness	185
	Appendix C Loads from prestressing	191
	Appendix D Cross sectional properties	197
	Appendix E Capacity control in accordance with EC2	209
	Appendix F Shear resistance at interface between beam and deck	217

Chapter 1

Introduction

In the past few decades, prestressed concrete has been widely used in bridges in Norway. From the 1970's to the 1990's, the prefabricated, pre-tensioned NIB beams (normalized I-beams) were used for the construction of over 150 bridges in Norway (Paciorek et al., 2017). The prefabricated NIB beams were combined with a cast-in-place bridge deck in order to establish either a continuous or a simply supported multi-spanned bridge.

Several of the bridges built with NIB beams are exposed to aggressive marine environment in the coastal areas. In these environments, reinforcement corrosion due to chloride penetration is considered the largest challenge to the durability of a reinforced concrete structure. The mechanism behind chloride induced reinforcement corrosion will be studied in this thesis, both for regular reinforcement and for prestressed reinforcement. Furthermore, the consequences that this deterioration mechanism may have for the material properties of the reinforcement bar, for the bond between the reinforcement and the concrete, as well as for the load bearing capacity of the entire structure will be looked into.

Shear capacity will be in focus for theory and calculations that is presented in this thesis. The shear capacity formulas have developed a lot over the years, as will be shown. Inclusion of corrosion induced damage in the capacity formulas is, on the other hand, still performed in a relatively simple manner.

Until the end of the 1980's, little attention was paid to the knowledge that reinforcement steel must be protected from the surface using sufficiently large concrete cover. Minimum requirements to concrete cover have in periods been extremely low, resulting in structures where the reinforcement is highly exposed to corrosion. It is therefore considered likely that several of the bridges built using NIB beams are extremely prone to reinforcement corrosion due to chloride attack.

Chapter 2

Standards and regulations

This chapter provides an overview of standards and regulations that are considered relevant for this thesis.

2.1 Standards

NS 3473 (Norske Sivilingeniøres Forening, 1973) is a nationally developed standard that provides design and detailing rules for concrete structures. The standard was developed by the then called Norwegian Society of Chartered Engineers, now Tekna, and the first edition was published in September 1973. In total six editions have been released, with the last edition published in September 2003.

In 1975 EU's Commission of the European Community decided on an action programme in the field of construction with the objective to eliminate technical obstacles to trade, in order to facilitate free flow of goods and services within the European Union. The action programme involved an initiative to establish a set of technical rules for the design of construction works, which initially would serve as an alternative to, and ultimately a replacement of, the national rules in the EU member states. The current versions of these European standards, called eurocodes, were developed during the 1990's.

Each eurocode contains a number of parameters that are to be decided on a national level. This may be parameters regarding safety, durability, use of resources in construction works, climatic or geographical relations, or other national concerns (Standard Online AS, 2003). These parameters are denoted Nationally Determined Parameters (NDP) and are given in the National Annex to the standard. The National Annex may only contain information on these NDP parameters, which are left open in the Eurocode for national choice.

The main European standard regarding design of concrete structures is Eurocode 2: "Design of concrete structures". Part 1-1 of this standard, "General rules and rules for buildings" (Norsk Standard, 2004), contains the information relevant for analyses in this thesis. The standard is shortened EC2. EC2 was released in 1992, and was adopted as Norwegian Standard in 2004. In November

2008 a Norwegian translation and the national annex NA:2008 was published. This version of the standard is valid today. Following the implementation of Eurocode 2 the 6th edition of NS 3473 was withdrawn in April 2010.

The analyses in this thesis are performed on an existing concrete bridge, designed in 1987. It has been decided to perform the capacity calculations of the bridge according to the standard that was valid at that time, i.e. the second edition of NS 3473 is to be used. This edition was released in 1977, and is denoted NS 3473:1977. Shear capacity is in focus in this thesis, and as Chapter 8 will show, the formulas regarding shear capacities have developed over the years. Because of this, a control of the calculated shear capacities will be performed using the most updated shear formulas, i.e. the shear formulas provided in EC2.

2.2 Regulations

The Norwegian Public Roads Administration (NPRA) provides manuals that supplement the standards by providing explanations, additional information or regulations to the information given in the standards. The handbooks are published on two levels: Level 1 contains norms and directions approved by the Directorate of Public Roads by authorisation. Level 2 contains guidelines approved by the individual department of the Directorate of Public Road when authorisation has been provided by the directorate.

For this thesis several manuals have been taken into use. N400 "Bridge design" (Statens Vegvesen, 2015) is a norm regarding design of bridges, ferry quays and other load-bearing structures in the public road network. It includes all phases of the structure's construction period and service life.

R412 "Bridge classification" (Statens Vegvesen, 2003) is the current manual providing directions regarding classification of existing bridges. Classification of bridges involve establishing the maximum allowed traffic loads that can load the bridge. R412 also contains an appendix which provides updated information regarding choices of various parameters for existing bridges.

Manual 100 "Bridge design-08 NIB beams" (Statens Vegvesen, 1983) is a norm published in 1983 by the NPRA, and will be referred to as the NIB manual. The manual provides information regarding the use of the standardized I-beams denoted "NIB", which are prefabricated beams that were used as the structural system in bridges together with a cast-in-place bridge deck. The manual was revised with a new edition released in 1989. This edition has also been taken into use for certain objectives in this thesis. After the release of the 1989 edition of the manual, NIB beams have been replaced by other standardized I-beams.

The Norwegian Concrete Society released two publications in 1981 regarding calculations of NIB bridges consisting of several spans. Publication 10 "Calculation and design of continuous NOB and NIB bridges" (Norsk Betongforening, 1981a) deals with bridge systems where continuity is established between the NIB beams, while Publication 11 "Multi-span NIB and NOB bridges - calculation and design of continuous bridge decks over the supports" (Norsk Betongforening, 1981b) deals with bridge systems where the NIB beams have not been made continuous.

Chapter 3

Durability

In this chapter concrete as a building material is introduced, and properties that are important regarding durability for reinforced concrete structures will be looked into. Different deterioration mechanisms are furthermore presented, distinguishing between reinforcement deterioration mechanisms and concrete deterioration mechanisms. The Hulvågen Bridge is located at the coastline, and the structure is therefore exposed to sea water. Reinforcement corrosion due to chloride penetration is considered one of the main deterioration mechanisms for concrete structures in coastal environments, and this deterioration mechanism will therefore be emphasized. This chapter also contains an overview of measures that can be taken in order to increase concrete durability.

3.1 Concrete

Reinforced concrete is the most used construction material in the world, with several billion tonnes produced worldwide each year.

Concrete is a mixture of aggregates, cement, water, admixtures and mineral additives. Aggregates used in the concrete vary with a distinct particle size distribution (PSD) from coarse aggregates (such as gravel or pebble) to fine aggregates (sand). The fraction between the two, as well as the smoothness of the PSD, affect the properties of the mixed concrete.

The mixture of cement and water is called cement paste. In the reaction between these components water is chemically bound to constituents of the cement, creating calcium-silicate-hydrates (approximately $C_3S_2H_3$, denoted C-S-H). This is the binder in the concrete, and the production of this controls the setting and hardening of the concrete. The composition of the cement, as well as the cement fineness (i.e. the surface area between water and cement in which the hydration process can take place) therefore has a large effect on the binder properties of the concrete. In addition the weight ratio between water and cement (the w/c-ratio) is an important factor regarding concrete properties. Use of mineral additives such as pozzolanic materials (silica fume or fly ash) produces excess C-S-H, altering

the binder composition and consequently also the property development of the concrete.

Admixtures are chemical agents that are added in small dosages, and which can have dramatic effect on certain concrete properties in fresh and/or hardened state. Examples of most-used admixtures are plastizers (or water reducing admixtures) which increase workability in fresh concrete without increasing the water content, and air entraining admixtures which increase the concrete's frost resistance by stabilizing and providing a more even distribution of the air bubbles in the concrete.

The components in the concrete are proportioned in order to obtain desired effects in both fresh, hardening and hardened concrete. The aggregates constitute approximately 70 % of the concrete volume, while the cement paste constitutes approximately 30 % of the volume. Pozzolanic materials can be used in somewhat larger dosages, either as a replacement for, or a supplement to, the cement. The volume fraction of admixtures is negligible.

The hydration process is an exothermic reaction, generating considerable amounts of heat. The hydration process is highly temperature dependent, and the process is accelerated when the temperature rises. This results in a faster strength development in the concrete. This may be advantageous as an acceleration of winter casting, where large heat loss to the surroundings may result in a slower strength development, but if too high temperatures occur in the concrete it may reduce the quality of the concrete, including a permanent reduction of strength. Furthermore the temperature rise will be higher in the core and lower at the surfaces where the heat loss to the surroundings is larger. This leads to strain differences in the concrete, giving a risk of crack formation. The progress of hydration and corresponding heat generation depends on the cement (amount, composition and fineness), the w/c-ratio, external conditions (temperature, wind conditions, rain, formwork, etc.), use of admixtures (accelerators or retarders) and more.

3.1.1 Porosity and permeability

Concrete durability is largely dependent on how easy fluids in the form of liquid (water), gas (carbon dioxide, oxygen) or ions (chlorides, sulfates) can move through the hardened concrete. Moisture movement can occur by capillary-suction-driven flow (absorption), concentration-driven flow (diffusion) or pressure-driven flow (permeation) through the porous concrete (Soutsos, 2010). The rate of flow of fluids into the concrete by these transportation mechanisms is called permeability.

The permeability is controlled by the amount, size and distribution of pores present. The porosity of fresh concrete is made up by the water surrounding the cement particles in the cement paste. This situation occurs right after mixing, as seen in Figure 3.1(a). During the hydration process C-S-H-binder grows from the cement particles and water in the surface between the two. With time the C-S-H-binder replaces a large part of the unhydrated cement materials and the water. Figure 3.1 illustrates the development of this process at time (b) seven days, (c) 28 days and (d) 90 days after mixing. The porosity in the concrete then consists of the space between the solid parts of the C-S-H phase, namely the gel pores, and

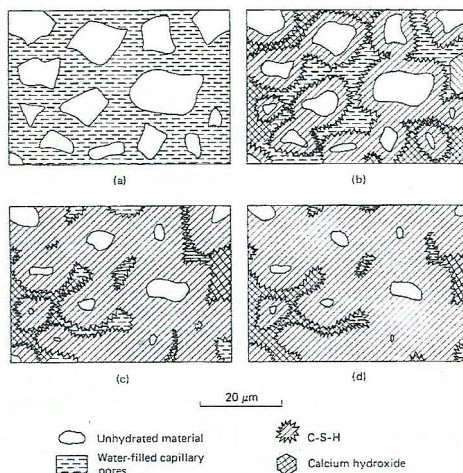


Figure 3.1: Microstructure of cement paste at: a = mixing, b = 7 days, c = 28 days and d = 90 days. $w/c < 0.5$. (Jacobsen et al., 2016)

those parts of the original water filled volume that did not fill up by hydration products, namely capillary pores.

The gel porosity is directly related to the amount of reacted cement while the capillary porosity increases strongly with the w/c -ratio and with decreasing degree of hydration. The gel pores are very small in size (2 nm) and the water contained in these pores are considered virtually immobile. The capillary porosity consists of larger pores (4-1000 nm), and its continuity plays a more important role regarding concrete permeability (Jacobsen et al., 2016).

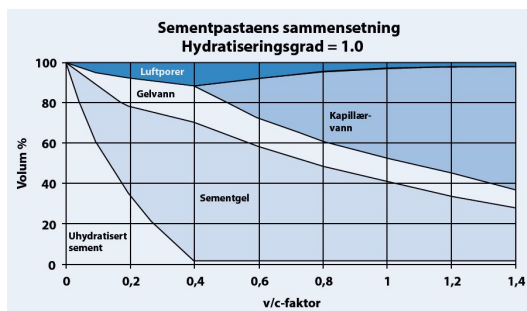


Figure 3.2: The concrete's pore system at maximum degree of hydration for increasing water/cement-ratio (Norcem)

The capillary porosity is a weak zone in the concrete, reducing its properties. This is particularly valid if the w/c -ratio is high enough to produce continuous capillary pores, i.e. above 0.5-0.6. The optimal w/c -ratio in order to produce

"watertight" concrete is lower than 0.50 (Jacobsen et al., 2016). This is given correct pouring, compaction and hardening of the fresh concrete, which is done in order to reduce the risk of crack propagation or badly compacted areas. It should be noted that with a w/c-ratio of less than 0.4 the concrete will contain unhydrated cement particles even after long time, in addition to C-S-H-binder, gel- and capillary pores. This is due to a lack of water compared to the amount of cement, and is illustrated in Figure 3.2. The degree of hydration will be dependent on for instance curing conditions, use of pozzolanas, etc. in addition to the w/c-ratio. For higher w/c-ratios (0.6-0.7) the continuity of the capillary system increases significantly more than the absolute value of the capillary porosity, meaning that the permeability will increase at a faster rate. This tendency can be seen in Figure 3.3. Figure 3.2 also illustrate how increasing the w/c-ratio increases the capillary porosity.

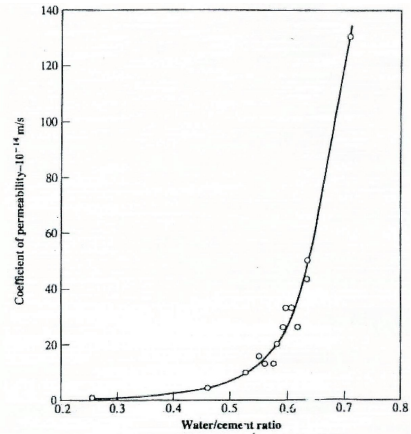


Figure 3.3: Relation between permeability and w/c-ratio for mature cement pastes (Jacobsen et al., 2016)

In addition to gel and capillary pores air voids occur in the concrete, either due to entrapped air during casting or intentionally entrained air using air-entraining admixtures. These air voids are bigger than the capillary voids, and can have a significant role in the permeability of concrete (Soutsos, 2010).

The permeability of the mixed concrete is always larger than for the cement paste used in the concrete, despite the fact that aggregates in Norway generally have low porosity. This is because of interfacial transition zones, where the cement particles are not able to be packed as densely towards larger surfaces such as aggregate and reinforcement.

Factors that influence the pore structure and hence the permeability of concrete include the w/c-ratio and degree of hydration as mentioned. Use of mineral additives such as pozzolana also influence the pore structure by producing excess C-S-H. Furthermore, the curing conditions and moisture history are of considerable importance. If drying of the concrete surface is allowed to occur during curing, the degree of hydration will become lower in this area, causing crack formation and higher permeability. Measures to avoid drying of the concrete surface during curing are therefore important. For hardened concrete, cycles of drying and re-wetting causes the pore structure to become coarser. This is also unfavourable with regards to permeability, and can be a problem for concrete surfaces exposed to weather (sun dries the surface, rain re-wets).

3.2 Reinforcement deterioration mechanisms

Reinforcement corrosion is one of the most important deterioration mechanisms of reinforced concrete, and has major financial implications around the world (Soutsos, 2010). In this section the common causes for reinforcement corrosion will be presented. Emphasis will be put on reinforcement corrosion due to chloride penetration, which usually is considered the main deterioration problem for concrete structures in coastal environments. In which manners corrosion of prestressed reinforcement differs from corrosion of regular reinforcement will also be looked into.

Section 3.1 presents concrete as a porous material, into which water and oxygen can diffuse quite easily. Regardless of the concrete cover over the reinforcement the water and oxygen can reach the reinforcement (Soutsos, 2010). Despite this porosity most concrete exposed to the outdoor environment does not corrode. This is because the concrete provides a chemical protection of the reinforcement steel, given by the alkalinity of the cement paste. The pore water in hardened cement usually has a pH in the range 12.5-13.5 (Soutsos, 2010). When reinforcement steel is exposed to a pH higher than about 10.5, a passive oxide layer will form on the surface of the reinforcement steel. This is called passivation, and inhibits corrosion from occurring on the steel surface.

When the concrete's protection of the reinforcement steel fails, corrosion can occur. Concrete is vulnerable to attack, and in Section 3.3 various mechanisms that break down the concrete will be presented. In addition there are two chemical species that can break down the passive layer without destroying the concrete first. They are the carbon dioxide molecule and the chloride ion. Carbonation attack is presented in Section 3.2.2. This mechanism causes pH reduction in the concrete pore water, depassivating the reinforcement so that corrosion can occur. Chloride attack lets the passive layer be broken down without the requirement of pH reduction. This mechanism is elaborated in Section 3.2.3.

Reinforcement corrosion consists of two stages. The initiation phase lasts until the passive oxide layer around the reinforcement is destroyed, i.e. the time it takes for aggressive elements, such as chloride or carbon dioxide, to penetrate the concrete. For carbonation attack it is sufficient that the carbonation front reaches the reinforcement, while for chloride attack the concentration of the chlorides must reach a sufficient level so that corrosion can begin. The corrosion phase is the time during which corrosion takes place after the passivation is dissolved.

The initiation phase will be described for carbonation attack and chloride attack in Sections 3.2.2 and 3.2.3. In the corrosion phase the same mechanism will occur regardless of the source of the depassivation of the steel. The corrosion mechanism that occurs in the corrosion phase will be elaborated shortly.

Hydrated ferric oxide, rust, which is the product from the corrosion process, has a volume of about 6.5 times that of the steel consumed (Soutsos, 2010). The formation of this expansive oxide leads to the cracking and spalling of concrete. This will initiate in corners and in areas of low cover, and if cracks propagate between adjacent reinforcing bars it may lead to delamination. Consequences of reinforcement corrosion on the reinforcement itself and on the concrete will be closer looked into in Chapter 10.

3.2.1 Corrosion mechanism

Reinforcement corrosion is an electrochemical process, consisting of an anode and a cathode that are connected through metallic contact and an electrolyte (a solution that can conduct ionic species). At the anode the oxidation, i.e. corrosion, occurs. Here the metal gives up electrons, and iron is dissolved to ferrous ions. The electrons are transferred from the anode to the cathode through the metallic contact provided by the reinforcement. Here the reduction process takes place, in which the electrons react with water and dissolved oxygen and produce hydroxide ions. These are transported through the electrolyte, made up by the pore water in the concrete, back to to the anode. The process is illustrated in a simplified manner in Figure 3.4. Secondary factors that affect the corrosion are temperature, pH, the electrolyte, the concentration of dissolved oxygen and more.

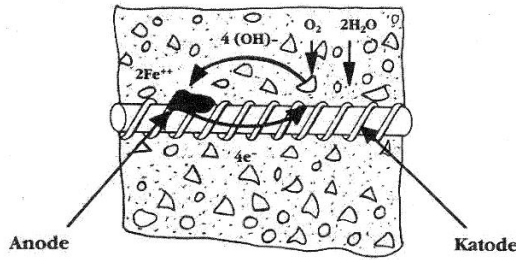
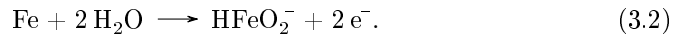


Figure 3.4: Simplified corrosion model

The reactions that are likely to occur at the anode, depending on among others the pH-value and the amount of negatively charged ions, are



Equation (3.1) normally occurs for $\text{pH} < 9$, while Equation (3.2) can occur for very high pH-values. The ferrous ions (Fe^{2+}) react with hydroxide ions (OH^{-}), water and oxygen to ultimately form rust (hydrated ferric oxide).

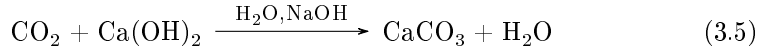
The cathode reactions depend on the availability of dissolved oxygen and the pH-value near the reinforcement steel's surface. The likely cathode reactions are



As can be seen from the reactions there is no initial requirement for oxygen at the anode, only at the cathode. Water is required at the anode in order to dissolve the ferrous ions. However, for rust to form both water and oxygen are required at the anode.

3.2.2 Carbonation

Carbonation is a chemical process between carbon dioxide (CO_2) from the air and the alkaline constituents of the concrete, that may lead to a neutralization of the concrete's alkalinity. The atmosphere typically contains between 0.03 and 1 % CO_2 . This is an acid gas, and when it is dissolved in water it forms carbonic acid. CO_2 from the air will migrate into the concrete through the pore system, and when the pores contain water the gas is dissolved. The weak acid reacts with calcium hydroxide ($\text{Ca}(\text{OH})_2$) in the pore water, and creates insoluble calcium carbonate (CaCO_3). The reaction is illustrated in Equation (3.5).



The insoluble calcium carbonate precipitates out of solution and lines the pores, causing increased density and solidity in the concrete. However, the reaction product take up less volume than the reactants, causing volume reduction and carbonation shrinkage which may lead to surface cracking. However, this effect that the carbonation process has on the concrete itself has no significant effect on the durability. The damage lies in the fact that the process reduces the pH in the pore water. When the pH is reduced below the critical threshold of 10.5, the reinforcement is depassivated and steel corrosion can initiate.

The carbonation advances as a front from the surface into the concrete. The carbonation rate is determined by the amount of moisture present, and particularly the amount of wetting and drying that occurs. CO_2 will penetrate when the concrete is dry, and then dissolve to form carbonic acid when the concrete is wet. Highest rate of carbonation is observed at around 60-70 % RH (Jacobsen et al., 2016). The porosity of the concrete and the amount of alkaline reserves in the concrete will also affect the carbonation rate. The carbonation front rate decreases further into the concrete because the transportation distance increases. Doubling the concrete cover over the reinforcement will therefore more than double the length of the initiation phase.

3.2.3 Chloride induced corrosion

In contrast to carbonation, which eventually will occur in all concrete exposed to the environment, chloride-induced corrosion will only occur in concrete that is exposed to chlorides. Chlorides are used in de-icing salt (CaCl_2) and are present at a concentration of about 3.5 % in seawater (NaCl) (Soutsos, 2010). Chloride from de-icing salts are considered more destructive than seawater. This is because the sea water contains several other compounds that can react with constituents in the concrete and form insoluble salts that give a clogging effect. This reaction does not occur for de-icing salt. The two corrosive agents CaCl_2 and NaCl are the most common causes of deterioration in reinforced concrete structures (Tahershamsi, 2016).

Chlorides enter the concrete either through constituents in the concrete containing chlorides or through migration of the ions from the environment. Chlorides

introduced during concrete mixing will spread evenly throughout the concrete. Increased knowledge regarding the effect of chlorides on reinforcement corrosion has led to more strict requirements regarding chloride content in the constituent materials. An example is the use of calcium chloride as a hardening accelerator. Since 1885 this had been considered the best hardening accelerator available, but in the 1970s the admixture was banned due to too high chloride content (Jacobsen et al., 2016; Soutsos, 2010). Other constituent materials can also contain chlorides, like the aggregate, cement and water, either unknowingly or deliberately. Chloride containing constituents can be considered as non-existent in concrete structures that are built today (SINTEF Byggforsk, 2009).

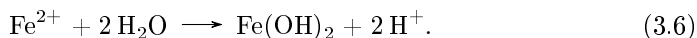
Migration of chloride ions from the environment into the concrete is a consequence of diffusion due to concentration gradients or capillary transport following freeze-thaw-cycles. The relative humidity of the concrete decides which of the two transport mechanisms that dominate. Capillary transport dominates when the concrete alternates between dry and moist, while diffusion dominates when the concrete alternates between moist and completely saturated (Stemland, 2007). The migration rate is largest for capillary transport, and depend among other things on the w/c-ratio, cement type, temperature, porosity and cover.

Both when chlorides are introduced during concrete mixing and when they migrate from the environment, some of the ions will bind to the solid structure while the rest act as free chlorides in the pore water. It is the free chlorides that are of importance regarding reinforcement corrosion. The concrete's ability to bind chlorides will therefore affect the length of the initiation phase.

Pitting corrosion

While carbonation advances like a front into the concrete, chlorides can attack the reinforcement's steel passive oxide layer in a point or small area. The corrosion initiates when a chloride ion replaces a hydroxide ion in the passive oxide layer, going from $\text{Fe}(\text{OH})_2$ to $\text{Fe}(\text{OH})\text{Cl}$. While $\text{Fe}(\text{OH})_2$ is passivating, $\text{Fe}(\text{OH})\text{Cl}$ is water soluble. In this area the passive oxide layer will therefore disappear, and the reinforcement below lies exposed to corrosion. The corrosion takes the form of pits or cavities, and this localized attack can often go deeper than the general corrosion.

When a pit is created the geometry of the pit will prevent mass transport, and the oxygen can be used up. As a result reduction of the oxygen will be limited to the surface near the pit, while inside the pit a slow build up of iron oxide (Fe^{2+}) will occur. Repassivation of the surface is prohibited by an acidification caused by hydrolysis of the dissolved iron oxide,



The acidity is maintained by the spatial separation of the cathodic and anodic half-reactions, where the cathodic half-reaction is the reduction of oxygen occurring at the reinforcement surface outside the pit while the anodic half-reaction is the oxidation of iron that occurs inside the pit.

The localised production of positive metal ions in the pit gives a local excess of positive charge. In order to maintain electronegativity the anion (ion of negative charge) must move into the pit and the cation (ion of positive charge) must move out. In neutral and alkaline solutions hydroxide (OH^-) will migrate to the pit and prevent a reduction of the pH-value. Acidification of the pore water in the pit can therefore only occur at the presence of other anions than hydroxide that can take it's place, like the chloride ions. If the content of Cl^- is low compared to OH^- repassivation of the steel can occur, causing the corrosion process to stop. A higher ratio will on the other hand lead to "excavation" of the reinforcement steel, growing into large pits.

Dissolved ferrous ions (Fe^{2+}) in the pit can react with water and chloride ions and create acidic H^+ -ions. If these ions accumulate in the pit hydrochloric acid (HCl) can be formed. This will make the water in the pit very acidic, which can cause further oxidation of the reinforcement steel (SINTEF Byggforsk, 2009). This process can self accelerate (become autocatalytic), and the corrosion rate in this kind of pit can become very high. Substantial local reduction of reinforcement cross section can occur, making pitting corrosion potentially more severe than corrosion caused by carbonation. Pitting can occur in one or several locations in a steel bar.

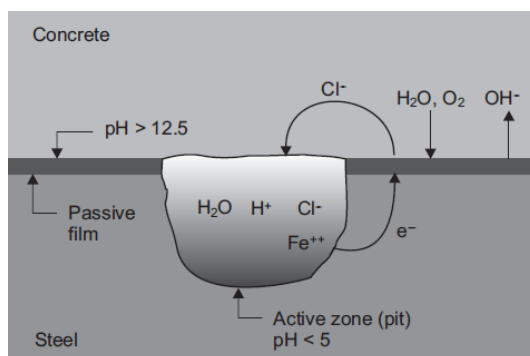


Figure 3.5: Mechanism of pitting corrosion

Figure 3.5 shows the mechanism of the pitting corrosion. First, iron is dissolved at the anode in the pit. Then a transportation of electrons occurs through the metal. The cathodic reaction where water is reduced to OH^- occurs on the reinforcement surface outside of the pit, and anions are finally transported through the concrete pore water back to the pit.

Critical chloride content

The critical chloride content denotes the threshold value of chloride concentration that is necessary for initiation of corrosion in a given concrete structure. This threshold value is highly uncertain, and dependent on many factors. One of the most important factors is the concrete's pH-value. The reinforcement can sustain a higher content of Cl^- compared to OH^- if the pH value is higher. The cement's

properties regarding chloride binding, the steel's electrochemical potential and the presence of cavities between the reinforcement and concrete layers also affect the critical chloride content.

As has been mentioned previously, carbonation will always occur in concrete exposed to the environment. For concrete structures that are exposed to chlorides, both mechanisms can therefore occur simultaneously. The influence of carbonation on chloride induced carbonation may become relevant when there is a certain amount of chlorides in the concrete which is not yet enough to depassivate the passive oxide layer in the reinforcement. In this case the influence of the CO_2 is twofold: Firstly, the pH-value will decrease with increasing uptake of CO_2 , which decreases the amount of chlorides that is needed to depassivate the reinforcement. Secondly, a certain amount of chloride bound to the cement will be set free, thus increasing the amount of free Cl^- -ions. This interaction between carbonation and chloride containing concrete is the likely cause of most severe corrosion problems that occur in practise (Schiessl, 1988).

Similar as for carbonation, measures to avoid chloride attack regards prolonging the initiation phase. Increasing the concrete cover is the most effective measure for both mechanisms, and for chloride attack a doubling of the concrete cover will quadruplicate the initiation phase (SINTEF Byggforsk, 2009). Low w/c-ratio with increased amount of pozzolana will make the concrete denser and less permeable. For chloride attack details which avoid contact between the sea water and concrete, for instance gulleys, can be used to limit the amount of chlorides entering. Surface treatment in order to reduce the amount of water (for chloride attack) or CO_2 (for carbonation attack) that enters the concrete can also be highly effective.

3.2.4 Corrosion of prestressed reinforcement

The information given above regarding reinforcement corrosion is quite general, and applies for both reinforcing steel and prestressing steel. While the underlying principles of the corrosion mechanism are the same for both reinforcing steel and prestressing steel, differences in mechanical and physical conditions of the steels give rise for the need to examine the corrosion propagation in prestressed concrete structures separately (Li et al., 2011). Mechanical and physical conditions that distinguish prestressed structures from regularly reinforced structures are in particular the high level of stresses in prestressing steels, their microstructure, smooth surface and small cross-sectional areas. Furthermore the effects of corrosion on the structural behaviour is different, as will be looked further into in Chapter 10.

Experiments performed by Li et al. (2011) shows that more corrosion occurs for steel bars than for unstressed strands, when the two are exposed to the same conditions. This suggests that it may be more difficult for corrosion to initiate on strands than on bars under the same conditions. Li et al. (2011) arguments that this may be due to the higher quality of the passive oxide layer on the surface of steel strands, which stems from higher carbon content than that of reinforced steel bars, as well as a smoother surface from manufacture. A higher carbon content causes more passivating reactions to occur, while the smooth strand surface causes finer and firmer passive oxide layer, both chemically and physically. The micro-structural

characteristics of the strands lead to less corrosion initiation, i.e. fewer corrosion cells, in the prestressing steel. Fewer corrosion cells will, however, result in faster growth of local corrosion at already corroded spots. Pitting corrosion dominates, and because the electrochemical characteristics can be different for each strand, local and uneven corrosion often occurs. For reinforcing bars the lower quality of the passive oxide layer of deformed bars allows chloride ions to penetrate more easily, causing initiation of corrosion over the whole surface. This causes relatively uniform corrosion of deformed bars.

The corrosion rate of prestressing steel strands increases with the increase of the level of stress applied. This increase occurs in an approximately linear manner. Hence, the higher the stress level in the prestressing strand is compared to its ultimate tensile strength, the faster the corrosion will occur.

It is evident from these observations that detection of corrosion in prestressing structures may be harder than in reinforcing steel. With a uniform corrosion of the reinforcing steel the chances of leakage of rust products to the surface are increased, which can make the corrosion process more visible and hence easier to detect. Pitting corrosion at fewer cells in the prestressing steel may on the other hand occur with little or no leakage to the surface, while the load-carrying capacity is being drastically reduced. The corrosion rate moreover increases with increased stress levels. If the mounting reinforcement around the prestressing steel is of low diameter, this may also corrode without leakage to the concrete surface. As a result, severe corrosion can occur in the prestressed reinforcement without any danger signs visible at the surface. These effects may explain why there are more structural collapses of prestressed concrete structures without warning than those of reinforced concrete structures (Li et al., 2011). It can be concluded that the corrosion of prestressing steel poses higher risk than that of reinforcing steel, from a structural point of view.

3.3 Concrete deterioration mechanisms

In the following different deterioration mechanisms for concrete structures will be presented. The deterioration mechanisms are generally divided into two parts: Chemical deterioration mechanisms and physical deterioration mechanisms.

3.3.1 Chemical deterioration mechanisms

Chemical deterioration of concrete is either due to contaminants added in the concrete mix during manufacturing, due to the action of external aggressive agents or due to a combination of both. Common to all chemical deterioration is a need for water (or moist environment) for the chemical deterioration reactions to occur (Norsk Betongforening, 2003).

There are two main forms of chemical deterioration, namely dissolution of the concrete binding material and the creation of reaction products with an associated volume increase. Both mechanisms can lead to an increase in porosity and permeability, a decrease in strength, cracking, dissolving or spalling (Soutsos, 2010).

Some different forms of chemical deterioration of concrete are briefly reviewed in this section. Reinforcement corrosion is also considered a form of chemical deterioration, but because it regards deterioration of the reinforcement instead of the concrete it has been treated in its own section.

Alkali-aggregate reaction (AAR)

Alkali-aggregate reactions are direct reactions between the cement and aggregate in hardened concrete. There are two main forms of AAR, namely the alkali-silica reaction (ASR) and the alkali-carbonate reaction (ACR), with ASR by far being the most common of the two. ASR is a chemical reaction that can occur between certain aggregate types and alkaline pore water in the concrete. The aggregate must be alkali-reactive, i.e. contain a reactive form of silica as a mineral constituent. The alkaline pore water originates from cement with a high alkali content due to alkali hydroxides (sodium or potassium). Typical cements used in Norway have a high alkali content. In addition water is necessary for the reaction to occur.

The product from the chemical reaction is an alkali-silica gel. The gel has the ability to absorb water and expand, creating a volume increase and internal stresses that can crack and disrupt the concrete. Over time the reaction gives a characteristic crack pattern (map cracking) on the concrete surface. Norwegian alkali-reactive aggregates are considered slowly reactive aggregates, and normally it takes at least 10 - 15 years before signs of ASR are visible on the concrete structures. (Jacobsen et al., 2016).

In order to avoid ASR there exists recommended upper values of alkali contents in the cement and concrete if alkali reactive aggregates are to be used. Relying on elimination of water in the structure is not sufficient according to today's regulations. For existing structures with ASR, or structures that are prone to future ASR, not much can be done except for an attempt to dry out the structure (Jacobsen et al., 2016).

Sulfate attack

Sulfate attacks can be external or internal. External sulfate attacks are caused by solution of sulfates penetrating the concrete. Sources of sulfates can be groundwater, seawater, bacterial action in sewers, clay adjacent to the concrete and more (Soutsos, 2010). Sulfates react with the products from hydration and lead to an alteration of the paste composition. Ettringite is formed, and because this has a larger volume than the reactants the cement paste will expand. In hardened concrete this reaction leads to extensive cracking and loss of bond between the cement paste and aggregate.

Internal sulfate attacks occur when a source of sulfate is incorporated into the concrete during mixing. This can for instance be sulfate-rich aggregates, excess gypsum added in the cement or contamination. Delayed ettringite formation is a special case of internal sulfate attack which can occur if the concrete reaches very high temperatures (65-70 degrees Celcius) during curing (Winter, 2005).

Sulfate attack can be prevented by the use of sulfate resistant cement. A low w/c-ratio is also important, and use of pozzolana like silica fume may also be advantageous (Norsk Betongforening, 2003).

Ammonium nitrate attack

Ammonium nitrate attacks are most common in concrete which is in contact with fertilizer. Similar to sulfate attacks, an ammonium nitrate attack leads to a chemical expansion where the reaction products demand larger volume than the reactants. In addition, large amounts of nitrates from chemical fertilizer can lead to corrosion and brittleness in the reinforcement. Measures to avoid ammonium nitrate attacks correspond with measures to avoid sulfate attacks.

Acid attack

Concrete is normally very alkaline with a pH of around 13. Acids have pH of below 7, and acid attacks, dependent on type and concentration of acid, can be severe. When exposed to acids, the binders in the concrete are transformed into new non-binder chemical compounds (Norsk Betongforening, 2003). The attack begins in the surface and leads to a dissolution of the concrete.

Acids can be present in acid rain, groundwater, sewage or soil, and in industrial environments leakage or random spillage of acids can occur. Precautions to avoid acid attacks includes using concrete with a low w/c-ratio. Use of pozzolanas results in a denser concrete, which can have a positive effect.

Lime leaching

Leaching of lime compounds is dissolution and removal of calcium hydroxide from the concrete, and occurs due to contact with water containing easy-soluble lime. This is mainly a structural problem for concrete of bad quality (high w/c-ratio), and can lead to destruction of the concrete binder, and with that destroying the protection against reinforcement corrosion. However it is seldom that this form of deterioration reaches far (Norsk Betongforening, 2003). For concrete of normal quality lime leaching is mainly an aesthetic problem. Structures exposed to one-sided water pressure (dams, supporting walls, etc.) are most exposed to lime leaching, and a low w/c-ratio and use of pozzolanas to secure a denser concrete will have a positive effect in order to avoid this deterioration form.

3.3.2 Physical deterioration mechanisms

There are a range of different mechanisms that can result in physical deterioration of concrete. Static loading (overloading, repeated loading or fatigue loading) and dynamic loading (impulse) are obvious sources of deterioration in form of crack propagation which make the concrete less sustainable. In addition frost damage and thermal damage can cause crack propagation as well as a reduction of the concrete structure's load capacity.

Frost damage

Normal concrete has a pore volume in the order of 120-180 litres per cubic meter. The pore system near the surface can easily fill with water, especially if the concrete is in direct contact with a water source. Freezing of water gives a volume increase of approximately 9 vol-% (Soutsos, 2010). This volume increase leads to internal pressure in the pores, which lead to tensile stress in the surrounding concrete. When this tensile stress exceeds the tensile strength of the concrete, this will result in crack propagation. With time freeze-thaw cycles cause scaling and crumbling of the surface.

As mentioned in Section 3.1 a stable and even distributed pore structure by use of air entraining admixtures increases the concrete's frost resistance. Furthermore a low w/c-ratio, protection from water and good drainage is advantageous.

Thermal damage

Concrete can be exposed to temperature differences from the environment or from the hydration process. The concrete expands during temperature increase and contracts during temperature decrease. If the structure is restrained from movement constraining forces occur and may lead to crack propagation.

As explained in Section 3.1 the temperature rise which follows the curing process may cause strain differences in the concrete because the core will have a higher temperature than the surfaces. This temperature difference causes *internal restraint* in the concrete, and the temperature difference should be less than 20 degrees in order to reduce the risk of crack propagation (Jacobsen et al., 2016). The heat production during curing may also cause *external restraint* if casting of concrete is done next to previously cast structural members, rock or similar. Bond between the new and old structural member will develop while the newly cast concrete is heated due to the hydration process, and when the hydration process finishes and the temperature sinks, the newly cast concrete will contract, leading to propagation of cracks perpendicular to the contact surface.

Thermal damage can be reduced by calculating and controlling the heat development during the curing. An increase in reinforcement amount (number of bars) leads to a denser distribution of cracks with smaller crack widths, which in many cases may give acceptable conditions.

Overload and impact

Overload damage can occur for a variety of reasons, for example early removal of formwork when the concrete has not yet reached design strength, a change in the use of a structure without proper structural upgrades, unintentional overloading or damage caused by impact. Overloading is particularly common in bridges, parking decks and similar which are exposed to large loads from heavy vehicles. The cracks in these structures will open and close depending on the current load on the structure. Overloading amplifies the deterioration of the concrete by allowing leakages to occur or aggressive ions to enter the concrete through the cracks.

Abrasion

Wear on the concrete surface caused by rubbing and friction can lead to abrasion damage. As the cement paste on the surface wears the fine and coarse aggregates in the concrete are exposed, and continued abrasion and impact lead to further degradation. Vehicular traffic surfaces is a typical example of concrete abrasion. If the concrete is of good quality and the aggregates are wear resistant, abrasion is not a large problem. A sufficiently high compressive strength is the most important factor in controlling the abrasion resistance of concrete (Portland Cement Association, 2002).

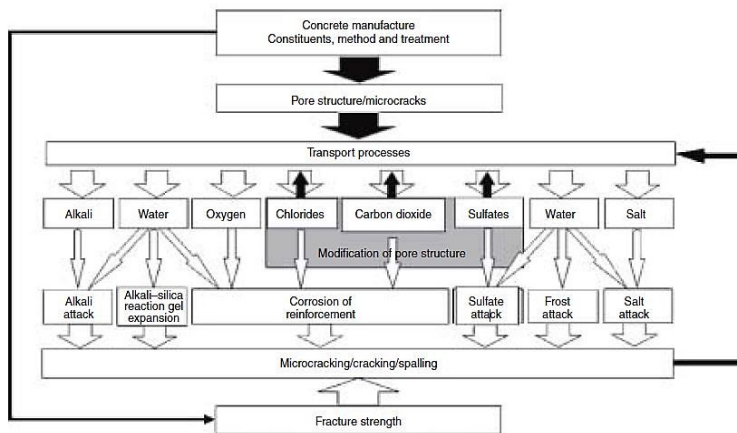


Figure 3.6: Overview of deterioration mechanisms (Soutsos, 2010)

Figure 3.6 shows an overview of several of the deterioration mechanisms that have been described in these sections. The figure gives a simplified overview of the substances that need to be present for the different mechanisms to occur, as has been elaborated. All mechanisms lead to microcracking, cracking or spalling of the concrete. Furthermore the figure illustrates the loop process of how the harmful substances are transported through the concrete's pore structure and cracks, cause further cracking of the concrete, which again allows for further transportation of harmful substances through the concrete. The effect the mechanisms have on the reinforcement is not included in this figure.

3.4 Measures to increase concrete durability

Measures to secure durable concrete begin in the design phase when materials are chosen, calculations are performed and drawings are made. Furthermore choice of components in the concrete, as well as casting and curing conditions are important. Preventative work to avoid deterioration continue throughout the service life of the structure with regular inspections and maintenance.

Important factors that affect the durability have been mentioned for the different deterioration mechanisms presented in Sections 3.2 and 3.3. On the basis of this, taking into account the relevance of the different mechanisms (probability of occurring and consequences if present) for The Hulvågen Bridge, measures that are of particular importance regarding durability can be summarized. The Hulvågen Bridge is exposed to aggressive environment through its location at the coast, and chloride induced corrosion is considered the greatest challenge for the structure's durability. Due to their importance in connection with reinforcement corrosion, concrete cover, concrete quality and cracking are elaborated in the following sections.

3.4.1 Concrete cover

Concrete cover is measured from the concrete surface and into the edge of the closest structural reinforcement bar. Securing sufficient cover is one of the most effective measures of increasing concrete durability.

The knowledge that reinforcement steel must be protected from the surface using sufficient cover has existed for as long as reinforced concrete has been used as a building material (Kompen and Liestøl, 1995). It has also been known that the necessary size of the cover depends on the environment that the structure is exposed to, and must be increased for more aggressive environments. However, until the end of the 1980's little attention was paid to this knowledge in the industry, both nationally and internationally.

Minimum requirements regarding concrete cover have developed over the years in various standards and regulations. A presentation by The Norwegian Public Roads Administration (NPRA) from 2014 regards the regulations for concrete related to durability (Reidar, 2015). Here a historical perspective has been presented regarding cover requirements. In 1926 the then called Norwegian Engineering Society, now Tekna, released directives stating that concrete structures exposed to sea water must have a concrete cover of minimum 4 cm. In 1962 the Norwegian Standard NS 427 A stated a minimum requirement of 5 cm for structures close to but not submerged in sea water. The first edition of NS 3473 released in 1973 stated that a cover of 25 mm was sufficient for outdoor structures, not differentiating between concrete exposed to sea water or less aggressive environment. This value remained in the second edition of NS 3473, which is the edition that was in use when The Hulvågen Bridge was built. In the third edition of the standard, released in 1989, the minimum requirements were increased back to 50 mm. This value was kept for the remaining editions of the NS 3473. When the Norwegian standard was replaced by the Eurocodes much higher cover was demanded for the structures that were exposed to the most aggressive environment. EC2 recommends a cover of 120 mm for prestressed structures exposed to marine environment (Statens Vegvesen, 2015).

Figure 3.7, from the presentation by the NPRA, shows an overview of the development of cover requirements. The drastic reduction in cover introduced in the first edition of NS 3473 is described in the presentation as a large blunder, not at all providing sufficient cover. It is stated that no development parallel

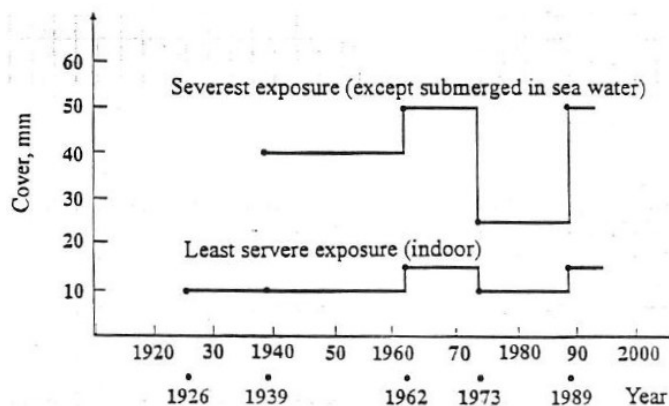


Figure 3.7: Development of cover requirements in standards (Reidar, 2015)

to this has been seen in other countries. No standard has included realistic or practically usable tolerance for reinforcement layout, reinforcement spacers have not been considered, etc. Large deviations from the required covers have therefore been common, both in Norway and internationally.

As mentioned in Section 3.2, concrete cover has large effect on the penetration rate of carbon dioxide and chlorides, and is therefore one of the most important factors that control the length of the initiation phase with regards to reinforcement corrosion. It is natural to assume that The Hulvågen Bridge will have problems with reinforcement corrosion, due to the fact that it was built while the requirements to concrete cover were very low. However it should be noted that prestressing reinforcement in general has been placed with larger cover than regular reinforcement, indicating that the prestressing strands may be slightly better protected from aggressives. The state of The Hulvågen Bridge will be looked into in Chapter 4.

3.4.2 Concrete quality

The quality of concrete is a term regarding a wide range of properties including its composition and the care of which it is executed. Important items regarding concrete quality are (Bertollini et al., 2013)

- Water/cement ratio
- Cement content
- Cement type
- Mixing, placing, compacting and curing
- Cracking, both on the macroscopic and microscopic scale
- Other aspects, such as air content

Of these items the water/cement ratio is a property of particular importance. This ratio controls the permeability of the concrete to a large extent. A dense concrete (with low permeability) will reduce the danger of harmful substances to

enter the concrete, and thus delay the deterioration. The quality of the aggregate, particle size and composition of the constituents also affect the permeability.

3.4.3 Cracking

The risk of reinforcement corrosion has often been correlated to the width of cracks. However, several studies show that as long as the crack widths remain below 0.5 mm no precise correlation occurs (Bertollini et al., 2013). For such small cracks the risk of corrosion will instead depend on factors such as environmental conditions (in particular the humidity), concrete cover and the concrete quality (in particular related to permeability). Cracks of sufficient width may on the other hand reduce the length of the corrosion initiation phase by providing a preferential path for the penetration of carbonation or chlorides. The risk of corrosion of prestressing steel has been observed to have a similar correlation with cracks and cracks widths (ElBatanouny et al., 2014).

Figure 3.8 illustrates how cracks may move the depassivation front closer to the reinforcement in a region around the crack. Experiments with sectioned steel bars in intentionally cracked concrete beams have shown that the initiation phase decreases in length as the crack width increases (Bertollini et al., 2013). On the other hand no relationship between crack width and the corrosion phase have been observed in these experiments, i.e. the crack width is not observed to affect the corrosion rate.

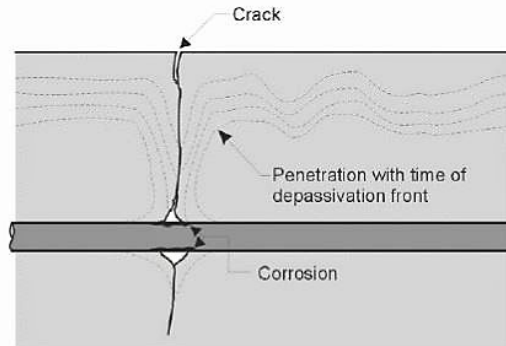


Figure 3.8: Illustration of the depassivation front near cracks (Bertollini et al., 2013)

Requirements regarding crack widths are given in the standards depending on the environment that the structure is exposed to and the reinforcement type that is chosen.

Cracking in end regions of prestressed concrete beams

Prestressed concrete structures are exposed to additional loads from the prestressing, especially in the end regions where transfer of the prestress by bond between

the prestressing strands and the concrete takes place. In this area the prestressing loads cause transverse tensile stress in the concrete, which can lead to cracking of the end regions, either during or immediately after the prestress is transferred from the prestressing jack to the concrete. I-shaped beams, like the structural beams that are used in The Hulvågen Bridge, are particularly prone to cracking due to their slender cross sectional geometry. The cracks that occur may, as explained in this chapter, provide a path for corrosive agents to reach the reinforcement bars or the prestressing strands. In order to avoid durability problems or structural capacity losses as a consequence of this Oliva and Okumus (2011) look into various solutions that can control cracking in these end regions. The cracks observed in the performed experiments are categorized into three: inclined cracks, horizontal web cracks and Y cracks, with marked examples of each category shown in Figure 3.9. A study is conducted in order to evaluate the impact modifications to the end region have on the occurrence of the cracks.

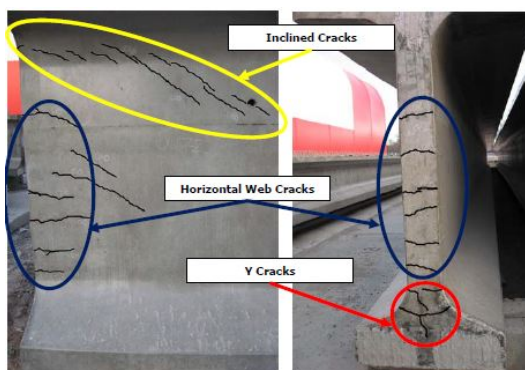


Figure 3.9: Marking of typical cracks categorized according to Oliva and Okumus (2011)

It is found that the choice of end zone reinforcement and debonding of strands in the beam end are the two most important factors affecting the cracking in the end regions. Using larger sized vertical bars in the end zone reinforcement mainly affects the strains in the web area, reducing the occurrence and size of the horizontal web cracks. Larger sized vertical bars also reduce the inclined cracking slightly, but the improvement in the inclined strains is not as significant as for the horizontal strains because the vertical rebars do not cross the inclined cracks perpendicularly.

Debonding strands at the beam end directly lowers the stresses that are transferred to the concrete at the end, and therefore affects cracking of each type. Debonding some strands in the bottom flange at the beam end has the potential to completely eliminate the inclined cracking problem. It can furthermore reduce the number of horizontal web cracks and the size of these cracks significantly. If debonding is performed on the strands as close to the exterior face as possible, reducing the resultant eccentricity of the strands, it also has the potential of significantly reducing or eliminating the hazardous Y cracking strains. However, the

selection of strands to debond should be made carefully, as debonding also has the potential of increasing the size of the Y cracks.

The results found from the study performed by Oliva and Okumus (2011) show that a combination of both an increasing in end zone reinforcement and debonding of strands is the most ideal solution in order to reduce the three categories of cracking in the end regions. Other factors that have been shown to have less effect on the end zone cracking are other parts of the end zone reinforcement (vertical bars further away from the beam end, stirrups in the bottom flange) and the cutting order of the prestressing strands.

It should be noted that a factor which has not been considered in this study is strengthening the beam webs in the end zones. This is often done by increasing the thickness of the web to the width of the lower flange for some length over each beam end. Strengthening the ends regions is consistently done for I-sectioned beams in Norway, while the I-beams that have been tested in this experiment do not have thicker end zones. A larger concrete cross section will contribute to reducing the risk of cracking in the end zone.

Chapter 4

The Hulvågen Bridge

In this chapter a presentation of The Hulvågen Bridge is given. The continuity of the bridge will be discussed, and the drawings that the analyses in this thesis are based on will be presented. Additional information is also given regarding the bridge's structural beams, which will be the focus of the analyses in this thesis. The current state of the bridge, based on information registered in NPRA's bridge management system Brutus, will also be presented.

4.1 Presentation of The Hulvågen Bridge

The Hulvågen Bridge lies on the Atlantic Ocean Road, a National Tourist Route which connects the island and municipality of Averøy with the mainland at Eide. Near The Hulvågen Bridge the road has an annual average daily traffic of 1730 vehicles and a speed limit of 60 km/h.

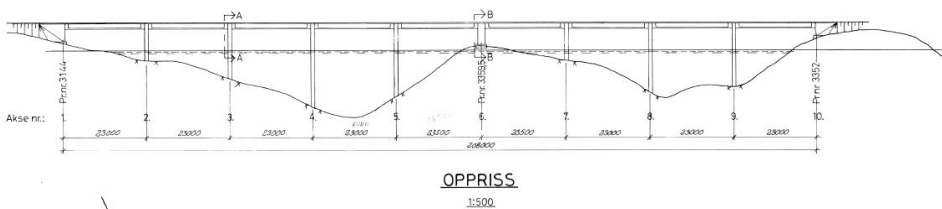


Figure 4.1: Profile of the Hulvågen Bridge

The bridge was designed by Johs Holt AS in 1987 and built by The Norwegian Public Roads Association (NPRA). It opened for traffic in 1989. The profile of the bridge is shown in Figure 4.1. It is a 208 meter long concrete element bridge, consisting of nine spans of 23 to 23.5 meters, with eight transversal supports between the bridge ends, anchored to rock. The support in axis 6 is anchored on a reef above water level, while the rest are anchored beneath water level. The structural system of the bridge consists of four rows of prefabricated pre-tensioned concrete

beams, in total 36, and with a cast-in-place bridge deck. The beams are supported on rubber bearings over the transversal supports. The transversal supports are also cast-in-place, and the bridge has a clearance of 3.5 meters over sea level.

The bridge has a horizontal curvature with a radius of 250 meters in the west end, which straightens out to no curvature between axis three and six. The bridge has no vertical curvature, and the cross section of the bridge is continuous throughout the bridge. In the area with horizontal curvature the bridge has a slope of 64 ‰ to one side, which is gradually reduced to a 25 ‰ slope from the middle and downwards to each side of the bridge.

A pavement is required on top of the bridge deck as an extra layer to protect the structural system from wear and tear. Modern pavements can consist of a damp-proof insulating layer, a screed, a base course and a wearing course of asphalt. It is not known what the pavement on The Hulvågen Bridge consists of, however, as Section 4.2 will introduce, registered damages to the bridge deck may indicate leakage of sea water through the deck, which may indicate that there is no waterproof layer in the pavement. The bridge has two traffic lanes, one in each direction. A guard rail is placed on either side of the bridge, and there are no sidewalks, cycle lanes or curbstones.

With its location in the coastal area and low clearance over sea level the bridge is exposed to extremely aggressive marine environment. Considering the age of the structure, the increase in service loads that in general has occurred for old structures when comparing to design values, the low demands to concrete cover at time of building and the registered deterioration damages to the bridge (both of which shall be elaborated in this chapter), there are strong indications that this bridge possibly can have large problems with deterioration in several structural elements.

4.1.1 The continuity of The Hulvågen Bridge

Continuous concrete element bridges are built in stages, one span at a time. First, the transversal supports are cast in order to act as supports for the beams. The beams are then placed in position, simply supported at both ends on the transversal supports as seen in the left case in Figure 4.2. Next, concrete is cast in between the beams over the transversal supports in order to make connect the beams in the longitudinal direction, making the bridge continuous. The bridge deck is then cast over the beams using formwork in between the beams, and when the bridge deck has sufficient strength the pavement layer on top is cast. When the bridge deck is hardened both the beams and the bridge deck will behave as a continuous structure over the entire length of the bridge, and the bridge is a continuous multi-span structure where each span behaves as given in the right case in Figure 4.2.

The drawings provided of The Hulvågen Bridge state that the concrete element bridge is continuous. This has been the basis of the calculations for the majority of this thesis. On an excursion to the Atlantic Ocean Road performed from the 9th to the 10th of May 2017, it was discovered that the bridge in fact was not made continuous when it was built. Instead the bridge is a multi-span simply supported bridge, where the beams have not been made continuous at the transversal sup-

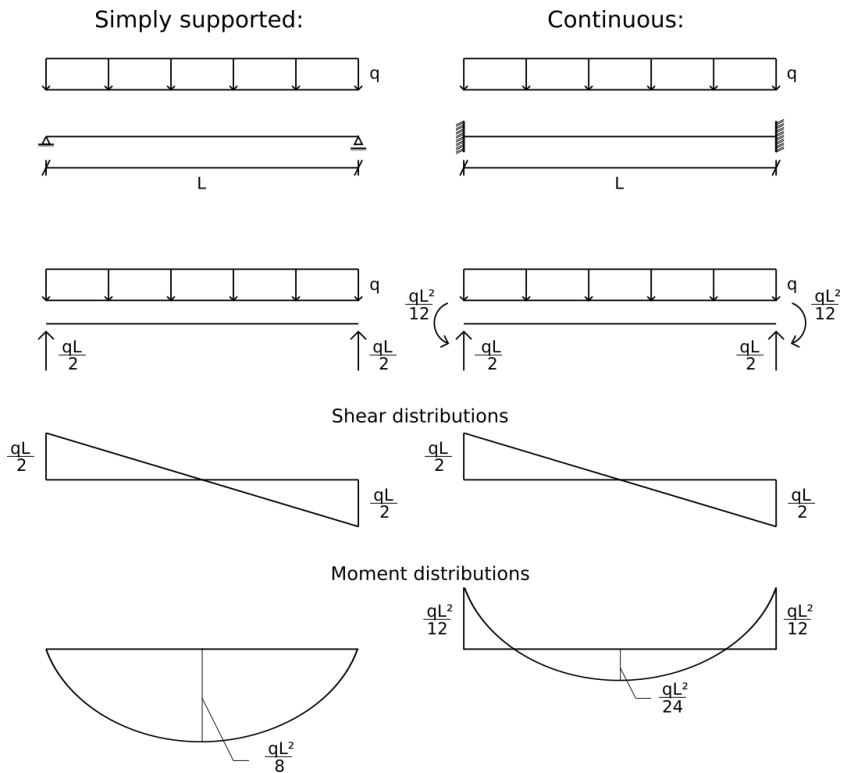


Figure 4.2: Load effects from distributed load on simply supported and continuous system

ports, but instead are resting as individual simply supported beams. Figure 4.3 shows that the beam ends are in fact not connected. The continuous bridge deck cast over the beams, as well as friction in the bearings between the beams and transversal supports will bring some continuity to the bridge, which means that the bridge in reality will have a structural system which lies somewhere in between the two idealized extremes. Nevertheless, the NIB beams are the most important factor with regards to continuity, and so the structural system will be closest to the simply supported bridge system.

The calculations that are to be performed in this thesis regard in particular the regions around the supports, where shear forces will be largest, and shear and anchorage failure can occur. As illustrated in Figure 4.2 the continuous system generally will cause larger shear forces and moment in the support regions than the simply supported system. This indicates that a continuous bridge system will be decisive rather than a simply supported bridge system with regards to shear capacity. Because the bridge has a structural system which lies somewhere in between simply supported and continuous it has been decided to consider the beam as continuous in all relevant manners throughout this thesis. Furthermore it will



Figure 4.3: Image from the excursion showing the simply supported NIB beams

be controlled that the design loads for the corresponding simply supported system do not exceed the design loads that are derived for the continuous bridge system. If both the continuous bridge system and the simply supported bridge system have sufficient shear capacity, it can be assumed that any situation with partial continuity in between the two extremes also will have sufficient capacity.

4.1.2 Drawings

The calculations performed in this thesis are based on working drawings of The Hulvågen Bridge produced by Johs Holt AS in February 1987, and production drawings of the NIB beams produced by Vestlandske Spennbetong AS in May 1987. Both sets of drawings are included in Appendix A.

The Appendix furthermore contains a drawing of the completed bridge, produced by the NPRA in August 1999. This drawing contains various information that has been included in the thesis, and provide a basis for assumptions and calculations. For instance is the thickness of the bridge deck given as 250 mm in this drawing, while it is not given in the working drawings from Johs Holt AS.

The span lengths in the drawing of the complete bridge vary from the span lengths given in the working drawings by Johs Holt, with differences up to 3500 millimetres in certain spans. Based on recommendations from the NPRA it has been decided to use the dimensions given in the working drawings by Johs Holt AS as the basis for analyses in this thesis. This recommendation is based on the knowledge that drawings of complete bridges as old as this had very little quality demands, and were only meant to illustrate the basic shape, placing and spans of the bridge. In general the working drawings had higher quality demands than the drawings of the complete bridges.

4.1.3 NIB beams

The Hulvågen Bridge consist of four rows of precast, pre-tensioned I-beams of type NIB 500/1435, in total 36. NIB stands for normalized I-beams. The beams were

normalized in a publication from The Norwegian Concrete Society, "Publikasjon nr. 3: Normerte I-tverrsnitt NIB", released in 1974. According to NPRA's bridge management system Brutus, more than 150 bridges have been built using NIB beams (Paciorek et al., 2017). 61 of these bridges are located in coastal areas and 13 in harsh coastal environment, where the latter category includes The Hulvågen Bridge.

The beams used in this bridge were produced by Vestlandske Spennbetong AS, now Spenncon. The production drawings provided in Appendix A are from May 1987. Appendix A also includes a bar schedule providing further information regarding placing, amount and type of pre-tensioned and regular reinforcement, as well as concrete quality of the beams.

The NIB beams have an I-shaped cross section as can be seen in Figure 5.1. In the beam ends there are several conditions that will change the capacity of the cross section, a fact which will be elaborated later. The shear loading will furthermore be at its largest in these areas. In order to assure sufficient capacity the beam is strengthened by increasing the thickness of the web from 100 mm to the width of the lower flange, 300 mm, over a length of 1425 mm in both beam ends. This change in the cross section in both beam ends will have marginal effect on the load distribution over the length of the beam, and it has therefore been decided to neglect this effect when establishing design loads. For capacity control however, where the capacity is controlled section-wise along the beam end, the change in cross section will be included.

Concrete cover over the NIB beams

As Section 3.4.1 has shown, minimum requirements to concrete cover have varied over the years, with a large reduction in the requirements around the time that The Hulvågen Bridge was designed and built. Figure 3.7 illustrates the development, and shows how low the demand was around 1987, with only 25 mm cover required for outdoor structures.

Recommendations regarding concrete cover over NIB beams is presented in the NIB manual (Statens Vegvesen, 1983). Section 080.3 of the 1983-edition recommends a concrete cover of 25 mm, in accordance with the recommendations given in NS 3473:1977 as presented in Section 3.4.1. Section 080.3 of the 1989-edition, released two years after the beams for The Hulvågen Bridge were produced, recommends a concrete cover of 40 mm. It can be seen from the production drawings of the NIB beams produced by Vestlandske Spennbetong AS that the minimum cover used for the beams in The Hulvågen Bridge is 40 mm. This indicates that it was known in the academic environment that 25 mm is not sufficient cover, especially for beams used in bridges exposed to aggressive marine environment.

In order to secure sufficient cover without reducing the capacity of the NIB beams, the total height of the NIB beams has been increased with increasing cover recommendations. The NIB 500/1435 beams used in The Hulvågen Bridge had in the 1983-edition of the NIB manual a total height of 1400 mm. In the 1989-edition of the manual the beams have a total height of 1430 mm. The beams used in The Hulvågen Bridge have a height of 1435 mm, as the name indicates.

4.1.4 Composite beams

The bridge deck is cast in place, as mentioned in the beginning of this section. The deck is cast directly onto the NIB beams, and when it has obtained sufficient strength the two components will work as a continuous cross section which is approximately T-shaped. This T-shaped beam is denoted the composite beam for the remainder of the thesis. The coupling between the two members is assumed to be maintained regardless of the loads a section is subjected to. The validity of this assumption will be studied in Section 8.6 and 9.5.

The height of the bridge deck is 250 mm as given in the drawings. The width of the bridge deck that is to be included in the composite beam must be decided. In EC2 a calculation procedure for calculating the effective width of the deck in the composite beam is given in Section 5.3.2.1, but no corresponding calculation procedure has been found in NS 3473:1977 or supplementing literature. Norsk Betongforening (1981a) provides a calculation example of a similar situation. Here the entire deck width between the beam is used as the effective width of the deck. Based on this it has been decided to use the distance of 2000 mm between the NIB beams as the effective width of the bridge deck that is to be included in the composite beam.

4.2 Current state

This chapter describes the current state of the Hulvågen bridge, based on various inspections performed by the NPRA. The NPRA administrates approximately 18 000 bridges in Norway through a self-developed system called Brutus. Brutus contains information regarding the structures, load capacities of the bridges, performed inspections, the current state of the bridges, planned measures and more.

In the following an overview of the inspections and maintenance that have been performed on The Hulvågen Bridge is given. Furthermore an overview of the damages to the NIB beams and the bridge deck will be provided. How the observed damages may affect the capacity of the bridge will be discussed further in Chapter 11. The damages that are registered in Brutus to the transversal supports and abutments are not given here, but can be found in the master's thesis by Opedal (2016).

4.2.1 Inspections and maintenance

The Hulvågen Bridge has an expected remaining service life of 70 years, meaning the bridge is expected to last until year 2087. Inspections have been performed several times after the bridge has been taken into use. This includes major inspections in 2009 and 2015, a special purpose inspection in 1998 and a simple inspection in 2000.

The aim of a major inspection is to perform a control of the state of all bridge elements over water and suggest a plan for possible needs for service or maintenance actions (Statens Vegvesen, 2000). Special purpose inspections are performed when there is a need to further map out damages or causes of damages that have

been discovered at previous inspections. The aim of a simple inspection is to control whether serious damage has originated which over short time can affect the bridge's structural capacity, traffic safety, future service or maintenance or environment/aesthetics.

Maintenance has been performed on the Hulvågen Bridge at five occasions. As will be elaborated shortly, the underside of the NIB beams and the bridge deck were covered in 1994 in order to protect the structure from sea spray. In addition, flushing and washing has been performed in 1999, the NIB beams and the underside of the bridge deck was treated with silane/siloxane-impregnation in 2000, unknown maintenance was performed in 2004 and in 2006 injuries in the cover underneath the bridge beams and deck are reported to have been repaired.

The NIB beams and underside of the bridge deck were originally exposed to the environment on the underside of the bridge, until it was decided that further protection against deterioration was needed. Drawings made by the NPRA in April 1994 shows how plywood boards are placed underneath the beams, covering the entire superstructure of the bridge in order to protect from sea spray. Inspection lids were included near the abutments in order to make it possible to supervise the progress of deterioration in the bridge, but the largest parts of the NIB beams are no longer easily accessible.

4.2.2 Damages on the NIB beams

Registration of current state of bridges in Brutus is done in accordance with Manual V441 (Statens Vegvesen, 2000), "Inspection manual for bridges". The manual provides guidelines regarding most aspects of inspection. Different types of damages or defects are systematised in a set of categories and subcategories. Furthermore an evaluation of the damage is performed through the use of degrees and consequences. Damage degrees vary from 1 (small damage or defect, no actions necessary) to 4 (critical damage, action necessary immediately or within half a year). Damage consequences concerns what kind of consequence a damage or defect can have for the bridge or the environment. The following categories are in use:

- B: Damage/defect that threatens the load bearing capacity
- T: Damage/defect that threatens the traffic safety
- V: Damage/defect that may increase cost of maintenance
- M: Damage/defect that may affect ambient environment / aesthetics

Damage degrees and damage consequences are used together in order to evaluate the damage or defect. The causes of the damage or defects are also systematised through the use of categories and subcategories.

In the following an overview of the damages and defects that have been registered in Brutus on the NIB-beams in the Hulvågen bridge is given. In Brutus the NIB-beams are registered with damages in three of nine spans. The spans are numbered in accordance with Figure 4.1.

Beam axes 2 to 3

The beam in span 2 - 3 is reported to have small diagonal cracks near the pillar in the second axis, discovered during a major inspection in 2015. The extent of damage is evaluated to a degree 2V. In V441 this degree of damage is described as a medium damage which can develop in such a way that maintenance can become more comprehensive, complicated and expensive if not attended to for more than 4 to 10 years. It is stated that the damage should be repaired within this time range.

The cause of the damage is not described in Brutus. In addition, images of the damage are not provided, making it harder to make assumptions regarding possible causes. Diagonal cracks near the pillar might indicate cracking due to shear forces, because there will be large shear forces acting in this area and because cracks due to shear generally will be inclined. Further inquiries must be made in order to establish a cause with more certainty.

Beam axes 4 to 5

In Brutus there is a report from the same inspection regarding efflorescence due to lime. The damage is characterized as 1V, which according to V441 means a small damage that is assumed not to affect cost of maintenance, and which will not be repaired. On the excursion to the Atlantic Ocean Road from 9th to 10th of May 2017 samples were taken of similar, more extensive efflorescence from the bridge deck, for further examination. The results of this will be presented in Section 11.2.



Figure 4.4: Efflorescence on the NIB-beam. Picture taken slanted upwards from the inspection hatch

Beam axes 7 to 8

From the inspection in 2015 there are also reports regarding efflorescence due to lime on the main beams between axes 7 and 8. The efflorescence is visible through the inspection hatch, and an image from the 1998 inspection is given in Figure 4.4.

The damage is given a characterization 2V, and no information regarding repair is given.

4.2.3 Damages on the bridge deck

There are reports regarding damaged plates in the lower edge of the bridge deck between axes 7 and 8, registered in the special purpose inspection done in 1998. This damage is evaluated to a degree of 3V, which V441 describes as a large damage that can make maintenance more comprehensive, complicated and expensive if not attended to for more than 1 to 3 years. In Brutus the damage is registered to be due to sea current, and as shall be elaborated in Section 11.2 it is considered likely that the damages are caused by leakage of sea water through the bridge deck. Similar damages caused by sea current are registered in the underside of the bridge deck between axes 8 and 9 and axes 9 and 10, all with a consequence of 3V. Though not explicitly given in Brutus, it can be assumed that the damages refer to efflorescence due to lime, similar to what is registered in the beams between axes 7 and 8. Figure 4.5 shows the efflorescence in the bridge deck, taken from the inspection hatch.



Figure 4.5: Efflorescence in the underside of the bridge deck.
Picture taken vertically upwards from the inspection hatch

The inspection in 1998 also revealed reinforcement corrosion due to chloride attack on the underside of the bridge deck. The damage is evaluated to a degree of 3V. Despite the fact that V441 states that damages of classification 3V should be attended to within 1 to 3 years, no signs of repair were visible when inspecting the bridge on the excursion to the Atlantic Ocean Road in May 2017.

Chapter 5

Basis for design

This chapter provides information regarding material and cross sectional properties that constitute the basis for the analyses that will be performed on the composite beam in the bridge. Properties regarding concrete quality for both the NIB beams and the bridge deck will be established. Furthermore amount, placing and steel quality for both the regular reinforcement and the prestressing reinforcement will be provided, in addition to further information that is relevant for the analyses that will be performed in this thesis. This chapter also provides an overview of certain simplifications and assumptions that the analyses will be based on.

5.1 Materials and cross sectional properties

Information regarding the materials and cross sectional properties of the structural components in The Hulvågen Bridge is taken from the drawings given in Appendix A. All analyses in this thesis will focus on the beams in the bridge superstructure. Because the NIB beams work together with the bridge deck as one composite cross section after the bridge deck is cast, the properties of the bridge deck is also relevant. Hence, the materials and cross sectional properties of the NIB beams and the bridge deck will be presented here. The remaining structural components of the bridge will not be looked into.

The original design of the bridge was carried out in accordance with the standard at the given time, NS 3473:1977. The material properties and characteristics from this standard is therefore used as a basis. When material properties in NS 3473 conflict with properties given in R412 (Statens Vegvesen, 2003), R412 is used. This is because R412 is published more recently and provides information regarding how calculations on existing bridges should be performed, and should therefore be more conservative than NS 3473. Properties that are introduced in calculations according to EC2 will be taken from EC2 for corresponding concrete quality in order for the calculations according to EC2 to be consistent.

5.1.1 Concrete

NIB beams

The concrete quality used in the NIB beams is given as C55(65) in the production drawings by Vestlandske Spennbetong AS. Presentation of a concrete quality on the form "C55" is an old Norwegian notation for concrete quality, and the number refers to the concrete's characteristic cube strength $f_{ck,cube}$ (Lenschow, 1979). With the introduction of the eurocodes the international CEN notation on the form "C45/55" replaced the former notation. By now characteristic cylinder strength f_{ck} had been taken into use, representing the first number in the notation for the concrete quality. The second number represents the characteristic cube strength. In Norway the notation B45 has become common for a C45/55 concrete, denoting only the characteristic cylinder strength.

The notation used for the NIB beams, C55(65), is not on standardized form, and despite consulting with professionals in the academic environment a dependable explanation of the notation has not been given. Characteristic cylinder strength had not yet been introduced as a way of classifying concrete quality, so the number in parenthesis does likely not represent the characteristic cylinder strength. The notation might indicate that a concrete quality of $f_{ck,cube} = 55$ MPa is required in this prestressed beam type, while $f_{ck,cube} = 65$ MPa is what is used in this production. The NIB manual (Statens Vegvesen, 1983) states a required concrete quality of C55 for this type of NIB beams. It has been decided to use the conservative concrete quality of C55 (with $f_{ck,cube} = 55$ MPa) for the analyses in this thesis.

Section 4.3.2 of NS 3473 defines the design concrete compressive strength f_c and the design shear strength f_v as

$$f_c = \frac{f_{cn}}{\gamma_m},$$

$$f_v = \frac{f_{vn}}{\gamma_m},$$

f_{cn} and f_{vn} are given in Table 4.4.1 of NS 3473. γ_m is the material coefficient for projects executed under extended or normal control, given in Section 4.3.3 of NS 3473.

Different expression for the elasticity modulus of concrete are given in the various editions of NS 3473 and EC2. Common for all is that the elasticity depends in some way on the compressive strength of concrete. In the second edition of NS 3473, which was in use when the bridge was designed, the elasticity modulus was calculated using the formula given in Section 3.3.1,

$$E_{ck} = 5000 \times \sqrt{f_{ck}},$$

Here f_{ck} denotes the characteristic concrete cube strength, i.e. $f_{ck} = f_{ck,cube} = 55$ MPa. The third edition of NS 3473 gives the elasticity modulus in Section 9.2.1 as

$$E_{ck} = k_E \times f_{cck}^{0.3},$$

where $k_E = 9500$ and where $f_{cck} = 45$ MPa is the cylinder strength as defined in Table 5 in NS 3473. The Eurocode 2 defines the secant modulus of elasticity in Table 3.1 as

$$E_{cm} = 22((f_{cm})/10)^{0.3}.$$

Here E_{cm} is found in GPa while f_{cm} is the mean concrete compressive strength given in MPa.

The relation between the characteristic concrete compressive strength and the mean concrete compressive strength is given in EC2 Section 3.1.2 as $f_{cm} = f_{ck} + 8$ MPa, where f_{ck} here denotes the characteristic cylinder strength, i.e. $f_{ck} = f_{cck}$. Using this relation for the first two equations for the elasticity modulus results in the secant moduli of elasticity given in Table 5.1, rounded down to the closest thousand. It should be noted that using this relation on the first equation will give some error because this formula uses the cube strength instead of the cylinder strength.

Table 5.1: Secant modulus of elasticity

Standard	Secant modulus of elasticity E_{cm} , [MPa]
NS 3473 2nd edition	39 000
NS 3473 3rd edition	31 000
EC2	36 000

The Eurocode 2 gives a relation between elasticity and compressive strength which is assumed to be valid for all the countries using the eurocode in Europe. It has been found that the given relation is not in conformity with the most commonly used Norwegian concretes. Norwegian aggregates generally give a lower elasticity modulus for the concrete than what is given in EC2. As is seen in Table 5.1 the Norwegian standard in use when the bridge was designed leads to a modulus which is even higher than the one derived using the formulas in EC2. The third edition, on the other hand, gives a much lower value. It is recognized that this relation corresponds better with Norwegian conditions.

In this thesis the elasticity modulus will only be used when calculating secondary moments from prestressing. The choice of modulus will not have large effect on this result, as the modulus is most important regarding calculations of deformations. Despite the fact that the modulus given in the third edition of NS 3473 is known to correspond better with Norwegian conditions, it is for this thesis chosen to perform calculations with the median modulus of the three given in Table 5.1, i.e. the modulus given in EC2. This choice has partly been made because the modulus from EC2 corresponds better with the modulus from the second edition of NS 3473, which is assumed to have been used in the original calculations of the

bridge. Using this may therefore provide better correspondence with the original calculations when capacities are established.

A summary of relevant material properties is given in Table 5.2.

Table 5.2: Concrete properties of NIB beams in accordance with NS 3473:1977 (or R412)

Material properties		Value
Concrete quality		C55 (B45 in EC2)
Characteristic cube strength	$f_{ck,cube}$	55 MPa
Material coefficient for projects executed under extended or normal control	γ_m	1.25
Characteristic compressive strength	f_{cn}	28 MPa
Characteristic shear strength	f_{vn}	0.7 MPa
Design compressive strength	f_c	$f_{cn}/\gamma_m = 22.4$ MPa
Design shear strength	f_v	$f_{vn}/\gamma_m = 0.56$ MPa
Density of reinforced concrete (R412)	ρ_c	25 kN/m ³
Secant modulus of elasticity (EC2)	E_{cm}	36 000 MPa
Properties used for EC2 calculations		
Mean cylinder compressive strength	f_{cm}	53 MPa
Mean axial tensile strength	f_{ctm}	3.8 MPa
Partial safety factor for concrete	γ_c	1.5
Long term loading coefficient	α_{cc}	0.85
Design compressive strength	f_{cd}	$\alpha_{cc}f_{ck}/\gamma_c = 25.5$ MPa
Characteristic axial tensile strength	$f_{ctk,0,0.05}$	2.7 MPa
Long term loading coefficient	α_{ct}	0.85
Design axial tensile strength	f_{ctd}	$\alpha_{ct}f_{ctk,0,0.05}/\gamma_c = 1.53$ MPa

Bridge deck

After the bridge deck is cast the beams will work in union with the deck as a composite T-sectioned beam. The material and cross sectional properties of the bridge deck may therefore be relevant for capacity calculations which will be performed in Chapter 9.

Little information is provided about the bridge deck in the drawings presented in Section 4.1.2. From the drawings of the complete bridge provided by the NPRA it is given that the thickness of the bridge deck is 250 mm. The concrete quality and reinforcement solution has on the other hand not been provided. For this thesis it has been decided to use values recommended in the NIB manual, which was valid when the bridge was designed. In Section 080.4 of the manual it is stated that the bridge deck shall have a concrete quality of C35 in accordance with NS 3474.

Shear failure usually occurs in the beam web, as shall be elaborated in Section 8.2. The shear capacity will therefore be decided by the material properties at the web, which is a part of the NIB beam. The material properties for the bridge deck

will only be used when controlling the interface between the two members that constitute the composite beam, as will be introduced in Section 8.6 and calculated in Section 9.5. The material properties for the bridge deck that are relevant for these calculations will be provided in these sections. More information regarding properties for concrete of quality C35 can be found using NS 3473 and R412.

5.1.2 Regular reinforcement

NIB beams

The NIB beam's cross section and reinforcement are given in Figure 5.1, gathered from the production drawings by Vestlandske Spennbetong AS. Parts of the in-

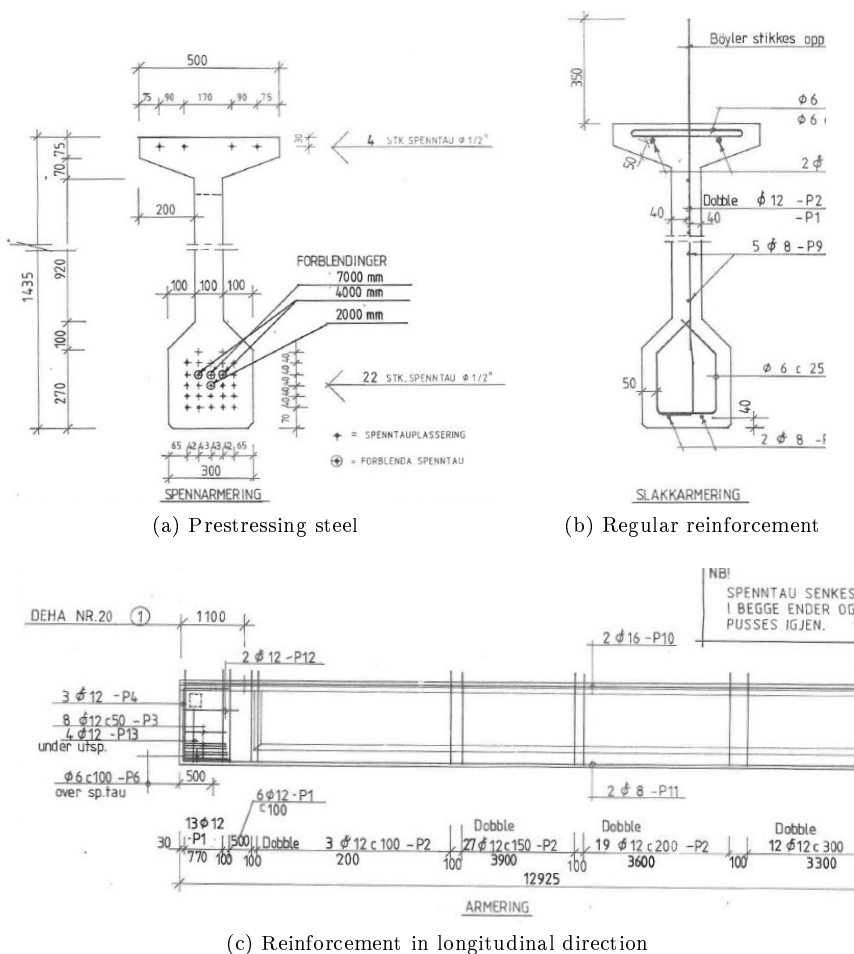


Figure 5.1: Reinforcement in NIB 500/1435 beams

formation regarding diameter and central distance of the regular reinforcement is missing in the figures, but all necessary information can be found from the drawings and bar schedule in Appendix A.

Regular reinforcement is placed with a cover of 50 mm (minimum 40 mm). Three steel qualities are used: St. 37, K400TS and K500TS. St. 37 is a mild steel bar. This is not ribbed, so it has a smooth surface. 37 is the material's guaranteed ultimate strength given in kp/mm^2 , which corresponds to an ultimate strength of $f_u = 370 \text{ N/mm}^2$. The yield strength of the St. 37 is $f_y = 235 \text{ N/mm}^2$ (Statens Vegvesen, 2003).

K400TS and K500TS are deformed steel bars. The K stands for ribs (Norwegian "kammer"), and the bars are ribbed in order to bind the rebars mechanically to the concrete and secure higher bonding between the concrete and the reinforcement, so that the two materials act as a unity. The S stands for weldable, while the T stands for Tempcore. Tempcore is a special process where the steel after hot-rolling is quenched and then self-tempered. The numbers 400 and 500 indicate the yield strength (in N/mm^2) of the material. Due to metallurgical properties the yield strength may be reduced for larger diameters in bars that are not Tempcore. Due to this it is common to use two yield strengths for these steel qualities, as can be seen in the overview in Table 4.2-3 in the Appendix of R412 Statens Vegvesen (2003). Because the rebars in the beam are Tempcore this will not be relevant here.

The drawings in Figure 5.1 show both general reinforcement throughout the beam, and additional reinforcement that is placed in the beam ends. The additional reinforcement in the beam ends is due to local force concentration and anchorage of the tensile forces caused by the prestressing reinforcement. The latter will be elaborated in Section 5.1.3. For shear capacity calculations in this thesis only the stirrups and longitudinal bars that are placed throughout the length of the beams are included. Anchorage reinforcement is only included in the calculations when the anchorage of the prestressing reinforcement is considered.

Regular longitudinal reinforcement over the length of the beam includes the bars denoted P9, P10 and P11 in Figure 5.1b. P9 consists of five K400Ts bars with diameter 8 mm, placed along the height of the web. Exact placement of these bars is not given, and it has been decided to neglect these bars in all analyses in this thesis in order to simplify the calculations. Because these bars are mounting bars of low diameter it can be assumed that they will not contribute noticeably to the capacity. P10 makes up two K500Ts bars of diameter 16 mm underneath the stirrups in the upper flange. P11 makes up two similar bars of diameter 8 mm placed underneath the stirrups in the lower flange, with steel quality K400Ts. P10 and P11 are also included as mounting reinforcement, and will not have a large contribution to the total longitudinal reinforcement when compared with the total area of the prestressing strands and the longitudinal reinforcement in the bridge deck. Nevertheless it is decided to include them in the capacity calculations.

Over the length of the beam three sets of stirrups denoted P2, P5 and P7 are placed. P2 is given in Figure 5.1b, and consists of double stirrups with diameter 12 mm of steel type K400Ts. The stirrups reach from the bottom flange and up

over the top of the NIB beams, so that they lie exposed until the bridge deck is cast above. The central distance varies over the length of the beam as shown in Figure 5.1c. P2 is the only stirrup placed vertically through the beam's web, and this will therefore amount to the total shear reinforcement in the beams. As will be elaborated in Section 8.6, P2 will also function as reinforcement of the interface between the NIB beam and the bridge deck, an area which must be controlled in particular with regards to shear capacity. P5 is the stirrup in the upper flange of the beam, with a diameter of 6 mm. The central distance is missing in the figures, but based on the total amount given in the associated bar schedule a central distance of 200 mm can be assumed. P7 is the stirrup in the lower flange, of diameter 6 mm and with a central distance of 250 mm. Both P5 and P7 are of steel quality St. 37.

Bridge deck

As mentioned little information is given regarding the bridge deck. Reinforcement layout is for this thesis assumed to be similar to the layout presented in Section 081.6 in the NIB manual. The NIB manual divides between sections with one-sided slope and sections with two-sided slope in the transverse direction. For bars in the bridge's longitudinal direction the same reinforcement layout is recommended for both situations. The manual recommends placing reinforcement bars with 12 mm diameter and central distance 150 mm in the upper edge, and bars with 16 mm diameter and central distance 250 mm in the lower edge. Section 080.4 of the NIB manual states that a steel quality Ks 40 is to be used for the 12 mm bars, and Ks 50 is to be used for the 16 mm bars. R412 and Lenschow (1979) show that Ks 40 has a yield strength of $f_y = 400$ MPa for diameter 8 - 20 mm, and Ks 50 has a yield strength of $f_y = 500$ MPa for diameter 8 - 16 mm.

Reinforcement in the transverse direction is also necessary in the deck. The manual recommends the same diameter in the upper and lower edge as for the longitudinal direction. The transverse bars are placed on the outer sides of the longitudinal bars. Besides affecting the cover for the longitudinal reinforcement and hence the centre of gravity of the reinforcement, the transversal reinforcement is not included in any way in the calculations. For the capacity calculations in this thesis, the bridge deck is assumed not to have shear reinforcement. This assumption is based on the fact that no information regarding shear reinforcement is given in the NIB manual, in addition to the fact that NS 3473:1977 does not require minimum shear reinforcement in plates.

In order to find the centre of gravity for the reinforcement in the bridge deck, the cover from the surface to the bars must be known. This decision has been made based on the development of covers in the NIB beams that are given in the NIB manuals. As described in Section 4.1.3 the 1983-edition of the NIB manual recommends a general cover of 25 mm for the NIB beams, while the 1989-edition recommends a cover of 40 mm.

As can be seen from the production drawings produced by Vestlandske Spennbetong AS in Appendix A the dimensions of the NIB beams in this bridge correspond better with the beam dimensions given in the 1989-edition of the NIB manual than in 1983-edition, despite the fact that the bridge beam was designed in 1987, i.e.

before the second edition was published. The production drawings also states a minimum reinforcement cover of 40 mm, corresponding with the 1989-edition of the NIB manual. This indicates that it might have been customary to use a larger cover than what is given in the 1983-edition in some time before the 1989-edition was published. Due to this it has been decided to assume a cover corresponding to the value recommended in the 1989-edition of the NIB manual for the reinforcement in the bridge deck, i.e. 40 mm. This leads to a reinforcement layout in the bridge deck as given in Figure 5.2, where a section of the bridge deck in the transversal direction is viewed.

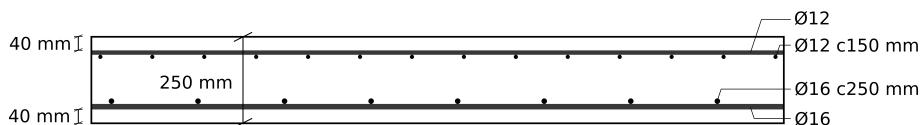


Figure 5.2: Reinforcement layout in the bridge deck

A summary of the properties of the regular steel used in the NIB beams and bridge deck is given in Table 5.3. The design strength of the reinforcement is given in Section 4.3.2 of NS 3473 as

$$f_s = \frac{f_y}{\gamma_m},$$

with f_y as the steel's yield strength and γ_m being the material coefficient for projects executed under extended or normal control, given in Section 4.3.3 of NS 3473.

Table 5.3: Regular reinforcement steel properties in accordance with NS 3473:1977 (or R412)

Material properties		St. 37	K400TS, Ks 40	K500TS, Ks 50
Yield strength	f_y	230 MPa	400 MPa	500 MPa
Material coefficient	γ_m	1.25	1.25	1.25
Design strength	f_s	240 MPa	320 MPa	400 MPa
Elasticity modulus	E_s	210 000 MPa		

5.1.3 Prestressed reinforcement

Prestressing reinforcement is used in the prefabricated NIB beams. There are 26 prestressing strands with a diameter of 1/2 inch in each beam, and each strand has a given cross sectional area of $A_s = 100 \text{ mm}^2$. 22 of these strands are placed in the lower part of the cross section which will be in tension in the Ultimate Limit State, while four strands have been placed in the upper part of the cross section and will be in compression.

Prestressing strands in the parts of the cross section that will be in compression in the Ultimate Limit State will increase the compressive stresses in the concrete and therefore reduce the cross section's moment capacity. Despite this a few strands are often used in the compression zone, both in order to simplify mounting of stirrups and in order to give better control of other limit states (stresses in Serviceability Limit State, capacity of the cross section at transfer of prestressing forces, etc.) (Thorenfeldt, 1990).

In the production drawings of the NIB beams it is given that the prestressing strands are of type St. 170/190. This notation describes the same bar type as explained for the St. 37 steel in Section 5.1.2. When St is followed by two numbers the first one represents the yield strength in kp/mm^2 , and the second represents the ultimate strength. This means that the strands have a yield strength of $f_y = 170 \text{ kp/mm}^2 = 1700 \text{ N/mm}^2$ and an ultimate strength of $190 \text{ kp/mm}^2 = 1900 \text{ N/mm}^2$ (Lenschow, 1979). The prestressing will cause axial compression in the concrete, and compressive axial stress is therefore defined as positive throughout this thesis. The strands in the lower edge are pre-tensioned to a force of 139 kN including anchor loss. The strands in the upper edge are pre-tensioned to a force of 131 kN. Furthermore it is given that the prescribed prestressing force is 134 kN in the lower edge and 126 kN in the upper edge.

Similar as with the notation regarding concrete quality it has been difficult to establish a dependable explanation for the notation of the prestressing, despite consulting with professionals in the academic environment. It is considered likely that the prescribed prestressing force is the force that is prescribed in manuals and therefore is the force that has been used in calculations and design, while the pre-tensioning force including anchor loss is the actual force that the beams were tensioned up to. As seen, the actual force is higher than what is prescribed, rendering a conservative solution in the Ultimate Limit State. In this thesis it is decided to base the analyses on the prescribed prestressing forces, because it is assumed that this is what has been used when designing the bridge in 1987. As mentioned this will be the conservative solution in the Ultimate Limit State. Furthermore it is evident that the beams have not failed at other limit states (such as at the transfer of the prestressing forces to the concrete), and hence it can be assumed that the beams are able to sustain the extra loading from the increased prestressing force without failing.

A summary of the properties for the prestressing steel is given in Table 5.4.

Special considerations near the end region

In pre-tensioned beams the force from the prestressed strands is transferred to the concrete by bond in the end regions of the beam. The length over which the effective prestress is developed in each strand is called the transmission zone. At the beam ends the force in the prestressing strands is zero. The force increases gradually over the transmission length and reaches its maximum value at the end of this zone.

The prestressing reinforcement causes transverse tensile stress in the concrete, and may cause cracking of the concrete. The stress is largest during the transfer of

Table 5.4: Prestressing steel properties

Material properties for St. 1700/1900		
Yield strength	f_y	1700 MPa
Ultimate strength	f_u	1900 MPa
Other properties		
Diameter	\emptyset	12.7 mm
Number of strands		26
Area per strand	$A_{p, \text{strand}}$	100 mm ²
Total area	$A_{p, \text{tot}}$	2600 mm ²
Prescribed prestressing force, lower and upper edge	$F_{p0, \text{lower}}$	134 kN
	$F_{p0, \text{upper}}$	126 kN

the prestress, and is negligible over the rest of the beam (Sengupta and Menon). As discussed in Section 3.4.3, the most effective measures in order to reduce cracking in the end region caused by this effect is to use larger sized vertical bars through the web in the end zone reinforcement and debond certain prestressing strands. For The Hulvågen Bridge it can be seen from Figure 5.1c that transverse reinforcement in the form of additional vertical stirrups (in addition to the reinforcement for shear) is provided at each end of the beam along the transmission zone. The stirrups denoted P1 are equally shaped as P2 mentioned in the previous section, where P2 denotes the general stirrups throughout the length of the beam while P1 is placed with a much lower central distance in the beam ends. As explained in the previous section these stirrups are 12 mm in diameter, and reach vertically from the bottom of the lower flange up to the bridge deck. Despite the fact that the bars are not larger sized in the end region, it can be assumed that the lower central distance will have a similar effect of reducing the strains occurring in the web area.

In addition to the additional stirrups in the end region, four of the prestressing strands in the lower part of the beam are coated near the beam ends in order to debond the strands. One strand is coated over 2000 mm at both ends of each beam, two are coated over 4000 mm while the fourth is coated over 7000 mm. This moves the transmission zone so that the transverse tensile stresses begin acting on the concrete when bond is re-established. In effect the tensile stresses are distributed over a larger area, hence reducing the total magnitude (Sengupta and Menon). The coating of the prestressing strands will cause a step by step increase of the prestressing load, either during the transmission length or after all the load has been transferred to the concrete. This effect, combined with the gradual increase due to transfer of prestressing by bond, will hence cause both a step by step and a linear reduction of the axial load in a certain region when approaching the beam ends.

Debonding of four of the 22 strands in the beam's lower edge causes 18 % debonding in the outermost 2000 mm of the beam ends. Oliva and Okumus (2011) state that for certain I-beams, 25-35 % debonding can reduce the web strains by approximately 50-70 %. It can therefore be assumed that the debonding performed here can have a large effect regarding the reduction of crack occurrence in the beam

ends.

It should be noted that the strands that are debonded in these NIB beams lie several rows of strands up from the lower edge in the lower part of the beam, see Figure 5.1a. This implies that the resultant eccentricity between the strands and the concrete centre of gravity will increase. As described in Section 3.4.3 Oliva and Okumus (2011) state that this may be disadvantageous regarding cracking of the lower flange, and that this has the potential of increasing the size of the Y cracks that may arise here.

As stated in Section 3.4.3 the strengthening of the beam web which is performed in both beam ends by increasing the web width to the width of the lower flange will contribute to reducing the risk of cracking due to transversal stresses in the beam ends.

5.2 Simplifications and assumptions

A main assumption that has been made in this thesis is assuming that continuous linear strains will occur in the composite beam consisting of the NIB beam and bridge deck. In reality the strains will be discontinuous between the two members, especially in early phases. Figure 5.3 illustrates the development of strains in the composite beam in a section near mid-span where tension occurs in the lower edge (Hermundsdal and Pétursson, 2015). The numbered list refer to the stages in the figure, with explanations of how the strains develop.

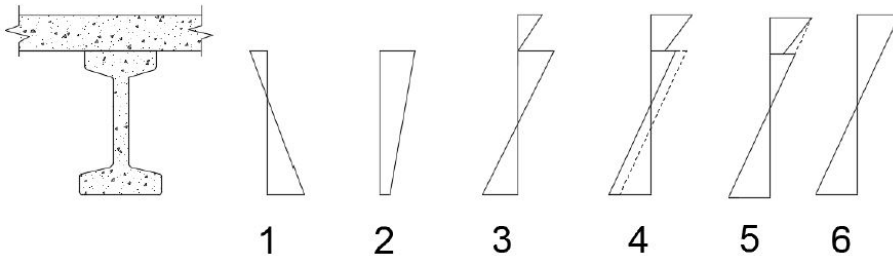


Figure 5.3: Development of strain in the composite beam with time (Hermundsdal and Pétursson, 2015)

1. At the transfer of prestressing of the NIB beam the prestressing strands in the lower edge will cause compression in the lower edge and tension in the upper edge of the beam
2. When the self weight of the beam is applied (usually at the transfer of prestressing) this will counteract the strains from prestressing in the span. If the beams are sufficiently prestressed this stage will result in compression over the the entire cross section.
3. The bridge deck is cast, and when it reaches sufficient strength the beam and bridge will work together. When the formwork is removed and self weight of

the bridge deck is applied, a moment will be applied to the composite beam causing tension in the lower edge and compression in the upper edge

4. With time strains will increase due to time-related effects such as creep in the concrete and relaxation of the prestressing steel.
5. After 100 years the strains in the composite beam will be approximately as illustrated.
6. For simplification of the calculations the strains can be assumed to be linear from the lower edge of the beam to the upper edge of the bridge deck.

Further assumptions that have been made in this thesis are:

- The horizontal curvature, as well as the slope of the bridge deck, has been neglected in all analyses in this thesis, both when establishing design load actions and calculating capacities.
- The fact that the bridge deck is cast with a different concrete quality than the NIB beam is neglected for the behaviour of the composite beam

Assumptions that are made during the modelling of the bridge, assumptions that the standards are based on, and other possible assumptions are presented when relevant.

Chapter 6

Loads and load combinations

This chapter will lay the basis for establishing the design loads that are acting on the composite beams in The Hulvågen Bridge. Which loads that are included in the analyses, time related load effects and load combinations that are used to establish the total design loads in the bridge are presented in this chapter. Chapter 7 will perform the actual analyses of establishing the critical design loads. The results from these two chapters will in Chapter 9 be used to get an insight into how utilized the composite beam is with regards to shear capacity. Finally, in Chapter 11, possible effects that corrosion damage may have on the utilization of the beams will be studied.

Capacity control is performed in the Ultimate Limit State. In this thesis the capacity control will be performed after 100 years. As shall be seen in this chapter, the time of consideration will for the calculations in this thesis only be relevant for the redistribution of self loads for the continuous system, as well as for the secondary moment occurring due to prestressing after the system has become continuous. According to N400 (Statens Vegvesen, 2015) the capacity of the bridge should also be controlled when the bridge is opened. This has not been performed in this thesis.

For the establishment of design loads working on the structure it has been decided to neglect the altered cross section in the beam ends, as well as the gradual transmission of the prestressing loads and the coating of four of the prestressing strands in the beam ends. This choice is made in order to simplify the loading situation. The altered cross section in the beam ends will primarily affect the stiffness and hence the deformation of the beam, while the effect it will have on the load distribution can be considered negligible. Furthermore the gradual transmission of prestressing will lead to a gradual increase of the primary moment in the beam ends. The coating of certain prestressing strands will increase this region of nonconstant primary moment somewhat more. Both these effects will furthermore cause slight variation in the shear distribution. It is assumed here that these effects also will have negligible effect on the total loading and the distribution of loads, and are therefore neglected for the establishment of design loads. For control of shear capacity however, the three effect will be included.

As mentioned in Section 4.1 The Hulvågen Bridge is conservatively assumed to be a continuous bridge, which will be the basis for this chapter. A control of the bridge where a multi-span simply supported bridge system is assumed will be performed in Chapter 7. As shall be seen most of the theory provided in this chapter will be directly applicable for the control.

6.1 Classification of actions

Actions are classified based on their variation over time between permanent exposure, variable exposure and accidental exposure (Statens Vegvesen, 2015). Here the loads are divided into the following categories, with common examples of loads included in each category:

- Permanent action: Self weight, earth pressure, water pressure, etc.
- Variable action: Traffic loads, nature loads, impact and mooring loads from ferries, temperature loads, etc.
- Deformation load: Applied deformations, prestressing, shrinkage, creep, relaxation, etc.
- Accidental action: impact, falling objects, explosions, fire, avalanches, etc.

6.2 Permanent action

Permanent loads are loads that remain constant during the considered time period. This includes the self weight of the structure and weight of permanent ballast or equipment that will not be removed during the considered time period. Earth pressure and water pressure are other permanent loads. In this thesis self weight of the structure is the only permanent action that is considered.

6.2.1 Self weight

As Figure 6.1 shows The Hulvågen bridge consists of a deck of width 7.3 meters, and it has with a constant thickness of 250 mm. Self weight of reinforced concrete can be assumed as 25 kN/m^3 (Statens Vegvesen, 2003), giving a total self weight from the deck of $25 \text{ kN/m}^3 \times 7.3 \text{ m} \times 0.250 \text{ m} = 45.6 \text{ kN/m}$.

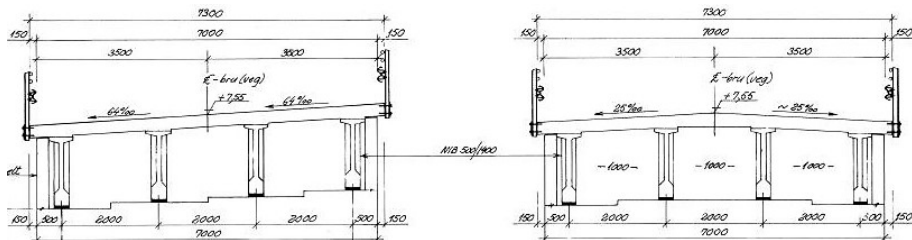


Figure 6.1: Section showing beams and deck in The Hulvågen Bridge

The four prestressed NIB beams are shaped as presented in Figure 5.1 and each has a cross sectional area of $A = 251\,500\text{ mm}^2 = 0.2515\text{ m}^2$. With a self weight of reinforced concrete of 25 kN/m^3 the total self weight for each NIB beam is $25\text{ kN/m}^3 \times 0.2515\text{ m}^2 = 6.3\text{ kN/m}$. With four parallel beams in the longitudinal direction the contribution to the total self weight is $4 \times 6.3\text{ kN/m} = 25.2\text{ kN/m}$. In these calculations the change in concrete cross section near the beam ends have been neglected, in accordance with what is stated in the introduction to this chapter.

In general the load caused by the pavement layer on top of the bridge deck has to be documented, but for smaller bridges documentation is not necessary if the load is set to a minimum of 3 kN/m^2 (Statens Vegvesen, 2003). N400 gives a minimum pavement load of 3.5 kN/m^2 for bridges with largest spans of less than 50 meters. Despite the fact that the carriageway width of the bridge is 7 meters it is assumed that the whole pavement load (including the asphalt wearing course) is placed over the entire width of the bridge (7.3 meters) in order to protect the structure against wear from the environment. With a pavement load of 3.5 kN/m^2 the total load is $3.5\text{ kN/m}^2 \times 7.3\text{ m} = 25.6\text{ kN/m}$.

On each side of the bridge there is a guard rail. The self weight of each guard rail is chosen to 0.5 kN/m based on R412 (Statens Vegvesen, 2003), giving a total load of 1.0 kN/m .

Table 6.1 gives a summary of the self weights imposed on the structure.

Table 6.1: Evenly distributed self weight on NIB-beams

Element	Load [kN/m]
Deck	45.6
NIB beams	25.2
Pavement	25.6
Guard rail	1.0
Total	97.4

6.3 Variable action

Variable loads can be traffic loads, nature loads, impact and mooring loads from ferries, or other loads that vary with time. Traffic loads are assumed to be the most important variable load for this bridge. Other loads that can be of importance are nature loads like wind, waves, change in tide, ice, temperature and earthquakes. These loads are neglected for this thesis in order to simplify the loading situation. Variation of temperature in the surroundings may result in large loads on a bridge and is therefore often important to consider, but because they have relatively small effect on the shear forces in the system it has been decided to neglect also this source of action in this thesis. Loads from ferries are not relevant for this bridge.

6.3.1 Traffic loads

Classification of existing bridges is to be done with respect to traffic loads given in R412. Traffic loads include loads in vertical and horizontal direction on carriageway, hard shoulder, sidewalk and cycle lanes, and they originate due to pedestrians and light and heavy vehicles that can load the structure during the bridge's service life.

Traffic loads are divided into three groups: regular transports, special transports and non-returnable transports. Regular transports include all loads that travel on the roads without dispensation, while for special transport and non-returnable transport special dispensation is necessary for the vehicles to be allowed to utilize the carriageway. Special transport and non-returnable transport will not be treated in this thesis, but in reality these criteria should also be considered in classification of the bridge.

Regular transport is specified either as use classes or axle loads/total loads. Use classes gives a description of the weights that roads can permit. Here weights are specified as the largest accepted axle loads, loads from an axle combinations and total weights depending on the distance between the axles. Use of axle loads/total loads is most relevant for bridges that can't be classified based on use classes, and is most commonly necessary for bridges with a lower load capacity. For this classification the largest total axle load and the largest total weight that can be allowed to pass the bridge is decided. For The Hulvågen Bridge the system of use classes can be used.

Use classes

Bridges are to be given a use class that reflects the use load that can traffic the bridge without restrictions. The four use classes are:

- Use class 10 (Bk10)
- Use class T8 (BkT8)
- Use class 8 (Bk8)
- Use class 6 (Bk6)

All bridges designed after 1969 are designed to sustain use class Bk10, and further classification is therefore not necessary. This applies for The Hulvågen Bridge, which was designed in 1987. Furthermore, it is given explicitly in the drawing of the complete bridge given in Appendix A that the bridge is designed for use class Bk10.

Each use class has restrictions regarding wheel load, axle load, tandem axle load, tri-axle load, light and heavy vehicle load. Only one of the given loads are to be chosen. In practise design loads for short bridges and secondary structures will be decided by the axle, tandem axle or tri-axle load, while the main structure for longer bridges will be decided by the light or heavy vehicle load (Statens Vegvesen, 2003). The latter of the two will be relevant for The Hulvågen Bridge. With the bridge's location along the Atlantic Ocean Road, heavy vehicle traffic is not very likely. However it may occur, and heavy vehicle load is therefore assumed to be the design load situation for this bridge.

Longitudinal direction

In the longitudinal direction heavy vehicle loads are represented as a distributed load with an extent of 16 meters with a total weight of 500 kN for Bk10. In addition an axle load of magnitude 40 kN for Bk10 shall be positioned in the least favourable position within the range of the distributed load. In front and/or behind the distributed total load a distributed load of 6 kN/m representing lighter traffic can be included if this is unfavourable.

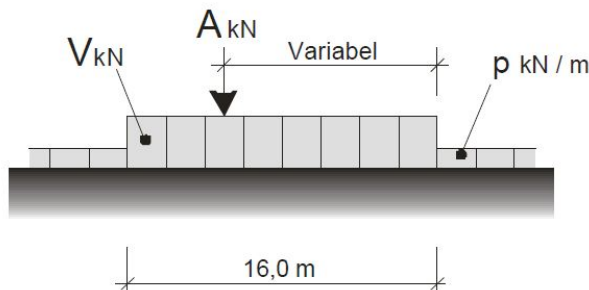


Figure 6.2: Load configuration for heavy vehicles (Statens Vegvesen, 2003)

The load configuration is represented in Figure 6.2 where V is the total weight of 500 kN, A is the axle load of 40 kN and p is the distributed load of 6 kN/m. The positioning of the load components in order to achieve the most unfavourable load effects in a critical section of the Hulvågen Bridge will be studied further in Section 7.1.3.

Transversal direction

In the transversal direction the vertical loads on the bridge are to be placed in the least favourable position within the available carriageway width. The carriageway width is given as the smallest of the horizontal widths between two curbstones, a curbstone and high vertical edge or rail guard, or between two high vertical edges or rail guards. In this bridge there are no curbstones or high vertical edges, and the carriageway is therefore given as the distance between the rail guards. This renders a carriageway width of 7.0 meters as seen in the bridge drawings given in Figure 6.1.

R412 states that heavy vehicles demands a lane width of 3.0 meters. Hence, there will be room for two heavy vehicles next to each other on The Hulvågen Bridge. With a carriageway width of 7.0 meters the vehicles can either be placed towards the outer ends of the carriageway with an extra meter in the middle, or towards the middle of the road with up to 0.5 meters extra on each side. The least favourable position will be studied further in Section 7.2.3. The axle load is divided into two for each vehicle, placed with a two metre space between them in the middle of each vehicle load.

In addition to the vertical loads that have been given above traffic loads induce horizontal loads on the structure that must be designed for. Horizontal loads include braking loads, centrifugal loads and by-weight loads, for instance induced by lopsided braking or transversal impact. The effect of horizontal loads have been neglected in this thesis.

6.4 Deformation loads

There are several sources that can lead to deformation loads in a structure. For prestressed structures the prestressing of reinforcement, both pre-tensioning and post-tensioning, is an important source. Characteristics of the construction material, such as shrinkage and creep of concrete and relaxation of the reinforcement, are important for all types of concrete bridges. Temperature deformations due to expansion of structural members are also a common source of deformations loads. Other factors that can deformation loads are settling of the structure, or factors that come as a result of the production or design process. Deformation loads are often time dependent, and the characteristic load is defined as the largest expected value within the considered time period.

6.4.1 Prestressing loads

According to N400 the load effect from prestressing must include both loads that works directly on the prestressed structural member in addition to secondary load effects that occur in statically indeterminate structures. In concrete element bridges secondary moments occur due to the continuity of the bridge which is established after the bridge deck is cast. This will be looked further into in Section 6.6.2. In this section the prestressing force in the beam will be established, as well as expressions for characteristic axial load and primary moment due to the axial load.

Loss of prestress

When regarding moments, which normally is the load effect that has to be designed for in a beam, load effects from prestressing normally counteracts the load effects from self weight of a beam, making it a favourable load in the Ultimate Limit State. Performing calculations with the minimum value of the prestressing load will therefore often be the most conservative. Due to various reasons the measured force in the jack at prestressing will always be reduced slightly, where the loss of prestress occurs both momentarily and over time.

There are three main forms of loss of prestress:

- Loss of strain difference between prestressing steel and concrete. This occurs when there is no bond between the steel and concrete, and is therefore mainly relevant for post-tensioned concrete or for unbonded pre-tensioned concrete. Loss of strain difference can be due to anchor loss caused by sliding of the prestressing steel in the active anchor when the jack is removed, friction loss

due to frictional forces between steel and concrete and temperature loss due to hydration heat.

- Stress change due to short time loading. In pre-tensioned concrete this loss is due to cutting of the prestressing steel in the casting beds, while in post-tensioned concrete this loss can occur when several units of prestressing steel are tensed successively, for instance when building cantilever bridges.
- Time related losses due to creep and shrinkage in the concrete and relaxation of the prestressing steel. These types of losses occur both in pre-tensioned and post-tensioned concrete.

Because The Hulvågen Bridge is a bridge with bonded pre-tensioned reinforcement the prestressing losses that are relevant here are anchor loss, stress change due to cutting of the prestressing steel and time related losses. Chapter 5 and 6 in Part 2 of Sørensen (2013) shows how these losses generally are calculated. However, when performing calculations regarding shear of a prestressed beam it is considered sufficient to instead include an approximate loss factor $\alpha' = 0.85$. This simplification is made because large shear forces normally will occur at beam ends where regular beam theory will not be valid. There are a number of reasons for why the capacity will change in the beam ends (Thorenfeldt, 1990), some of which are the following,

- Cross sectional change of the concrete where the web width is increased to the width of the lower flange in a certain length in the beam ends
- The prestressing force is reduced from maximum to zero over a certain transmission length in each beam end
- Certain prestressing strands are coated
- The design moment will change from tension in the upper end to tension in the lower edge in some distance from the continuous support (as the right case in Figure 4.2 illustrates), which cause a number of factors which influence the shear capacity to vary
- The shear reinforcement amount near the beam end varies
- Possible reinforcement corrosion and spalling of the concrete

All these factors will cause uncertainty regarding the capacity calculations in the beam ends. Careful calculations of the loss will therefore be superfluous, and instead the simplified value α' is chosen. The approximate factor is larger than for equivalent regularly reinforced concrete. This is justified by the fact that in prestressed concrete structures extra loss can occur due to relaxation of the prestressing steel and particularly large creep due to early loading, and because the entire axial load is a long-time load (Thorenfeldt, 1990).

Creep

When calculating secondary moments occurring in the beam, effective stiffness at different points of time reduced due to creep will be used. For this reason an introduction into calculations of creep is given here.

Concrete that is exposed to compressive forces over time will continue to deform beyond the instantaneous deformation that occurs when the load is applied. This additional deformation is called creep (Sørensen, 2013). For prestressed concrete the additional deformation in the beam causes straining of the prestressing steel, which causes reduction of the prestressing forces.

Creep calculations have been performed in various ways throughout the various editions of the Norwegian Standard (Norske Sivilingeniøres Forening, 1973) and the EC2. For this thesis it has been decided to use the most updated formulas in order to minimize the sources of error in these calculations. Creep calculations are therefore performed in accordance with EC2.

For loads with a duration that cause creep, calculations may be performed using an effective modulus of elasticity for concrete according to the following expression,

$$EI_{\text{beam},t,t_0} = \frac{E_{cm} I_z}{1 + \phi(t, t_0)},$$

given in Section 7.4.3(5) in EC2. Here E_{cm} is the secant modulus of elasticity of concrete, I_z is the second moment of area of the concrete section around the horizontal axis, and $\phi(t, t_0)$ is the creep coefficient. t is the age of concrete in days at the considered point in time, and t_0 is the age of concrete in days at loading.

The creep coefficient is calculated in Appendix B in EC2 as

$$\phi(t, t_0) = \phi_0 \times \beta_c(t, t_0),$$

where ϕ_0 is the notional creep coefficient. This may be estimated from

$$\phi_0 = \phi_{RH} \times \beta(f_{cm}) \times \beta(t_0).$$

ϕ_{RH} is a factor which allows for the effect of relative humidity on the national creep coefficient. For mean compressive strength $f_{cm} > 35$ MPa, which will be the case here, ϕ_{RH} is

$$\phi_{RH} = \left(1 + \frac{1 - RH/100}{0.1 \times \sqrt[3]{h_0}} \times \alpha_1 \right) \times \alpha_2.$$

RH is the relative humidity of the ambient environment in percent. N400 states that the relative humidity should be assumed to be 70 % for the superstructure of a bridge. h_0 is the notional size of the member in mm,

$$h_0 = \frac{2A_c}{u},$$

where A_c is the cross-sectional area and u is the perimeter of the member in contact with the atmosphere and which allows for the structure to dry out. α_1 and α_2 will be defined shortly.

$\beta(f_{cm})$ is a factor which allows for the effect of concrete strength on the notional creep coefficient,

$$\beta(f_{cm}) = \frac{16.8}{\sqrt{f_{cm}}}.$$

Here f_{cm} is the mean compressive strength of concrete in MPa at the age of 28 days, and $\beta(t_0)$ is a factor that allows for the effect of concrete age at loading on the notional creep coefficient,

$$\beta(t_0) = \frac{1}{0.1 + t_0^{0.20}}.$$

$\beta_c(t, t_0)$ is a coefficient to describe the development of creep with time after loading, and may be estimated using the following expression,

$$\beta_c(t, t_0) = \left(\frac{t - t_0}{\beta_H + t - t_0} \right)^{0.3}.$$

With t_0 and t as given above, $t - t_0$ is the non-adjusted duration of loading in days. β_H is a coefficient depending on the relative humidity (RH) and the notional member size (h_0). For $f_{cm} > 35$ MPa this is estimated from

$$\beta_H = 1.5 (1 + (0.012RH)^{18}) h_0 + 250\alpha_3 \leq 1500\alpha_3$$

$\alpha_{1/2/3}$ are coefficients to consider the influence of the concrete strength. They are as follows:

$$\alpha_1 = \left(\frac{35}{f_{cm}} \right)^{0.7} \quad \alpha_2 = \left(\frac{35}{f_{cm}} \right)^{0.2} \quad \alpha_3 = \left(\frac{35}{f_{cm}} \right)^{0.5}$$

Prestressing force

As given in Section 5.1.3 there are 26 prestressing strands in each NIB 500/1435 beam, each with a given cross sectional area of $A_p = 100 \text{ mm}^2$. 22 of these strands are placed in the lower part of the cross section, and four strands are placed at the top. As given the prescribed prestressing force is 134 kN in each strand in the lower edge and 126 kN in each strand in the upper edge. This gives a characteristic prestressing force

$$F_{p0} = 22 \times 134 \text{ kN} + 4 \times 126 \text{ kN} = 3452 \text{ kN}.$$

Reducing the force with the approximate loss factor $\alpha' = 0.85$ gives an effective characteristic prestressing force

$$F'_{p0} = \alpha' F_{p0} = 0.85 \times 3452 \text{ kN} = 2934 \text{ kN} \quad (6.1)$$

As mentioned both gradual transmission of prestressing forces and coating of certain prestressing strands will cause exceptions from this loading in the beam ends. Because shear calculations are performed at the beam ends these factors may affect these calculations, and both effects should in theory be taken into account when establishing design loads. However, as shall be seen when the calculation procedures for shear capacity is presented in Chapter 8, the relevant edition of NS 3473 does not take the gradual transfer of axial load by bond into consideration. Instead full axial load is assumed from the beam ends.

Furthermore it is assumed that the coating of certain prestressing strands will not affect the prestressing force considerably because it only concerns four out of in total 26 strands. The effect this will have on the moment distribution and the shear forces that will arise from this can therefore be assumed to be negligible. In order to simplify the calculations this is therefore not taken into account.

Not taking the reduction in the axial load into account will be non-conservative because the axial load is favourable with regards to shear capacity. However, near the continuous support the beam experiences tension in the upper edge as the next chapter will show, and the moment occurring from the prestressing will therefore be unfavourable.

As Section 6.7 will elaborate, characteristic loads are transformed to design loads by the use of load coefficients for different load combinations. Load combinations and load coefficients will be introduced in Section 6.7. For prestressing loads the factor is denoted γ_D . This load factor roughly only covers the uncertainty in the prestressing force itself (Thorenfeldt, 1990). Including the load factor leads to the following expression for the design axial load N_{Ed} in the beam,

$$N_{Ed} = \gamma_D F'_{p0} = \gamma_D \alpha' F_{p0} \quad (6.2)$$

From the axial load the primary moment M_0 can be calculated. The primary moment originates due to an eccentricity e between the centre of gravity for the concrete cross section and the centre of gravity of the prestressing steel. The characteristic primary moment is given as

$$M_{0, \text{char}} = F'_{p0} \times e = \alpha' F_{p0} \times e,$$

while the design primary moment is given as

$$M_0 = N_{Ed} \times e. \quad (6.3)$$

The prestressing strands that will be in the compression part of the cross section will give contributions to the primary moment in the opposite direction as the prestressing strands in the tensile part of the cross section, causing a reduction of the total moment that will occur. All the strands are therefore be included in the calculation of e .

In reality the eccentricity will vary over the length of the beam. Change in the concrete cross section near the beam ends will change the centre of gravity for the concrete. Furthermore, as Chapter 7 will show, the beam will be subjected to tension in the lower edge and compression in the upper edge in the greatest part of the beam, while near the critical support the beam tension will occur in the upper edge and compression in the lower. The centre of gravity of the prestressing steel in tension will therefore also shift. As mentioned it has been decided to neglect the change in the concrete cross section for the establishment of design loads. Furthermore it is decided to simplify the distribution from the primary moment by using a constant eccentricity. Because the beam is in tension in the lower edge in the greater part of the beam, with the exception of a part near the beam end, it is decided to derive the eccentricity based on tension in the lower edge. The cross

sectional details and placing of the prestressing strands are given in Figure 5.1, and based on this calculations of the eccentricity e is performed in Appendix C. This will be utilized further in Section 7.3.

The assumed constant cross sectional and prestressing properties over the length of the beam means that the primary moment will be constant throughout the beam, with equivalent forces corresponding to applied moments in both beam ends. Because the prestressing strands have a centre of gravity that lies lower than the centre of gravity for the concrete cross section the prestressing compressive force will lead to a moment with compression in the lower edge and tension in the upper edge of the beam. This is defined as a positive moment in this thesis. Because the prestressing leads to tension in the upper edge of the beam which induces an uplift of the beam, counteracting the deformation from the beam's self weight, it will be a favourable load in the greater part of the beam. However, as shall be seen in Chapter 7, near the critical support tension will occur in the upper part of the beam from the other design loads as well, meaning that the prestressing force will be unfavourable. With constant cross sectional and prestressing properties over the length of the beam the prestressing does not induce shear forces in the beam.

6.5 Accidental action

Accidental actions are loads that the structure can be exposed to due to an abnormal incident, accident or incorrect use. This can for instance be impact loads from vehicles or vessels, falling objects, explosion, fire or avalanches. Loads on the bridge from accidental actions will not be studied further.

6.6 Time related load effects

Time related effects such as creep and shrinkage in the concrete and relaxation of the prestressing steel may affect the load distribution acting on a system over time. In the following sections the effect that time related effects have on the distribution of self weight and on the moment occurring from prestressing will be looked into.

6.6.1 Redistribution of self weights

The construction method of continuous concrete elements bridges, as described in Section 4.1.1, brings forth a challenge regarding calculation of self weights: The self weights from the different bridge components will work on both the initial simply supported system as well as on the continuous system after the bridge deck has been cast. The distribution of the self weights from each bridge component between the two systems is dependent on time of loading as well as time of consideration. This has been looked into in a previous master thesis written for the Department of Structural Engineering at the Norwegian University of Science and Technology (NTNU) in 2015, by students Anders Hermundsdal and Andrés Pétursson (Hermundsdal and Pétursson, 2015). A simplified approach has been taken here, based on the results discovered in this master thesis.

In the master thesis written by Hermundsdal and Pétursson it is assumed that the prestressing steel is cut after three days, and the self weight is applied. Furthermore it is assumed that the bridge deck is cast and has reached sufficient strength for the system to become continuous when the beams have attained 28 days strength. The pavement and guard rail is assumed to be cast after the bridge has become continuous, i.e. after 28 days.

Deformations are the basis of the deduction performed by Hermundsdal and Pétursson. Looking at the placing of the beams and at the casting of the bridge deck as two separate cases, one set of systems of equations is produced for each case based on how the structural members will deform over time. Deformation of the beams due to self weight will occur as simply supported systems (as the left case in Figure 4.2) from day three to day 28. From day 28, when the bridge deck is cast, until 100 years the beams will deform as part of a continuous system (as the right case provided in the same figure). Deformation of the bridge deck occurs in the same manner as for the beams, with the difference that the self weight of the bridge deck does not contribute to deformations in the first 28 days but instead provides a momentary deformation when the bridge deck is cast. A more detailed description of the process can be found in the master thesis by Hermundsdal and Pétursson (Hermundsdal and Pétursson, 2015).

The contribution to self weights from each structural member in The Hulvågen Bridge is given in Figure 6.1. Here the contributions are numbered as follows: $g_1 = g_{\text{beams}}$, $g_2 = g_{\text{deck}}$, $g_3 = g_{\text{pavement}} + g_{\text{guard rail}}$.

The self weight is multiplied with a factor x_i that gives the portions of the component's self weight that works on the continuous system. This makes it possible to find how much of the self weights that work on the simply supported and on the continuous system. x_1 shows the portion working on the continuous system for the beams' self weight while x_2 shows the portion working on the continuous system for the bridge deck's self weight. The systems of equations deduced by the process described above lead to the following expressions for the factors x_i (Hermundsdal and Pétursson, 2015).

$$x_1 = \frac{\Delta g_{\text{beam}}}{g_{\text{beam}}} = \frac{\frac{1}{EI_{\text{beam},36500,3}} - \frac{1}{EI_{\text{beam},28,3}}}{\frac{1}{5EI_{\text{composite beam},36500,28}} + \frac{1}{EI_{\text{beam},36500,28}}}$$

$$x_2 = \frac{\Delta g_{\text{deck}}}{g_{\text{deck}}} = \frac{\frac{1}{EI_{\text{beam},36500,28}} - \frac{1}{EI_{\text{beam},0,0}}}{\frac{1}{5EI_{\text{composite beam},36500,28}} + \frac{1}{EI_{\text{beam},36500,28}}}$$

Hermundsdal and Pétursson (2015) find the factors as $x_1 = 39.1\%$ and $x_2 = 48.1\%$. Because the pavement and guard rail is cast after the bridge is made continuous it is assumed that this self weight acts only on the continuous system, rendering $x_3 = 100\%$.

For this thesis it has been decided to use the values found by Hermundsdal and Pétursson (2015) directly. Both bridges are made of reinforced concrete, built with the same method and with spans of similar length. Both bridges have bridge decks with thickness 250 mm. The beams in Hermundsdal and Pétursson (2015) are of type MOT 1200, which is slightly smaller than The Hulvågen Bridge's NIB

500/1435 beams. There are also seven instead of four beams. However, based on the similarities between the two bridges it has been assumed that the factors used by Hermundsdal and Pétursson (2015) are directly transferable to The Hulvågen Bridge. The magnitude of the error this assumption makes will not be examined further here.

With the self weights of each bridge component given in Table 6.1 the distribution of self weights working on each of the two systems can now be found. Table 6.2 gives a summary of the information given in Table 6.1 and in the previous paragraphs, while the self weights working on the continuous and simply supported systems for The Hulvågen Bridge are calculated in Table 6.3 and Table 6.4, respectively. When the total self weights working on each system is found, a model can be made for each system assigning the associated self weight. This will be done in Section 7.1.2.

Table 6.2: Self weights with fractions on continuous systems

Structural member	Self weights	Fraction of g_i on continuous system $x_i = \frac{\Delta g_i}{g_i}$
Beam	$g_1 = g_{\text{beam}} = 25.2 \text{ kN/m}$	$x_1 = 39.1 \%$
Deck	$g_2 = g_{\text{deck}} = 45.6 \text{ kN/m}$	$x_2 = 48.1 \%$
Pavement + rail	$g_3 = g_{\text{pavement}} + g_{\text{rail}} = 26.6 \text{ kN/m}$	$x_3 = 100 \%$

Table 6.3: Self weights on continuous system

Structural member	On continuous system Δg_i
Beam	$\Delta g_1 = 0.391 \times 25.2 = 9.9 \text{ kN/m}$
Deck	$\Delta g_2 = 0.481 \times 45.6 = 21.9 \text{ kN/m}$
Pavement + rail	$\Delta g_3 = 1.0 \times 26.6 = 26.6 \text{ kN/m}$
Total	$\Delta g_{\text{tot}} = 58.4 \text{ kN/m}$

Table 6.4: Self weights on simply supported system

Structural member	On simply supported system $g_i - \Delta g_i$
Beam	$g_1 - \Delta g_1 = 25.2 - 9.9 = 15.3 \text{ kN/m}$
Deck	$g_2 - \Delta g_2 = 45.6 - 21.9 = 23.7 \text{ kN/m}$
Pavement + rail	$g_3 - \Delta g_3 = 26.6 - 26.6 = 0 \text{ kN/m}$
Total	$g_{\text{tot}} - \Delta g_{\text{tot}} = 39 \text{ kN/m}$

As stated it is only for the self weights that this problem arises when using concrete elements in continuous bridges. The variable load that is considered here,

traffic load, is applied after the bridge has become continuous, and it is therefore assumed that all traffic loads work on the continuous system. Furthermore the prestressing loads are applied to the isolated NIB beams, and the effects they provide are only transformed to the continuous system through long term effects such as creep and shrinkage of the concrete beams and relaxation of the steel, which may cause cracking of the beams when made continuous with the bridge deck. This will be most relevant for Serviceability Limit State calculations, and is not looked further into in this thesis.

6.6.2 Secondary moments from prestressing

When prestress is applied in the NIB beams they are simply supported, statically determined beams. Due to this, no secondary moments occur in the beams initially. However, when the bridge deck is cast the simply supported beams are made continuous and the system becomes statically indeterminate. Then secondary moments can, and will, occur. Just as for the calculations regarding redistribution of self weights, the calculations regarding secondary moments are dependent on the stiffness at different times of loading.

The prestressing steel is assumed to be cut after three days, and the primary moment M_0 which subsequently is applied leads to an uplift of the beam, causing the beam to be loaded by its self weight which counteracts the uplift. From three to 28 days the beams will rest in this simply supported system. Time related effects, mainly creep, cause a reduction of the beam's stiffness over time, which initially means that the uplift from the primary moment will increase over time to a maximum uplift or to fracture (Yin, 2004). However, after the bridge deck is cast at 28 days the beam and deck will work in union, and further uplift will be prevented due to the symmetry in the system. This prevention is caused by a secondary moment which has appeared in the beam. The secondary moment is low in the beginning, but increases with time as the beam stiffness decreases. The secondary moment alone will induce tension in the lower edge of the structure and compression in the upper edge, and it is therefore a negative moment. The bridge is considered after one year, or 36 500 days, which is the service life that the bridge is designed for.

A set of systems of equations describing the situation is created by Hermundsdal and Pétursson (Hermundsdal and Pétursson, 2015). The following expression for the secondary moment is derived based on the equations,

$$M_{\text{sec}} = \left(-\frac{M_{0, \text{char}}}{EI_{\text{beam}, 36500, 3}} + \frac{M_{0, \text{char}}}{EI_{\text{beam}, 28, 3}} \right) EI_{\text{beam}, 36500, 28} \quad (6.4)$$

$M_{0, \text{char}}$ denotes the characteristic primary moment as given in Equation (6.4.1). The stiffness of the beam for the different time of loading and time of consideration has been found in Appendix B. The calculations are done in accordance with EC2, using the formulas for creep provided in Section 6.4.1. As elaborated in Section 5.1.1 the elasticity modulus given in EC2 can be used in the calculations.

The total characteristic moment which will occur from the prestressing after long time will then be given as

$$M_{\text{tot}} = M_0 + M_{\text{sec}} \quad (6.5)$$

This moment is defined as positive when it leads to tension in the upper edge of the cross section.

6.7 Limit states and load combinations

Design of structures is done by proving that the structure satisfies the design requirements in the following limit states:

- Ultimate Limit State (ULS)
- Serviceability Limit State (SLS)
- Accidental Collapse Limit State (ALS)
- Fatigue Limit State (FLS)

For each limit state there are specified load combinations that must be used in order to control the capacity when loads act simultaneously from several load sources. The load combinations consists of a selection of the characteristic loads acting on the structure, combined with specified load coefficients, in order to establish the design loads acting on the structure. The least favourable load combination makes the basis of the design. Design for ULS and SLS is most common, and will therefore be explained in more detail.

6.7.1 Ultimate Limit State

Ultimate Limit State (ULS) includes collapse or similar forms of failure of a structural member or of the entire structure. In ULS the capacity against failure of a structural member is decided based on calculations of the strain characteristics and design strength of the materials.

Load effects of interest are bending moments, axial loads, shear loads and torsional moments. When the load effects act simultaneously the capacities must be decided based on combinations of the load effects.

Load combinations in ULS

In ULS there are two sets of load combinations that must be controlled, *a* and *b*. Load coefficients for the two combinations are given in Table 6.5, with following choices of values for the various parameters.

Table 6.5: Load coefficients in ULS (Statens Vegvesen, 2003)

Load group Combination	Permanent loads		Deformation loads, <i>D</i>	Variable loads, <i>Q</i>
	Earth pressure	Other		
a	1.0	1.15 [†]	γ_D	$\gamma_1 \cdot Q_1$
b	1.0	1.0	1.0	$\gamma_2 \cdot Q_1 + 0.8 \cdot \sum Q_n$

[†] Load coefficient for permanent load is set to 1.0 if this is unfavourable.

$\gamma_D = 1.1/0.9$ for unfavourable/favourable direct effects of prestressing forces,
otherwise $\gamma_D = 1.0$.

$\gamma_1 = 1.4$ for normal transports
 $= 1.2$ for special transports
 $= 1.15$ for mobile cranes
 $= 1.1$ for one time transport
 $= 1.0$ for temperature load, variable part of water pressure and impact
 mooring loads from ferries
 $= 1.6$ for other variable loads

$\gamma_2 = 1.2$ for normal transports
 $= 1.1$ for special transports
 $= 1.05$ for mobile cranes
 $= 0.8$ for temperature load, variable part of water pressure and impact
 mooring loads from ferries
 $= 1.3$ for other variable loads

Q_1 is the characteristic value of the variable load that is least favourable for the considered load situation, while Q_n is the characteristic value of other variable loads that act unfavourable for the load situation.

It should be noted that NS 3473:1977, which was the in use when The Hulvågen Bridge was designed, states that for prestressing a load coefficient of $\gamma_p = \gamma_D = 0.88$ should be chosen if the prestressing load acts favourably. It is natural to assume that this is the value that has been used in the original designing of the bridge. However, for consistency it has been decided to follow the regulations in R412 here, with a prestressing load coefficient of $\gamma_D = 0.9$.

6.7.2 Serviceability Limit State

For the Serviceability Limit State (SLS) the structure has to be designed to fulfil given performance criteria in order to secure normal use throughout it's service life. SLS defines criteria in order to limit deflection, vibration, cracking tendency and penetrability of fluids into the concrete.

Load combinations in SLS

Also in SLS there are two sets of load combinations that must be controlled. Combination a is assumed to represent the worst expected load situation in the structure's service life and is used for controlling displacements in supports and joints, while combination b is assumed to represent a load situation that will not be exceeded more than 100 times during the structure's service life. This combination is used for control of deflections and crack widths. Load coefficients for the two combinations are given in Table 6.6.

Combination factors, Ψ_1 , are given in Table 6.7.

Table 6.6: Load coefficients in SLS (Statens Vegvesen, 2003)

Combination	Permanent loads, P	Deformation loads, D	Variable loads, Q		
			Traffic loads, T	Nature loads, E	Ballast etc, L
a	1.0	1.0	$Q_1 + 0.7 \cdot \sum Q_n$		1.0
b	1.0	1.0	$\Psi_1 \cdot Q_1 + 0.7 \cdot \sum \Psi_1 \cdot Q_n$		

Table 6.7: Combination factors

Variable loads, Q		Combination factors, Ψ_1
Traffic loads	T	0.5
Nature loads	E	0.5
Ballast, etc.	L	1.0

Control of crack widths is generally not necessary for bridges with a planned remaining service life of less than 25 years. This is also applicable for bridges with a remaining service life of more than 25 years when the exposure to chlorides is low. Otherwise the crack widths should be considered with regard to durability for the following types of elements:

- Regularly reinforced beams
- Prestressed beams with direct bond to the concrete (for instance NIB beams) and with cover of the same order of magnitude as regular reinforcement
- Bridge decks covered with asphalt pavement without membranes

According to R412 control of crack widths can be omitted if utilization in ULS does not exceed 90 % of the reinforcement capacity.

Chapter 7

Design loads

In this chapter the design load effects acting on The Hulvågen Bridge are established. The calculations are based on the information given in the previous chapter regarding loads and load combinations. In this chapter the design load effects acting in the critical composite beam from self weight, traffic loads and prestressing loads will be established, and in Chapter 9 this will be used to control the capacity of the composite beam with respect to shear.

The loads working on the beams from prestressing can be established directly based on the formulas presented in Section 6.4.1. In order to find the load effects from self weight and traffic load the analytical program Frame Analysis Program (fap2D) is used. Fap2D is a program for static and dynamic analysis of 2D frame type structures, developed at the Department of Structural Engineering at NTNU in 2006.

The aim of modelling the bridge in fap2D is to find the design shear loads that act in the critical beam. In order to achieve this two models are made of the bridge, one showing the load distribution in the longitudinal direction and the other showing the load distribution in the transversal direction. When modelling the bridge in the longitudinal direction it is desired to find the total critical load that must be transported through the four beams in the critical span over the length of the bridge. How the load is distributed between the four beams is investigated when modelling the bridge in the transversal direction. With a combination of the two models the load effects in the critical beam can be found.

As shall be seen in Chapter 8, some of the formulas that are used for calculating shear capacity include the design axial load and moment that is working in the critical beam. Therefore, in addition to establishing the design shear load, the design axial load and design moment will also be established in this chapter.

As elaborated in Section 4.1 the bridge will initially be considered as continuous. In Section 7.5 the bridge will be calculated as a multi-spanned simply supported bridge system, and the design loads found here will be compared with the design loads found for the continuous bridge system for further evaluation of this choice.

7.1 Fap2D: Longitudinal direction

In this section the longitudinal model of the bridge will be established. How the model is assembled, including how the critical region is located and simplifications in the modelling, will be given. Furthermore the model is used in order to establish the total load effects that will occur in the critical span of the bridge due to self weight and traffic.

7.1.1 Assembling the model

When modelling a bridge idealizations, assumptions and simplifications will always be necessary, and will affect the accuracy of the results. For this thesis it has been decided to simplify the loading situation that the bridge is exposed to, as has been explained in Chapter 6. Only loads from self weight, traffic and prestressing is considered. Neglecting the cross sectional change of the beam near the beam end, as well as the gradual transmission and coating of the prestressing, provides a simple and predictable model. The basic shape of the load distribution over the length of the bridge can then easily be derived, which makes it possible to locate the regions of the bridge that will be critical with respect to loading without performing complex calculations.

Section 6.4.1 gives an overview of some of the factors that will vary in the beam end, and that will cause variation in the shear capacity in the end regions of the beams. These factors make it more complicated to determine the exact section that will be critical with regards to utilization of the total shear capacity. Furthermore shear capacity control involves checking the capacity with regards to several failure mechanisms, and the critical section for the various failure mechanisms may vary in the beam end.

As shall be elaborated shortly, the only load that can be positioned freely over the length of the bridge is the traffic load, while the loads from self weight and prestressing are determined by the structural system of the bridge and the beam. For this thesis it has been decided to place the traffic loads in order to induce the largest possible shear load in a region near a beam end when the traffic loads interworks with the self loads and prestressing loads. Hence, when establishing the critical load configuration, it has been decided to overlook the fact that the capacity near the beam end may vary. For more exact calculations, the critical load configuration should be found using numerical analysis through an iterative process where the shear capacity of each section can be taken into account. Several hundreds load configurations can easily be controlled using computational software that is designed for this, in order to assure that no load configuration will lead to a more critical combination of load effects in another section of the bridge.

The procedure that is performed here, where the loads are positioned solely based on the load effect they will induce in a beam with assumed constant cross section, makes it possible to reduce the complexity of the computational model by only modelling the factors that are relevant for the load effects in the critical region of the bridge.

Locating the critical region of the bridge

In Chapter 6 it is established that the loads that are to be included when finding the design load effects in the critical beam is the self weight of all the relevant structural members, traffic load as well as direct and indirect prestressing loads from the beams. The other loads that are mentioned are not considered relevant for this bridge, or they are neglected in order to simplify the calculation procedure.

The self weight induces a static load effect in the composite beams. As Section 6.6.1 has introduced the loads from self weight are redistributed from the simply supported to the continuous system over time. For establishing the critical span over the length of the bridge, only the component of the self weight that is acting on the continuous system will be relevant. The prestressing of the beams induce loads that will vary with time, but the load distribution will be constant over the length of the beams. Hence, the only load that can be positioned freely over the length of the bridge is the traffic load. Based on this the most critical load effect one can induce in a section is by placing the traffic load in such a position that it induces as large shear forces as possible in the same region that has the largest shear forces from the self weight.

Because of the continuity in the bridge the largest shear force due to self weight will appear at the outer two spans, as can be seen in Figure 7.1. Idealized, these spans will be simply supported at the outer end and somewhere between simply supported and continuous at the inner ends (rotation around the support is possible but will be counteracted by the structure's stiffness as well as loading in the adjacent spans). The maximum shear load will appear at the inner axes of the two outer spans (axis 2 and 9, enumerated in Figure 4.1).

Simplifications in the modelling of the bridge

In addition to the simplifications and assumptions that have been made above in order to locate the critical span in the bridge, further simplifications and idealizations are made regarding the modelling of the bridge in fap2D.

Because the critical region of the bridge is near one end of the bridge a simplification of the model can be made by only modelling the outer four spans of the bridge. All five transversal supports are modelled as simply supports for the beam, the outer support is pinned while the rest are roller supports. To produce a more realistic model the fifth support should be modelled as something in between a simple and a fixed support, but because the difference between the two systems is very small it has been chosen to model the conservative of the two, rendering the largest load effects in the critical region. Furthermore it has been controlled that the number of spans modelled beyond the first four spans has little effect on the load effects in the critical region. Adding an extra span provides negligible difference in the load effects in the critical region for all loading situations that are looked into.

The cross section of the bridge, consisting of four NIB beams and the bridge deck, has been simplified and modelled as one continuous rectangular beam. This simplification, and the simplifications that have been made regarding modelling of

the bridge in the longitudinal direction have several implications on the accuracy of the result, as will be discussed in the remainder part of this section.

In reality the composite beam stiffness varies over the cross section due to the four NIB beams supporting the bridge deck, and the composite beam could more correctly have been modelled as T-sections instead of a rectangular section. However, this should not affect the distribution of loads in the longitudinal direction when modelling in a 2D programme.

Furthermore, the choice of dimensions of the modelled rectangular beam's cross section mainly affects the deflection (due to change in stiffness), and has negligible influence on the load effects in the longitudinal direction. Simple assumptions regarding reasonable beam dimensions can therefore be made. For this thesis the composite beam is modelled with a width of 7300 mm in accordance with the deck width, and the beam height has been chosen as 250 mm in accordance with the deck height. Furthermore the horizontal curvature and the slope of the bridge deck has been neglected in the modelling.

The model may overestimate the continuity of the bridge, as the bridge in real life consists of precast concrete elements that are made continuous by concrete cast in between the beams and the cast-in-place deck. The two-layer effect of the precast beam and the cast-in-place deck with shear stresses introduced between the members will not be included in this simple model.

Modelling the transversal supports as simply supported implicates that the stiffness in these structural members is ignored. This results in a model where deformation of the top part of the transversal supports is neglected, while rotation around the transversal supports can occur. Hence axial compression set and other deformations of the transversal supports is neglected in this model. Depending on the dimensions and stiffness of the transversal supports this may have substantial impact on the accuracy of the model, and may render a model that is too simplified to be able to produce accurate results.

Neglecting the stiffness of the transversal supports results in a system where only the span lengths affect the loads acting on the beams, given constant cross sectional properties. It is therefore indifferent whether axis 2 or 9 is viewed, despite the height difference of the transversal supports as can be seen in Figure 4.1. In practise different heights of the transversal supports will induce varying degree of displacement and rotation of the support, affecting the shear forces appearing in the beams. Here it has been chosen to model the west end of the beam, where the maximum shear force will appear in the first span near axis 2.

7.1.2 Self weights

In Section 6.2.1 the magnitudes of the self weights from each bridge component has been calculated, and in Section 6.6.1 the distribution of the self weights between the simply supported system and the continuous system has been found.

As is given Tables 6.3 and 6.4 in Section 6.6.1 the total self weight working on the continuous system is $\Delta g_{\text{tot}} = 58.4 \text{ kN/m}$, and the total self weight working on the simply supported system is $(g - \Delta g)_{\text{tot}} = 39.0 \text{ kN/m}$. Each of the systems are modelled separately in fap2D.

The model for the continuous system includes four spans of the bridge, as explained in the previous section. The distributed self weight $\Delta g_{\text{tot}} = 58.4 \text{ kN/m}$ is placed over all the modelled beams, as shown in Figure 7.1a. This leads to a shear and moment distribution over the modelled beams as shown in Figure 7.1b and Figure 7.1c.

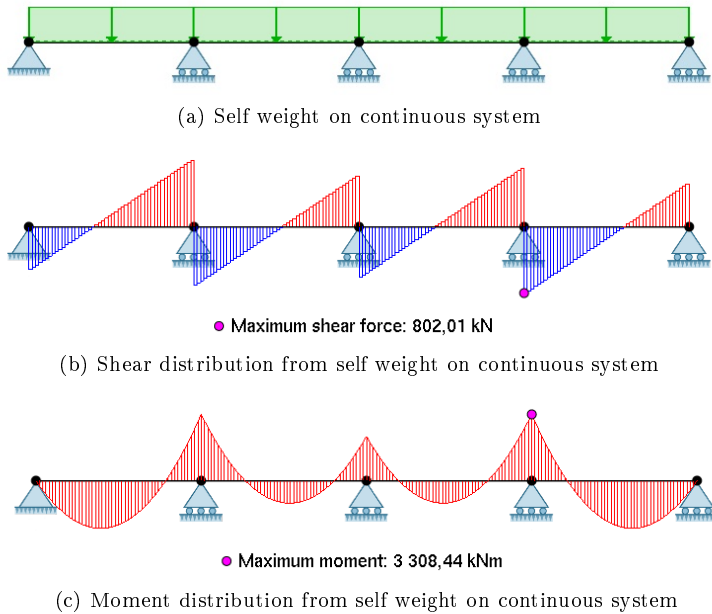


Figure 7.1: Self weight, shear and moment distribution on continuous system

Furthermore the model for the simply supported system is a one-span-beam of 23 meters, simply supported on both ends. The distributed self weight $(g - \Delta g)_{\text{tot}} = 39.0 \text{ kN/m}$ is placed over the entire beam as given in Figure 7.2a. This leads to a shear and moment distribution over the modelled beam as shown in Figure 7.2b and Figure 7.2c.

The characteristic load effects that arise in the beam from these two systems is established. For comparison between the different loads the characteristic shear force and moment acting at the support are given in Table 7.1.

Table 7.1: Characteristic load effects at support from self weights

Characteristic load effects	On continuous system	On simply supported system	Total load from self weights
Shear load [kN]	826.8	456.1	1282.9
Moment [kNm]	3308.4	0	3308.4

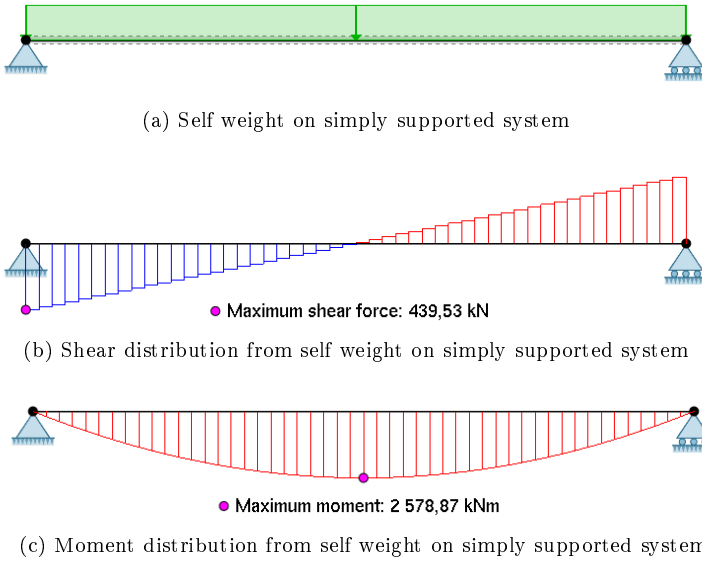


Figure 7.2: Self weight, shear and moment distribution on simply supported system

7.1.3 Traffic loads

In general design of bridges all load situations must be controlled for all placements on the bridge. As given in Section 6.3.1, it has been assumed that a heavy vehicle load will be critical for this bridge. Furthermore, since the largest shear force from self weight will appear in the first span near axis 2, it has been decided to place the traffic load in order to induce largest possible shear force in the same area.

In accordance with the directive summarized in Section 6.3.1, this results in a distribution of the traffic loads as given in Figure 7.3a. The distributed heavy vehicle load $V = \frac{500 \text{ kN}}{16 \text{ m}} = 31.25 \text{ kN/m}$ is placed in the first span next to the support in axis 2.

The axle load $A = 40 \text{ kN}$ is placed at a distance $2d$ from the support, d being the effective depth of the cross section. As shall be elaborated in Section 8.3.1 the reduction factor $a/2d$ can be applied to all load that is placed within a distance a from the support. This is valid for all load types, but will have a much larger effect for point loads than for distributed loads. It has been decided to neglect this factor for the distributed loads that are applied to the system. However, for the axle point load, it has been decided to place this with a distance $2d$ from the support in order for this value not to be reduced. This is assumed to be the critical situation here without further examination of how a reduction of the point load which simultaneously can be brought closer to the support (which in itself is a more critical load situation) will affect the load distribution. For placing of the axle load it is decided to use the value for d which is valid when the beam has tension in the

lower edge of the cross section, i.e. the situation that will occur in the greatest part of the beam. This renders a value $d = 1550$ mm, as is calculated in Appendix D, meaning that the axle load is placed at a distance $2d = 3100$ mm from the support.

Furthermore the distributed load $p = 6$ kN/m, representing lighter traffic, is placed at the remainder part of the first span, in addition to the whole of the second and the fourth span. In theory the shear force in the viewed section would increase if the bridge had been modelled with all spans and with the distributed load over every other span for the remainder of the bridge, but in practise the increased load effect in the considered section from loading p on the sixth and eighth spans is negligible.

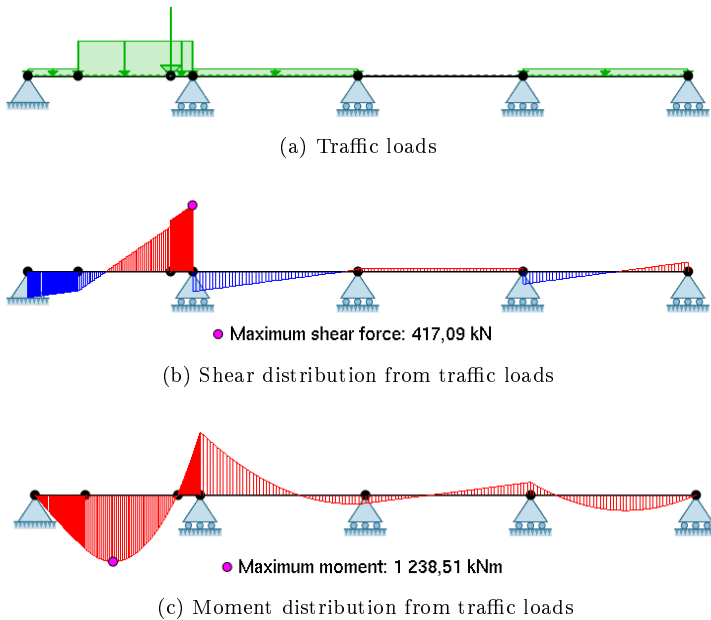


Figure 7.3: Traffic loads, shear and moment distribution

The distribution of the traffic loads leads to a shear distribution over the modelled bridge as shown in Figure 7.3b. Placing the axle load with a distance $2d$ from the support will give a jump corresponding to $A = 40$ kN in the shear force distribution, as can be seen in Figure 7.4. Figure 7.4 also shows how changing the magnitude of the distributed load changes the slope of the shear distribution. The moment distribution is shown in Figure 7.3c. The characteristic shear forces and characteristic moments acting at the support are given in Table 7.2. Positive moment is defined as moment that leads to tension in the upper part of the beam.

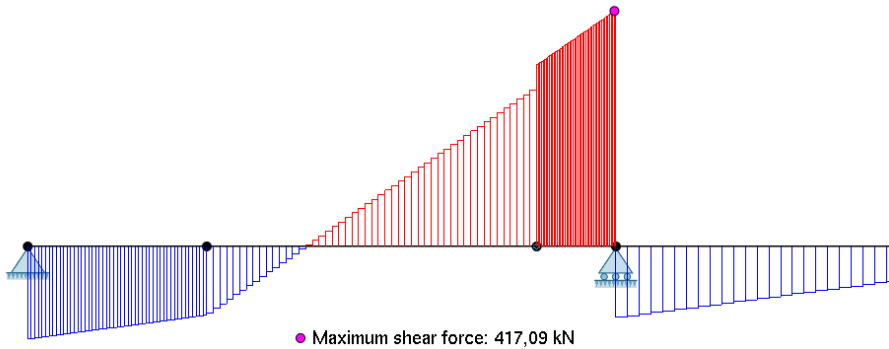


Figure 7.4: Close-up of shear distribution from traffic loads

Table 7.2: Characteristic load effects at support from traffic loads

Characteristic load effect	Total load from traffic
Shear load [kN]	418.9
Moment [kNm]	1172.3

7.2 Fap2D: Transversal direction

7.2.1 Assembling the model

Modelling the bridge in the transversal direction is done with the intention of discovering how the loads from traffic and self weight are distributed between the four NIB beams over the cross section of the bridge. This will provide the opportunity to establish the design load effects that act in the critical part of the critical beam. In this thesis the distribution of loads between the beams will only be considered in a simplified manner, with several simplifications that may have large impact on the accuracy of the results. A master thesis written this semester by Halvard Halsnes, Audun Fossum and Valon Hyseni is looking more closely into the distribution of the loads between the four beams in The Hulvågen Bridge.

The bridge deck is modelled as a rectangular cross sectioned beam with height 250 mm and width 7.3 meters, and is modelled as simply supported where the bridge deck rests on the beams. The positioning of the NIB supports is gathered from the working drawings produced by Johs Holt AS, given in Figure 6.1. Symmetry in the bridge deck and beams is utilized and only half the bridge is modelled. In the middle a boundary condition that allows vertical displacement but no rotation or horizontal displacement is applied. The no rotation criterion originates from the symmetry in the system, and is necessary in order to preserve a continuous deformation of the bridge deck.

Simplifications and assumptions

The chosen model of the bridge's cross section is very simplified, causing room for a substantial lack of accuracy in the results.

The NIB beams are modelled as simple supports instead of beams with a cross section. This causes the stiffness in the beams themselves to be neglected, and the beams are considered as point supports instead of supports with a reach or size. Furthermore possible deformation over the NIB beam supports are ignored, despite the fact that these deformations in reality can be relatively large in midspan. However, when shear is of interest in this thesis, the critical sections with large shear loads will be near the transversal supports, as has been seen in Section 7.1. The NIB beams can therefore only have little or no vertical deflections in the critical sections, and this simplification might therefore be okay.

The continuity of the bridge deck and NIB beams is furthermore not included in this simplified model. In reality the two will act as a composite T-sectioned beam. Excluding this from the model may provide inaccurate results.

Near the transversal supports the distribution of loads will be affected by the stiffness of the transversal supports that the NIB beams rest on. As can be seen from the shape of the transversal supports in the working drawings by Johs Holt AS in Appendix A, the stiffness of the transversal supports will be larger in the outer regions than towards the middle. Hence, the outer NIB beams are supported in stiffer areas of the transversal sections while the inner NIB beams are supported in less stiff areas. This means that in an area around the supports the outer beams will have larger stiffness than the inner beams. This effect decreases with increased distance from the transversal supports, and will have negligible effect on the load distribution at a certain distance from the supports. However, because the critical sections are located close to and at the transversal supports this is a phenomenon that may affect the load distribution, and which is neglected here.

It is assumed that the distribution of loads between the beams that is established in this section will be valid for all sections of the beam, both at the support and at a distance from the support.

Due to the large simplifications that have been made regarding distribution of the loads over the cross section of the bridge, it is necessary to take into consideration that there lies considerable uncertainty in the magnitude of the critical load effects that will be found in the critical beam. Further examinations regarding this, for instance through comparing the values established here with the values that Halsnes, Fossum and Hyseni find in their master thesis, should be made.

7.2.2 Self weights

In the transversal direction no distinction has been made between the simply supported system and the continuous system. All self weights are applied in an intuitive manner over the cross section from each bridge component.

In accordance with the self weights derived in Section 6.2.1 the self weight from the bridge deck and pavement layer, when distributed over the width of the bridge, is $\frac{45.6 \text{ kN/m}}{7.3 \text{ m}} = 6.3 \text{ kN/m}^2$ and $\frac{25.6 \text{ kN/m}}{7.3 \text{ m}} = 3.5 \text{ kN/m}^2$, respectively. This leads to

a distributed load of $6.3 + 3.5 = 9.8 \text{ kN/m}$ over the width of the bridge. The self weight from the guard rails is placed as 0.5 kN/m point loads on each side of the bridge. Because the beams are modelled as simple supports, the self weight from the NIB beams can not be included in this model and must be included manually. This load constitutes 6.3 kN/m for each beam, as calculated in Section 6.2.1.

Figure 7.5 shows the distribution of self weights over the cross section of the bridge. As mentioned only the left half the bridge is modelled. The resulting reaction force in each NIB beam supporting the bridge deck is given in Table 7.3, with the left beam in Figure 7.5 representing the outer beams and the right beam representing the inner beams. In the table the self weight of each NIB beam is included in the reaction force. The last column shows the percentage of the total self weight taken up by each beam.

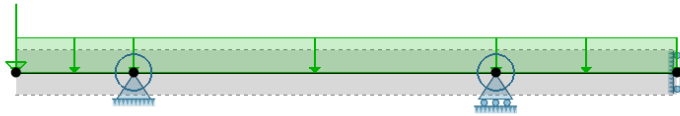


Figure 7.5: Self weight on bridge's cross section

Table 7.3: Reaction forces in each NIB beam from self weights

Beam	Reaction force F per beam, [kN]	Percentage of total self load per beam, [%]
Inner	26.42	27.0
Outer	22.45	23.0

7.2.3 Traffic loads

Traffic loads are to be placed in the least favourable position within the available carriageway width. As stated in Section 6.3.1, there is room for two vehicles next to each other, each of width three metres. With a carriageway width of seven metres this renders one extra meter within which the vehicles can be placed. Placing both vehicles at the outer ends of the carriageway width will lead to the largest possible reaction force in the outer beams, while placing the vehicle loads against each other towards the middle of the carriageway will lead to the largest possible reaction force in the inner beams. Both situations are studied here in order to find what will give the most critical loading situation.

As explained in Section 7.1.3 the vehicle load $V = 500 \text{ kN}$ is distributed over 16 metres in the longitudinal direction, rendering a distributed load of 31.25 kN/m . Divided over the vehicle width of three meters, this leads to a distributed load of $\frac{31.25 \text{ kN/m}}{3 \text{ m}} = 10.42 \text{ kN/m}^2$, which is placed in chosen positions. Furthermore the axle load $A = 40 \text{ kN}$ is divided into two axle loads of 20 kN , and placed with a two

metre space between them in the middle of each vehicle load. The two placings of the vehicle loads are given in Figure 7.6.

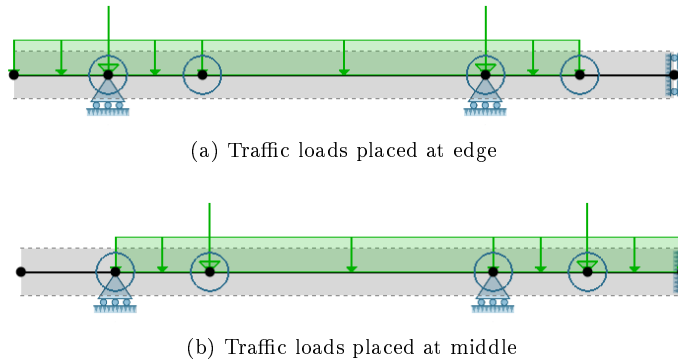


Figure 7.6: Traffic loads on bridge's cross section

Table 7.4: Reaction forces in the NIB beams from traffic loads

Beam	Reaction force, F	
	Loads at edge	Loads at middle
Inner	36.21	51.11
Outer	35.05	20.15

Table 7.4 shows the resulting reaction force in each NIB beam supporting the bridge deck for the two placings of the traffic loads. The table shows that both placings of the traffic loads lead to more load on the inner beams than on the outer beams, and that placing the loads towards the middle increases the difference in distribution between the two pairs of beams. As was found in Table 7.3, the self weight also leads to slightly higher percentage of loading on the inner beams. Based on this, the inner beams will be the most critically loaded beams, and the most critical loading situation will be to place the traffic loads towards the middle of the bridge. This results in a percentage of the reaction force on each beam from the traffic load as given in Table 7.5.

Table 7.5: Reaction forces in the NIB beams from traffic loads placed towards the middle of the carriageway width

Beam	Reaction force F , [kN]	Percentage of total traffic load per beam, [%]
Inner	51.11	35.9
Outer	20.15	14.1

Situations with asymmetrical loading have also been studied in a fap2D model where the entire bridge is modelled, but no situation leads to higher loads on the

inner (or outer) beams than what is given here.

7.3 Prestressing loads

In Section 6.4.1 the initial prestressing force $F_{p0} = 3452$ kN was found. Reducing the force with the approximate loss factor $\alpha' = 0.85$ gave the effective characteristic prestressing force $F'_{p0} = 2934$ kN. Furthermore, the expressions for the design axial load N_{Ed} and the characteristic and design primary moment, $M_{0, \text{char}}$ and M_0 , were established in the same section. The secondary moment M_{sec} due to the continuity of the bridge was established in Section 6.6.2, and the total characteristic moment from prestressing was given as $M_{\text{tot}} = M_0 + M_{\text{sec}}$.

The characteristic axial load and primary moment are calculated in Appendix C. Figure 7.7 shows the characteristic primary moment's eccentricity, which is calculated in the appendix. Furthermore the beam stiffness for various time of loading and consideration that are used in the expression for the secondary moment are calculated in Appendix B. The values for the stiffness are repeated in Appendix C so that also the secondary moment can be calculated here.

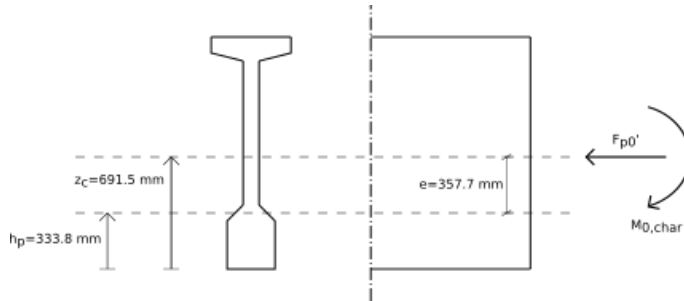


Figure 7.7: Loads on NIB beams from prestressing

Table 7.6 shows a summary of the characteristic prestressing loads working on the beam. For axial loads pressure is defined as positive, while positive moment is defined as moment that leads to tension on the upper edge of the beam, as seen in Figure 7.7. As the table shows, the secondary moment will reduce the magnitude of the total characteristic moment, but the total moment maintains the direction as Figure 7.7 illustrates for the characteristic primary moment. As explained in Section 6.4.1 the gradual transmission of prestressing forces to the concrete and the coating of certain prestressing strands is neglected in the establishment of design loads, leading to a constant axial load and constant primary moment over the length of the beam. All the characteristic load effects will therefore be constant over the length of the beam.

Table 7.6: Characteristic load effects at support from prestressing

Characteristic load effect	Total load from prestressing
Axial load F'_{p0} [kN]	2934
Primary moment $M_{0, \text{char}}$ [kNm]	1050
Secondary moment M_{sec} [kNm]	-570
Total moment M_{tot} [kNm]	$1050 - 570 = 480$

7.4 Load combinations and design load on critical beam

With all the characteristic load effects that are acting on the beams established in the previous sections, the design load effects can be found using load combinations presented in Section 6.7. In this thesis only the Ultimate Limit State is considered, so Table 6.5 is relevant here. The two given sets of load combinations, a and b , need to be controlled. Here it is clear that load combination a will give the largest design load. This increases the unfavourable effects from the self weight (with load factor 1.15 instead of 1.0 as for b), and increases the direct effects from prestressing if they are unfavourable and decrease them if they are favourable. Furthermore, with only one variable load taken into account in these calculations, no variable loads will be overlooked from the fact that load combination a only includes the least favourable variable load.

For self weights and traffic loads the characteristic load effects can be transformed to design load effects directly by multiplying the load coefficient with the characteristic load effects. Multiplying this with the percentage of the total load that is taken up by the critical (inner) beam, given in Tables 7.3 and 7.5 for self weights and traffic loads respectively, will give the total design loads on the critical beam from self weights and traffic loads. Performing these calculations for shear load and moment acting at the support gives

$$\begin{aligned}
 \text{Shear:} \quad V_{Ed} &= V_{Ed, \text{self}} + V_{Ed, \text{traffic}} \\
 &= 0.27 \times 1.15 \times 1282.9 \text{ kN} + 0.359 \times 1.4 \times 418.9 \text{ kN} \\
 &= 609 \text{ kN} \\
 \text{Moment:} \quad M_{Ed} &= M_{Ed, \text{self}} + M_{Ed, \text{traffic}} \\
 &= 0.27 \times 1.15 \times 3308.4 \text{ kNm} + 0.359 \times 1.4 \times 1172.3 \text{ kNm} \\
 &= 1616 \text{ kNm}
 \end{aligned}$$

It is assumed here that the distribution of shear loads and moments between the beams will be the same as the distribution of the reaction forces that have been established in the previous sections.

For prestressing loads, further considerations must be made. As stated in Section 6.7 the load coefficient γ_D is 0.9 or 1.1 for direct effects of loading when

the loading acts favourably or unfavourably, respectively. In addition it is stated $\gamma_D = 1.0$ for other load effects. The total prestressing moment causes compression in the lower edge and tension in the upper edge, as shown in Figure 7.7. The axial load and primary moment will therefore be favourable with load coefficient $\gamma_D = 0.9$ when the self weights and traffic loads give tension in the lower edge, and they will be unfavourable with load coefficient $\gamma_D = 1.1$ when the self weights and traffic loads give tension in the upper edge. Furthermore the secondary moment, which is an indirect load effect of prestressing, will have load coefficient $\gamma_D = 1.0$ for all load situations.

These considerations are taken care of in the calculations. It is found that the self weights and traffic loads cause a moment with tension in the upper edge from the critical support and to an approximate distance 3020 mm from the support. Here the moment from self weight and traffic loads is zero, and then it increases with tension in the lower edge for increased distance from the support. The load coefficient for prestressing is adjusted to account for this. The design load effects that will occur at the critical support due to prestressing are given in Table 7.7. Similar as for the characteristic moments, the total design moment M_{Ed} is positive, causing tension in the upper part of the composite beam as Figure 7.7 illustrates. The total design moment from prestressing will cause tension in the upper part of the cross section throughout the length of the beam.

Table 7.7: Design load effects at support from prestressing

Design load effect	Load coefficient at support	Total load from prestressing in each beam
Axial load [kN]	1.1	$1.1 \times 2934 = 3227$
Primary moment [kNm]	1.1	$1.1 \times 1050 = 1155$
Secondary moment [kNm]	1.0	$1.0 \times (-570) = -570$
Total moment [kNm]	-	$1155 - 570 = 585$

Finally, the design load effects from self weights, traffic loads and prestressing loads can be summed, resulting in the total design loads that will act on the critical beam. The axial load effect will be decided by the prestressing load, the shear load effect will be decided by the self weights and traffic loads, and the moment will be decided by the sum of all three.

Table 7.8: Design load effects in critical beam at support

Design load effects	Total load from self weight, traffic and prestressing in critical beam at support
Axial load [kN]	3227
Shear load [kN]	609
Moment [kNm]	$1616 + 585 = 2201$

Table 7.8 shows the total load effects acting at the support. The distribution

7.4. LOAD COMBINATIONS AND DESIGN LOAD ON CRITICAL BEAM 79

of each load effect over the entire length of the beam is given in Figures 7.8, 7.9 and 7.10. In these figures the x-axis denotes the distance from the critical support, but in order for the graphs to correspond with the figures for self weight and traffic load given in Figures 7.1 to 7.4 the x-axis is inverted in the graphs. Hence the area that is of interest for capacity control is given in the right end of the graphs.

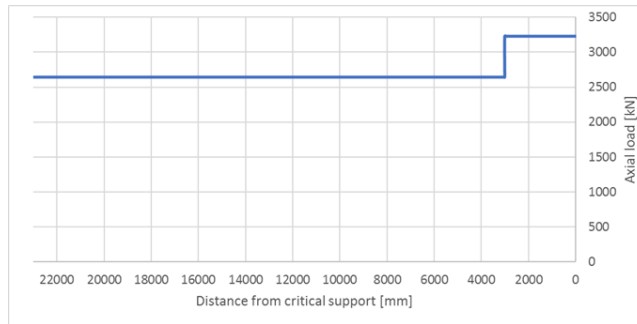


Figure 7.8: Design axial load on critical beam

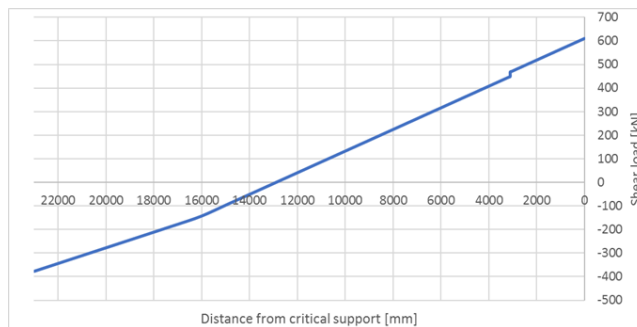


Figure 7.9: Design shear load on critical beam

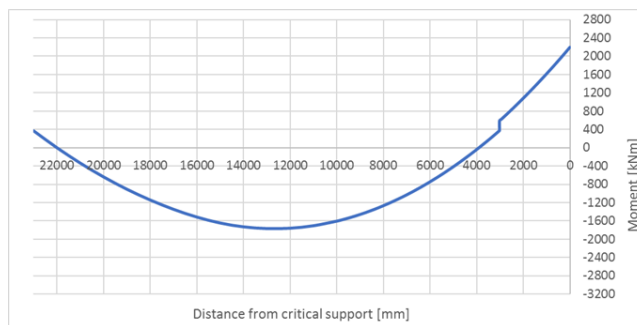


Figure 7.10: Design moment on critical beam

7.5 Design loads on a simply supported bridge system

As given in Section 4.1 it was primarily assumed, based on the provided drawings, that The Hulvågen Bridge is a continuous concrete element bridge. However, on an excursion to the bridge in May 2017 it was discovered that the bridge in fact was not made continuous when it was built. Instead the bridge is a multi-span simply supported bridge, where the beams are resting as individual simply supported beams over the transversal supports.

As Section 4.1 elaborates it can be assumed that the continuous bridge system will lead to larger shear loads and moment near the critical support than the simply supported bridge system, and that this bridge system therefore will be more critical. Nevertheless, a control of the load effects that arise from the simply supported bridge system will be performed in this section, in order to validate the assumption. A comparison of the load effects and a discussion regarding which bridge system should be used for the capacity control will be given in the last part of this section.

7.5.1 Fap2D: Modelling self weights and traffic loads

Similar to the continuous bridge system, the longitudinal direction of the bridge will be modelled using fap2D in order to establish the load distribution that will occur due to self weight and traffic. It will further be assumed that the distribution in the transversal direction will be the same as established for the continuous bridge system.

Assembling the model

When the bridge is to be calculated as a simply supported system with multiple spans each span can be assumed independent of the other spans. As a consequence, calculations can be performed on only one span, in the same manner as was done when considering self weights for the simply supported system. With the assumptions and simplifications given in Section 7.1.1, the critical spans will here be the longest spans, i.e. the span between axis four and five or between axis five and six, which both have lengths 23.5 meters (given in Figure 4.1).

Fap2D will be used to find the design loads from self weights and traffic loads. Similar as for the continuous bridge system, a region near the support will be critical regarding shear capacity, and it is of interest to maximize the load effects that occur here by optimizing the placing of the traffic loads. Like it was elaborated in Section 7.1.1 idealizations, assumptions and simplifications will affect the accuracy of the results also here.

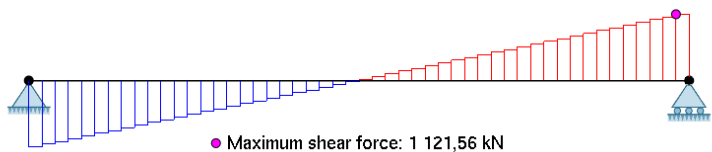
Self weights

The model for the self weights for this bridge system corresponds to the simply supported part of the continuous bridge system as given in Section 7.1.2. Then

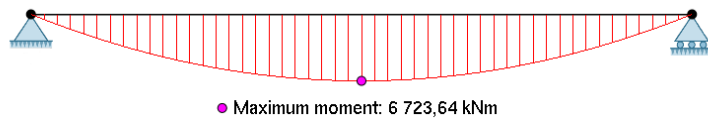
the simply supported system was only exposed to a distributed load $(g - \Delta g)_{\text{tot}} = 39.0 \text{ kN/m}$, but now the simply supported system is exposed to the entire distributed self weight of $g_{\text{tot}} = 97.4 \text{ kN/m}$. Figure 7.11 shows the distribution of loads as well as the shear and moment distribution over the modelled beam.



(a) Self weight on simply supported bridge system



(b) Shear distribution from self weight



(c) Moment distribution from self weight

Figure 7.11: Self weight, shear and moment distribution on simply supported bridge system

Traffic loads

The critical position of the traffic loads in order to induce largest possible forces near the beam end will for the simply supported bridge system be identical to the continuous bridge system. With only one span being modelled the distributed load p can only be placed in the remainder of this span, but with a total beam length of 23.5 meters p works over an extra 0.5 meters compared to the continuous bridge system. V and A are placed as explained in Section 7.1.3, and all magnitudes of the loads remain the same. This leads to a distribution of loads and shear and moment distribution as given in Figure 7.12.

7.5.2 Prestressing loads

Prestressing loads are given for each NIB beam and are independent of whether the bridge is continuous or simply supported. The loads from the prestressing will therefore be equivalent to the loads given in Table 7.6.

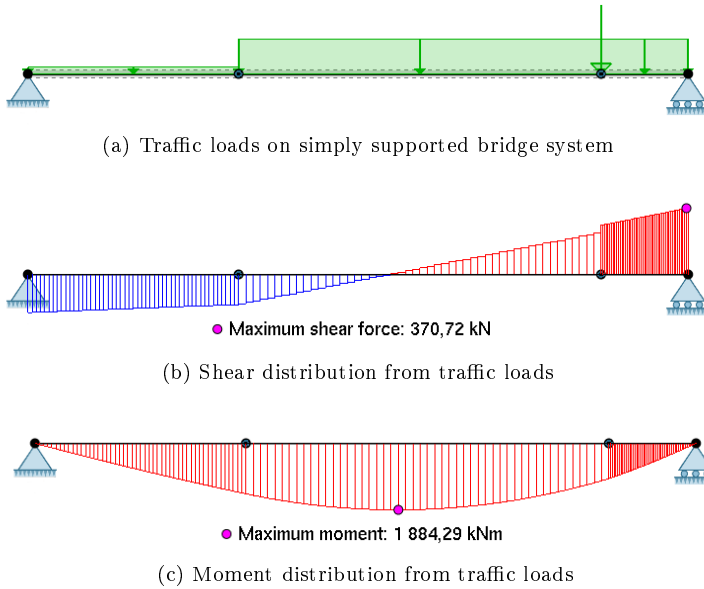


Figure 7.12: Traffic load, shear and moment distribution on simply supported bridge system

7.5.3 Load combinations and design load on critical beam

The total design load effects are found with the same procedure as in Section 7.4. The total design load acting at the support in the critical beam from self weight, traffic and prestressing is given in Table 7.9.

Table 7.9: Design load effects in critical beam at support

Design load effects	Total load from self weight, traffic and prestressing in critical beam at supports
Axial load [kN]	2640
Shear load [kN]	549
Moment [kNm]	374

7.5.4 Comparing the two bridge systems

The graphs in Figures 7.13 to 7.15 show the distribution of axial load, shear load and moment throughout the critical beam. The distributions are given for both the continuous bridge system and the simply supported bridge system.

The distribution of axial loads for the continuous system given in Figure 7.13a shows a jump in the axial load at an approximate distance $x = 3020$ mm from the critical support. This jump corresponds with a change in the load coefficient γ_D

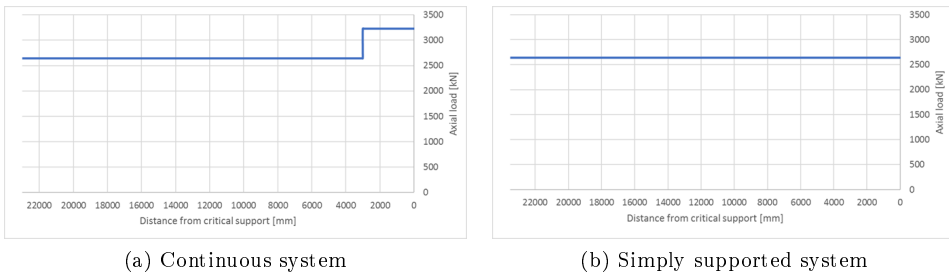


Figure 7.13: Axial load on critical beam

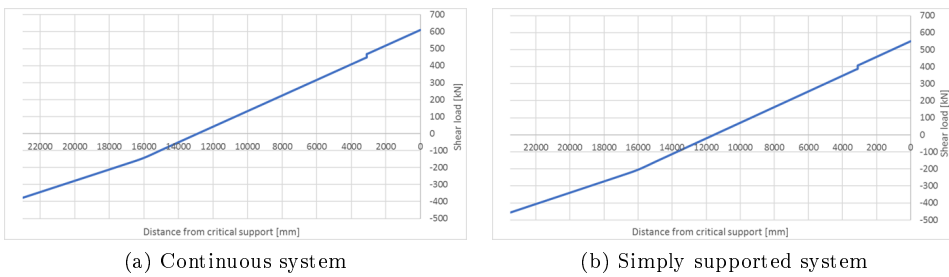


Figure 7.14: Shear load on critical beam

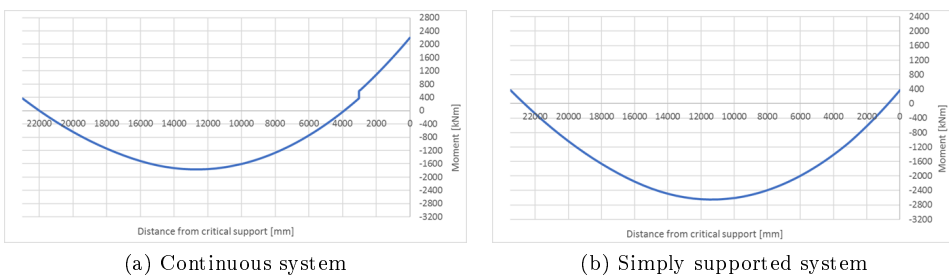


Figure 7.15: Moment on critical beam

for the prestressing load from $\gamma_D = 1.1$ to $\gamma_D = 0.9$, and occurs because the design moment from self weights and traffic loads changes from positive to negative value here. With the prestressing load giving positive moment (tensile in the upper edge) for the entire beam this means that the prestressing load goes from an unfavourable to a favourable load, resulting in a change of value of γ_D as explained previously. The change in γ_D can also be seen in the moment distribution in Figure 7.15a, and is caused by the abrupt change in the primary moment due to the change in the axial load. Figures 7.13b and 7.15b do not have corresponding jumps. This is because the design moment from self weights and traffic loads lead to tension

in the lower edge for the entire length of the beam when the beam is modelled as simply supported, causing the prestressing loads to be favourable throughout the beam.

The jump that occur at $x = 3100$ mm in the shear distribution for both systems, given in Figure 7.14, are due to the axle load $A = 40$ kN applied as part of the traffic load. Initially this point load leads to a 40 kN jump in the total shear distribution, but in these graphs the jump has been reduced in magnitude because only the load working on the critical beam is shown. The jump in the shear distribution will also have an effect on the moment distributions through a change in curvature, but this is not easily seen in the figures. The shear distributions have lower slopes from a distance $x = 16\,000$ mm from the beam end for both bridge systems. This marks the end of the distributed vehicle load V and the beginning of the distributed load p representing lighter traffic. The curvature in the moment distribution will also be reduced in this area, which again is hard to see in the moment distribution figures.

Comparing Table 7.8 and Table 7.9 makes it evident that the continuous bridge system leads to higher loads at the support than the simply supported bridge system, despite the fact that the beam in the simply supported bridge system has a slightly longer span than the beam that is considered in the continuous system. Figures 7.13 to 7.15 confirm that this also remains the case for all sections that are relevant for shear design, i.e. within some distance from the critical support where the design shear load is high.

On the basis of this it may be natural to perform a capacity control on the continuous bridge system, which might be assumed to be the most critical of the two based on the fact that both axial loads, shear loads and moment are higher in this bridge system. However, as shall be seen in Chapter 8, high shear loading and high moment is unfavourable with regards to shear capacity, while an increase in axial loading on the other hand increases the shear capacity (when the axial loading is in pressure). This means that the reduction in the axial load for the simply supported bridge system may reduce the shear capacity when compared to the continuous bridge system, which may make it more critical than the continuous bridge system. However, the increase in design moment from the simply supported bridge system to the continuous bridge system is much larger than the decrease in axial load. Based on this it will be assumed that the continuous bridge system will be the critical of the two, and capacity calculations will only be performed on this bridge system.

It should be noted that it is only at the support regions that the design loading is reduced when the bridge is considered as a simply supported system instead of a continuous system. When considering moment in the mid-span, which usually is the design load situation in beams, it is clear that the simply supported system is much more critical than the continuous system. If a complete control of the NIB beams in the Hulvågen Bridge had been performed, this must have been taken into account.

Chapter 8

Shear

This chapter contains two different aspects with regards to shear. The first sections introduce the shear phenomenon, as well as failure mechanisms that can arise in a beam subjected to shear load. The last sections give an overview of how control of shear capacity is performed according to the various standards. Section 8.3 shows the development of the shear capacity calculations in the various editions of NS 3473. Furthermore, calculations of shear capacity according to the present edition of EC2 is presented in Section 8.4. Section 8.5 introduce how the anchorage capacity of a beam is established and in Section 8.6 a basis for control of the interface between the NIB beam and the bridge deck in the composite beam is established. In addition to the standards, supplementing literature has been used in order to derive, explain or in other ways elaborate the formulas and information given regarding shear capacities.

8.1 Shear force and its effect

When designing a structure in the Ultimate Limit State it is necessary to study the effect that axial load, shear load and moment have on a structure. When considering moment, one usually designs in such a way that a possible failure will have a ductile development, giving clear preliminary warnings of imminent failure. Failure that occurs due to shear will on the other hand have a brittle nature, without preliminary warning. For this reason it is usually desired to design so that shear failure does not occur before the structure's moment capacity is reached.

With a correct amount of shear reinforcement, the cross sectional dimensions that are found when designing a beam for moment will usually be sufficient to secure against shear failure (Lenschow, 1979). Shear design will consequently be limited to deciding the amount of shear reinforcement that is necessary. For plates the occurring shear forces can be decisive with regard to cross sectional dimensions.

The shear fracture is a complicated mechanism, usually giving a combination of multiple fracture mechanisms. Due to this a number of shear fracture models exist, from which it is attempted to derive design methods. Most of the shear

capacity formulas in NS 3473:1977 and EC2 are empirical formulas that are based on experimental results. However, some of the formulas presented in NS 3473:1977 are theoretical and can be derived.

8.2 Shear failure mechanisms

Shear failure will always start with an inclined crack. This crack will either be initiated by flexural cracking due to moment loading (flexure-shear cracking) or they will originate from an interior point in the beam web as a result of the principal tensile stress exceeding the tensile strength of the concrete (web-shear cracking).

If the beam is not shear reinforced failure may either occur due to crushing of the concrete in the compression zone (compressive shear failure), or it may fail due to insufficient capacity of the anchorage of the tensile reinforcement (anchorage failure).

If the beam is shear reinforced with vertical or inclined shear reinforcement, often stirrups, there are three main failure mechanisms that can occur. The initiation of cracks will activate the bars. Dependent on the beam's capacity regarding the two failure mechanisms mentioned above, the stirrups may or may not begin to yield. From here, yielding of the stirrups and deformations in the end region of the beam may occur until either (1) yielding occurs until fracture of the stirrups, (2) crushing occurs in the compression zone, or (3) anchorage failure occurs near the tensile reinforcement. The first of these failure mechanisms is related to diagonal tension failure, while the other two are defined in the previous paragraph. If the beam end is sufficiently under-reinforced, both compressive shear failure and anchorage failure may occur before yielding of the shear reinforcement has initiated.

Which failure mechanism that will occur in a structural member when it is loaded to failure is dependent on which part of the considered beam that is the weakest. Some of the most important factors regarding this are (Lenschow, 1979):

- Material quality
- Cross sectional size
- Amount and layout of the shear reinforcement
- Amount of tensile reinforcement
- Aggregate size of the concrete
- The structure, structural system and load distribution
- Axial load due to prestressing

In addition to the three main failure mechanisms there exists transitional forms as well as other forms of failure like splitting or stability failure. Shear failure is often a complex mechanism, with several mechanisms involved in the final failure. In order to perform a complete control regarding shear capacity of a beam, calculations must be performed to assure that the beam has sufficient capacity both regarding diagonal tension failure, compressive shear failure and anchorage failure.

8.2.1 Diagonal tension failure

Diagonal tension failure is characterized by the inclined cracks which originate and develop until fracture occurs. The failure mechanism is sudden, causing a brittle failure of the beam. The diagonal tension capacity is related to yielding of the shear reinforcement, and is largely dependent on the amount of shear reinforcement in the beam. With correct amount and placing of shear reinforcement diagonal tension failure of the beam can be avoided. In general the design for shear is based on considerations regarding this failure mechanism.

As mentioned, two types of inclined cracking may occur in concrete beams. *Flexure-shear cracking* is initiated by flexural cracking due to moment loading. Cracks originate as vertical cracks in the tensile zone, increasing the shear stresses above the crack. The flexure-shear crack develops into inclined cracks and enter the compression zone of the beam when the combined shear and tensile stress exceeds the tensile strength of the concrete (Pezeshk, 2014). *Web-shear cracking* originates from an interior point in the beam web as a result of the principal tensile stress exceeding the tensile strength of the concrete. This cracking occurs independently of moment induced flexural cracking.

When inclined cracking arises in nonprestressed structural elements it is generally flexure-shear cracking that occurs. Prestressing will reduce or even fully prevent the occurrence of flexure-shear cracking through a reduction in the tensile stresses. However, in older prestressed structures flexure-shear cracking may occur due to an increase in service loads, concrete ageing or deterioration. As Figure 8.1 illustrates, web-shear cracking generally occurs near the supports of members with thin webs, or near the inflection point of continuous beams, particularly if the beam is subjected to axial tension. Web-shear cracking can also arise if the shear forces in a section is large compared to the moment, a situation that can occur if large point loads are applied near beam supports.

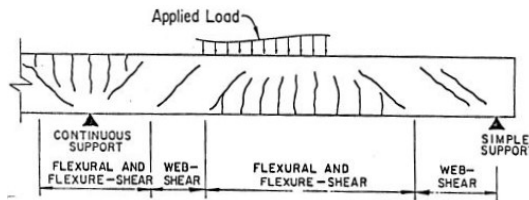


Figure 8.1: Illustration of failure mechanisms causing inclined cracking (Pezeshk, 2014)

It is important to state the difference between the capacity regarding inclined cracks and the capacity regarding ultimate failure of the structure. The load required for failure will generally be somewhat larger than the load required to initiate a crack, even for a structure without shear reinforcement. This is due to the redistribution of stresses that occurs in the beam when a crack is initiated. The compressive stresses in the concrete are arranged into an arch which, when working together with tensile stresses in the longitudinal reinforcement, gives the necessary

carrying effect for the structure to remain standing. In this cracked system it is the vertical component of the compression in the arch that carry the shear force. This arch effect is the reason that some structures, for instance concrete floors, can carry the necessary shear forces without a need for special shear reinforcement.

8.2.2 Compressive shear failure

If the diagonal cracks propagate across a large part of the cross section, the active compression zone becomes narrow and the beam may fail due to crushing of the concrete in the compression zone. This failure mechanism is called compressive shear failure, and is characterized by crushing near the edge of the beam that is in compression. For a simply supported bridge (with tension in the lower part of the cross section near the support) this will occur in the upper part of the beam, while for continuous beams (where tension will be in the upper part near the support) this will occur in the lower part of the beam.

This failure mechanism seldom occurs in rectangular beams without prestressing, but can be a risk for I-shaped beams with weak webs, and especially when the beams are prestressed. For I-shaped beams the crushing will in appear in the beam web, and can occur in the same regions as the shear reinforcement is placed. This failure mechanism is assumed independent of the development of inclined cracks, and the capacity can not be increased by increasing the amount of shear reinforcement.

8.2.3 Anchorage failure

The formation of diagonal cracks near the beam end will cause an increase in the force in the tensile reinforcement. In order to avoid fracture this increase must be designed for, by adding horizontal anchorage reinforcement at the beam end that can take up the additional longitudinal stresses. For I-shaped beams with thick lower flanges, fracture due to anchorage failure will normally occur through slipping of the tensile reinforcement from the beam end, causing successive collapse. It is normal to add anchorage reinforcement in the form of horizontal stirrups stacked over each other at the beam end. Anchorage failure will be looked further into in Section 8.5, and Figure 8.3 provided in this section illustrates the failure mechanism.

8.3 Shear calculations in NS 3473

As mentioned in Chapter 2, NS 3473 (Norske Sivilingeniøres Forening, 1973) is a nationally developed standard used for design and detailing of concrete structures in Norway between 1973 and 2010, ultimately replaced by EC2 (Norsk Standard, 2004). Six editions of NS 3473 were released,

- 2nd edition: February 1977
- 3rd edition: October 1989

- 4th edition: November 1992
- 5th edition: November 1998
- 6th edition: September 2003

Calculations of shear capacity of a cross section was introduced in the first edition of NS 3473. The formulas have in later editions been updated in accordance with development of new research and knowledge. This summary primarily contains the formulas regarding shear capacity of concrete beams, and the effect of axial load from prestressing on the capacity is emphasized. Supplementing literature has been used in order to derive, explain or in other ways elaborate the formulas and information given in NS 3473.

8.3.1 NS 3473:1973, 1st edition

In the 1st edition of NS 3473, procedures regarding shear capacity are given in Section 5.2. Capacity regarding shear forces are to be controlled for both diagonal tension failure and for compressive shear failure.

Compressive shear capacity

Compressive shear failure limits the concrete cross section's capacity for shear force. The capacity for compressive shear failure given in NS 3473 is

$$V_d = 0.3f_c b d, \quad (8.1)$$

where

- f_c is the design concrete compressive strength, defined in Section 4.3.2 of NS 3473
- b is the width of the beam's web
- d is the effective depth of the cross section from the compressive edge to the centre of gravity for the tensile reinforcement.

This formula is based on empirical results, and was considered a relatively safe lower limit of the actual capacity (Lenschow, 1979). Further limitation is given by the criteria that together with other design loads the design shear force can not give a larger principal compressive stress than the design concrete compressive strength f_c . An uncracked concrete cross section is to be assumed for these calculations.

Chapter 10 in NS 3473 contains particular rules for design of prestressed concrete. In Section 10.6 is it stated that if the shear reinforcement is placed approximately in the direction of the principal tensile stress and with distance of maximum $0.3 d$ or 200 mm, the compressive shear capacity can be increased to

$$V_d = 0.4f_c b d. \quad (8.2)$$

This is only valid if the capacity is not limited by the principal compressive stress stated above.

Diagonal tension capacity

The diagonal tension capacity is based on two formulas connected to the two failure mechanisms presented in Section 8.2. The capacity with regard to flexure-shear failure is given by an empirical formula consisting of the sum of the concrete and shear reinforcement capacities,

$$V_{d0} = f_v (bd + 75A_s) + f_s A_{sv} h'. \quad (8.3)$$

An upper limit of the shear capacity is furthermore given, in connection with web-shear failure, as

$$V_{d0} = 2f_v bd + f_s A_{sv} h'. \quad (8.4)$$

This formula is based on principal stresses, and its derivation can be found in Section 6.4.4 in Lenschow (1979). The two formulas have the following parameters:

f_v	is the design concrete shear strength, defined in Section 4.3.2 of NS 3473
f_s	is the reinforcement steel's design strength, defined in Section 4.3.2 of NS 3473
A_s	is the cross sectional area of the associated tensile reinforcement
A_{sv}	is the cross sectional area of the shear reinforcement divided by the centre distance measured perpendicular to the reinforcement direction
h'	is the distance between the tension and compression reinforcement's centre of gravity. For cross sections without compression reinforcement one can use $h' = 0.9d$

The last term is equal in both equations, $f_s A_{sv} h'$, and represents the shear reinforcement's contribution to the diagonal tension capacity. The calculation model resulting in this equation is presented in Section 6.4.6 in Lenschow (1979). Equation (8.4) gives an upper limit for the contribution from the tensile reinforcement to the capacity.

Only the reinforcement which constitutes an angle of minimum 45° with the system axis and which at least has a cross sectional area of the prescribed minimum shear reinforcement is counted as effective shear reinforcement. When the cross section is constituted by units or groups of shear reinforcement with different angles or centre distances the capacity is given as the sum of the capacities.

Shear reinforcement in beams can be stirrups or stirrups together with bent rods from the longitudinal reinforcement, where the stirrups must cover at least half of the total necessary amount of reinforcement. For beams a minimum reinforcement amount is given in Section 9.3.4 of NS 3473, $A_s f_s \geq 0.025 A_c f_c$. Here A_c is the concrete area of the cross section and f_c has a minimum value of 16 MPa. Maximum distance between the stirrups and more information regarding placing of reinforcement is also given in the same section.

Section 5.2.7 of NS 3473 states that loading which occurs at a distance $a < 2d$ from the edge of the support can, for control of diagonal tension capacity, be reduced with the factor $0.5a/d$. d should be chosen using its smallest value in the

area. The reduction of the load can be explained by the fact that the beam carries the load in a different manner near the support than for loads in the span. A part of the load acting near the support will be directly transmitted into the support, and hence the load can be reduced slightly to account for this.

Cross section subject to shear force and simultaneous axial compression or tension

Cross sections subjected to *axial compression*, for instance from prestressing, will have an increase in diagonal tension capacity. In NS 3473 Section 5.2.4 this increase is given as

$$V_d = V_{d0} + 0.2V_\gamma h N_\gamma / M_\gamma, \quad (8.5)$$

with a maximum value

$$V_d = (2f_v + 0.2N_\gamma/A_c) bd + f_s A_{sv} h'. \quad (8.6)$$

We have the parameters

V_{d0}	the diagonal tension capacity for a section without axial load, as given in Equation (8.3)
V_γ, N_γ and M_γ	the design load actions working in the considered section
h	the total height of the concrete cross section

As introduced in Section 5.1.3, the load from prestressing will be gradually increased by bond from zero load at the beam end to the maximum prestressing load at the end of the transmission zone. No information has been found regarding this effect, or how it should be included in the calculations, in the first editions of NS 3473. Neglecting this effect will be non-conservative because the axial load gives a favourable effect on the shear capacity.

The argumentation behind Equation (8.5) is as follows: Axial pressure will counteract the tendency to form moment induced flexural cracking, which again counteracts the formation of flexure-shear cracks because these are initiated by the flexural cracking (Lenschow, 1979). When considering shear capacity, the cross section will behave approximately as if the axial load did not exist from the state that gives flexural cracking. From the cracked state and until failure the capacity can therefore be calculated using Equation (8.3). Adding up the shear force that is applied at the cracked state will give the total shear capacity.

A homogeneous, elastic cross section will not be exposed to tensile stresses as long as the axial pressure force N_γ is applied within the central core of the cross section (illustrated in Figure 6.4.4 in Lenschow (1979)). The moment that will result in the first tensile stresses is $M_{\text{tensile}} = h/6 \times N_\gamma = 0.17h \times N_\gamma$. The moment which results in flexural cracking is set as approximately $M_{\text{flex. crack.}} = 0.2h \times N_\gamma$. By assuming a similar relationship between shear force and moment in the cracking state as in the Ultimate Limit State, the shear force in the cracking state can be found,

$$\frac{V_{\text{flex. crack.}}}{M_{\text{flex. crack.}}} = \frac{V_\gamma}{M_\gamma} \quad V_{\text{flex. crack.}} = \frac{V_\gamma}{M_\gamma} \times M_{\text{flex. crack.}}$$

Inserting the value for the flexural cracking moment results in $0.2V_\gamma h \frac{N_\gamma}{M_\gamma}$, i.e. the last term in Equation (8.5), which originates due to the prestressing load (Lenschow, 1979). This term combined with Equation (8.3) renders Equation (8.5).

Section 5.2.4 in NS 3473 states that if a cross section is subject to shear force and simultaneous *axial tension* the capacity can be calculated as the capacity of the shear reinforcement without contribution from the concrete. This is in line with Section 3.3.1 of NS 3473, where it is stated that the tensile strength of concrete is neglected.

As stated previously, Chapter 10 in NS 3473 contains particular rules for design of prestressed concrete. Chapter 10 provides no additional information regarding calculation of diagonal tension capacity, but in the Appendix belonging to this chapter, T10.6, two alternative formulas for the capacity are given,

$$V_d = f_v (bd + 75A_s) + V_0 + f_s A_{sv} h' (\sin \beta + \cos \beta), \quad (8.7)$$

$$V_d = (2f_v + 0.2\sigma_m) bd + f_s A_{sv} h' \frac{\cos(\beta - \alpha)}{\sin \alpha}. \quad (8.8)$$

These formulas have terms that include the effect of inclined shear reinforcement for diagonal tension failure. β is the angle between the direction of the shear reinforcement and the structure's system axis. α is the angle between the system axis and the principal tensile direction in the Ultimate Limit State, considered at the axis for centre of gravity for the crack free concrete cross section. For vertical shear reinforcement, which is the relevant case for the prestressed beams in The Hulvågen Bridge, $\beta = 90^\circ$. This gives

$$(\sin \beta + \cos \beta) = 1 \quad \text{and} \quad \frac{\cos(\beta - \alpha)}{\sin \alpha} = 1,$$

regardless of the value of α . σ_m is the mean effective concrete compression in the beam web in the Ultimate Limit State due to prestressing forces and possible external axial forces, expressed as $\sigma_m = N_\gamma/A_c$. $\sigma_m = 0.6f_c$ is a given maximum value.

V_0 in Equation (8.7) is defined as the shear force from the load which in the Ultimate Limit State gives no tension or compression in the concrete at the height of the tensile reinforcement's centre of gravity. V_0 is determined for the presumed interdependence between shear force and moment from the load that gives shear force, $V_0 = V_\gamma M_0/M_\gamma$. When establishing the associated "zero tension moment" M_0 , $x = d$ is chosen, and constant concrete tension over $0.8x$ can be assumed.

The explanation of V_0 gives a slightly different angle to the same phenomenon as is described regarding the axial load in Equation (8.5). Following a similar explanation we get $V_0 = 0.2V_\gamma h N_\gamma/M_\gamma$. Equations (8.5) and (8.7) are therefore identical, both expressing the capacity regarding flexure-shear failure.

Furthermore Equation (8.8) expresses the capacity regarding web-shear cracking, similar to Equation (8.6). With $\beta = 90^\circ$ and $\sigma_m = N_\gamma/A_c$ these two formulas are identical.

8.3.2 NS 3473:1977, 2nd edition

In the 2nd edition of NS 3473, no changes have been made to the relevant sections from the 1st edition regarding shear capacity.

8.3.3 NS 3473:1989, 3rd edition

The 3rd edition of NS 3473 is a complete revision of the two preceding editions. Design for shear in beams and plates in this edition is given in Section 12.3.

In this edition, the formulas for shear capacity are specified to be applicable for only beams, plates and ties where the ratio between span width and height is minimum 3.0 for two-sided support systems or 1.5 for a cantilevered structural member. Areas with smaller ratios than this are to be calculated as discontinuous parts in accordance with Section 12.6 of NS 3473.

Also in this edition the shear capacity must be established for diagonal tension failure ($V_{cd} + V_{sd}$) and compressive shear failure (V_{ccd}). Three alternative procedures for calculating the capacity are given: The simplified method is given in Section 12.3.2, the truss model is given in Section 12.3.3 and the general method is given in Section 12.5.

Section 12.3.1.4 in NS 3473 states that an inner force system is to be established around the supports in accordance with Section 12.6. Control of diagonal tension capacity for a direct load applied at a distance $a \leq 2d$ from the edge of the support can be performed with the simplification of multiplying the load with the factor $a/2d$ when establishing the shear force. For loads that are approximately evenly distributed one can, as a simplification, use the value of the shear force in a critical section with distance d from the edge of the support as the basis of calculating the diagonal tension capacity at the support. The compressive shear capacity must be established for the entire shear load that acts at the edge of the support.

As in the 1st edition of NS 3473, the shear reinforcement can only be included in the calculations if it fulfils the minimum requirements (for beams, here given in Section 18.3.6). The reinforcement must consist of stirrups or stirrups together with bent rods from the longitudinal reinforcement, and also here at least half of the necessary reinforcement must consist of stirrups. Maximum distance between the stirrups, and more information regarding placing of reinforcement is also given.

Design for shear capacity following the simplified method is given below.

Diagonal shear capacity without shear reinforcement

For a structural member without shear reinforcement, the diagonal tension capacity is given in Section 12.3.2.1 of NS 3473 as

$$V_{cd} = V_{co} = 0.33 \times \left(f_{td} + \frac{k_A A_s}{\gamma_c b_w d} \right) \times b_w d k_v \leq 0.66 f_{td} b_w d k_v \quad (8.9)$$

where

- f_{td} is the design tensile strength of the concrete, defined in Section 10.4.2 of NS 3473
 $k_A = 100 \text{ kN/mm}^2$
 A_s is the cross sectional area of the tensile reinforcement with sufficient anchorage
 γ_c is the material coefficient, given in Table 4 in NS 3473
 b_w is the width of the beam's web
 d is the effective depth of the cross section from the compressive edge to the centre of gravity for the tensile reinforcement
 k_v is a scale correction factor of magnitude $1.5 - d/d_1$, $d_1 = 1.0 \text{ m}$, and has a lower limit of 1.0 and upper limit of 1.4

Capacity for shear and simultaneous axial compression/tension without shear reinforcement

Diagonal tension capacity for a structural member subjected to shear and simultaneous *axial compression* can according to Section 12.3.2.2 in NS 3473 be assumed as

$$V_{cd} = V_{cd1} \leq V_{cd2}, \quad (8.10)$$

where

$$V_{cd1} = V_{co} + 0.8 \frac{M_o}{M_f} V_f \quad (8.11)$$

$$V_{cd2} = \left(f_{td} k_v - \frac{0.25 N_f}{A_c} \right) b_w z_1. \quad (8.12)$$

We have

- $M_o = -N_f W_c / A_c$
 N_f is axial load, positive in tension
 V_f is design shear load for the cross section in studied state
 M_f is the moment in the cross section working simultaneously as the shear force V_f
 N_f / A_c , where A_c is the concrete cross section, is not to have a larger value than $0.4 f_{cd}$
 W_c is the concrete's elastic section modulus with respect to the cross sectional edge in tension or with the lowest pressure
 I_c is the second moment of area for the uncracked concrete section
 z_1 is the largest of $0.7d$ and I_c / S_c

The formula is based on similar theory as in the 1st edition of NS 3473. The capacity V_{cd1} can be apprehended as an expression for the capacity with regard to flexure-shear failure, i.e. when inclined cracks are assumed to develop from a flexural crack. As is seen from the formula, V_{co} , expressing the shear capacity

when the cross section is not exposed to axial load, is dependent on a modified tensile strength (f_{td}) and the reinforcement ratio $\rho = A_s/bd$. The influence from the tensile reinforcement A_s on the shear capacity can be argued for with basis in the effect that ρ is known to have on the compressive zone height for a cracked cross section, and effect that the compressive zone height has on the initiation of a flexural crack. The upper limit for V_{co} , $0.66f_{td}b_wdk_v$, gives a restriction on how much the compressive zone height can be increased by increasing the tensile reinforcement in the cross section. This will have effect in sections subjected to large moments.

In this edition of NS 3473, the longitudinal reinforcement is included as a term that is added to the tensile strength, instead of as a multiplier with the shear strength, as is the case in Equation (8.3). This means that the tensile reinforcement will give the same contribution to the capacity independently of the tensile strength, and that the necessary reinforcement amount in order to reach a high shear capacity increases proportionally with the tensile strength. This relation gives better conformity with experimental results (Thorenfeldt, 1990).

For beams with axial load, the compressive zone height for bending will be dependent on the ratio between moment and axial load. If this eccentricity is within the central core of the cross section, the elastic theory will lead to compression in the entire cross section. This is in accordance with the derivation of the second term in Equation (8.5) from the 1st edition of NS 3473. Here the distance from the centreline to the edge of the central core of the cross section is expressed as W/A for a homogeneous cross section. The moment $M_o = N(W/A)$ is therefore the moment that can be applied together with the axial load without flexural cracks initiating. In the formula for V_{cd1} , $\frac{M_o}{M_f} V_f = V_f N_f \frac{W_c/A_c}{M_f}$ can be apprehended as the part of the shear force that can be applied without flexural cracking occurring. As in the 1st edition, this assumes that the shear force is proportional with the moment in the section. The factor 0.8 in the formula can be interpreted as a purely empirical reduction factor, but it may also be assumed to cover the loss due to redistribution of effective compression stresses in reinforced cross sections due to shrinkage and creep, assuming a normal ratio for long time loading.

The maximum capacity V_{cd2} is a simplified expression for the capacity with regard to web-shear failure, where the principal tensile stresses at the centreline in the web exceeds the concrete's tensile strength. The derivation for this formula can be found in Part 6.3, Section 1.1 b), from the course material given in (Thorenfeldt, 1990).

The capacity for diagonal tension failure for shear with simultaneous *axial tension* is given in Section 12.3.2.3 in NS 3473 as

$$V_{cd} = V_{co} (1 - N_f / (1.5f_{td}A_c)) \geq 0. \quad (8.13)$$

In a section where bending moment occurs simultaneously as the axial tension, the capacity can be set to

$$V_{cd} = V_{co} (1 - M_o / |M_f|) \geq 0 \quad (8.14)$$

if this equation provides a larger capacity than the latter. Here we have

$$M_o = N_f W_c / A_c$$

W_c is the concrete's elastic section modulus with respect to the cross sectional edge in pressure

Diagonal shear capacity with shear reinforcement

For areas where the design shear load is larger than the capacity, $V_f \leq V_{cd}$, the beam needs shear reinforcement in accordance with Section 12.3.2.4 in NS 3473. The capacity for structural members with shear reinforcement distributed over the length can be assumed to be the sum of the capacity V_{cd} and an addition V_{sd} from the reinforcement,

$$V_{sd} = \sum (f_{sd} A_{sv} \sin \alpha) \quad (8.15)$$

V_{sd} can be explained using a truss model with 45° diagonals, placed within a height z from the longitudinal reinforcement. z can be chosen as $0.9d$ if the cross section has a pressure zone. f_{sd} is the design reinforcement strength, defined in Section 10.4.2 of NS 3473. A_{sv} is the shear reinforcement area, and α is the angle between the shear reinforcement and the structural member's system axis. For shear reinforcement that consists of units with centre distance s measured along the system axis, the capacity becomes

$$V_{sd} = \frac{f_{sd} A_{sv}}{s} z (1 + \cot \alpha) \sin \alpha \quad (8.16)$$

Using vertical stirrups, giving $\alpha = 90^\circ$, this capacity becomes

$$V_{sd} = \frac{f_{sd} A_{sv}}{s} z \quad (8.17)$$

Compressive shear capacity

The capacity for compressive shear failure is to be calculated as

$$V_{ccd} = 0.25 f_{cd} b_w z (1 + \cot \alpha) \leq 0.45 f_{cd} b_w z \quad (8.18)$$

according to Section 12.3.2.5 of NS 3473. Vertical stirrups give

$$V_{ccd} = 0.25 f_{cd} b_w z. \quad (8.19)$$

Also here z can be chosen as $0.9d$ if the cross section has a pressure zone. In this edition of NS 3473, no change in capacity due to an introduction of axial load is given, in contrary to the previous editions. It can be assumed that the formula gives a certain reserve for the increase in principal compressive forces that normal prestressing will induce. For prestressed beams the principal compressive forces should be considered closely. For I-beams with strengthened webs in the beam ends, the critical section will often be in the section where the web width changes.

Force contribution in the tensile reinforcement due to shear forces

NS 3473:1989 introduces a force contribution that should be included in the tensile reinforcement due to the formation of inclined cracking when a cross section is subjected to shear. With vertical stirrups this contribution is

$$F_{sv} = V_f - 0.5V_{sd}$$

as given in Section 12.3.4 in NS 3473. This is connected to anchorage failure as introduced in Section 8.2.3, and for prestressed beams with straight prestressing reinforcement this will only have effect when controlling the reinforcement's tensile capacity near the supports.

8.3.4 NS 3473:1992, 4th edition

In the 4th edition of NS 3473 only one relevant change has been made from the 3rd edition regarding procedures for calculating shear capacity. As in the previous edition, it is given that the capacity for structural members with shear reinforcement distributed over the length can be assumed to be the sum of the capacity V_{cd} and an addition V_{sd} from the reinforcement. However, in this edition it is specified that for calculations of V_{cd} in this situation one can use a scale correction factor $k_v = 1.0$ for structures where stirrups constitute the shear reinforcement.

8.3.5 NS 3474:1998, 5th edition

In the 5th edition of NS 3473, design for shear in Section 12.3 is expanded to include design of bars and shells in addition to beams and plates. The general information in the beginning of the section is mostly the same as in the previous editions, with minor adjustments to the presentation of the content as well as a few details added, for instance requirements regarding anchorage of the reinforcement.

The formula for diagonal tension capacity of a structural member without shear reinforcement (Equation (8.9)) has been given minor adjustments (0.33 and 0.66 is changed to 0.3 and 0.6), rendering

$$V_{cd} = V_{co} = 0.3 \times \left(f_{td} + \frac{k_A A_s}{\gamma_c b_w d} \right) \times b_w d k_v \leq 0.6 f_{td} b_w d k_v \quad (8.20)$$

The formula for diagonal tension failure for shear with simultaneous axial pressure has also had minor alterations for clarification, where V_f/M_f has been given an absolute value sign.

Equation (8.14) has been changed from $V_{cd} = V_{co} (1 - M_o/|M_f|) \geq 0$ to $V_{cd} = V_{co} \left(1 - \frac{\epsilon_s}{\epsilon_{sy}} \right)$, where ϵ_s is the strain in the most stressed tensile reinforcement calculated from all simultaneously acting loads, including effects from restraints. With this calculation of V_{cd} , no part of the tensile reinforcement in the considered section should have a larger strain than ϵ_{sy} .

The formula given for compressive shear capacity has a minor change in factor (from 0.25 to 0.3):

$$V_{ccd} = 0.3f_{cd}b_wz(1 + \cot \alpha) \leq 0.45f_{cd}b_wz \quad (8.21)$$

8.3.6 NS 3473:2003, 6th edition

In the 6th edition of NS 3473, no changes have been made to the relevant sections from the 5th edition regarding shear capacity.

8.4 Shear calculations in EC2

The beams in The Hulvågen Bridge will be controlled for shear capacity in a similar manner that was performed when the bridge was designed, using NS 3473:1977. As mentioned in the introduction to this chapter, the shear formulas have developed much over the years, and it can be assumed that the newer formulas provide more accurate results than the previous.

Several of the shear capacity formulas presented in NS 3473:1977 are theoretical, and can be derived based on assumed failure mechanisms. They show the capacity contributions of each component (concrete, shear reinforcement, axial load) clearly. This may give the possibility to provide good approximations of the capacity, but the shear problem is complex and perhaps not all factors are taken into account. The shear capacity formulas presented in EC2 are purely empirical, and should therefore correspond well with observed shear capacities in real structures.

It has been decided to perform shear calculations of the beams in The Hulvågen Bridge using the shear capacity formulas presented in EC2, as a form of control of the capacity formulas used in NS 3473:1977. These calculations will also illustrate whether or not the bridge has sufficient capacity using today's design regulations. The calculations will provide a stronger basis for evaluating how safe the structure can be considered with regards to shear capacity of the beams.

Shear capacity calculations are presented in Section 6.2 of EC2. Unlike for NS 3473:1977, the shear capacity are only to be controlled in two sections. Section 6.2.1(8) states that for members that predominantly are subjected to uniformly distributed loading, the diagonal tension capacity $V_{Rd,c}$ or $V_{Rd,s}$ does not need to be checked at a distance less than d from the edge of the support, d being the effective depth of the cross section. If it is found that shear reinforcement is required, the calculated reinforcement amount must be continued to the support. The compressive shear capacity $V_{Rd,max}$ should always be controlled for the design shear load working at the support.

8.4.1 Members not requiring design shear reinforcement

The shear capacity of members not requiring design shear reinforcement is given in Section 6.2.2 of EC2. When no shear reinforcement is required on the basis of the design shear calculation, minimum shear reinforcement for beams should nevertheless be provided in accordance with Section 9.2.2 in EC2.

Diagonal tension capacity

Section 6.2.2(1) states the capacity for the diagonal tension failure for general members, given by Equation (6.2.a) in EC2 with a minimum value given by Equation (6.2.b). For prestressed members these requirements are valid for regions that are cracked in bending. However, for regions that are uncracked in bending the shear resistance of the prestressed members should be limited by the tensile strength of the concrete. In these regions the shear resistance is given by Equation (6.4) in EC2. It shall be shown in Section 9.3 that the considered section of the beam is not cracked in bending. It is therefore Equation (6.4) that is relevant for these calculations, and only this equation will be reproduced here. We have

$$V_{Rd,c} = \frac{I b_w}{S} \sqrt{(f_{ctd})^2 + \alpha_l \sigma_{cp} f_{ctd}}, \quad (8.22)$$

with the parameters

- I as the second moment of area
- b_w as the width of the cross section at the centroidal axis, i.e. the width of the web for the considered composite beam
- S as the first moment of area above and about the centroidal axis
- $\alpha_l = l_x / l_{pt2} \leq 1.0$, with l_x and l_{pt2} explained below
- $\sigma_{cp} = N_{Ed} / A_c$ in MPa, as the concrete compressive stress at the centroidal axis due to prestressing (N_{Ed} positive in compression)
- f_{ctd} as the design tensile strength of the concrete, defined by Equation (3.16) in EC2

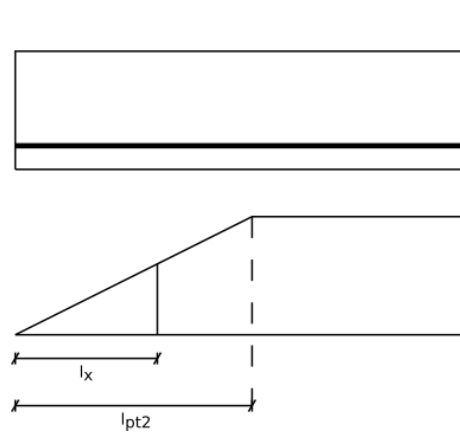


Figure 8.2: Gradual transfer of prestress by bond

As mentioned earlier, the prestressing force in pre-tensioned members will be gradually transferred to the concrete by bond. Along this transmission length the axial load in the concrete will increase gradually, from zero axial load in the beam end until the entire prestressing load has been transmitted to the concrete. In

contrary to NS 3473:1977 where this effect is neglected, EC2 includes this in the capacity control. The factor α_l reduces the contribution to the diagonal tension capacity from the prestressing axial load, assuming a linear increase in the axial load. As Figure 8.2 illustrates, l_x is the distance of the considered section from the starting point of the transmission length, which for these beam will correspond to the distance from the beam end. l_{pt2} is the upper bound value of the transmission length of the prestressing element. This value is calculated in Section 8.10.2.2 in EC2, as

$$l_{pt2} = 1.2l_{pt}.$$

l_{pt} is the basic value of the transmission length, given by

$$l_{pt} = \frac{\alpha_1 \alpha_2 \phi \sigma_{pm0}}{f_{bpt}}.$$

Here,

- α_1 = 1.0 for gradual release
- = 1.25 for sudden release
- α_2 = 0.25 for tendons with circular cross section
- = 0.19 for 3 and 7-wire strands
- ϕ is the nominal diameter of the tendon
- σ_{pm0} is the tendon stress just after release

f_{bpt} is the constant bond stress by which the prestressed is assumed to be transferred to the concrete at release of the tendons. It is given by

$$f_{bpt} = \eta_{p1} \eta_1 f_{ctd}(t),$$

where

- η_{p1} is a coefficient that takes the type of tendon and the bond situation at release into account
- = 2.7 for indented wires
- = 3.2 for 3 and 7-wire strands
- η_1 = 1.0 for good bond conditions
- = 0.7 otherwise, unless a higher value can be justified with regard to special circumstances in execution
- $f_{ctd}(t)$ is the design tensile value of strength at time of release,
- $f_{ctd}(t) = \alpha_{ct} \times 0.7 f_{ctm}(t) / \gamma_c$. See Sections 3.1.2(8) and 3.1.6(2)P in EC2.

Shear compressive capacity

The shear compressive capacity is denoted $V_{Rd,max}$ and limits the capacity of the member through crushing of the concrete.

For members without shear reinforcement, the design shear force V_{Ed} should always satisfy the condition given in Equation (6.5) in EC2,

$$V_{Ed} \leq V_{Rd,max} = 0.5b_w d \nu f_{cd}. \quad (8.23)$$

Here,

- b_w is the width of the cross section at the centroidal axis, i.e. the width of the web for the considered composite beam
- d is the effective beam depth
- $\nu = 0.6(1 - f_{ck}/250)$ is a strength reduction factor for concrete cracked in shear
- f_{cd} is the design compressive strength of the concrete, defined by Equation (3.15) in EC2

8.4.2 Members requiring design shear reinforcement

In regions where the design shear force exceeds the design shear resistance of the member without shear reinforcement, $V_{Ed} > V_{Rd,c}$, sufficient shear reinforcement should be provided so that $V_{Ed} \leq V_{Rd,c}$.

The shear capacity for members with shear reinforcement is based on a truss model. The shear resistance is given in EC2 as the smaller value of $V_{Rd,s}$ and $V_{Rd,max}$, the first equation denoting the diagonal tension capacity and the second the compressive shear capacity.

Diagonal tension capacity

For the diagonal tension capacity the entire shear load shall be taken up by the shear reinforcement, any contribution from the concrete is neglected in these empirical formulas. Assuming vertical shear reinforcement, the diagonal tension capacity is given in Equation (6.8) of EC2 as

$$V_{Rd,s} = \frac{A_{sw}}{s} z f_{ywd} \cot \theta, \quad (8.24)$$

where

- A_{sw} is the cross sectional area of the shear reinforcement
- s is the spacing of the stirrups
- z is the inner lever arm
- f_{ywd} is the design yield strength of the vertical shear reinforcement in the web, defined in Figure 3.8 of EC2
- θ is the angle between the concrete compression strut and the beam axis perpendicular to the shear force

According to EC2, the angle θ can be chosen between the values 21.8° and 45° , so that $1 \leq \cot \theta \leq 2.5$. The NPRA have recommended an upper limit of $\cot \theta = 2.0$ for design of bridges, which corresponds to a maximum crack angle of

26.6° (Statens Vegvesen, 2015). Choosing a smaller crack angle will increase the diagonal tension capacity. Furthermore EC2 states that if Equation (6.10) in EC2 is taken into use for calculations of the compressive shear capacity, f_{ywd} should be reduced to $0.8f_{ywk}$, where f_{ywk} is the characteristic yield strength of the vertical shear reinforcement in the web.

Compressive shear capacity

The compressive shear capacity is given for vertical shear reinforcement in Equation (6.9) in EC2 as

$$V_{Rd,max} = \frac{\alpha_{cw} b_w z \nu_1 f_{cd}}{\cot \theta + \tan \theta}, \quad (8.25)$$

where

- α_{cw} is a coefficient taking the state of the stress in the compression chord into account, defined in NA.6.2.3(3)
- ν_1 is a strength reduction factor for concrete cracked in shear, defined in NA.6.2.3(3)

The favourable effect from compression in the cross section is included in α_{cw} , to a certain degree. The factor is defined in NA.6.2.3(3), dependent on the ratio between the compressive stress from prestressing and the design compressive strength of the concrete, σ_{cp}/f_{cd} . ν_1 is a strength reduction factor for concrete cracked in shear, defined in NA.6.2.3(3). The crack angle θ is also included in the formula for the compressive shear capacity, and must be chosen as the same angle used when establishing diagonal tension capacity. For compressive shear capacity the capacity will decrease for lower values of θ .

8.5 Anchorage capacity

Sections 8.3 and 8.4 contain information regarding calculations of diagonal tension capacity and compressive shear capacity of beams according to NS 3473 and EC2. As introduced in Section 8.2, anchorage failure is the third failure mechanism that must be controlled in order for the shear control of the beam to be complete. A common procedure for controlling the anchorage capacity will be presented in this chapter.

The overview of the development of the shear capacity formulas in the various editions of NS 3473 which is given in the previous sections shows that anchorage failure has not been introduced into NS 3473 before the 3rd edition, NS 3473:1989. The reinforcement layout in the NIB beams at The Hulvågen Bridge suggest that the failure mechanism may nevertheless have been designed for before the release of NS 3473:1989. In EC2, Section 6.2.3(7) contains regulations regarding how to handle anchorage failure.

For control of anchorage failure for shear reinforced beams it is assumed that the first crack initiates at the edge of the support and exceeds into the compression zone with an approximate angle θ as seen in Figure 8.3.

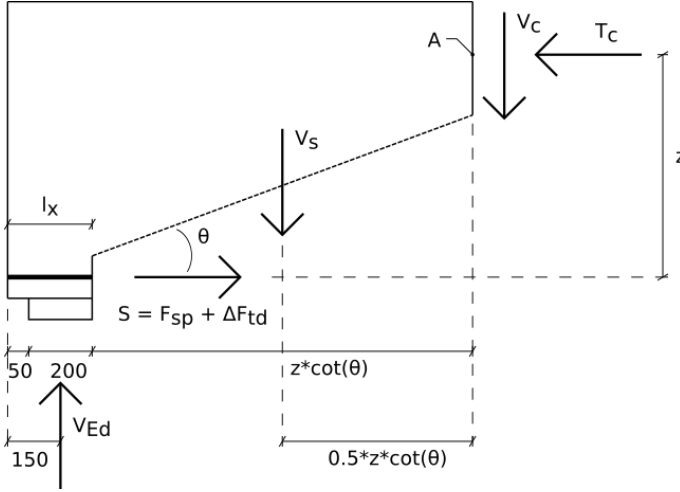


Figure 8.3: Force model for anchorage failure

The anchorage calculations that are performed in this thesis will be somewhat simplified. It is assumed that the entire shear load is taken by the shear reinforcement, $V_s = V_{Ed}$, while the contribution to the shear capacity from the concrete is neglected, $V_c = 0$. If the region has sufficient amount of reinforcement, this simplification will be relatively close to reality. Furthermore it can be assumed that the width of the support is relatively small compared to the inner moment arm z , and that it can be neglected when considering the horizontal distance from the reaction force at the support to the end of the cracked area. If the crack angle θ is arbitrary, the horizontal distance from the support to the end of the crack will be $z \cot \theta$. Assuming vertical shear reinforcement, moment equilibrium about point A renders the following force in the tensile reinforcement,

$$\sum M = V_{Ed} z \cot \theta - S z - 0.5 V_{Ed} z \cot \theta = 0,$$

which gives

$$S = \frac{1}{2} V_{Ed} \cot \theta. \quad (8.26)$$

As mentioned in Section 8.2.3, the diagonal crack will lead to an additional force ΔF_{td} in the tensile reinforcement. This force arises because the vertical shear reinforcement is only able to take up the vertical component of the stresses that cause the cracking (Lenschow, 1979). Because the principal tensile stresses act perpendicular to the crack, there will also be a horizontal component of the stresses, which must be taken up by the tensile reinforcement. For prestressed concrete this additional force ΔF_{td} will act in addition to the prestressing load F_{sp} that is already acting in the prestressed strands.

Taking the gradual transfer of the prestressing by bond into account, the prestressing load in the considered section can be established by reducing the total

prestressing load F'_{p0} in accordance with the regulations provided in Section 6.2.2(2) in EC2. Figure 8.2 illustrates the reduction of the prestressing force near the beam end. If the prestressing strands reach to the end of the beam, l_x will denote the distance from the considered section to the beam end, and the total transmission length l_{pt2} is calculated according to Section 8.10.2.2 in EC2. The prestressing load in the considered section will then become

$$F_{sp} = \frac{l_x}{l_{pt2}} F'_{p0}. \quad (8.27)$$

The additional force that arises due to the cracking can then be established using Equations (8.26) and (8.27),

$$\Delta F_{td} = S - F_{sp}. \quad (8.28)$$

Finally, it must be assured that sufficient horizontal anchorage reinforcement is placed at the beam end, in order to take up this additional force in the tensile reinforcement. This is done by assuring that the reinforcement area is sufficient so that yielding does not occur. The necessary amount of horizontal anchorage reinforcement is therefore given as

$$A_s = \frac{\Delta F_{td}}{f_{yd}}, \quad (8.29)$$

where f_{yd} is the design yield strength of the reinforcement. As stated in Section 8.2.3, the anchorage reinforcement is normally added in the form of horizontal stirrups stacked over each other at the beam end.

As the expression for S shows, the necessary amount of horizontal reinforcement is dependent on what assumptions that are made regarding the angle of the crack that will occur next to the support. In NS 3473:1977 it is given that the crack angle is $\theta = 45^\circ$, while for EC2 the crack angle can be chosen following restrictions presented in Section 8.4.2. As stated, the diagonal tension capacity of the beam increases with a lower crack angle. However, the compressive shear capacity decreases with a lower crack angle, and the expression for S also shows that the lower the angle is assumed to be, the higher the additional load at the beam end that require anchorage reinforcement will become. Because the same crack angle has to be used for all capacity controls of the beam, the choice of the crack angle should be based on an evaluation where the capacity regarding all three failure mechanisms are taken into consideration.

If the capacity of the anchorage reinforcement is insufficient and yielding initiates, deformation and crack propagation will occur until fracture. The tensile reinforcement may slip out of the concrete at the beam end, causing the whole beam to collapse. As stated in Section 8.2 anchorage failure can occur independently of diagonal tension capacity and compressive shear capacity. If the reinforcement that is placed at the beam end in order to anchor the additional tensile forces is insufficient, failure will occur.

It should be noted that using inclined shear reinforcement perpendicular to the crack may remove the force increase in the tensile reinforcement, which removes

the need for anchorage reinforcement. Inclined shear reinforcement will have the ability to take up both vertical and horizontal stress components acting in the concrete, and the tensile reinforcement will therefore not be additionally loaded due to the cracking (Lenschow, 1979).

8.6 Shear stresses at the interface between concrete cast at different times

The NIB beams in The Hulvågen Bridge is in this thesis assumed to work together with the bridge deck as a composite beam in order to resist the acting shear loads. For this assumption to be valid it is necessary to control that the interface between the two parts of the composite beam has sufficient capacity to work as a continuous cross section. The basis for this will be provided in this chapter.

8.6.1 Shear stresses induced by shear loads

The stresses that a shear force will induce in a concrete cross section depends largely on the state of the cross section. The concrete cross section can either be uncracked (stage I) or cracked (stage II).

A concrete cross section in the uncracked stage can be considered linear elastic on both the tension and compression side. Here the shear stress will be distributed as a parabola over the height of the cross section, with a maximum value

$$\tau_{\max} = \frac{3}{2} \frac{V_{Ed}}{A_c}. \quad (8.30)$$

at the neutral axis, i.e. at the centre of gravity for the concrete cross section. V_{Ed} is the design shear load in the section and A_c is the concrete cross section.

When bending cracks occur in the tension side of the cross section, the neutral axis will move to the compression side of the cross section. Assuming that the concrete will have no capacity regarding tensile stresses in the cracked state, the stress distribution described for the uncracked section will gradually change to a distribution where the shear stress is constant between the tensile reinforcement and the neutral axis, and then gradually decrease in a parabola shaped manner to zero stress at the compression edge. The maximum shear stress is then

$$\tau_{\max} = \frac{V_{Ed}}{b_z} \quad (8.31)$$

The two situations are illustrated in Figure 8.4 for a cross section which is exposed to tension in the upper part, i.e. the situation that will occur near the beam end of a continuous structural system.

The situation with constant shear stress in the tensile zone assumes that the cracks can transfer tensile, compression and shear stresses. This can occur through friction in the cracks (Stemland, 2007). The state with constant shear stress will nevertheless be an idealization compared to what will actually occur when a stable system of inclined cracking has been established.

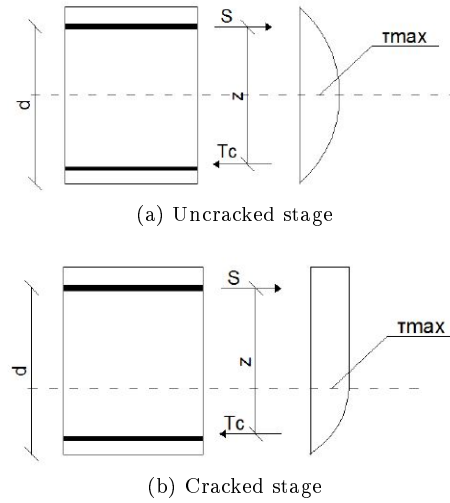


Figure 8.4: Distribution of shear stresses (Munthe-Kaas, 2014)

8.6.2 Shear stresses at the interface

Using prefabricated concrete beams with, a bridge deck cast directly onto the beams, will lead to a construction joint or interface which separates the two concretes cast in different points in time. Avoiding mutual slippage at this interface level will greatly increase the moment of inertia for the composite cross section, which increases the load-bearing capacity of the cross section. Coupling of the two members is therefore desired.

Shear stresses will be induced in the contact area between the two coupled members. The longitudinal shear stresses are caused by the difference in bending moment over the length of the member (Kovačovic, 2013), as illustrated in Figure 8.5. At each level of the cross section the stress is transmitted by the monolithic behaviour of the concrete. At the interface level however, the stresses must be transferred by the shear resistance of the coupling between the two members.

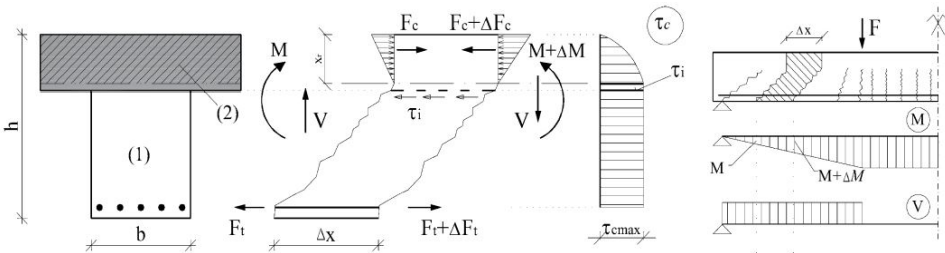


Figure 8.5: Shear stresses in the interface between concrete cast at different times (Kovačovic, 2013)

The beam in the figure is loaded with tension in the lower edge, rendering the the opposite distribution of shear stresses compared to what is given in Figure 8.4b. Furthermore the shear stress distribution illustrated in Figure 8.5 does not take the change in cross section into account. In reality the increase in b from the beam to the deck will give an abrupt reduction in τ at the interface, in addition to the gradual decrease.

In general it will be conservative to consider a cracked cross section for the control of the shear resistance at the interface. Moment equilibrium of the element given in Figure 8.5 gives the same expression for τ_{\max} as given for a cracked cross section in Equation (8.31). When considering the expression for the shear stress it is clear that it will be conservative to use the smallest width of the two surfaces in the interface, in order to obtain the largest possible τ_{\max} . Furthermore the interface should be controlled at the support in order to have the largest design shear load V_{Ed} acting in the section.

8.6.3 Shear resistance at the interface

Shear resistance at the interface is dependent on cohesion, friction and shear reinforcement (Kovačovic, 2013). Cohesion is the ability of two contact surfaces to resist shear loading without any compressive force up to the point of mutual slippage. Friction depends on the contact force perpendicular to the interface area and the coefficient of friction μ . Both cohesion and friction for a specific interface are dependent on the roughness of the interface.

Shear reinforcement is the factor that has the largest effect on the shear resistance of the interface. Transverse shear reinforcement with a certain angle to the interface can provide a large contribution to the total shear resistance of the interface.

NS 3473:1977 does not provide formulas for control of shear stresses at the interface between concrete cast at different times, indicating that this phenomenon might not have been considered in older structures with prefabricated elements. The capacity will in this thesis therefore be controlled using EC2. Section 6.5.2 of EC2 provides the calculation basis. The design shear resistance at the interface is given in Equation (6.25) in EC2 as

$$v_{Rd} = cf_{ctd} + \mu\sigma_n + \rho f_{yd} (\mu \sin \alpha + \cos \alpha) \leq 0.5\nu f_{cd} \quad (8.32)$$

where

- c and μ are factors depending on the roughness of the interface, given in Section 6.2.5(2) of EC2
- σ_n is the stress normal to the interface
- $\rho = A_s/A_i$
- A_s is the area of the reinforcement crossing the interface with adequate anchorage at both sides of the interface
- A_i is the area of the joint
- α is the angle between the reinforcement and the interface surface, limited to $45^\circ \leq \alpha \leq 90^\circ$

ν is the strength reduction factor for concrete cracked in shear, defined in NA.6.2.3(3)

The three terms in the equation represent the contribution to the total shear resistance from cohesion, friction and shear reinforcement, respectively.

The upper limit of the shear resistance, $v_{Rd} \leq 0.5\nu f_{cd}$, is related to the compressive shear capacity of members requiring design shear reinforcement in accordance with EC2 (Statens Vegvesen, 2013). Assuming no axial load in the section, NA.6.2.3(3) in EC2 gives $\alpha_{cw} = 1$, and Equation (8.25) can be rewritten to the form

$$\frac{V_{Rd,max}}{b_w z} \leq \frac{\nu_1 f_{cd}}{\cot \theta + \tan \theta} = \nu_1 f_{cd} \sin \theta \cos \theta. \quad (8.33)$$

With $\nu_1 = \nu$ in accordance with NA.6.2.3(3) in EC2 and choosing $\theta = 45^\circ$, the equation becomes $\frac{V_{Rd,max}}{b_w z} = v_{Rd} \leq 0.5\nu f_{cd}$, which gives the upper limit of the shear resistance at the interface between concrete cast at different times.

Chapter 9

Shear capacity control

In this chapter the design loads acting on the critical beam that were established in Chapter 7 will be used to control the shear capacity of the composite beams. The diagonal tension capacity and the compressive shear capacity will first be established using the formulas presented in Chapter 8 for the second edition of NS 3473, NS 3473:1977, which is the standard that was valid when the bridge originally was designed. Furthermore the capacities will be controlled using the updated shear capacity formulas given in EC2, which is in use today. In addition the anchorage capacity of the beam end will be established, and further controls will be made of the interface between the NIB beam and the bridge deck. Concluding remarks regarding the shear capacity of the critical beam will be provided in the last section. Here, the assumptions that have been made regarding the continuity of the bridge will also be assessed.

9.1 Basis for the capacity calculations

Capacity control is performed in the Ultimate Limit State.

As seen in Chapter 5, the composite beam consists of a NIB beam and bridge deck of different concrete qualities. For the shear calculations in this chapter the material properties will in general be decided by the NIB beam. This is because it is the beam web that will be critical with regards to shear, and as seen in Section 8.2 any failure mechanism will occur here.

For all calculations in this chapter it is assumed that the NIB beam and bridge deck work together as a composite beam with full coupling between the two members, so that d , h' and z are calculated with basis in the total composite beam height $h_{\text{tot}} = h_{\text{beam}} + h_{\text{deck}} = 1435 \text{ mm} + 250 \text{ mm} = 1685 \text{ mm}$. The validity of this assumption will be looked further into in Section 9.5.

The NIB beams in The Hulvågen Bridge are supported at the beam ends by rubber bearings. The working drawings of the transversal supports made by Johs Holt AS, given in Appendix A, show the planned layout of the support. Here it is given that rubber supports of type Lasto-Block or similar with capacity of 75 MPa

and dimensions 200 x 300 x 52 mm shall be used. With the width of the lower flange in the NIB beam of 300 mm as Figure 5.1a shows, the support will in the longitudinal direction reach 200 mm.

None of the drawings that are provided in Appendix A describe how far from the beam end the support should be placed. An image taken from the excursion in May is given in Figure 9.1, and it shows how the rubber bearing is placed far out towards the beam end. With a bearing length of 200 mm it can be assumed that choosing a distance from the outer edge of the bearing to the beam end of 50 mm should be approximately correct. This image is of one of the two inner beams at the eastern end of the bridge, taken from inside the inspection hatch. The beam that is considered in this thesis lies on the west side of the bridge. It is assumed that the support in the image is representative for the layout of the rest of the supports in the bridge.



Figure 9.1: Image from the excursion showing the rubber bearing at the beam end

It should be noted that for the diagonal tension capacity and the compressive shear capacity it will be conservative to overestimate the distance from the beam end to the support. A large distance here will decrease the distance from the support to the cross sectional change, where the utilization of the shear capacity will increase largely for a given design load. However, when considering anchorage capacity, it will be conservative to underestimate the distance from the beam end to the support. This will be shown in Section 9.4.

Assuming a 50 mm gap from the beam end to the outer edge of the support, and a total length of the support of 200 mm, the distance from the beam end to the middle of the support is 150 mm, while the distance from the beam end to the inner edge of the support is 250 mm.

Over the previous chapters it has been established that there are several factors that will cause variation in the shear capacity near the beam end. For design loads acting on the beam, variation will primarily be caused by the gradual transmission of the prestressing forces and the coating of certain prestressing strands. The change in the cross section at the beam end (width of the beam web) may also have

a slight effect on the distribution of loads. As mentioned in the introduction to Chapter 6, these effects are neglected when establishing the design loads. However, for calculations of capacity which is performed section by section, these effects will be included.

For capacity calculations there are in addition several more effects that will cause variation in the beam ends. These effects are for instance caused by variation in shear reinforcement, or non-continuous effects from the design loading such as the axle load. Table 9.1 shows an overview of all the factors that will lead to abrupt or gradual changes in the shear capacity.

Table 9.1: Factors near the beam end causing variation in the shear capacity

Varying factor	Distance from beam end [mm]	Distance from support [mm]
Gradual transmission of prestressing loads	0, 2000, 4000, 7000	-
Concrete cross section (width of the web)	1425	1275
Shear reinforcement amount (change in central distance)	1800, 5800, 9500	1650, 5650, 9350
Number of uncoated prestressing strands (causes variation in d and h')	2000, 4000, 7000	1850, 3850, 6850
Design axial load (change in γ_D from unfavourable to favourable)	3170	3020
Axle load from traffic load (gives jump in design shear load)	3250	3100
Part of cross section in tension (gives jump in d)	4100	3950
Design shear load and moment	Continuously	Continuously

9.2 NS 3473:1977

For calculations according to NS 3473:1977, the diagonal tension capacity and compressive shear capacity must be controlled over a region near the beam end. As Section 8.3.1 has shown, the capacity depends on the design load that are acting in the section, and will therefore vary in accordance with the loading. In Chapter 7 the design loads were established over the entire length of the beam. In this section these design loads have been used in order to establish the diagonal tension capacity and compressive shear capacity over a majority of the beam.

Because the shear utilization will be highest near the critical support it is decided not to include the entire beam when displaying the resulting capacities in this section. As Table 9.1 illustrates, the factor that will cause an abrupt change in the shear reinforcement capacity at the furthest distance from the support is the

reduction in the shear reinforcement amount which occurs at a distance 9350 mm from the support. In order to include the effect of this in the displayed results, it is decided to include the shear capacities that have been calculated up to a distance of 9400 mm from the support.

As established in Section 8.3.1, no indications that the gradual transmission of prestressing loads near the beam ends is included for capacity calculations according to NS 3473:1977 has been found. Because it is uncertain whether or not this effect has been included in the original calculations of The Hulvågen Bridge, it is decided to assume in these calculations that the full amount of prestressing load acts on the beam from the beam end.

9.2.1 Compressive shear capacity

The capacity regarding compressive shear failure in NS 3473:1977 is given in Equation (8.1), reproduced here for simplicity,

$$V_d = 0.3f_c b d. \quad (9.1)$$

The concrete compressive strength $f_c = 22.4$ MPa is calculated in Appendix D. The web width varies from $b = 300$ mm for the beam ends to $b = 100$ mm for the regular cross section which begins at a distance $x = 1425$ mm from the beam end. The effective cross sectional depth d from the compressive edge to the centre of gravity for the tensile reinforcement varies, depending on whether tension is in the upper or lower edge, and depending on the number of prestressing strands that are uncoated. The values for d for the various distances from the beam end are calculated in Appendix D. As Section 5.1.2 indicates, the reinforcement in the composite cross section is constituted by reinforcement bars of several steel qualities. The effective cross sectional depth for each section i is therefore averaged using the area, yield strength and effective cross sectional depth of each contribution to the total reinforcement in the section,

$$d_i = \frac{f_{pdi} A_{pi} d_{pi} + \sum f_{sdi} A_{si} d_{si}}{f_{pdi} A_{pi} + \sum f_{sdi} A_{si}}, \quad (9.2)$$

where the subscript p denotes the prestressing reinforcement and the subscript s denotes the contribution from the regular reinforcement. The resulting compressive shear capacity V_d based on Equation (9.1) is calculated for sections with 50 mm distances in the considered region of the beam using Excel.

Furthermore, the compressive shear capacity is limited by the criteria that together with other design loads the design shear force can not give a larger principal compressive stress than the design concrete compressive strength f_c . For these calculations, an uncracked concrete cross section is to be assumed (Lenschow et al., 1978), i.e. theory of elasticity can be used.

The principal compressive stress is based on Mohr's circle and is given by Sørensen (2013) as

$$\sigma_1 = \frac{\sigma_x + \sigma_y}{2} + \sqrt{\left(\frac{\sigma_x - \sigma_y}{2}\right)^2 + \tau^2}.$$

Lenschow et al. (1978) show that σ_x is the stress occurring in the cross section due to the axial load, while τ is the maximum occurring stress due to the shear load. Furthermore $\sigma_y = 0$ because it is assumed that the normal stresses in the vertical direction are negligible. We have

$$\sigma_x = \frac{N_\gamma}{A_c} \quad \text{and} \quad \tau = \frac{V_\gamma S}{Ib}.$$

N_γ and V_γ are the design axial and shear load, A_c is the area of the composite concrete cross section and b is the width of the beam web. I is the cross section's second moment of area, while S is the cross section's first moment of area, defined as

$$S = \int y dA = \sum y_i A_i.$$

Here y_i is the distance from the centre of gravity for the area A_i to the centre of gravity, or neutral axis, for the total cross section. The maximum first moment of area occurs if the whole cross sectional area over or under the neutral axis is included, and will contribute to give the maximum principal compressive stress σ_1 .

All parameters in the expression for the principal compressive stress σ_1 will vary for varying distance from the beam end x , and the stress has to be controlled over a region from the critical beam end. This has been done in the excel sheet. A_c , S and I used in the excel sheet are calculated for both concrete cross sections in Appendix D.

As given in Equation (8.2), the compressive shear capacity can be increased for prestressed structures if certain criteria are fulfilled. These criteria are that the shear reinforcement is placed approximately in the direction of the principal tensile stress and that the maximum distance between the shear reinforcement is $0.3d$ or 200 mm. The direction of the principal tensile stress will be perpendicular to where the inclined cracks appear. In the second edition of NS 3473 it is assumed that cracks occur at an angle of 45° from the system axis. For the prestressed NIB beams in this bridge, the shear reinforcement is placed vertically, i.e. 45° away from the direction of the principal tensile stress. This means that the first criterion is not fulfilled, and so the increased capacity for compressive shear should not be used for this bridge.

Results

Figure 9.2 shows the design shear load together with the compressive shear capacity. The compressive shear capacity decreases with two thirds at a distance of 1275 mm from the critical support. This is due to the change in the concrete cross section which occurs at 1425 mm from the beam end, from the strengthened cross section with web width of 300 mm to the regular cross section with web width of 100 mm.

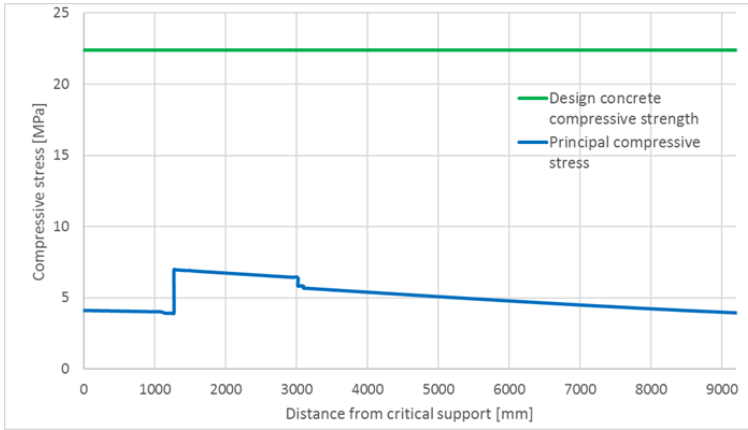


Figure 9.3: Control of principal compressive stress related to compressive failure

$$\eta = \frac{\sigma_1}{f_c} = \frac{7.0}{22.4} = 0.31. \quad (9.4)$$

Comparing the utilization ratios in Equations (9.3) and (9.4) shows that the latter indicates that the capacity of the cross section is less utilized than the first. This may indicate that Equation (9.1) will underestimate the capacity of this beam, and is in line with the fact that Equation (9.1) was considered a relatively safe lower limit of the capacity, as stated in Section 8.3.1.

9.2.2 Diagonal tension capacity

As described in Chapter 8, the formulas for diagonal tension capacity distinguish between flexure-shear failure and web-shear failure. The capacity for each failure mode is reproduced here in the given order for simplicity,

$$V_d = f_v (bd + 75A_s) + f_s A_{sv} h' + 0.2V_\gamma h N_\gamma / M_\gamma, \quad (9.5)$$

$$V_d = (2f_v + 0.2N_\gamma / A_c) bd + f_s A_{sv} h'. \quad (9.6)$$

It is clear from the formulas that the contribution from the concrete itself, the shear reinforcement and the axial load from the prestressing to the total capacity can be separated. The effect that the shear reinforcement and the axial load have on the shear capacity will be looked further into after the capacities have been established, by excluding the factors one by one.

Several material and cross sectional parameters need to be established for the calculations of the diagonal tension capacities. The design concrete shear strength $f_v = 0.6 \text{ MPa}$ is calculated in Appendix D. Furthermore the longitudinal and shear reinforcement steel's design strength f_s are calculated for all steel types in the same appendix. The total height of the composite cross section is $h_{\text{tot}} = 1685 \text{ mm}$.

The remaining parameters that are included in the formulas vary over the length of the beam, and all values are calculated in Appendix D for all relevant distances x from the critical beam end. The web width b varies as explained for the compressive shear capacity, with associated variations in the cross sectional area A_c .

The tensile reinforcement A_s and the shear reinforcement A_{sv} have been introduced in Section 5.1.2. The longitudinal reinforcement consists of prestressing steel and regular steel (P10 and P11) in the NIB beams, as well as regular steel in the bridge deck. When tension is in the upper part of the beam the prestressing steel in the upper part, P10 and the reinforcement in the bridge deck will be included, whereas when the tension is in the lower part of the beam P11 and the prestressing steel in the lower part of the beam will be included.

The areas and centres of gravity for the longitudinal reinforcement are calculated in Appendix D. For tension in the lower part of the beam, the coating of prestressing strands has been taken into consideration, resulting in parameters that are valid for certain ranges from the beam end. The effective cross sectional depth d and the distance between the tensile and compressive reinforcement's centre of gravity h' vary accordingly. h' is averaged based on the steel qualities' yield strength in the similar manner as d . Furthermore it is assumed that prestressing reinforcement in the compression zone acts as compressive reinforcement relative to the concrete, and that the initial tensile stresses in the prestressing steel will not affect this relation.

The shear reinforcement includes the stirrups denoted P2 in Figure 5.1b as introduced in Section 5.1.2. Potential shear reinforcement in the bridge deck has been neglected for these calculations, as explained in Section 5.1.2. The area A_{sv} is given as the cross sectional area of the shear reinforcement divided by the centre distance measured perpendicular to the reinforcement direction. P2 has varying central distance over the length of the beam, as can be seen in Figure 5.1b. The stirrups are placed very densely at the beam ends in order to take up transverse tensile stresses from the prestressing reinforcement as explained in Section 5.1.3. When these stresses are taken up the stirrups may have remaining capacity which can be used to take up shear stresses, but in order to avoid overestimating their capacity these additional stirrups are neglected for these capacity calculations. Instead it is assumed that the stirrups are placed with central distance 100 mm from the beam end until a distance $x = 1800$ mm from the beam end. Between $x = 1800$ mm and $x = 5800$ mm the central distance is 150 mm. The central distance increases further to 200 mm for $x = 5800$ mm to $x = 9500$ mm, and from $x = 9500$ mm to mid-span the central distance is 300 mm. The A_{sv} for the various ranges are calculated in Appendix D.

Results

Figure 9.4 shows the design shear load together with the flexure-shear capacity given by Equation (9.5) and the web-shear capacity given by Equation (9.6). The diagonal tension capacity of the beam is for each section decided by the lowest of the two capacity graphs. It is clear that for the strengthened cross section, occurring from the beam end and to a distance of 1275 mm from the support (1425

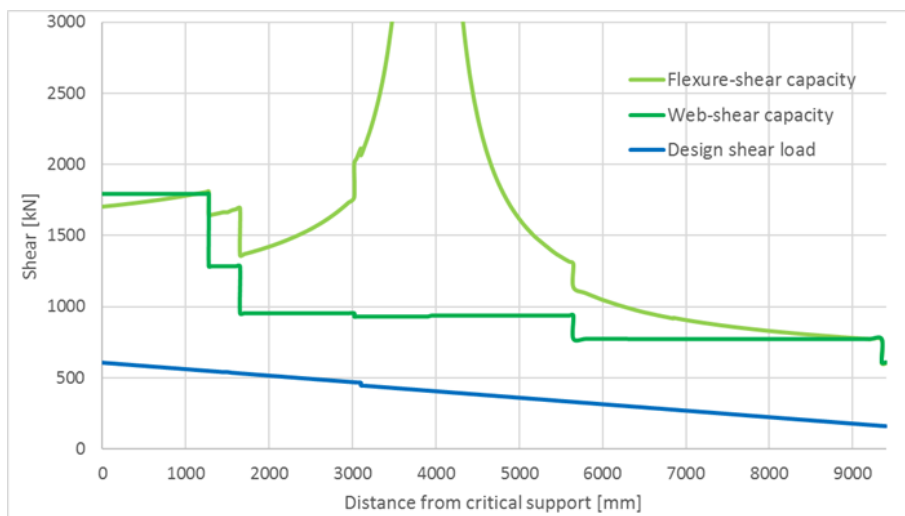


Figure 9.4: Capacity regarding diagonal tension failure

mm from the beam end), it is the flexure-shear capacity that limits the diagonal tension capacity of this beam, while for the rest of the beam the capacity is limited by the web-shear capacity. The critical section regarding both diagonal tension failure types is found at a distance of 1650 mm from the support, as can be seen in the figure. There, the utilization ratio of the diagonal tension capacities are

$$\text{Flexure-shear capacity: } \eta = \frac{V_\gamma}{V_d} = \frac{533}{1364} = 0.39$$

$$\text{Web-shear capacity: } \eta = \frac{V_\gamma}{V_d} = \frac{533}{955} = 0.56$$

Both capacity formulas are originally smooth formulas. However, Figure 9.4 shows that both graphs have jumps in several locations. Table 9.1 summarizes the factors that cause variations to the curve, and the effects they have are explained in further detail in the following paragraphs.

From the beam end both V_γ and M_γ decrease with increasing distance from the support. The flexure-shear capacity formula given in Equation (9.5) makes it evident that the capacity will increase for increasing V_γ and increase for decreasing M_γ . The fact that the capacity increases when both V_γ and M_γ decrease shows that the effect of M_γ overrides that of V_γ in this region. Furthermore, at a distance 1125 mm from the critical support the cross section is reduced, causing a reduction in the flexure-shear capacity. At distances 1650 mm, 5650 and 9350 mm from the critical support, the amount of shear reinforcement is reduced through an increase in the central distance of the P2 stirrups. This also causes reduction in the flexure-shear capacity.

At a distance of 3020 mm from the critical support, γ_D changes from 1.1 to 0.9,

reducing the value of N_γ . This gives a relatively large reduction in the primary moment M_0 , causing the total moment $M_{tot} = M_\gamma$ in V_d to be reduced. The reduction of M_γ has a positive effect on the capacity, while the reduction of N_γ has a negative effect on V_d . Figure 9.4 makes it evident that the change in moment outweighs the change in axial load, causing an increase of the total flexure-shear capacity. The small reduction of the flexure-shear capacity at the distance 3100 mm from the critical support is due to the axle point load from the traffic load. This gives a relatively large decrease in the design shear load V_γ while not affecting the design moment M_γ at this point, causing in total a reduction in the flexure-shear capacity. The increase in the number of prestressing strands (which increases A_s and gives variation in d) is not visible in the flexure-shear capacity curve.

At approximately 3950 mm from the critical support, the total design moment becomes zero because the moment from the prestressing load outweighs the moment from the self weight and traffic load exactly. As seen in Equation (9.5), the formula for flexure shear capacity has the design moment in the denominator. This causes the graph for the flexure-shear capacity to reach towards infinite here, as Figure 9.4 shows. In practise, the shear capacity in this area will always be limited by the web-shear capacity.

The graph for the web-shear capacity also displays several jumps in a similar manner to the flexure-shear capacity. At a distance 1275 mm from critical support the reduction of the web width has a large effect on the web-shear capacity. Furthermore at distances 1650 mm, 5650 mm and 9350 mm from the support the web-shear capacity is reduced as a consequence of reduced shear reinforcement amount. At a distance 3020 mm from the critical support the axial load N_γ is reduced as explained for the flexure-shear capacity. In the formula for the web-shear capacity the design moment is not included, and the decrease in the axial load therefore leads to a decrease in the capacity. At an approximate distance 3950 mm from the critical support, the total design moment changes sign, causing tension in the lower edge instead of in the upper edge as is the case closer to the support. This leads to a relatively large change in d , causing a visible nick in the capacity curve. The variation in d due to change in the number of prestressing strands is not visible in the graph.

As mentioned in the introduction to this chapter, a relatively large part of the beam is included in the figure. This is done in order to show the development of the shear capacities, and to show how the various factors will affect the capacities. The effect that the shear reinforcement amount has on the diagonal tension capacities is illustrated clearly in Figure 9.4.

Effect of shear reinforcement and axial load on the diagonal tension capacity

In order to study the effect that the shear reinforcement and the axial load have on the diagonal tension capacity in more detail, capacities where both factors are excluded, then included one by one, are calculated. Figures 9.5 and 9.6 show the flexure-shear capacity and web-shear capacity, respectively. V_d is used for the flexure-shear capacity, while V_{dmax} is used for the web-shear capacity. Furthermore

V_{d0} is used when axial load is not included, and V_d is used when axial load is included.

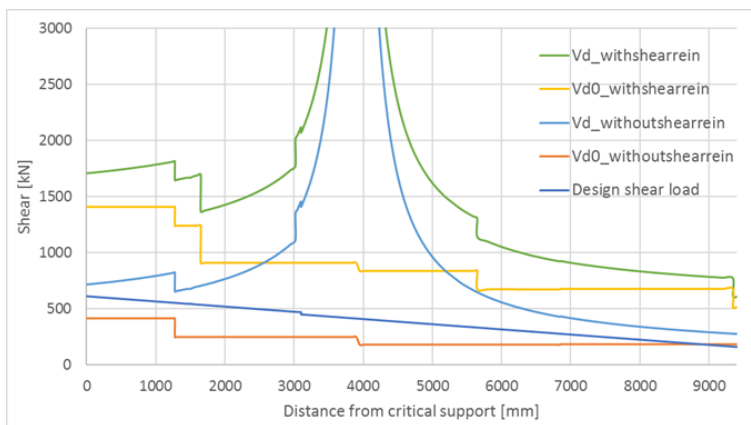


Figure 9.5: Influence of shear reinforcement and axial load on flexure-shear capacity

Figure 9.5 shows that as long as the beam is shear reinforced, the effect from prestressing is not necessary for the capacity. The figure also shows that the flexure-shear capacity would have been sufficient without shear reinforcement as long as the axial load from the prestressing is applied, however with high utilization ratio near the beam end and towards the middle of the beam. It is only when both the shear reinforcement and the axial load from prestressing are neglected that the design shear load exceeds the flexure-shear capacity.

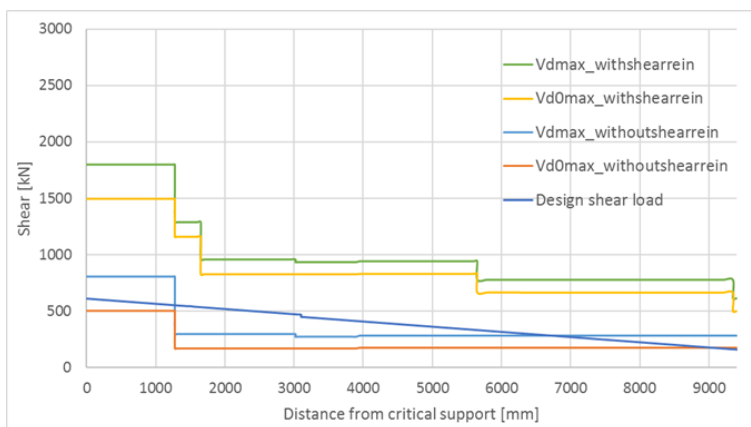


Figure 9.6: Influence of shear reinforcement and axial load on web-shear capacity

Figure 9.6 shows that the web-shear capacity is sufficient as long as the beam is shear reinforced (regardless of whether the prestressing axial load is applied). How-

ever, without shear reinforcement the capacity is insufficient both when including and excluding the axial load.

This assessment makes it evident that shear reinforcement is, in fact, necessary in order for the beam to withstand the design shear loading. It is clear from the figures that adding shear reinforcement in the beams in general has a larger effect on the diagonal tension capacity than prestressing of the NIB beams.

9.3 EC2

In this section the shear capacities established with NS 3473:1977 are to be controlled through the use of the updated shear capacity formulas provided by EC2.

As given in Section 8.4, Section 6.2.1(8) of EC2 states that control of the diagonal tension capacity $V_{Rd,c}$ or $V_{Rd,s}$ can be performed at a distance d from the edge of the support, while the compressive shear capacity $V_{Rd,max}$ is to be controlled at the support. It has been assumed in the introduction of this chapter that the outer edge of the bearing is placed 50 mm from the beam end, and that the bearing has an extent of 200 mm in the longitudinal direction of the beam. This means that the inner edge of the support is placed 250 mm from the beam end.

The effective depth d of the cross section varies depending on the concrete cross section and the number of uncoated prestressing strands. It is chosen to use the value $d = 1546.9$ mm, and control for diagonal tension failure at a approximate distance 1550 mm from the inner edge of the support. The chosen d is calculated in Appendix D, and corresponds with the effective depth of the composite beam that is valid in the majority of the beam, when the beam experiences tension in the lower edge and compression in the upper edge, and where all prestressing strands are uncoated. It is chosen to use this effective depth instead of $d_{ok} = 1494.8$ mm which is valid in the considered section, because the larger d provides the opportunity to control the diagonal tension capacity in the section that is critical according to the NS 3473:1977 formulas. Here the shear reinforcement amount is reduced by increasing the central distance of the stirrups from 100 mm to 150 mm, which is assumed to have an impact for the diagonal tension capacity of the beam according to EC2 as well.

The choice of controlling the diagonal tension capacity at a distance 1550 mm from the edge of the supports results in a distance from the middle of the support to the considered section of $1550 + 100 = 1650$ mm, and a distance from the beam end to the considered section of $1550 + 250 = 1800$ mm. The design loads in this section are given in Table 9.2. Table 9.2 also gives the design loads acting at the support, which is where the compressive shear capacity is to be controlled.

For the calculations that are performed according to EC2, the established design loads (using load coefficient according to R412 (Statens Vegvesen, 2003)), effective width of the bridge deck in the composite beam, etc. will remain unchanged from the NS 3473:1977 calculations. Material properties and material coefficients will on the other hand be used as given in EC2. This is done in order for the EC2 calculations to be consistent and thorough, without changing the basis for the calculations.

Table 9.2: Design load actions in the two considered sections

Design load	At distance 1650 mm from the support	At support
Axial load [kN]	3228	3228
Shear load [kN]	533	609
Moment [kNm]	1269	2201

9.3.1 Members not requiring design shear reinforcement

First, the shear resistance of the composite beam has been found without taking the shear reinforcement into account. This has been done in order to check whether or not the shear reinforcement is necessary to secure sufficient shear capacity of the beam. This will be of interest when corrosion of the shear reinforcement is considered.

In EC2 two equations exist for calculating the diagonal tension capacity of prestressed members not requiring shear reinforcement. As stated in Section 8.4.1, Equation (6.2.a) in EC2 (with a minimum value given by Equation (6.2.b)) is to be used for prestressed members in cracked regions, while Equation (6.3), reproduced in Equation (8.22), can be used for prestressed members in uncracked regions.

If the tensile strength of concrete is neglected, the cross section can be assumed to be cracked if it experiences tensile stresses in some part over the height of the cross section. The design axial load and the total design moment from prestressing, self weights and traffic loads in the considered section is known, and it is therefore easy to control whether or not the cross section will be in tension.

The axial load provides compressive stresses in the entire cross section, with a total magnitude of $N_{Ed} = 3228$ kN as given in Table 9.2. The coating of four of the prestressing strands to a distance 2000 mm from the beam end is not taken into account for the calculation of this design axial load, as elaborated in Section 6.4.1. The considered section lies 1800 mm from the beam end, and the exclusion of the four of the in total 26 prestressing strands that are coated can be done in a simple manner, by multiplying with the fraction $22/26$. The gradual increase of the axial load in the concrete which occurs from the beam end can also be included, using the factor α_l which was introduced in Section 8.4.1. α_l is calculated in Appendix E, and is found to be $\alpha_l = 0.761$. This gives an axial load in the section of

$$N_{Ed} = \frac{22}{26} \alpha_l N_{Ed} = \frac{22}{26} \times 0.761 \times -3228 \text{ kN} = -2079 \text{ kN}.$$

While axial compression generally is defined as positive in this thesis, here the axial load has been given a negative sign to indicate that it causes compression in the cross section. Dividing this by the area of the concrete cross section, $A_c = 751\,500 \text{ mm}^2$, gives the stresses in the cross section due to the axial load,

$$\sigma_n = \frac{N_{Ed}}{A_c} = \frac{-2079 \times 10^3 \text{ N}}{751\,500 \text{ mm}^2} = -2.77 \text{ MPa}.$$

Furthermore, the stresses in the cross section due to moment can be found. The total design moment working in the section is $M_{Ed} = 1269$ kNm as given in Table 9.2. The moment is positive, i.e. it leads to tension in the upper part and compression in the lower part of the cross section. Maximum tension will occur in the upper edge of the cross section. The stresses occurring here is given by the formula

$$\sigma_m = \frac{M_{Ed}z}{I},$$

where $I = 192.9 \times 10^9$ mm⁴ and z is the distance from the centre of gravity for the concrete cross section to the upper edge of the cross section. With the centre of gravity for the concrete cross section calculated in Appendix D as $z_{ctot} = 1269$ mm and the total height of the cross section $h_{tot} = 1685$ mm, we get $z = h_{tot} - z_{ctot} = 1685 - 1269 = 416$ mm. This gives the following tensile stress in the upper edge of the concrete cross section,

$$\sigma_m = \frac{1269 \times 10^6 \text{ Nmm} \times 416 \text{ mm}}{192.9 \times 10^9 \text{ mm}^4} = 2.74 \text{ MPa},$$

The resulting stress in the upper edge of the cross section can then be found,

$$\sigma_{tot} = \sigma_n + \sigma_m = -2.77 \text{ MPa} + 2.74 \text{ MPa} = -0.03 \text{ MPa}.$$

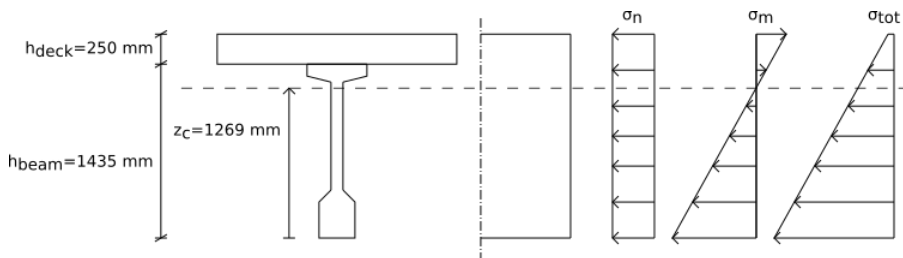


Figure 9.7: Stress distribution in the composite beam

The stress distribution over the height of the composite beam is illustrated in Figure 9.7. The calculations show that the section which is exposed to the highest tensile stress from the moment distribution will be in compression over, i.e. the entire cross section will be in compression. When the compressive stress is found to be as low as given here it might be more conservative to use the equations for cracked cross section. Nevertheless, Equation (8.22) has been used here to find the shear capacity of the cross section without shear reinforcement.

The shear capacity calculations have been performed in Appendix E. Choices regarding parameter values are given in the appendix. For calculations of the transmission length it has been assumed sudden release and that the bond conditions are not good, both rendering conservative values for the transmission length. From the calculations in Appendix E it is found that the shear resistance regarding diagonal tension failure for regions that are uncracked in bending is $V_{Rd,c} = 345$ kN.

Comparing this with the design shear load in this section, $V_{Ed} = 533$ kN, it is clear that the capacity is not sufficient, $V_{Ed} > V_{Rd,c}$, with a utilization of $\eta = \frac{V_{Ed}}{V_{Rd,c}} = \frac{533}{345} = 1.55$ in the section.

The capacity with regard to compressive shear failure without shear reinforcement is also found, using Equation (8.23). This gives a capacity of $V_{Rd,max} = 970$ kN. Comparing this with the shear load at the support, $V_{Ed} = 609$ kN, it is evident that the capacity regarding compressive shear failure is sufficient, $V_{Ed} < V_{Rd,max}$, and the section is utilized to a degree of $\eta = \frac{V_{Ed}}{V_{Rd,max}} = \frac{609}{970} = 0.63$. However, because the diagonal tension capacity is insufficient, shear reinforcement is necessary in the beam in order to avoid failure.

9.3.2 Members requiring design shear reinforcement

The diagonal tension capacity when the shear reinforcement in the NIB beam is taken into consideration is found using Equation (8.24). The angle between the concrete compression strut and the beam axis perpendicular to the shear force, θ , is to be chosen between the values 26.6° and 45° , so that $1 \leq \cot \theta \leq 2.0$. The angle of the compression strut corresponds with the principal compressive direction. With the principal tensile direction perpendicular to this, this is also the angle in which the cracks are assumed to appear.

First it is assumed that the angle θ is 45° ($\cot \theta = 1$). This will be in accordance with NS 3473:1977, where it is assumed that all cracks occur 45° from the system axis. This gives a diagonal tension capacity of $V_{Rd,s} = 336$ kN. Comparing this with the design shear load $V_{Ed} = 533$ kN in this section, it is clear that the capacity is not sufficient ($\eta = 1.59$).

If instead the angle θ is chosen as 26.6° ($\cot \theta = 2.0$), in correspondence with the recommendations given in N400 (Statens Vegvesen, 2015), the diagonal tension capacity is found to be $V_{Rd,s} = 671$ kN. With the design shear load $V_{Ed} = 533$ kN in the section, the capacity is now sufficient ($V_{Ed} < V_{Rd,s}$), and the section has a utilization ratio of

$$\eta = \frac{V_{Ed}}{V_{Rd,s}} = \frac{533}{671} = 0.79.$$

This shows how the EC2 formulas provide a possibility to utilize the shear reinforcement in a much more efficient way than NS 3473:1977 allows. In this thesis the minimum crack angle is limited by the recommendations given in N400, but EC2 allows for the direction of the cracks to be rotated to a minimum angle from the beam axis of 21.8° . Both N400 and EC2 allow for the calculations to include that any cracks that may appear may cross several more shear reinforcement bars, which in effect increases the utilization of each bar.

Finally, the compressive shear capacity, given by Equation (8.25), must be controlled. In Appendix E this capacity is found to be $V_{Rd,max} = 776$ kN, i.e. higher than the design shear load of $V_{Ed} = 609$ kN at the support, and with a utilization ratio of

$$\eta = \frac{V_{Ed}}{V_{Rd,max}} = \frac{609}{776} = 0.73.$$

Because there are so many factors changing near the beam ends, both the diagonal tension capacity and the compressive shear capacity of the beam should be controlled in more sections using the EC2 formulas. More critically utilized sections may be discovered than the two sections that have been considered here.

9.4 Anchorage capacity

The previous sections have performed control of the diagonal tension capacity and the compressive shear capacity of the composite beam in The Hulvågen Bridge using both NS 3473:1977 and EC2. In this section the anchorage capacity of the beam end will be established.

It has been established in Section 8.5 that the force ΔF_{td} which arises in the tensile reinforcement near the beam end when diagonal cracks appear, and which must be anchored using anchorage reinforcement, will be

$$\Delta F_{td} = S - F_{sp} = \frac{1}{2} V_{Ed} \cot \theta - \frac{l_x}{l_{pt2}} F_{p0'}. \quad (9.7)$$

l_x will be the distance from the beam end to the inner edge of the support, i.e. $l_x = 50 + 200 = 250$ mm as can be seen in Figure 8.3. The total transmission length l_{pt2} is calculated as $l_{pt2} = 2366$ mm in Appendix E.

It is chosen to only include the load from the prestressing strands that are placed in the lower part of the NIB beam when establishing the prestressing load $F_{p0'}$. Furthermore, it is chosen to take into account that four of the 22 prestressing strands in the lower part of the beam are coated over the first 2000 mm from the beam end. Using the loss factor and prescribed prestressing load as described in Section 6.4.1, gives the following prestressing load in the considered section (when gradual transmission of prestressing is not taken into account),

$$F'_{p0} = 0.85 \times 18 \times 134 \text{ kN} = 2050.2 \text{ kN}.$$

Including the gradual transmission of prestressing leads to

$$F_{sp} = \frac{l_x}{l_{pt2}} F_{p0'} = \frac{250}{2366} \times 2050.2 = 217 \text{ kN}.$$

As Figure 8.3 illustrates, the design shear load V_{Ed} must be taken from the support, i.e. $V_{Ed} = 609$ kN. Furthermore, the angle θ can be chosen as $\theta = 45^\circ$ in accordance with NS 3473:1977, or it can be chosen as $\theta = 26.6^\circ$ in compliance with the value that was ultimately chosen for control of diagonal tension and compressive shear capacity in the EC2 calculations. As stated previously, a lower value of θ will be critical for the anchorage capacity. Here it is decided to control whether the anchorage reinforcement amount that is placed in the beam is sufficient both when using $\theta = 45^\circ$ and $\theta = 26.6^\circ$.

Using Equation (9.7), ΔF_{td} can be established as a function of only θ ,

$$\Delta F_{td} = S - F_{sp} = \frac{1}{2}609 \text{ kN} \times \cot \theta - 217 \text{ kN}.$$

For $\theta = 45^\circ$ ($\cot \theta = 1$) this gives $\Delta F_{td} = 88 \text{ kN}$, and for $\theta = 26.6^\circ$ ($\cot \theta = 2$) this gives $\Delta F_{td} = 392 \text{ kN}$.

The amount of horizontal reinforcement required to maintain sufficient anchorage capacity is $A_s = \Delta F_{td}/f_{yd}$, where f_{yd} is the design yield strength of the reinforcement. The stirrups are denoted P3 in Figure 5.1c, and as the figure shows eight horizontal stirrups of diameter 12 mm placed above each other with a central distance of 50 mm. The bar schedule in Appendix A states that the steel quality is K400Ts. K400Ts has design yield strength of $f_{yd} = 348 \text{ MPa}$, as established in Appendix F. The required reinforcement for the two angles then become

$$A_{s,\theta=45^\circ} = \frac{88 \times 10^3 \text{ N}}{348 \text{ N/mm}^2} = 253 \text{ mm}^2,$$

$$A_{s,\theta=26.6^\circ} = \frac{392 \times 10^3 \text{ N}}{348 \text{ N/mm}^2} = 1126 \text{ mm}^2.$$

With two legs in each of the eight stirrups, the horizontal stirrups in the beam provide a total reinforcement amount of

$$A_s = 8 \times \frac{2 \times \pi \times (12 \text{ mm})^2}{4} = 1810 \text{ mm}^2.$$

Hence, it is clear that the anchorage capacity of the beam end is sufficient, both when considering the crack angle according to NS 3473:1977 and according to the performed calculations using EC2. The utilization ratios of the anchorage reinforcement for the two situations are

$$\eta = \frac{A_{s,\theta=45^\circ}}{A_s} = \frac{253}{1810} = 0.14,$$

$$\eta = \frac{A_{s,\theta=26.6^\circ}}{A_s} = \frac{1126}{1810} = 0.62.$$

It should be noted that the anchorage capacity that has been calculated here is dependent on the fact that the distance between beam end and the middle of the support in fact is 150 mm. If some supports in the bridge have been placed further towards the beam end, the anchorage capacity will be lowered due to a decrease in l_x , which increases ΔF_{td} . However, it is evident from the utilization ratios that there is more than sufficient anchorage capacity in the beam for both standards.

9.5 Shear stresses at the interface between the NIB beam and bridge deck

As mentioned in Section 8.6, it is necessary to control that the interface between the NIB beams and the bridge deck has sufficient capacity for the composite beam

to work as a continuous cross section. These calculations will be performed in this section.

9.5.1 Shear stresses at the interface

For the control of shear stresses at the interface between the NIB beam and the bridge deck it is assumed that the cross section is cracked. This will lead to the largest shear stresses in the considered section, and therefore be a conservative solution.

The Hulvågen Bridge is in general assumed to be a continuous bridge for the analyses in this thesis, meaning that tension will be in the upper edge of the cross section near the beam end. As Figure 8.4b illustrates, this will provide a shear stress of $\tau_{\max} = V_{Ed}/bz$ in the interface between the beams and bridge deck.

The largest shear stresses will act on the surface that has the smallest width of the two surfaces in the interface. For The Hulvågen Bridge this means that the width of the upper flange of the beam, $b = 500$ mm should be used in the expression for the shear stresses. Furthermore the shear resistance should be controlled at the support where the design shear load is largest, $V_{Ed} = 609$ kN. With an effective cross sectional depth of $d = 1494.8$ mm at the support, the lever arm of the composite section z can be assumed to be $z = 0.9d = 0.9 \times 1494.8$ mm = 1345.3 mm. Section 6.2.3 in EC2 states that the simplified value of $z = 0.9d$ primarily is valid for shear design of reinforced concrete sections that are not subjected to axial load. However, course material from the subject "TKT4220 Concrete Structures 2" at NTNU indicates that the simplification also is used for prestressed beams, and it has therefore been used for calculations according to EC2 in this thesis without further examinations of the validity of this assumption.

The design shear stress that occur in the interface are

$$v_{Ed} = \tau = \frac{V_{Ed}}{bz} = \frac{609 \times 10^3 \text{ N}}{500 \text{ mm} \times 1345.3 \text{ mm}} = 0.91 \text{ MPa.}$$

9.5.2 Shear resistance at the interface

Section 8.6.3 provides the basis for calculations of the design shear resistance at the interface between two parts of a composite section that are cast at different points in time, in accordance with EC2. Equation (8.32) shows the design shear resistance at the interface.

For the calculations on the composite beam in The Hulvågen Bridge it can be assumed that there are no stresses acting normal to the interface, and the reinforcement which crosses the interface lies perpendicular to the interface. This gives $\sigma_n = 0$ and $\alpha = 90^\circ$, which gives $\sin \alpha = 1$ and $\cos \alpha = 0$. Hence, Equation (8.32) can be reduced to

$$v_{Rd} = cf_{ctd} + \rho f_{yd} \mu \leq 0.5 \nu f_{cd} \quad (9.8)$$

Section 6.2.5(2) of EC2 provides regulations regarding the cohesion and friction coefficients c and μ depending on the roughness of the interface. In the absence

of more detailed information, surfaces may be classified as very smooth, smooth, rough or indented, with examples provided in the standard. For a free surface left without further treatment after vibration, which can be assumed to be the case for The Hulvågen Bridge, a smooth surface should be assumed, and recommended value are $c = 0.20$ and $\mu = 0.6$.

Furthermore it is decided to use the design axial tensile strength f_{ctd} and the design compressive strength f_{cd} of the concrete that is of the lowest material quality of the two. As presented in Section 5.1.1 the NIB beams are of concrete quality C55 while the bridge deck can be assumed to be of concrete quality C35. The material properties that are relevant for the bridge deck will therefore be used here. Table 3.1 in EC2 shows that a concrete with characteristic cube strength $f_{ck,cube} = 35$ MPa does not exist in the overview of the concrete qualities that are defined in EC2. The extensive damages that have been registered in the bridge deck in Brutus (see Section 4.2.3) indicate that the quality of the bridge deck is somewhat reduced. Because of this it is decided to underestimate the concrete quality by using material properties associated with a B25 concrete, which has characteristic cube strength $f_{ck,cube} = 30$ MPa. The material properties used in Equation (9.8) are given in Appendix F, where the calculations are performed.

Figure 5.1b shows how the P2 stirrups (denoted P1 at the beam end) of steel quality K400Ts reach through the beams and vertically up into the bridge deck after the deck is cast. These stirrups will provide reinforcement over the interface between the two parts of the composite beam, and will increase the capacity of the interface. Figure 5.1c shows that near the beam end, 13 single stirrups are placed over a distance of 770 mm.

The calculations of the shear resistance near the beam end are performed in Appendix F. It is found that the design shear resistance is $v_{Rd} = 0.94$ MPa. With design shear stresses of $v_{Ed} = 0.91$ MPa acting in the interface it is evident that the shear resistance at the interface is only barely sufficient to sustain the design shear stresses that are acting in the critical section near the beam end. The utilization of the shear resistance amounts to

$$\eta = \frac{v_{Ed}}{v_{Rd}} = \frac{0.91}{0.94} = 0.96.$$

The design shear load will decrease with increasing distance from the support, but at the same time the central distance of the P2 stirrups will increase, which decreases the amount of shear reinforcement crossing the interface. If each term that contributes to the shear resistance is considered individually, it becomes evident that it is the shear reinforcement that contributes most to the total shear resistance, in total 78 %. Reducing the amount of shear reinforcement is therefore likely to have a large impact on the shear resistance of the interface. Calculations should therefore be performed over a larger part of the composite beam in order to control whether the shear resistance is sufficient. This has not been performed here.

It should be noted that when the utilization ratio of the shear resistance at the interface is as high as it is, the capacity has very little tolerance regarding factors that may reduce the shear resistance. The material properties of the bridge deck

are not established with certainty, as Section 5.1.1 elaborates. Furthermore, with several extensive damages registered in the bridge deck, as elaborated in Section 4.2.3, the quality of the bridge deck can be questioned. This may affect the concrete properties that are relevant regarding the shear resistance of the interface.

In addition to the registered damage to the concrete in the bridge deck, there is a relatively large possibility that corrosion is occurring in the shear reinforcement stirrups if sea water is leaking through the bridge deck. If so, the shear resistance of the interface is decreasing, and at a certain point the shear resistance of the interface may no longer be sufficient to maintain the shear stresses occurring here. Slippage between the bridge deck and NIB beams may then occur, which destroys the coupling between the two members. The bridge deck will in that case no longer be active in resisting the design load actions in the section, and the NIB beams have to carry the entire design loads by itself.

Given the high utilization ratio of the shear resistance at the interface between the NIB beam and the bridge deck, further calculations should be made in order to control whether the NIB beams have sufficient capacity to carry the design loads by themselves. In addition, if uncoupling of the structural members occur in a section that is exposed to considerable moment, the moment capacity of the section may be reduced to a point where it is no longer sufficient. Calculations regarding this have not been performed in this thesis.

9.6 Concluding remarks regarding the shear capacity

In the previous sections the shear capacity with regards to diagonal tension failure, shear compressive failure and anchorage failure has been studied. In addition it has been looked into whether or not the interface between the NIB beam and the bridge deck has sufficient capacity to resist the shear stresses that will occur here.

Calculations have been performed using NS 3473:1977, the standard that was valid when The Hulvågen Bridge was designed, and using EC2, which is the design standard that is valid today.

Table 9.3: Overview of utilization ratios for the different shear failure mechanisms

Shear failure mechanism	Utilization ratios, η	
	NS 3473:1977	EC2
Diagonal tension	0.56	0.79
(Flexure-shear)	0.39	-
(Web-shear)	0.56	-
Compressive shear	0.55	0.73
Anchorage	0.14	0.62
Interface between beam and deck	-	0.96

A summary of the established utilization ratios is given in Table 9.3. The sum-

mary makes it clear that the capacity regarding the three main failure mechanisms is plenty, while the interface between the beam and bridge deck is almost entirely utilized. It is evident that capacity formulas in EC2 result in higher utilized shear capacity for all the considered shear failure mechanisms. In the following sections the difference for each failure mechanism is looked further into.

It is important to remember that in reality, several more factors will cause loading on the bridge (i.e. temperature loads), and that only one load configuration is considered here. There might exist other combinations and configurations of loads that lead to higher loads in the critical sections of the beam. Furthermore, the distribution of loads between the four NIB beams in the transversal direction has been performed in a simplified manner. The share of the total self loads and traffic loads that act on the critical beam may be higher, which in that case will result in higher utilization of the shear capacities.

Diagonal tension failure

For diagonal tension failure a large difference between the two standards is that EC2 takes the gradual increase in prestressing load that occurs in the beam end into account, while NS 3473:1977 assumes full prestressing load at the beam end. NS 3473:1977 will therefore overestimate the favourable effect that compression in the cross section has on the shear capacity. At the same time, the beam will have tension in the upper part of the beam over the critical support, so that the prestressing will contribute to increase the total moment acting in the section. This is an unfavourable effect. Nevertheless, it is likely that the gradual increase in prestressing loads in EC2 is one of the reasons why the diagonal tension capacity according to EC2 is utilized higher than the NS 3473:1977 capacity in the critical section.

The diagonal tension capacity according to EC2 is furthermore largely dependent on the choice of crack angle θ , while for NS 3473:1977 this angle is set to 45°. The possibility of decreasing this angle in EC2 provides the opportunity for the shear reinforcement to be higher utilized, because any cracks that may appear will cross several more shear reinforcement bars. This means that if the beam had a larger amount of shear reinforcement, the diagonal tension capacity according to EC2 would increase faster than the diagonal tension capacity of NS 3473:1977 (given that the angle of the crack is chosen to be less than 45°). At some point the capacity according to EC2 would have exceeded the NS 3473:1977 capacity.

Compressive shear failure

The favourable effect of the prestressing load is also included at for the compressive shear capacity in EC2. However, as this capacity is calculated at the support, the contribution from the prestressing is very low. The formulas for the compressive shear capacity are relatively different for the two standards. While NS 3473:1977 solely is based on the concrete quality, effective depth and beam web, the EC2 formula is given by the truss model and also includes the assumed crack angle θ and the favourable effect from prestressing. However, for the compressive shear

capacity a lower crack angle will be unfavourable. Hence, because the crack angle is chosen with a low value in order to assure sufficient diagonal tension capacity, the compressive shear capacity according to EC2 will be reduced. This can be assumed to be an important reason for the difference between the utilization ratios according to the two standards.

It should also be noted that the compressive shear capacity according to NS 3473:1977 is calculated using a conservative formula. The procedure using principal compressive stresses provided a utilization ratio of $\eta = 0.33$, and this may be considered to be closer to the actual capacity according to NS 3473:1977. The differences between the two standards with regards to compressive shear capacity is therefore high.

Furthermore are the two compressive shear capacities calculated with different web widths (NS 3473:1977 has the critical section at 1425 mm where the web width is reduced, while EC2 controls the compressive shear capacity at the support). The design shear load is somewhat higher at the support, but the shear capacity according to EC2 is nevertheless much lower than according to NS 3473:1977.

Anchorage capacity

The control of the anchorage capacity is not expressed explicitly in any of the two standards, but is based on equilibrium at the beam end when a diagonal crack is initiated. As seen, the crack angle is chosen both to comply with NS 3473:1977 and with EC2, with the two resulting utilization factors given in Table 9.3. As for the compressive shear capacity, the choice of a low crack angle in compliance with EC2 will reduce the anchorage capacity. It should be noted that for both calculated anchorage capacities the reduction of the prestressing load near the beam end is included despite regulations for this not being given in NS 3473:1977. The utilization ratio of $\eta = 0.14$ will therefore not be entirely in compliance with NS 3473:1977. However, including the reduction of the prestressing is conservative when considering anchorage capacity, and if this had not been done it would have been found that very little or no anchorage reinforcement was necessary at the beam end.

Interface between the NIB beam and bridge deck

Procedures for control of the interface between concrete cast at different times has not been found in NS 3473:1977, and may not have been taken into consideration for design of bridges that were built at this time. The calculation procedure according to EC2 indicates that the shear resistance is utilized almost to the maximum. Very little damage to the deck or reinforcement is necessary for the capacity to become insufficient, according to these calculations. It is evident from the summary in Table 9.3 that this is the most critical part of the complete shear capacity control of the beam.

As has been stated a failure of the shear resistance in the interface will not necessarily cause collapse of the structure. The coupling effect of the NIB beam and the bridge deck will instead be lost, so that the bridge deck will no longer

contribute to resisting loads, and the NIB beams have to take up all the loads acting on the section by itself.

The relatively low utilization ratios that have been established for the various shear failure mechanisms above indicate that the NIB beams may be able to carry the design shear load without contribution from the bridge deck. Furthermore the NIB beams are designed in order to be able to carry the design axial loads from prestressing by themselves, so that this should not be a problem either.

However, if uncoupling occurs in a section where the beam is exposed to considerable moment, the NIB beam may no longer have sufficient capacity to take up the entire moment without contribution from the bridge deck.

Further examinations of the bridge deck, and of the interface between the beam and deck, should be performed. If repairs are performed where necessary, sufficient capacity can be secured without too costly measures. Nevertheless, based on these results, it is clear that further analysis in order to establish the structural capacity of the NIB beam alone is necessary.

Considering the continuity of the bridge

As Section 4.1.1 introduced, The Hulvågen Bridge is in fact not fully continuous, as the calculations in this chapter is based on. Instead the NIB beams are simply supported, with a continuous bridge deck cast over them. This renders a partly continuous bridge system, instead of a fully continuous system as has been assumed for the calculations.

Table 9.4: Design loads at support

Design loads	Continuous bridge system	Simply supported bridge system
Axial load [kN]	3227	2640
Shear load [kN]	609	549
Moment [kNm]	2201	374

Table 9.4, which combines the information given in Table 7.8 and Table 7.9, gives an overview of the design loads acting at the critical support when comparing the continuous bridge system with the simply supported bridge system modelled in Section 7.5.

The table makes it evident that the increase in design loads at the end region when considering the continuous bridge system instead of the simply supported bridge system is not drastic. It is primarily the design moment that will increase. As Chapter 8 showed, the design moment in the section is included in the capacity formulas according to NS 3473:1977. Overestimating the design moment in the section has therefore reduced the diagonal tension capacity and the compressive shear capacity calculated according to NS 3473:1977 to some degree. However, as Table 9.3 shows, NS 3473:1977 provides sufficient capacity when regarding the utilization of these capacities. The design moment does not affect the diagonal tension capacity and the compressive shear capacity according to EC2.

Furthermore the design axial load effect is increased when the continuous bridge system is considered instead of the simply supported bridge system. As shown this is favourable with regards to shear capacity, and it has caused an increase in the calculated shear capacity both according to NS 3473:1977 and EC2. However, the increase is not very large, and will only occur in the outer 3020 mm of each beam end.

Finally, the design shear load effect is increased slightly, from $V_{Ed,ss}$ 549 kN in the simply supported bridge system to $V_{Ed,cont}$ 609 kN in the continuous bridge system. This increase is relatively small, but because it is directly compared with the calculated shear capacity for each failure mechanism, this will probably constitute the largest difference between the continuous bridge system and the simply supported bridge system. Calculating new utilization ratios using the design shear load from the simply supported bridge system, without changing the basis for the shear capacities, show that the reduction in design load does not have drastic effect on the calculated utilization ratios. The utilization of the shear resistance in the interface between the beam and deck, which is the most critical as Table 9.3 shows, is reduced to $\eta = 0.87$ instead of $\eta = 0.96$.

As was stated in Section 4.1.1, The Hulvågen Bridge likely has a structural system that lies closer to the simply supported system than to the continuous system. It is however difficult to quantify this. Nevertheless, it can be concluded that the utilization ratios of the various shear failure mechanisms likely are somewhat lower than what is presented in Table 9.3.

Chapter 10

Consequences of reinforcement corrosion

Chapter 3 gave an introduction into the durability of reinforced concrete structures, and different deterioration mechanisms were introduced. The Hulvågen Bridge is exposed to extremely aggressive marine environment due to its location at the coast. Chloride induced corrosion is therefore considered the most dangerous deterioration mechanism for this bridge. Combined with low demands to concrete cover when the bridge was built, it is considered likely that chloride induced reinforcement corrosion is occurring in the bridge.

This chapter deals with the consequences that chloride-induced reinforcement corrosion may have on the structural capacity of the bridge. Both the effect that corrosion can have on the mechanical properties of reinforcement bars (regular and prestressed), on the bond between the reinforcement and concrete, and on the entire reinforced structure will be considered. In addition, the effect that reinforcement corrosion has on the shear capacity of a structure in particular will be looked further into, including a suggested calculation procedure to account for this in the capacity calculations.

10.1 Mechanical properties of corroded reinforcement bars

There are two main mechanical properties of reinforcement bars that are of importance for the structural capacity and that change when steel reinforcement bars experience corrosion. These are the reinforcement cross section and the ductility of the material.

10.1.1 Reduction of reinforcement cross section

As has been introduced in Section 3.2 reinforcement corrosion can occur due to carbonation or chloride attack. Carbonation is associated with corrosion that is uniformly distributed along the reinforcement, called uniform corrosion, while chloride attack typically is associated with pitting corrosion, where localized corrosion forms local pits along the reinforcement bar. As stated in Section 3.2.4 pitting corrosion on prestressed reinforcement typically is in the form of few corrosion cells, with localized deep pits, while for reinforcing bars pitting corrosion can be initiated over the whole surface, causing a more uniform corrosion of the bar.

When uniform or pitting corrosion of a steel bar occurs, the effective reinforcement area is either evenly or locally reduced. The degree of corrosion is often specified as a weight loss in percent of the original reinforcement weight. For structures in use however, the weight loss can be difficult to acquire. For uniform corrosion, direct measurement of the remaining bar diameter can be used in order to establish the degree of corrosion. For a corroded structure with cover spalling the remaining bar diameter can be measured directly on the exposed bars. For less corroded structures where the cover has not yet spalled off, small parts of the cover can often be removed at non-critical locations for measurements to be made, and then be repaired afterwards. Stemland (2007) states that around 1 - 2 % of the reinforcement area can normally be corroded when the first cracks appear, while it is normal with around 5 - 20 % corrosion before spalling occurs. The area reduction is largest before signs occur for smaller bar diameters.

Effective reinforcement due to more localized pitting corrosion can be found based on the experimentally confirmed assumption that the pits are circular cross-sectioned, with widths averaged slightly less than twice the depth (Hanjari, 2010). This assumption leads to a cross section loss that is approximately proportionate to the square of the pit's depth.

An alternative to direct measurement is to estimate the penetration of corrosion from the concrete surface, based on corrosion rate and time of corrosion initiation. Several models have been suggested.

10.1.2 Ductility

Ductile behaviour is desired in concrete structure so that preliminary warnings in the form of deformations will occur before the structure collapses. In order to achieve this concrete structures are under-reinforced, so that plastic yielding will occur in the reinforcement before fracture in the concrete occurs. For under-reinforced cross sections, the deformation and capacity is therefore largely dependent on the ductility of the reinforcement material.

Hanjari (2010) has looked into several studies that have investigated the effects of corrosion on the mechanical properties of reinforcement. For uniform corrosion it has been shown that the ultimate and yield strength are reduced proportionally with the degree of reinforcement corrosion, so that the ultimate to yield strength ratio is not significantly affected by the corrosion. Furthermore the elasticity modulus of steel reinforcement is not significantly affected. The values valid for uncorroded

reinforcement will therefore also be valid for corroded reinforcement. While both the ultimate and nominal yield strength are reduced proportionally with the degree of reinforcement corrosion, the true yield strength and the true ultimate strength, calculated according to the actual area of the cross section, are not influenced by the level of reinforcement corrosion (Paciorek et al., 2017; Hanjari, 2010).

The ultimate strain, on the other hand, is significantly reduced by uniform corrosion, meaning that ductility is reduced. Measured reductions in ultimate strain and elongation of bars with smaller diameters were in the studies by Hanjari (2010) shown to be greater than for those of larger diameters. However, the observed differences were small, and the reduction of the ductility of corroded reinforcement was concluded to primarily be a function of the amount of corrosion rather than the bar type and diameter. Figure 10.1 shows the load-elongation curves that resulted from an experiment performed on a six mm steel bar for various degrees of uniform corrosion (Almusallam, 2001). Despite the general agreement that the reinforcement becomes less ductile for increasing reinforcement corrosion, opinions vary regarding exactly when the reinforcement goes from a ductile to a brittle behaviour.

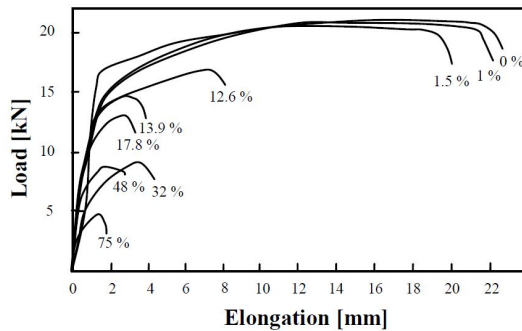


Figure 10.1: Load-elongation curves for various degrees of uniform corrosion (Almusallam, 2001)

As has been stated earlier, with its limited reach, chloride induced pitting corrosion is limited to affect only a very small extent of the reinforcement bar. Hanjari (2010) states that a length of approximately twice the bar diameter is affected. Furthermore the maximum penetration of pitting corrosion is given as about four to eight times the average corrosion penetration of uniform corrosion (Hanjari, 2010). This notch effect will therefore induce large and very localized strain in the bar. The average strain of the whole bar will as a result be less than the local strain at the pit. This causes the bar to fail at an average strain which is lower than the ultimate strain of the uncorroded bar, and the ductility of the entire bar is therefore impaired. According to Palsson and Mirza (2002), very brittle behaviour can be expected when 50 % of the cross section of the reinforcement is locally corroded.

10.1.3 Prestressed reinforcement

In Section 3.2.4 the differences between corrosion of reinforcing steel and prestressing steel is given. The mechanical and physical conditions that distinguishes prestressing steel from reinforcing steel will also cause differences in the consequences that are observed from the reinforcement corrosion.

Prestressing steel in the form of strands consist of several wires of small diameter (typically 4 mm) that are twisted around each other. Considering the small size of a single wire, a relatively great reduction of the cross sectional area will occur rapidly once corrosion is initiated (Paciorek et al., 2017). A local increase of the stresses in the wire will occur, which again leads to higher corrosion rate as stated in Section 3.2.4.

Similarly to reinforcing steel, the change in reinforcement behaviour from ductile to more brittle is observed for corrosion of prestressing steel. For reinforcing steel the reduction of ultimate strain occurs primarily due to pitting corrosion or chloride-induced corrosion, as explained in Section 10.1.2. Risk of brittle failure is even more pronounced for corroded high strength steel, where fracture can occur due to several different mechanisms in addition to the usual chloride-induced corrosion. Sudden failure of the prestressing strand can be the result of stress corrosion cracking, hydrogen-induced cracking or hydrogen-induced stress corrosion cracking (Paciorek et al., 2017). These failure modes can only occur if the surface has defects like notches, sharp cracks or corrosion pits due to chloride attack.

While the true yield strength of corroded reinforcing bars is not significantly affected by the corrosion, the true yield strength of prestressing steel is decreased for increased degree of corrosion. The elasticity modulus is also affected by corrosion in prestressed steel. This dependence can be explained by the material damage that occurs due to evolution of microcracks and microvoids in the wire when the steel is exposed to stress corrosion cracking (Paciorek et al., 2017).

As stated in Section 3.2.4 the corrosion rate of corroded prestressing reinforcement is strongly dependent on the stress level in the strands. This dependence is also seen on the mechanical behaviour and the maximum mass loss of the reinforcement (Paciorek et al., 2017). Experiments performed by Vu et al. (2009) gave 10 - 15 % higher mass loss for wires loaded up to 80 % of the yield strength than for unstressed wires. Furthermore, the reduction of the elastic modulus and yield strength was exclusively observed for the stressed wires. The brittle failure mode induced by stress corrosion cracking was only observed in wires exposed to high levels of stress (over 70 % of the yield strength (Vu et al., 2009)). Consequently it can be concluded that the stress level has a high influence on the mechanical properties of corroded prestressed reinforcement, and the service life of the reinforcement is reduced with increased of stress level.

In addition to the loss of cross section and the degradation of mechanical properties of corroded prestressed steel, the degradation of the bond between the prestressing steel and the concrete need to be taken into consideration when assessing the structural behaviour of prestressed concrete. How the bond is affected for prestressed reinforced structures compared to regularly reinforced structures will not be looked into in this thesis.

10.2 Bond between corroded reinforcement and concrete

Bond between reinforcement and concrete is the most important parameter providing the composite action in reinforced concrete (Tahershamsi, 2016). The load transfer is achieved by transferring bond stresses in the interaction zone between the two materials. The bonding mechanism is made up by three components: chemical adhesion, friction and the mechanical interaction between concrete and steel (Hanjari, 2010). Low bond stresses are resisted mainly by chemical adhesion. This chemical adhesion is weak, and fails for moderate stresses. This leads to the occurrence of radial micro cracks in the concrete.

When slipping occurs between the reinforcement and the concrete, bond resistance acts mainly in the form of friction for plain bars. For ribbed bars bond strength initially comes from friction, but mechanical interlocking between the ribs and surrounding concrete quickly becomes dominant. For ribbed bars the bond stresses cause transverse cracks radiating from the tip of the bar ribs, as can be seen in Figure 10.2. The bond stress can then be divided into longitudinal bond stress alongside the reinforcement and normal splitting stress perpendicular to the reinforcement. The splitting stresses are resisted by ring stresses that occur in the concrete around the bar.

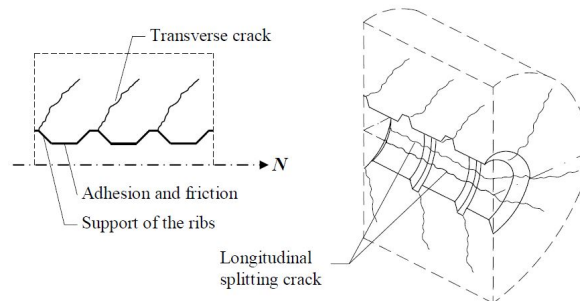


Figure 10.2: Illustration of cracking caused by bond (Hanjari, 2010)

Bond characteristics are influenced by several parameters, such as concrete strength, yielding and spacing of the reinforcement bars, lateral pressure and confinement by concrete cover and the amount of transverse reinforcement (Hanjari, 2010). The interaction between the reinforcement and the concrete is governed by the splitting stresses, as well as by the friction between the reinforcement and the concrete. Corrosion causes volume expansion which lead to splitting stresses that act on the surrounding concrete, which lead to a reduction in the bond properties.

Change in bond strength due to corrosion will primarily be a problem for anchorage of bars at the supports, and may affect the anchorage capacity of a beam. It can also affect areas where the reinforcement has been joined (Stemland, 2007). In a normal beam span the bond stresses are normally sufficiently low so that the reinforcement can transform them to the concrete despite large amounts of the

concrete cover having spalled off. At supports simultaneous compressive stress in the transversal direction appear, which usually causes the bond strength to decrease less here than in the spans. In addition the supports normally are placed more favourably, making the concrete less exposed to attack than other parts of the structures. This is particularly true regarding chloride attack (Stemland, 2007).

Based on this, it is mainly areas where reinforcement is joined, de-escalated or ended that need to be paid special attention to. One example of this is over supports where extra reinforcement is placed in the upper part of the cross section in order to take up the support moment. Low bond strength in these areas can make it difficult to build up the tension in the reinforcement, which ultimately may reduce the moment capacity over the support. Extra reinforcement over the supports in bridge decks will lie close to the surface, usually without transversal stirrups surrounding them. This makes the reinforcement bars extra exposed to chloride attack, especially if de-icing salt is used on the bridge.

10.3 Mechanical behaviour of corroded reinforced concrete structures

The mechanical behaviour of reinforced concrete structures, such as the load-carrying capacity, stiffness and force redistribution, will be affected by the corrosion of reinforcement (Tahershamsi, 2016). This is illustrated in Figure 10.3. Both uniform corrosion and pitting corrosion of a rebar cause a reduction in the cross sectional area and a reduction in the ductility of the reinforcement. The formation of rust causes volume expansion, which leads to concrete cracking and eventually spalling, causing a reduction of the concrete cover and the concrete cross section. Cracking and spalling may also ultimately increase the corrosion rate. Spalling of the cover on the compressive side of a concrete element will decrease the internal lever arm, which in turn decreases the bending capacity.

The reduction of the cross sectional area of the rebars leads to decreased moment and shear capacities, as well as decrease structural stiffness. A reduction in the rebar ductility directly influences the possibility of force and moment redistribution, and limits the load-carrying capacity of a statically indeterminate structure through a reduction in the structure's moment capacity. The structure's shear capacity is not directly influenced by the rebar ductility.

The reduced confinement which is caused by the reduction in the concrete cross section and concrete cover will influence the interaction between the reinforcement and the concrete. This in turn affects the bond strength between the reinforcement and concrete, which can affect the anchorage capacity as described in Section 10.2. In addition, both the load-carrying capacity and ductility in the Ultimate Limit State, as well as stiffness distribution and deflection in the Serviceability Limit State, may be influenced by the corrosion effects on the bond mechanism (Tahershamsi, 2016). The reduction in the concrete cross section and concrete cover due to spalling will also affect both moment and shear capacity. For structures exposed to axial compression a reduction in the concrete cross section will imply an increase

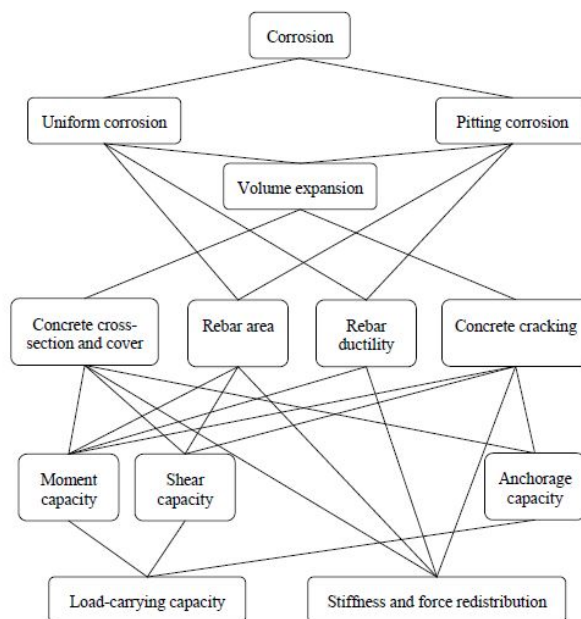


Figure 10.3: Effects of corrosion on load-carrying capacity, stiffness and force redistribution of a concrete structure (Hanjari, 2010)

in the cross section's slenderness. In order to prevent buckling, slenderness should therefore be controlled for corroded cross sections in axial compression (Hanjari, 2010).

As Figure 10.3 illustrates, cracking of the concrete around the reinforcement bars and stirrups will influence the anchorage capacity, shear capacity and moment capacity of the structure. If the concrete in this region has been cracked by corrosion it has reached its maximum tensile strength. Thus, any further tensile stress which can be induced by mechanical loading will contribute to opening larger cracks. This not only affects the shear and anchorage capacities directly, but by giving less protection to the reinforcement and by allowing an aggressive environment direct access to the reinforcement this also reduces the moment capacity of the structure over the longer term. Moreover, the cracks may also change the stiffness of the structure, depending on their direction. This will in turn alter the force distribution in the structure.

10.4 Effect of reinforcement corrosion on shear capacity

As elaborated in Section 8.2, shear failure may occur in the beam end due to three mechanisms. When a diagonal crack is initiated near the beam end, yielding of the

shear stirrups may or may not occur. From here (1) yielding of the shear stirrups may occur until fracture, (2) the concrete in the compressive zone may be crushed, or (3) anchorage failure may occur near the tensile reinforcement.

If reinforcement in the beam end is corroded, this will have an effect on these failure mechanisms. Primarily, diagonal cracks may be initiated due to corrosion of the reinforcement, which leads to tensile stresses in the concrete due to expansive corrosion products. If the shear reinforcement corrodes, the cross sectional area is reduced, which can reduce capacity so that yielding is initiated. Furthermore Section 10.1 elaborates on how ductility is reduced for increasing amounts of corrosion in the reinforcement. This may affect the yielding of the shear stirrups and of the tensile reinforcement if yielding is initiated here. Reduction in the ductility may cause fracture to occur faster than what would be the case for uncorroded reinforcement.

There exists few methods to accurately predict remaining capacity of corrosion damaged structures. This is particularly true regarding shear capacity. Higgins, Farrow and Turan present an American-published paper (Higgins et al., 2012) where four different approaches are used in order to predict the shear capacity of undamaged and corrosion damaged beams. Each methods is modified to account for corrosion induced damage induced to both the shear reinforcement (stirrups) and to the the concrete section. The accuracy of the estimated capacities are controlled through experiments where the capacities of undamaged elements and elements subjected to accelerated corrosion of embedded stirrups are found.

The four methods that are used in the study are:

- Conventional ACI-AASHTO standard specification approach
- Strut and tie method (STM)
- Modified compression field theory (MCFT)
- Analysis by the computer program Response 2000TM

The conventional ACI-AASHTO standard specification approach is the traditional method for computing the shear strength of corroded reinforced concrete elements in the United States. It provides a reasonably simple approach to estimate shear capacity of reinforced concrete structures, where, similar to the NS 3473:1977, the contributions from the concrete and stirrups to the total shear capacity are summed.

The suggested modification of the method in order to account for reinforcement corrosion provides a hands-on procedure, with suggestions on how to handle the various consequences that reinforcement corrosion is known to have on both the reinforcement, concrete and the interaction between the two. Due to the study's simplicity, credibility and it's relevance to this master thesis, the method will be studied further in the remainder part of this chapter. The study will also provide the theoretical basis of the information presented in this thesis regarding how reinforcement corrosion affects the shear capacity of a structure, complimented by the more general information given in the preceding sections.

The conventional ACI-AASHTO standard specification method sums the contributions from the concrete and stirrups to the total shear resistance,

$$V_n = V_c + V_s,$$

where

$$V_c = 2\sqrt{f'_c}b_wd$$

$$V_s = \frac{A_v f_{yt} d}{s}$$

V_n	is the normal shear resistance (lb)
V_c	is the shear resistance of the concrete (lb)
V_s	is the shear resistance of the transverse reinforcement (lb)
f'_c	is the compressive strength of the concrete (psi)
A_v	is the area of the transverse steel (in ²)
f_{yt}	is the yield strength of the transverse steel (psi)
d	is the effective depth (in)
b_w	is the beam width (in)
s	is the spacing of the transverse steel (in)

This method of superposing the contributions from the concrete and the stirrups corresponds to the shear capacity formulas in NS 3473:1977 as presented in Section 8.3. The formula is repeated here for convenience,

$$V_{d0} = f_v (bd + 75A_s) + f_s A_{sv} h',$$

where the first term represents the shear resistance of the concrete and the second term represents the shear resistance of the transverse reinforcement. As can be seen, the transverse reinforcement terms are almost identical (A_{sv} represents the cross sectional area of the shear reinforcement divided by the centre distance s). The terms providing the contribution from the concrete have larger differences, with the American formulas not including the tensile reinforcement's contribution to the capacity as the most marked difference. Despite this, it can be assumed that the approach taken in the study can be transferable to the Norwegian formulas.

Higgins et al. (2012) states that the given formula for V_c tends to underestimate the contribution from the concrete to the total shear strength for deep members (members with shear span-to-depth ratio below 2.5, with the shear span a_v being the portion of the beam in which the shear stresses are high, and depth being the effective depth d of the cross section). The underestimation is a consequence of the fact that it becomes easier for the shear to be transmitted directly to the support by a compression strut for deeper members, and as a consequence the average shear stress at failure becomes progressively larger than in slender beams. Because beams with shear span-to-depth ratio of approximately 2 is used in Higgins et al. (2012), experimental results are used to adjust the formula to accord for this, by changing the factor 2 in the formula for V_c to 5. Testing of uncorroded test specimen similar to the NIB beams used in The Hulvågen Bridge can provide information regarding

whether or not this would be necessary for similar calculations on The Hulvågen Bridge.

The damage on the corroded reinforced concrete is included in the conventional standard specification method through modelling of the damage to the concrete from cracking and spalling as well as the section loss and debonding of the shear reinforcement.

Damage to the concrete from cracking and spalling

In order to establish the shear resistance of the concrete, the concrete damage from corrosion must be estimated. Higgins et al. (2012) use empirical evidence and theoretical computation from observed cover damage due to spalling.

The amount of concrete damage that is observed due to corrosion depend primarily on stirrup spacing, cover distance and degree of corrosion to the underlying rebar. For larger spacing between the stirrups and smaller cover, it is found that the cracks may extend directly towards the surface rather than reach out between the bars (Dagher and Kulendran, 1992). Example of spalling given in Figure 10.4 illustrates that for closer spaced stirrups spalling may interact and occur in the entire cover area, while for more widely spaced stirrups the spall damage is non-overlapping.

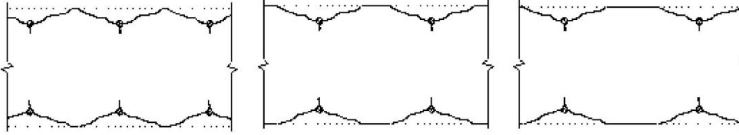


Figure 10.4: Effects of stirrup spacing on cover spalling (Higgins et al., 2012)

Based on the experimental results from the studies by Higgins et al. (2012), it is established that the angle of discrete spalls is approximately 20° . The spalling originates at the intersection of the concrete core (the region within the concrete cover and stirrup layer) and the rebar cross section, as seen in Figure 10.4. Based on these observations expressions to estimate the average remaining beam width $b_{w\text{eff}}$ which is available to resist shear within a stirrup spacing s is established,

$$b_{w\text{eff}} = b_w - 2(c_v + \phi_v) + \frac{s}{5.5} \quad \text{if} \quad s \leq 5.5(c_v + \phi_v) \quad (10.1a)$$

$$b_{w\text{eff}} = b_w - \frac{5.5}{s}(c_v + \phi_v)^2 \quad \text{if} \quad s > 5.5(c_v + \phi_v) \quad (10.1b)$$

Here,

- b_w is the original undamaged beam width (in)
- c_v is the concrete cover (in)
- ϕ_v is the stirrup diameter (in)
- s is the stirrup spacing (in)

Equation (10.1a) shows that as the stirrup spacing becomes smaller, the effective concrete width approaches the core width. Hence Equations (10.1a) and (10.1b) assume that the concrete cover is no longer effective, and can be used when significant corrosion induced cracks are formed on the concrete surface. In the experiments performed by Higgins et al. (2012), corrosion induced cracking was observed in specimens at relatively small section losses of stirrup area, on average 2 %. This observation is in conformity with what was registered by Stemland (2007) as discussed in Section 10.1.1. When section loss in the stirrups occurs to a small degree, there may be some strength contribution attributed to a partially damaged concrete cover. As expected, the damage observed by Higgins et al. (2012) progressed as additional corrosion occurred, with the cracks becoming larger and sounding indicating de-laminations. The concrete cover will then provide less and less contribution to the shear resistance of the concrete, ending at no contribution when all the cover has spalled off.

If this method was to be applied on the NIB beams in The Hulvågen Bridge, the validity of using the formulas for $b_{w\text{eff}}$ on the NIB beams would have to be considered. Whether or not the spalling angle of 20° is directly transferable to other concrete qualities, cover distances, etc. should be controlled, and a new factor valid for the metric system, replacing 5.5, would have to be found.

Section loss and debonding of the shear reinforcement

The section loss of the shear reinforcement is in Higgins et al. (2012) directly quantified through measurements using either digital calipers or a contour gauge. Experimental results from the study showed that despite the fact that the cross sections of highly-corroded rebars appeared quite random on the outward facing side, the surface in contact with the concrete core region tended to be semi-circular. Using a contour gauge to capture the outward facing random rebar perimeter, the cross sectional area can be estimated by assuming the back half as semi-circular.

Two methods were used to include the section loss of the shear reinforcement in the calculations: The average areas over the lengths of stirrups and the local minimum areas of stirrups within a span length equal to the effective depth d of the section. It is recommended to use at least three measurements on a stirrup leg in order to establish the average stirrup area.

The number of stirrups n crossing a potential diagonal crack which is oriented at an angle of 45° is

$$n = \frac{d}{s}, \quad (10.2)$$

where d is the effective depth of the cross section and s is the stirrup spacing. For regular stirrups the *average area* \bar{A}_{v_i} for each stirrup is determined by summing the average area measurements for each of the two legs,

$$\bar{A}_{v_i} = \bar{A}_{leg_1} + \bar{A}_{leg_2}.$$

Within the region of the diagonal crack the average stirrup area is determined

by computing an equivalent stirrup area to be applied at the same spacing as that of the undamaged stirrups,

$$\bar{A}_v = \frac{\sum_{i=1}^n \bar{A}_{v_i}}{n}.$$

When calculating the *local minimum area* of stirrups the number of stirrups crossed by an assumed 45° diagonal crack are computed using Equation (10.2). The minimum area for each stirrup within this region is determined through measurements. The smallest area \dot{A}_{v_i} for each stirrup is determined by summing the local minimum area measurements for each of the two legs,

$$\dot{A}_{v_i} = \dot{A}_{leg_1} + \dot{A}_{leg_2}.$$

However, as described in Section 10.1.2, corrosion has been shown to decrease the ductility of reinforcement steel. For cases where two legs of the same stirrup exhibit significantly different degrees of corrosion the reduced ductility of one leg may therefore limit the ability to achieve the combined strength of both legs. Higgins et al. (2012) suggest that the reduced ductility of the stirrup due to corrosion can be included through the recommendation that if one leg exhibits 75 % more section loss than the other, the area of both legs is set to that of the smallest area. Furthermore, if a stirrup has undergone complete section loss in one leg, it should be assumed that the stirrup is not capable of effectively restraining a diagonal crack due to loss of bond around the legs (see Section 10.2). Because of this the area for both legs should be set equal to zero.

Within the region of the diagonal crack the minimum stirrup area is determined by computing an equivalent stirrup area to be applied at the same spacing as that of the undamaged stirrups,

$$\dot{A}_v = \frac{\sum_{i=1}^n \dot{A}_{v_i}}{n}.$$

Once the equivalent corrosion-damaged stirrup area is determined using the two methods above, the shear resistance of the transverse reinforcement is calculated for each case.

Evaluation of the method based on results from Higgins et al. (2012)

The proposed equations provide a reasonably simple method to estimate shear capacity of corrosion damaged reinforced concrete structures.

Using the average area over the length of the stirrups as the corroded cross sections provided a mean value for the ratio of experimental to calculated shear strength (V_{exp}/V_n) of 1.13, with a coefficient of variation of 0.120 (Higgins et al., 2012). Using the minimum stirrup area gave a mean value for V_{exp}/V_n of 1.28, with a coefficient of variation of 0.263.

The results shows that using the minimum stirrup area in general predicted conservative results. For cases where stirrups were completely corroded the approach of using the minimum area was overly conservative. Use of average values

for stirrup area tended to provide better correlation with experimental results, indicating that some partial bonding of the stirrups may have permitted transfer of stress between the rebar and concrete, even for locally significant section loss (pitting corrosion). The partial bond may shield the locally reduced stirrup area from strain concentrations, except when diagonal cracks are formed adjacent to the pit location.

Furthermore it is evident that the corroded pairs of rebar legs have retained sufficient ductility to prevent the locally reduced cross sectional areas from controlling the strength of the specimen. This is in accordance with the findings by Tahershamsi (2016), see Section 10.3, where it was stated that the structure's shear capacity is not directly influenced by the rebar ductility. It can be concluded that despite having regions where concrete cover is completely spalled it will be overly conservative to fully discount the contribution of any discontinuous stirrups by using the minimum stirrup area. Instead the average area over the stirrup length should be used.

(Higgins et al., 2012) also studies three other methods that were listed in the beginning of this section. These methods are based on more complicated models, and provide highly accurate results when the calculated shear capacities are compared to the shear capacities of the uncorroded test specimen. However, for the corroded test specimen the other methods provide roughly the same mean values and coefficients of variation for V_{exp}/V_n as the conventional standard specification approach. The ratio for the mean values does in fact correspond best for the conventional approach, while the coefficients of variation are somewhat lower for some of the other methods.

In all methods the corrosion damage is incorporated by modifying model attributes so that cross sectional loss in stirrups and damage of concrete cover is included. The fact that the conventional method includes the corrosion damage in the similar manner as the more complicated methods, and results in approximately the same accuracy, may indicate that it is the corrosion assumptions that all the methods are based on that is the most deciding factor regarding the accuracy of the results, while the explored methods all provide relatively accurate results in themselves. Based on this it be concluded that the method described above provides reasonable accuracy despite it's simplicity, and it can be a valuable approach in order to establish the shear capacity of corrosion damaged reinforced concrete structures.

As mentioned, some adaptations are necessary if the conventional ACI-AASHTO standard specification approach is to be used for the beams in The Hulvågen Bridge. The expression for $b_{w\text{eff}}$ must be adopted, and furthermore it must be taken into account that the shear reinforcement in the NIB beams are not regular two-legged stirrups, but instead one-legged bars through the web. However, since the stirrups are placed double, as described in Figure 5.1, similar effects to what is described by Higgins et al. (2012) may occur.

Because there does not exist detailed information regarding reinforcement corrosion of The Hulvågen Bridge, the conventional ACI-AASHTO standard specification approach can not be used in this thesis. A simplified approach will instead

be taken, where only the reduction in the cross sectional area of the stirrups is included when the corroded shear capacity is established. However, if more accurate information regarding the scope of corrosion damage on the bridge is established, this approach can be used in order to assess the effect that corrosion damage will have on the shear capacity.

Chapter 11

Shear capacity control of the corroded structure

In this chapter the information presented in Chapter 3 and Chapter 10 regarding deterioration of reinforced concrete structures and consequences of reinforcement corrosion is utilized in order to assess the effect that various consequences of corrosion will have on the shear capacities established in Section 9. In the second part of this chapter, the established information is used to assess the damages that have been observed on The Hulvågen Bridge. In addition, a similar bridge which shows more extensive visible corrosion near the beam ends will be assessed using the information established in this and previous chapters.

11.1 Capacity calculations

In Chapter 9 the capacities and utilization ratios with regards to shear are established assuming that no corrosion damage has occurred in the structural members. The previous chapter establishes a theoretical basis regarding the consequences reinforcement corrosion will have on the shear capacity of a structure. In the following sections an assessment of the tolerance of the composite beams with regards to reinforcement corrosion will be performed.

Similarly as for the study performed by (Higgins et al., 2012), the consequences of shear reinforcement corrosion that constitute the basis for this assessment are reduction of reinforcement area and reduction in concrete cover due to spalling. Only spalling in the beam web, which is caused by shear reinforcement corrosion, will be relevant for the shear capacity. Reduction of reinforcement area will be considered both for the shear reinforcement in the web and for the tensile reinforcement in the upper part of the beam. It has previously been established that change in reinforcement ductility has little effect on the shear capacity of a structure (see Sections 10.2 and 10.4).

In the following a sensitivity study, where the consequences each factor has on the total shear capacity, will be performed. The sensitivity study will be strictly

theoretical, in that spalling is assumed to occur without corrosion of the underlying reinforcement. This approach is chosen in order to get a clear overview of how large effect each factor will have on the shear capacity. The capacities will be reduced in the sections that have been established as critical for each shear failure mechanism, in order to be able to establish the amount of area reduction or spalling that will be critical according to the two standards.

11.1.1 Reduction in shear reinforcement area

The effect of reducing the shear reinforcement area will be studied in this section. For both NS 3473:1977 and EC2 the shear reinforcement area is only included in the diagonal tension capacities.

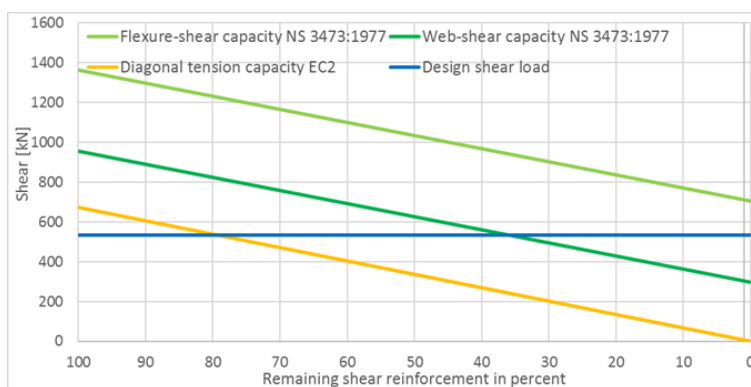


Figure 11.1: Diagonal tension capacity for increasing degree of stirrup corrosion at section 1800 mm from beam end

NS 3473:1977

Considering loss in cross sectional area of the shear stirrups in the critical section at 1800 mm from the beam end, results in the graphs given in Figure 11.1. As the figure shows, both the flexure-shear capacity and the web-shear capacity calculated according to NS 3473:1977 decrease linearly with decreasing amount of remaining shear reinforcement. Because the term that gives the contribution from the shear reinforcement to the total shear capacity for the two capacities is the same (see Equation (8.3) and Equation (8.6)), the capacities will decrease at the same rate.

It is clear from the flexure-shear capacity curve in Figure 11.1 that in the section of the beam where this capacity is highest utilized, the capacity remains sufficient even when all the shear reinforcement is corroded and assumed inactive. The flexure-shear capacity when all shear reinforcement is corroded is 52 % of the original capacity. Due to the low utilization ratio of only $\eta = 0.39$ for flexure-shear capacity (as seen in Table 9.3) in the uncorroded state, this is evidently sufficient.

This finding corresponds with Figure 9.5, from which it was concluded that the flexure-shear capacity is sufficient for all sections of the beam without taking

the shear reinforcement into account, as long as the axial load from prestressing is applied.

This result makes it evident that the flexure-shear capacity according to NS 3473:1977 is not very vulnerable to shear reinforcement corrosion. As long as the load from prestressing acts on the beam, considerable shear reinforcement must be combined with concrete spalling if the flexure-shear capacity is to become insufficient. However, as Figure 9.4 illustrated, the beam will likely fail due to web-shear failure before flexure-shear failure will occur.

In Section 9.2.2 it was found that shear reinforcement is necessary for the web-shear capacity to be sufficient, regardless of whether or not the beam is prestressed. However, the prestressing increases the capacity compared to beams without prestressing as can be seen in Equation (8.6), and therefore has a favourable effect. These findings were illustrated in Figure 9.6.

Figure 11.1 shows that the web-shear capacity according to NS 3473:1977 becomes insufficient if more than 36 % of the shear reinforcement area is lost. In reality this value will be slightly lower in the considered section because the fact that certain prestressing strands are coated is not included in the establishing of the design axial load N_γ , and the transmission of the prestressing forces is not taken into account either. However, for approximately 36 % corrosion of the shear reinforcement, the shear capacity according to NS 3473:1977 is no longer on the safe side, and failure of the structure may occur.

EC2

For EC2 the amount of shear reinforcement in the beam is included in the diagonal tension capacity given by Equation (8.22). The section d from the edge of the support in which the diagonal tension capacity was calculated according to EC2 corresponded with the section 1800 mm from the beam end which was found to be critical for diagonal tension capacity according to NS 3473:1977. The diagonal tension capacity according to EC2 was calculated in Appendix E, and as Chapter 9 found the EC2 formula rendered a lower diagonal tension capacity than NS 3473:1977, with a utilization ratio of $\eta = 0.79$ in the uncorroded state. This can also be seen in Figure 11.1.

The capacity decreases in a linear manner, similar to the NS 3473:1977 formulas. The term including the shear reinforcement area is denoted as $A_{sw}szf_{ywd}$ in the EC2 formula in contrary to $f_sA_{sv}h'$ for the NS 3473:1977 formulas. However, because A_{sv} in NS 3473:1977 is defined as the shear reinforcement area divided by the central distance (s), and it is assumed that both $h' = 0.9d$ and $z = 0.9d$ in the calculations, the contribution will be identical. EC2 will therefore also decrease with the same slope as the NS 3473:1977 formulas for increasing amount of corrosion.

As can be seen in Figure 11.1 the diagonal tension capacity according to EC2 reduces to zero when the shear reinforcement is completely corroded. This corresponds with the assumptions behind Equation (8.22), where only the contribution of the shear reinforcement to the total shear capacity of the beam is considered. When 21 % of the total shear reinforcement's area has corroded the diagonal tension

capacity according to EC2 is no longer sufficient.

11.1.2 Reduction in tensile reinforcement area

The effect of reducing the cross sectional area of the longitudinal reinforcement has furthermore been studied. The tensile reinforcement is included in the flexure-shear capacity formula in NS 3473:1977, as seen in Equation (8.3). The considered section has tension in the upper part of the composite beam, so only the longitudinal reinforcement in the bridge deck and in the upper flange of the beam will affect the corrosion. The tensile reinforcement amount is not included in the compressive shear capacity formula in NS 3473:1997, nor is it included in any shear capacity formulas in EC2.

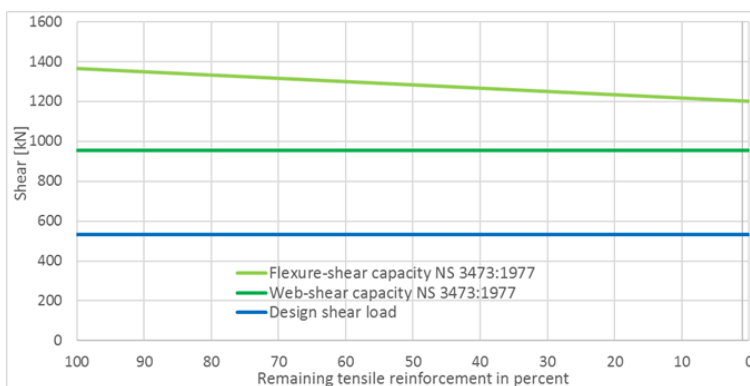


Figure 11.2: Diagonal tension capacity for increasing degree of tensile reinforcement corrosion at section 1800 mm from beam end

Assuming equal amount of corrosion in all steel bars so that d is not altered, a graph showing the effect that the reduction of the total tensile reinforcement area has on the diagonal tension capacity in the critical section at a distance 1800 mm from the beam end is given in Figure 11.2. The assumption of equal amount of corrosion in all steel bars is only performed in order to simplify the calculations. As damages on the bridge deck, reproduced in Section 4.2.3 have indicated, sea water may be leaking through the deck. This means that the longitudinal reinforcement in the bridge deck is vulnerable with regards to corrosion. The prestressing steel and the two mounting bars in the upper part of the NIB beam are slightly more protected. If corrosion occurs primarily in the reinforcement in the deck the effective depth d of the composite beam will be reduced, causing further reduction in the shear capacity.

As the figure illustrates the web-shear capacity is not affected by the reduction in the tensile reinforcement, while the flexure-shear capacity is reduced linearly with increasing degree of corrosion. Both capacities will be affected if d is altered. When considering the unaltered d , it is evident that the total reduction in the flexure-shear capacity is very small, the flexure-shear capacity of a section where all

tensile reinforcement is corroded is still 88 % of the original flexure-shear capacity. This indicates that the effect that the tensile reinforcement has on the total shear capacity in this composite beam is minimal.

Because the total longitudinal reinforcement in the lower part of the composite beam is lower than the total longitudinal reinforcement in the upper part ($A_{s,uk} = 1900 \text{ mm}^2$ compared to $A_{s,ok} = 3919 \text{ mm}^2$), the contribution to the flexure-shear capacity will be even less for the regions of the beam that experience tension in the lower part of the cross section.

It is evident from these results that the contribution from the shear reinforcement and/or the axial load will provide a much larger contribution to the total flexure-shear capacity given by Equation (8.3) than the tensile reinforcement for this composite beam. For beams without axial load, or where the amount of shear reinforcement is much lower, the contribution from the tensile reinforcement may be larger.

It can be noted that corrosion will decrease the ductility of the longitudinal reinforcement, which will reduce the amount of yielding that can occur before the reinforcement fractures. The possibility that structural failure will occur in a ductile manner with preliminary warnings will decrease, while the risk of brittle failure increase of increasing amount of corrosion. This is, however, more relevant for failure due to exceeded moment capacity than for shear failure.

11.1.3 Reduction in beam web concrete cover

The width of the beam web is included in both diagonal tension capacities and in the compressive shear capacity formula given in NS 3473:1977. In EC2 only the compressive shear capacity contains the width of the web when considering members that require shear reinforcement.

While the critical section with regard to diagonal tension capacity is 1800 mm from the beam end, the critical section when regarding compressive shear capacity was found to be at the cross sectional change occurring 1425 mm from the beam end. Here the design shear load is $V_{Ed,1425} = 550 \text{ kN}$, while at the critical section with regards to diagonal tension capacity the design shear load is $V_{Ed,1800} = 533 \text{ kN}$. For EC2 the compressive shear capacity is controlled at the support, where the design shear load is $V_{Ed,support} = 609 \text{ kN}$.

The beam web consists of stirrups of diameter 12 mm placed vertically through the beam web. In addition there are five longitudinal mounting bars of diameter 8 mm that are spread through the beam web, and that are neglected for all analyses in this thesis. In the regular cross section the reinforcement is covered by 40 mm concrete on each side, rendering a total web width of 100 mm. From the beam end and up to a distance of 1425 mm the web has a total width of 300 mm. In this region the concrete cover has a width of 140 mm on each side. Because the beam consists of only one stirrup the cover over the stirrup will correspond to the width of the web.

Figure 11.3 gives an overview of the effect that reducing the width of the beam web has on diagonal tension capacity and the compressive shear capacity according

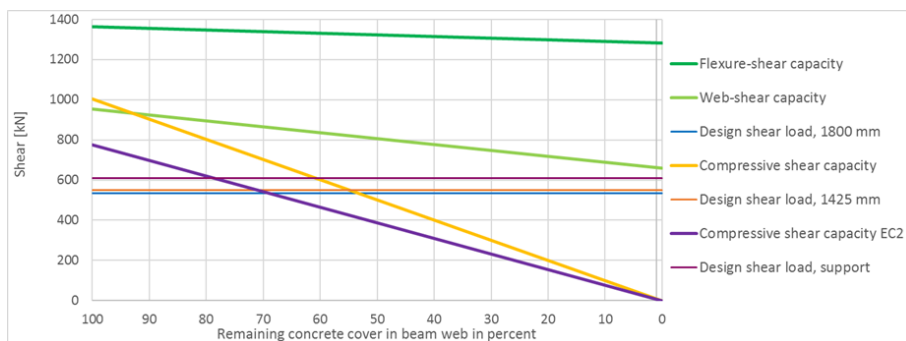


Figure 11.3: Diagonal tension capacity for increasing degree of beam web cover spalling in various sections

to NS 3473:1977, as well as on the compressive shear capacity according to EC2. The figure also gives the design shear load occurring in each of the three sections.

It is important to note that the reduction from 100 % to 0 % concrete cover will involve a lot more concrete spalling for compressive shear capacity according to EC2, which is controlled at a section with a 300 mm wide beam web, than what is necessary to achieve the same percentage reduction of the concrete cover for the two capacities according to NS 3473:1977, which are controlled at sections where the beam web is 100 mm.

NS 3473:1977: Diagonal tension capacity

Figure 11.3 shows that the flexure-shear capacity of the beam is not noticeably affected by the reduction in the beam width. This, combined with the low impact that the tensile reinforcement is established to have, indicates that the contributions from the shear reinforcement and the prestressing load are sufficient to resist the design shear load alone.

Furthermore it is evident from the figure that the web-shear capacity is affected more by the reduction in the web width than the flexure-shear capacity. When comparing Equation (8.6) with Equation (8.3) it can be seen that the concrete's contribution to the total shear capacity is twice as high for the web-shear capacity than for the flexure-shear capacity. However, when comparing with the design load occurring at a distance 1800 mm from the beam end it is clear that also for web-shear failure the capacity is still sufficient despite no contribution from concrete.

It should be noted that the fact that the diagonal tension capacities do not decrease towards zero for 100 % corroded concrete cover is strictly theoretical. In reality failure will occur in the beam when the spalling of the concrete cover has reached a critical value, where the assumptions that lie behind the capacity formulas regarding how the stresses are absorbed and distributed through the beam no longer are valid.

NS 3473:1977: Compressive shear capacity

The compressive shear capacity according to NS 3473:1977 consists of one term, which includes the beam width b . This causes the compressive shear capacity to reduce to zero when the entire concrete cover has spalled off. When 45 % of the concrete cover has become ineffective the compressive shear capacity is no longer sufficient when compared to the design load acting at the section 1425 mm from the beam end.

EC2: Compressive shear capacity

The compressive shear capacity according to EC2 reduces in a similar manner as for NS 3473:1977. When no spalling has occurred the capacity is lower than for NS 3473:1977, despite the web having a three times larger cross section. The capacity is reduced at a slower rate, and results in zero capacity when all the concrete in the web is spalled.

11.1.4 Anchorage capacity

Equation (8.29) makes it clear that the anchorage capacity primarily depends on the horizontal stirrup area, and a reduction in the stirrup area will give a linear decrease in the capacity. The utilization of the anchorage capacity of $\eta = 0.62$ leaves tolerance for some corrosion of the horizontal stirrups, but if more than 38 % of the reinforcement area is corroded the anchorage capacity is no longer sufficient when considering the crack angle that is valid for EC2. The stirrups lie close to the concrete surface with minimum amount of cover in several directions, and are therefore prone to chloride attack.

Furthermore the anchorage capacity is dependent on the bond between the concrete and the reinforcement. This is not quantified in the capacity formulas, but bond contributes to resist the mechanism that occurs due to anchorage failure. As elaborated in Section 10.2, corrosion leads to a reduction in the bond properties. Hence, if corrosion in the prestressing steel in the lower part of the beam occurs, this may contribute to reducing the anchorage capacity of the beam. However, as established in Section 10.2, the bond strength is decreased less near supports due to simultaneous compressive stress in the transversal direction.

11.1.5 Resistance at the interface between the beam and deck

It has been shown that the shear resistance at the interface between the beam and bridge deck is almost entirely utilized in the critical section at the support. The shear reinforcement is also highly exposed to reinforcement corrosion if sea water is leaking through the deck.

With the reinforcement in the interface contributing to 78 % of the total resistance as established in Section 9.5.2, only a small amount of corrosion is necessary for the shear resistance to become insufficient. Also here the shear resistance will

be reduced linearly for increasing amount of corrosion. If all reinforcement across the interface is assumed to be corroded the shear resistance in the interface will be $v_{Rd} = 0.20$ MPa, i.e. the shear resistance of the interface have utilization ratio of $\eta = v_{Ed}/v_{Rd} = 0.91/0.20 = 4.5$.

11.1.6 Concluding remarks

In the preceding sections a sensitivity study regarding the effect that various consequences of corrosion will have on the shear capacity of the composite beam in The Hulvågen Bridge has been studied isolated. In reality, spalling of cover will not occur without corrosion of reinforcement underneath. Corrosion of tensile reinforcement and reinforcement of shear stirrups may occur independently because the two are located in different parts of the composite beam.

As stated in Section 10.1 normally around 5 to 20 % of the reinforcement bar is corroded before spalling occurs. The corrosion will progress further before spalling occurs for smaller bar diameters. This indicates that a substantial amount of shear reinforcement corrosion will occur before cracking and spalling initiates.

Because concrete spalling in the beam web only comes as a consequence of shear reinforcement corrosion it can be assumed that the diagonal tension capacity, which is the only failure mechanism that is affected by shear reinforcement corrosion, will become the decisive factor over the compressive shear capacity when the composite beam is exposed to corrosion, both when considering NS 3473:1977 and when considering EC2.

For NS 3473:1977 the web-shear capacity has the lowest tolerance for corrosion, and this is will also be more effected by concrete spalling once this initiates than the flexure-shear capacity. The compressive shear capacity according to NS 3473:1977 requires a substantial amount of concrete spalling before the utilization ratio becomes critical. It is therefore likely that web-shear capacity will become decisive.

For EC2 only 21 % of the shear reinforcement has to corrode for the diagonal tension capacity to become insufficient. Spalling will not contribute to reducing the diagonal tension capacity, so when spalling occurs only the compressive shear capacity will be affected by this. However, it is likely that sufficient amount of shear reinforcement corrosion can occur before spalling reduces the compressive shear capacity to a critical level.

However, it is clear from the preceding chapters, in particular from Table 9.3, that the structure is relatively robust against corrosion with regards to shear capacity. In general a substantial amount of reinforcement corrosion can occur before the shear capacity becomes critical. It is primarily the shear resistance at the interface between the beam and deck that should be studied more closely. If the interface is examined more closely and repairs are performed where necessary, shear failure will likely not be the relevant unless large amounts of the reinforcement has corroded.

11.2 Evaluation of corrosion damage in The Hulvågen Bridge

As stated in Chapter 3 the main challenge for durability of reinforced concrete bridges in coastal environments is chloride induced corrosion. In this section the damages on The Hulvågen Bridge is considered in more detail, using the theory and calculations that have been performed in this and the preceding chapters. An assessment of the effect that the observed damages may have on the shear capacity of the structure is also given based on this. In addition to this, the next section contains a discussion regarding corrosion damages observed in another bridge similar to The Hulvågen Bridge, where the damages are more extensive.

The previously registered damages on The Hulvågen Bridge are collected from Brutus, and were presented in more detail in Section 4.2.2. These damages primarily regard efflorescence due to lime on the beams and on the underside of the bridge deck in the spans near the inspection hatch at axis 10. The damages are most comprehensive on the underside of the bridge deck, registered with a consequence of 3V, while the efflorescence on the beams are registered with consequences 1V or 2V. In addition to the efflorescence small diagonal cracks near the pillar in the second axis are registered on a beam between axes 2 and 3, with a consequence of 2V. Reinforcement corrosion due to chloride attack is also registered on the underside of the bridge deck near axis 10, with a consequence of 3V.

11.2.1 Observed damages from inspection in May 2017

On the excursion to the Atlantic Ocean Road from the 9th to the 10th of May 2017 several forms of examinations were performed in order to assess the state of The Hulvågen Bridge. Visual inspections where further signs of damage beyond what is registered in Brutus was looked for. As stated in Section 4.1.2 the underside of the NIB beams were covered with plywood in 1994 as an attempt to protect the beams and bridge deck from sea spray. Inspection lids were included in the plywood in order to make it possible to supervise the beams near the abutments, but the largest parts of the NIB beams and underside of the deck is no longer easily accessible. In addition the beams and underside of the deck were surface treated with silane/siloxane-impregnation in 2000. Visual inspection of the accessible area around both abutments gave no visible indications of chloride induced corrosion or any other deterioration mechanisms of the beams or bridge deck. Due to inaccessibility it was not possible to further examine the small diagonal cracks that are registered in Brutus in a beam near the pillar in the second axis.

Dust samples were taken from three NIB beams in order to examine for chloride content. In total four samples were taken; one at each side the sea exposed beam, one at a inner beam and one at the outer beam surface of the fjord exposed beam. These tests are not concluded, and so the results are not available at this time.

Further inspections of the beams and deck were performed by entering the inspection lid at axis 10. In conformity to what is registered in Brutus, efflorescence was observed on the underside of the bridge deck in this area. Figure 11.4 shows a

photo taken between two beams inside the inspection hatch, where the efflorescence in the bridge deck is visible. A smaller amount of efflorescence on the beams are also visible in the image, in conformity with what is registered in Brutus.



Figure 11.4: Efflorescence on the underside of the bridge deck near axis 10

Further examinations have been performed on samples of the efflorescence that were taken during the inspection. X-Ray Diffraction analysis has been performed on the white powder, and the analysis showed that the powder indeed is a form of lime (CaCO_3 , calcium carbonate), as is registered in Brutus. It was found that the powder mainly consists of aragonite, which can be formed through precipitation of sea water. Based on this analysis it can be assumed that the lime efflorescence is caused by leakage of sea water through the bridge deck.

If sea water is in fact leaking through the bridge deck, this indicates that the reinforcement in the bridge deck may be exposed to corrosion. This theory may be strengthened by the observance of reinforcement corrosion in the underside of the bridge deck in the same area as the efflorescence, as is registered in Brutus. Corrosion damage can also be seen in Figure 11.4, and several spots like this was visible in the area. The localized leakage of rust products to the surface may indicate pitting corrosion.

11.2.2 Damages in connection with shear capacity

In this section discussions will be made regarding how the damages that have been observed in the bridge may affect the shear capacity of the composite beam. These discussions are based on the information established in this and previous chapters.

Corrosion of shear stirrups

As the previous section shows, no visible corrosion and no extensive cracking or spalling has been observed on the surface of the NIB beams near the examined supports. However, as previously established, the fact that corrosion can not be observed, does not necessarily mean that it does not occur.

Section 3.2.4 states that chloride induced corrosion of regular reinforcement generally occurs in a relatively uniform manner, and the probability of leakage of rust products to the surface is relatively high. If the reinforcement bar is of small diameter however, corrosion may occur without giving visible signs on the surface.

The shear reinforcement in the beam has diameter 12 mm. This diameter is relatively low, and there exists therefore a chance that corrosion has initiated in the stirrups. However, it can be assumed that visible signs of corrosion should leak to the surface if extensive corrosion is taking place. No rust products on the surface therefore indicates that the shear reinforcement in the beam web is not exposed to extensive corrosion.

Cracking and spalling of the concrete web

As was established in the parameter study in the preceding sections, the shear capacity can mainly be reduced through reduction of the shear reinforcement area and spalling of the concrete of the web. As stated in Sections 10.1.1 and 10.4 around 1 - 2 % of the reinforcement area can normally be corroded when the first cracks appears, while it is normal with around 5 - 20 % corrosion before spalling occurs. When no spalling has occurred in the examined part of the beam, and no cracks were discovered during visual inspection, it can be assumed that the amount of shear reinforcement corrosion in the beam is low.

Corrosion of tensile reinforcement

Because the tensile reinforcement also influences the diagonal tension capacity according to NS 3473:1977, possible corrosion of this will also be discussed here. As stated in Section 3.2.4, corrosion of prestressing steel usually occurs in the form of pitting corrosion, with little or no leakage of corrosion products to the surface. It can therefore not be known without further examinations whether or not corrosion is occurring in the prestressing steel.

When the structural system of the bridge is considered continuous, tension will be in the upper part of the beams near the supports. Corrosion of the prestressing may therefore not be crucial with regards to shear capacity, because the majority of the prestressing is placed in the lower part of the cross section and do therefore not contribute to the shear capacity. However, if the structural system is assumed to be more or less simply supported, which in fact will be closer to reality for the beams in this bridge, tension will occur in the lower part of the beam. Corrosion of the prestressing reinforcement may then have an affect on the diagonal tension capacity of the beams.

The assumed leakage of sea water through the bridge deck indicate that the reinforcement of the bridge deck is exposed to a highly corrosive environment. If corrosion is occurring here, and the structural system of the bridge is considered partly continuous with tension in the upper part of the section near the beam ends, corrosion in the longitudinal reinforcement in the deck may affect the shear capacity. Figure 11.4 indicates that corrosion may be occurring in the bridge deck.

Based on the quality of the bridge deck, corrosion of the tensile reinforcement in the deck is considered much more likely than corrosion of reinforcement in the beam.

However, as it has been established in Section 11.1.2, corrosion of tensile reinforcement causes very small reduction of the diagonal tension capacity for this bridge system. Corrosion of the longitudinal reinforcement is therefore not considered crucial with regards to diagonal tension capacity. It should be noted that if corrosion is in fact occurring in the prestressing steel this will have an impact when considering the moment capacity of the beam.

Anchorage

Due to the covering of the superstructure with plywood boards, the underside of the NIB beams are no longer available for inspection, neither outside nor inside the inspection hatch. Corrosion of the anchorage reinforcement is often primarily visible on the underside of the NIB beams, as the images provided in the next section may indicate. The covering of the beams therefore makes it difficult to establish whether or not visible corrosion of the anchorage reinforcement has occurred. As established, no indications of corrosion was found on the sides of the beams.

The interface between the beams and deck

In addition to the tensile reinforcement, leakage of sea water through the bridge deck may also be crucial for the bridge deck's contribution to the shear capacity of the composite beam. It is considered likely that corrosion may be occurring in the reinforcement crossing the interface, due to the assumed leakage of sea water through the bridge deck. As has been established, very little corrosion can occur here before the shear resistance in the interface becomes insufficient according to EC2.

As mentioned previously this failure mechanism will not necessarily cause collapse of the structure. Nevertheless it is evident that the consequences of insufficient shear resistance in the interface between the beam and deck must be looked into.

Concluding remarks

Taking the observed damages in the NIB beam and the bridge deck into consideration, it is evident that there is little evidence indicating that an imminent shear failure is prone to occur in the beam. Further examinations and repairs of the interface between the bridge deck and beam is necessary in order to avoid de-coupling of the two members, but with regards to shear capacity this is nevertheless assumed to not be critical.

Fossum, Halsnes and Hyseni have found in their master thesis that the moment capacity is approximately 100 % utilized in mid-span when considering a span of length 25.8 meters in The Hulvågen Bridge (this group has based their calculations on the span widths described in the drawings of the complete bridge instead of the working drawings that are the basis here, see Section 4.1.2). In this section the design shear stresses at the interface will be very low. However, if uncoupling of the

bridge deck occurs in a section where the shear stress is relatively high, combined with considerable moment, the capacity of the beam may become insufficient.

If corrosion in the prestressing reinforcement is occurring without visible signs on the beam surface, and/or loss of compressive strength in the bridge deck occurs as a result of the damages that are observed in the deck, the moment capacity of the beam may be reduced to a critical level, even with coupling of the beam and deck. As Section 10.1.3 has shown, both yield strength and elasticity modulus is reduced for increasing amount of corrosion in prestressed reinforcement that is exposed to stress. Mass-loss will also occur faster if the strands are exposed to high levels of stress (up to 80 % of the yield strength), and very brittle failure modes can occur in strands loaded up to over 70 % of yield strength. Simplified calculations of the levels of prestress in the strands in the lower part of the beam, overlooking loss of prestress, can be found by establishing

$$\sigma = \frac{F}{A_s} = \frac{134 \text{ kN}}{100 \text{ mm}^2} = 1340 \text{ MPa.}$$

Comparing this with the yield strength of the prestressing steel, $f_y = 1700 \text{ MPa}$, makes is clear that the strands are wired up to $1340/1700 = 0.79 = 79 \%$ of the yield strength. This shows that several of the factors above may assert themselves when corrosion occurs in the prestressing strands.

It is clear that The Hulvågen Bridge may be risking failure due to other failure modes than shear failure. The quality of the bridge deck and whether or not corrosion has initiated in the prestressing steel should be looked further into.

11.3 Similar bridge with more extensive corrosion damage near the supports



Figure 11.5: Bridge between Amundsøya and Brattøya

With the inaccessibility of the beams in The Hulvågen Bridge, and the lack of observable corrosion damage in the accessible parts of the beams, it can be of

interest to study a similar bridge in the similar region, which displays more visible corrosion damage.

On the Flatøy road, between the two islands Amundsøya and Brattøya, a small one-lane bridge of approximately 100 meters is located. As seen in Figure 11.5 the bridge consists of three spans with two rows of prefabricated NIB beams placed over transversal supports, and with a cast-in-place bridge deck over the beams. The beams in this bridge are exposed to the seawater (not covered using plywood), and no surface treatment is visible on the beams or underside of the bridge deck.

While The Hulvågen Bridge is located on the outer coastal area and is directly exposed to the open sea, the bridge between Amundsøya and Brattøya is located in an inner coastal area, somewhat more shielded from the most aggressive harsh coastal environment caused by sea spray, etc. Despite this, extensive corrosion damages can be seen in the beams and bridge deck near the abutments.



Figure 11.6: Corrosion near the east abutment



Figure 11.7: Close-ups of corrosion area 'C' near the east abutment

Figures 11.6 and 11.7 show leakage of rust products to the beam surface next to the abutment in the eastern part of the bridge. Figure 11.7 shows two close-ups of the corrosion close to the area denoted 'C', somewhat further away from

the abutment. The beams near the west abutment show similar damages. It is natural to assume that this bridge does not have sufficient concrete cover over the reinforcement according to today's standard, similar to The Hulvågen Bridge. This is likely a contributing cause to the large amount of visible corrosion on the concrete surface. Spalling of some of the concrete cover also appears to have occurred in the examined parts of the beams.

The corrosion appears to be more or less uniform over a larger area, which in accordance with Section 3.2.4 may indicate that it is the corrosion of regular reinforcing steel that is seen, and not corrosion of prestressing steel. Because the corrosion is concentrated around the supports it can be assumed that it is the additional reinforcement placed here as anchorage reinforcement that shows visible signs of corrosion.

It is clear from the calculation procedure established in Section 8.5 that corrosion of the horizontal stirrups will affect the capacity with regards to anchorage failure. Horizontal stirrups often lie near the concrete surface, with a minimum amount of cover to protect the stirrups. If the stirrups are sufficiently corroded, yielding and possible fracture of the stirrups may occur, and the entire beam may collapse.

It should be noted that with this extensive corrosion visible on the concrete surface it can be considered likely that the chloride concentration near the prestressing steel has reached sufficient levels for corrosion to occur also here. As elaborated in Section 11.1.4, corrosion of prestressing steel will reduce the bond to the concrete, which may increase the danger of slipping of the reinforcement relative to the concrete. The combination of this effect with corrosion of anchorage reinforcement may be devastating.

Chapter 12

Future work

The suggestions to future work that should be performed as a follow-up to this thesis can be considered as threefold.

Shear failure is a complex phenomenon which often is an outcome of several failure mechanisms occurring simultaneously. Several calculation procedures exist today, both in old and current national and international standards. In addition there exists literature where more specialized or more complex calculation models are suggested. However, due to the complexity of the mechanisms behind shear failure, further development of more accurate methods to predict shear capacity will always be necessary.

Furthermore, more research into how reinforcement corrosion affects the shear capacity of a structure, as well as its influence on the shear failure mechanisms that may occur, is necessary. As it has been elaborated in this thesis, it is known that reinforcement corrosion affects a number of properties in the reinforcement, the concrete and the interaction between the two. However, when the remaining capacity of a corroded structure is calculated, simple assumptions are often made and only a few of the properties that are affected are directly included in the calculations. At this time there exists few calculation models where the more complex properties that are affected by corrosion can be included. When corrosion becomes as extensive as presented for the bridge between Amundsøya and Brattøya, large uncertainties exist when assessing the remaining capacity and the risk of failure of the bridge.

Finally, more specific information regarding future work on The Hulvågen Bridge should be provided. First and foremost, there are a few uncertain factors that should be worked out:

- The actual length of the bridge's spans is not certain. As has been mentioned, there exists two sets of drawings that provide very different information regarding spans.
- Information regarding the bridge deck is scarce. The concrete quality and the quality, amount and layout of the reinforcement that is used in the deck has only been based on recommendations in the NIB manuals (Statens Vegvesen,

1983), and is not established with certainty.

- The amount of reinforcement corrosion in the structural members of the bridge is not known. There are few signs of visible corrosion on the NIB beams, but as established prestressing reinforcement is known to corrode without visible signs on the concrete surface. Further examinations of chloride content in various parts of the bridge should be performed.

Based on the assumptions that have been made in this thesis, it can be concluded that the risk of shear failure in the NIB beams and bridge deck is not imminent. However, as Fossum, Halsnes and Hyseni have established in their master's thesis, the moment capacity of the beams in mid-span can be questioned, particularly if corrosion has occurred in the prestressing reinforcement or if the quality of the bridge deck is substantially reduced due to leakage of sea water through the deck. Furthermore, as established in this thesis, the interface between the beams and bridge deck is highly utilized near the beam ends, and corrosion in the reinforcement crossing the interface due to leakage of sea water may cause this capacity to be exceeded. Further examinations of the NIB beam's capability to carry all design loads in sections where decoupling may occur is necessary. In addition, further examinations of the damages to the bridge deck and the interface, and repairs where necessary, is recommended.

Chapter 13

Conclusion

In this thesis, shear capacity calculations have been performed on the structural beams in The Hulvågen Bridge. NS 3473:1977, which was the standard valid when the bridge was designed in 1987, and Eurocode 2, which is valid today, have both been used as basis for the calculations.

The bridge is exposed to extremely aggressive marine environment, and the effect that reinforcement corrosion can have on the shear capacity of the beams has been studied. Examinations of the bridge from an excursion in May indicate leakage of sea water through the bridge deck, which increases the risk of reinforcement corrosion in the deck. No visual signs of corrosion in the NIB beams have been found.

It has been established that the utilization ratios in the uncorroded state are well below 1.0 for all the three main failure mechanisms, i.e. diagonal tension failure, compressive shear failure and anchorage failure. Based on the fact that the bridge has more than sufficient capacity in the uncorroded state, and that little or no damage is observed in the NIB beams, it has been concluded that neither of the three main shear failure mechanisms are likely to occur at this time.

Furthermore it is found that the shear resistance in the interface between the beams and bridge deck is utilized to a degree of $\eta = 0.96$. Leakage of sea water through the bridge deck indicates that this resistance may be lessened due to corrosion of the reinforcement crossing the interface. Exceeding the capacity of the interface will not necessarily cause failure of the beam, but will require that the NIB beams must carry all design loads in the section without contribution from the bridge deck. The consequences of this must be further examined. In addition, it is recommended to further examine the damages to the bridge deck and interface, and perform repairs where necessary.

Even if corrosion has not yet occurred in the NIB beams, it is only a question of time before it will initiate. The bridge was designed for a service life of 100 years, and should therefore in theory have a remaining service life of 70 years. Several factors including the small concrete cover that has been used in the bridge, as well as how fast the bridge deck has deteriorated, indicate that the bridge in all likelihood will not remain standing for this long.

Bibliography

- A. A. Almusallam. Effect of degree of corrosion on the properties of reinforcing steel bars. *Construction and Building Materials*, 15(8):361–368, 2001.
- Luca Bertollini, Bernhard Elsener, Pietro Pedferri, and Rob Polder. *Corrosion of Steel in Concrete: Prevention, Diagnosis, Repair*. Wiley-VCH, Weinheim, 2013.
- H.J Dagher and S. Kulendran. Finite element modeling of corrosion damage in concrete structures. *ACI Structural Journal*, 89 (6)(699-708), 1992.
- Mohamed K. ElBatanouny, Jesé Mangual, Paul H. Ziehl, and Fabio Matta. Early Corrosion Detection in Prestressed Concrete Girders Using Acoustic Emission. *Journal of Materials in Civil Engineering*, 26(3):504–511, 2014.
- Kamyab Zandi Hanjari. *Structural Behaviour of Deteriorated Concrete Structures*. Gothenburg, 2010.
- Anders Hermundsdal and Andrés Pétursson. *Beregning av en betongelementbru*. Master's thesis, NTNU, 2015.
- Christopher Higgins, William C. Farrow, and O. Tugrul Turan. Analysis of reinforced concrete beams with corrosion damaged stirrups for shear capacity. *Structure and Infrastructure Engineering*, 8(11):1080–1092, 2012.
- S. Jacobsen, M. Maage, S Smeplass, K.O. Kjellsen, E.J. Sellevold, J. Lindgård, R. Cepuritis, R. Myrdal, Ø. Bjøntegaard, M. Geiker, and M.fl. *Concrete Technology 1 TKT 4215*. Norwegian University of Science and Technology, Trondheim, 2016.
- Reidar Kompen and Gunnar Liestøl. *Publikasjon nr. 78*. Oslo, 1995.
- Marek Kovačovic. Shear Resistance between Concrete-Concrete Surfaces. *Slovak Journal of Civil Engineering*, XXI(4):25–34, 2013.
- Rolf Lenschow. *Betongkonstruksjoner*. Tapir, 1979.
- Rolf Lenschow, Erik Thorenfeldt, and Hans Thomas Øderud. *Dimensjonering for skjærkraft*. 1978.

- Fumin Li, Yingshu Yuan, and Chun Qing Li. Corrosion propagation of prestressing steel strands in concrete subject to chloride attack. *Construction and Building Materials*, 25(10):3878–3885, 2011.
- Oda Munthe-Kaas. *Beregning og dimensjonering av korrosjonsskadet betongbru*. Master's thesis, NTNU, 2014.
- Norcem. *God betong er bestandig*.
- Norsk Betongforening. *Publikasjon nr. 10: Beregning og dimensjonering av kontinuerlige NOB- og NIB-broer*. 1981a.
- Norsk Betongforening. *Publikasjon nr. 11: Flerfelts NIB- og NOB-broer Beregning og dimensjonering av kontinuerlig broplate over støttene*. 1981b.
- Norsk Betongforening. *Bestandighet av betongkonstruksjoner Del 1: Skadeårsaker*. 2003.
- Norsk Standard. *NS-EN 1992-1 Eurocode 2: Design of concrete structures - Part 1-1: General rules and rules for buildings*. 2004.
- Norske Sivilingeniøres Forening. *NS 3473 Prosjektering av betongkonstruksjoner. Beregning og dimensjonering*. 1973.
- Michael G. Oliva and Pinar Okumus. *Finite element analysis of deep wide-flanged pre-stressed girders to understand and control end cracking*. 2011.
- Sigurd Helle Opedal. *Evaluering av korrosjonsskadet betongbru med betydelig skadeomfang*. Master's thesis, NTNU, 2016.
- Magdalena Jadwiga Paciorek, Terje Kanstad, and Max Hendriks. *The effect of reinforcement corrosion on the structural behaviour of prestressed bridges in the Norwegian coastal regions*. 2017.
- R. Palsson and M. S. Mirza. Mechanical response of corroded steel reinforcement of abandoned concrete bridge. *ACI Structural Journal*, 9(2):157–162, 2002.
- Shahram Pezeshk. *Chapter 9. Shear and Diagonal Tension 9.1*. 2014.
- Portland Cement Association. *Types and Causes of Concrete Deterioration*. 2002.
- Kompen Reidar. *Betongregelverk relatert til bestandighet*. 2015.
- P Schiessl. *Corrosion of Steel in Concrete*. Chapman and Hall, 1988.
- Dr. Amlan K Sengupta and Prof. Devdas Menon. *7. 1 Transmission of Prestress, Part I*.
- SINTEF Byggeforsk. 520.061 Armeringskorrosjon. In *Byggeforskserien*. 2009.
- Svein Ivar Sørensen. *Betongkonstruksjoner*. Akademika forlag, Trondheim, 2013.

- Marios Soutsos. *Concrete durability: A practical guide to the design of durable concrete structures*. Thomas Telford Ltd, London, 2010.
- Standard Online AS. Eurokoder, 2003. URL <http://www.standard.no/fagomrader/bygg-anlegg-og-eiendom/eurokoder1/>.
- Statens Vegvesen. *Håndbok 100 Bruprosjektering 08 NIB-BRUER*. 1983.
- Statens Vegvesen. *Håndbok V441 Inspeksjonshåndbok for bru*. 2000.
- Statens Vegvesen. *Håndbok R412 Bruklassifisering*. 2003.
- Statens Vegvesen. *Prosjektering av bru, Skjærdimensjonering*. 2013.
- Statens Vegvesen. *Håndbok N400 Bruprosjektering*. 2015.
- Hans Stemland. *Betongkonstruksjoners Livsløp, DP2 B3 Styrkeberegninger ved korrosjonsskader*. Number 16. Oslo, 2007.
- Mohammad Tahershamsi. *Structural Effects of Reinforcement Corrosion in Concrete Structures*. Gothenburg, 2016.
- Erik Thorenfeldt. *Dimensjonering av spennbetong etter ny NS 3473*. 1990.
- N.A. Vu, A. Castel, and R. Francois. *Effect of stress corrosion cracking on stress-strain response of steel wires used in prestressed concrete beams*. 2009.
- Nick Winter. Sulfate Attack in Concrete and Mortar, 2005. URL <http://www.understanding-cement.com/sulfate.html{#}>.
- Libin Yin. *Continuity of bridges composed of simple-span precast prestressed concrete girders made continuous*. 2004.

Appendix A

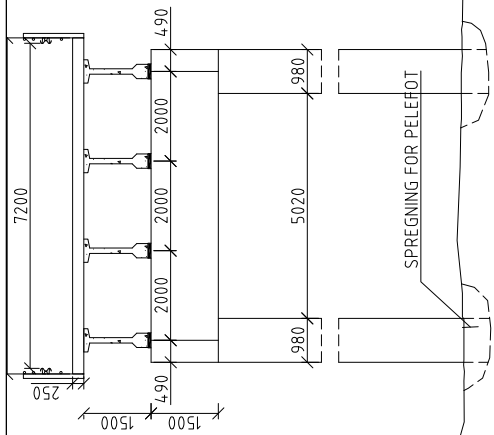
Drawings of The Hulvågen Bridge

In this appendix the following drawings of various structural members in The Hulvågen Bridge is presented, in the given order:

- The drawing of the completed bridge produced by The Norwegian Public Roads Administration in August 1999
- Production drawings of the prefabricated NIB 500/1435 beams produced by Vestlandske Spennbetong AS in May 1987, also containing a bar schedule and information regarding properties of the materials used in the beams
- Working drawings of the cast-in-place substructure of The Hulvågen Bridge produced by Johs Holt in 1987, including an overview showing the profile and cross section of the bridge
- Drawings made by the NPRA in April 1994 showing the plywood boards that have been placed underneath the NIB beams, covering the entire superstructure of the bridge in order to protect from sea spray

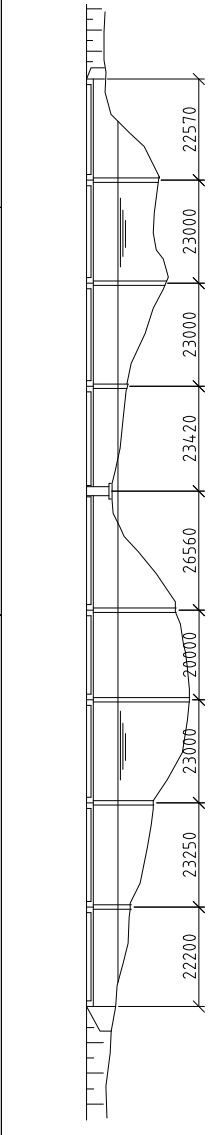
The production drawings of the prefabricated beams include a scanned page where parts of the information regarding regular reinforcement in the NIB beam is missing. Combining the drawings with the bar schedule makes it possible to establish the missing information with relative certainty, as elaborated in Section 5.1.2.

IVERSSNITT M= 1:100

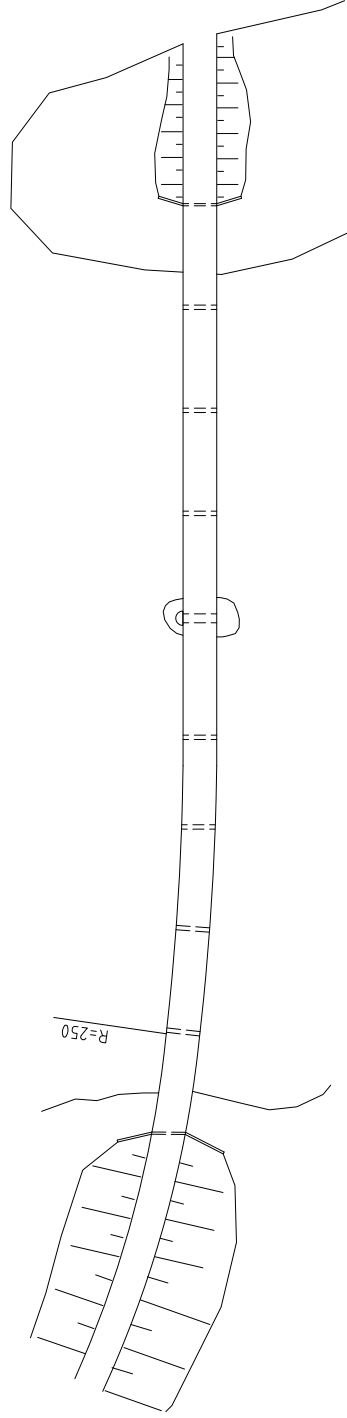


HULVÅGBRUA	bru	64	2182	1987	arkiv nr. 68 - 2182
FYLKE	KOMMUNE	nr.	brunnr.	bygd år	
MØRE OG RØMSDAL	EIDE	Kilometering (beliggende)	HP 15	KM 2,973	MOLDE
BRUSYSTEM	KONTINUERLIG NIB-BJELKEBRU				
KONSTRUKSJON (MATERIALER)	ARMERT BETONG				
BRUDEKKE	ARMERT BETONG				
UNDERBYGNING (MATERIALER)	ARMERT BETONG				
FUNDAMENTERING	PÅ FJELL				
SPENNVIDDE/FRI LENGDE	207,8 M				
KURVEUTV. B=	M	GANGBANER	G=	M	FØRINGSÅVSTAND F=
fri bredde over fering	999	fri bredde over rekkverk	999	fri høyde over c bru	1
konstruert for lasth.	SVV 1971	konstruert for akseltrykk	BK 10	fritt settip	3,5x 20,0
OVERBYGNING	STATENS VEGVESEN MØRE OG RØMSDAL				
KONSTRUERT AV	STATENS VEGVESEN MØRE OG RØMSDAL				
BYGD AV	STATENS VEGVESEN MØRE OG RØMSDAL				

OPPERISS M= 1:1000



GRUNNRISS M= 1:1000

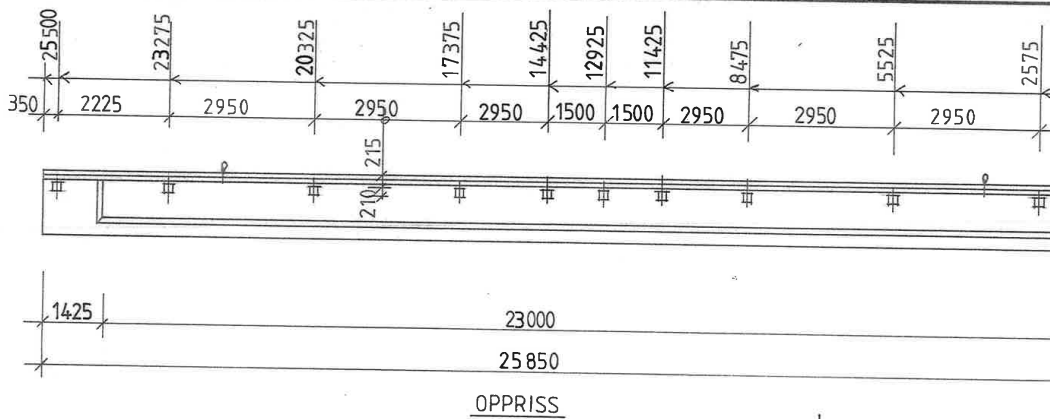


skisse tegnkunnsvar

forsterket/utv.
TEGN. 13.08.1999 ORS.
TRAC.

8-4056-A1 LANDKAR, FORM OG ARMERING
8-4058-A1 OVERBYGNING

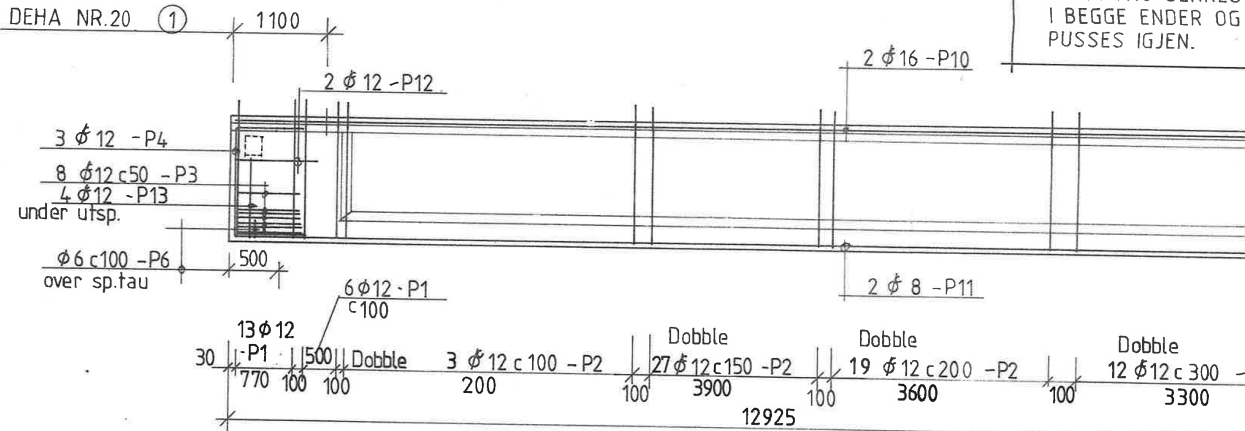
Tegn nr.



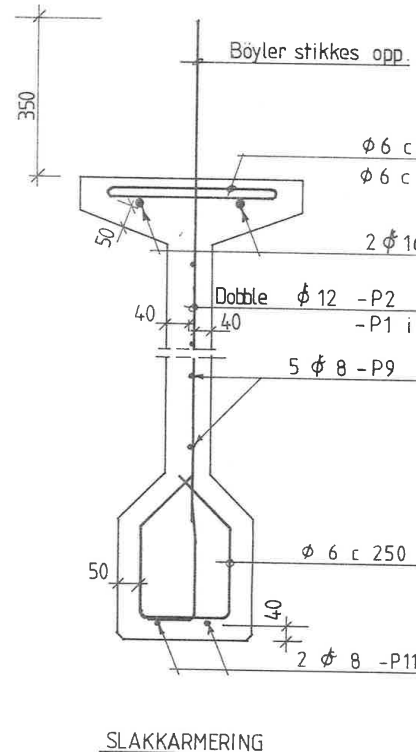
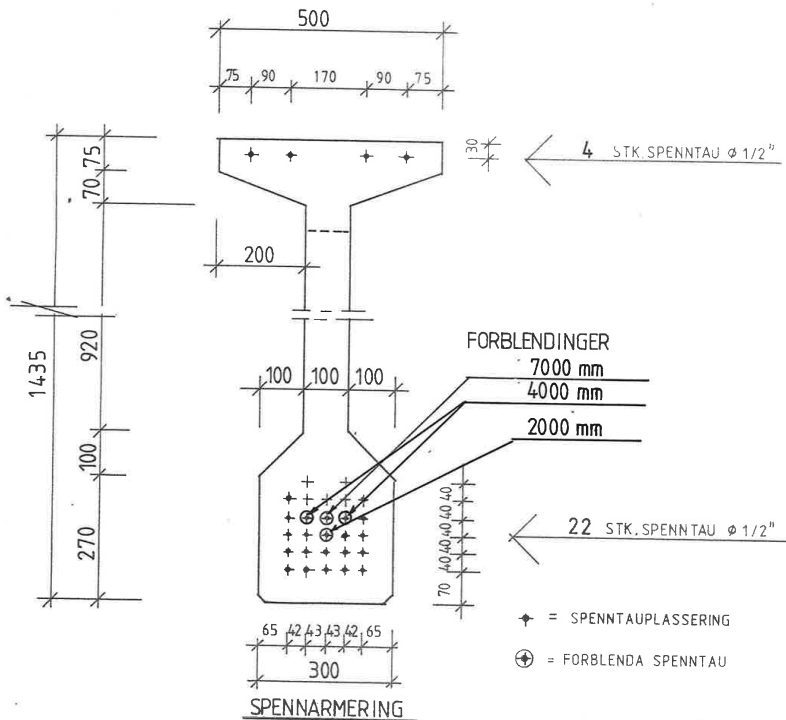
OPPRISS

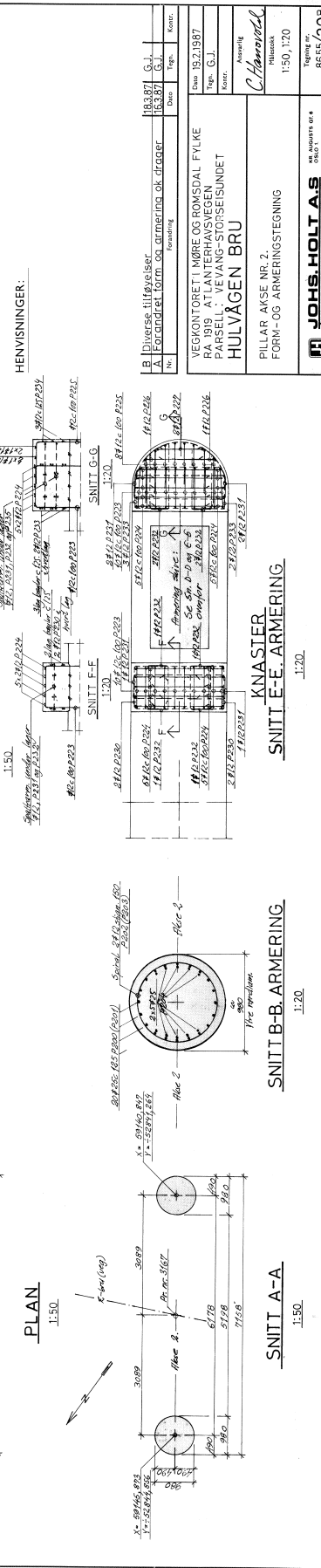
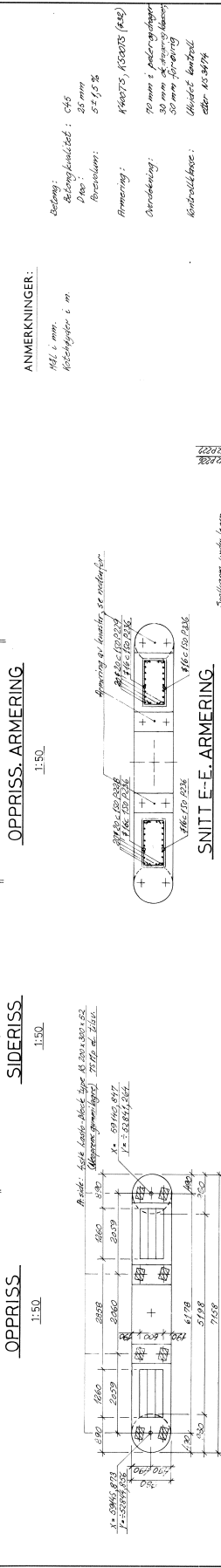
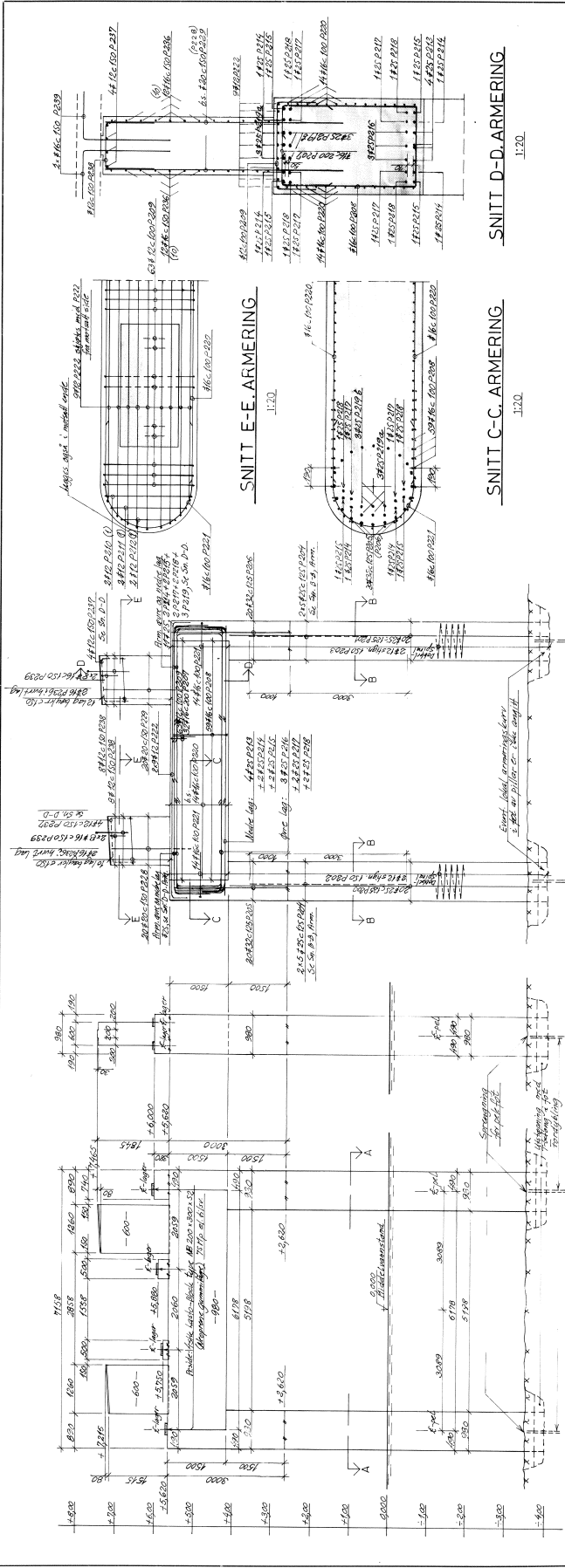
NB!

SPENNTAU SENKES I BEGGE ENDER OG PUSSES IGJEN.



ARMERING





SNITT D-D ARMERING
1:20

OPPRISS ARMERING
1:50

OPPRISS ARMERING
1:50

SIDERISS
1:50

OPPRISS
1:50

SNITT C-C ARMERING
1:20

OPPRISS ARMERING
1:50

SIDERISS
1:50

OPPRISS
1:50

ANMERKNINGER:
 HØI i mm.
 Røstehøyder i m.
 Betongtykkelse: 045
 Dece: 25 mm
 Forstevolum: 5 ± 1,5 %
 Armering: A400T5, A320T5 (A32)
 Overdekning: 70 mm i påstrøketlag
 30 mm af retningsbetong
 50 mm forovering
 Udviklet kantbet
 efter NS 3474

HENVISNINGER:

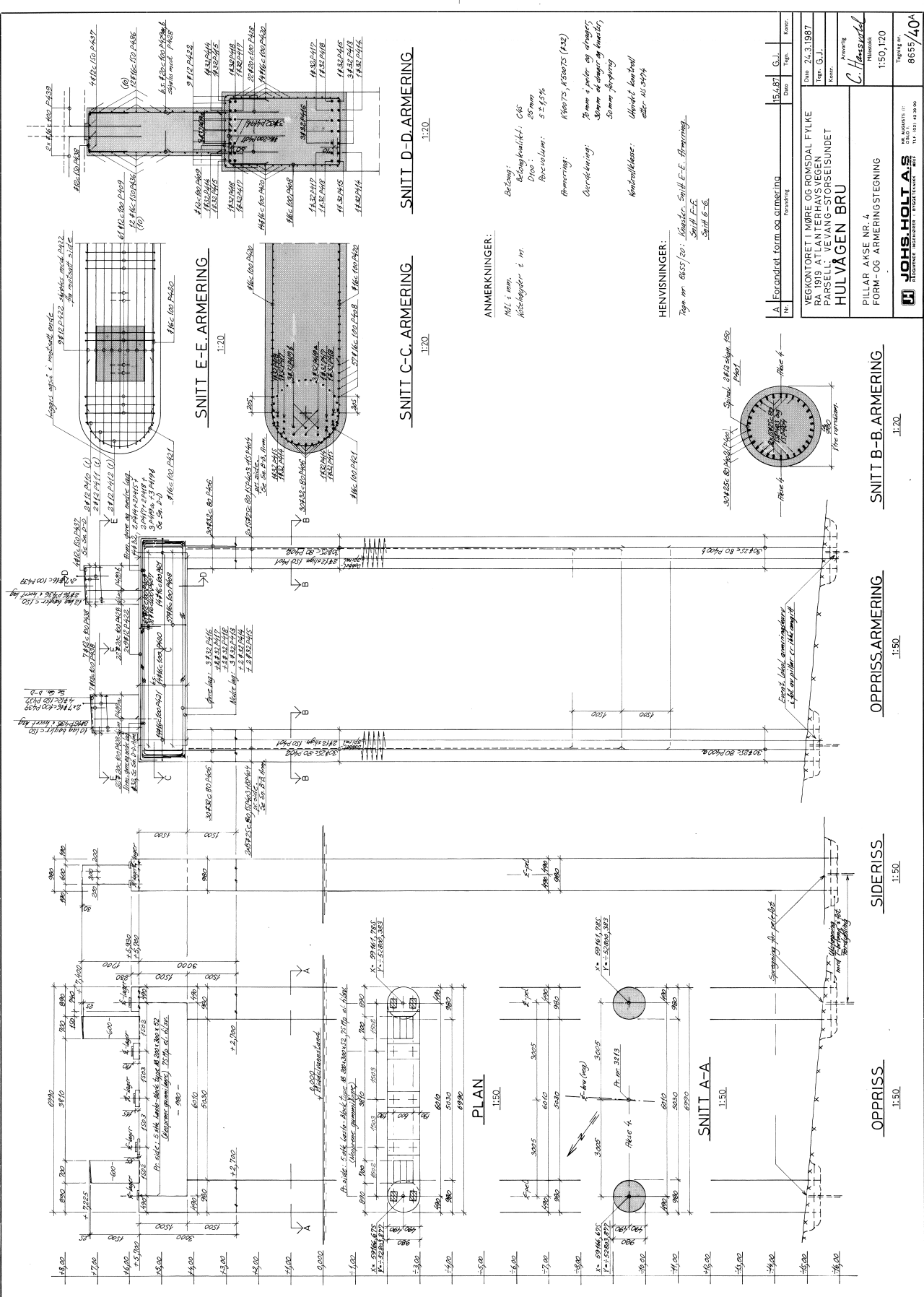
B Diverse tilføjelser
 For ændret form og armering se drøbet
 Udgivelsesdato: 19.11.1987
 Tegner: G.J.
 Kontor: G.J.
 Udgivelsesdato: 19.11.1987
 Tegner: G.J.
 Kontor: G.J.

VEKONTOR ETI MØRE OG RØMSDAL F.V.VE
 RA 1919 ATLANTERHAVSVEJEN
 PARSELL: VEVANG-STORSEI-SUNDET
 HULVÅGEN BRU

PILLAR AVISE NR. 2
 FORM- OG ARMERINGSTEGNING

JOHNS HOLTAS
 Byggetekniker i Trondheim

Udgivelsesdato: 19.11.1987
 Tegner: G.J.
 Kontor: G.J.



SNITT D-D ARMERING
1:20

SNITT C-C ARMERING
1:20

SNITT B-B ARMERING
1:20

SNITT E-E ARMERING
1:20

SNITT A-A
1:50

PLAN
1:50

ANMERKNINGER:

Nett i mm.
Abtøringer i m

HENVISNINGER:

Tegn nr. 0625/20, Skovde, Snitt E-E, Armering.
Snitt F-F.
Snitt G-G.

Betong:
Betongkvalitet: C25
Densitet: 2500 kg/m³
Arbeidsvolum: 0,215 m³
Armering: A400/25, A500/25 (A32)
Overdekning: 20 mm i øverste og nederste, 30 mm på de andre tre sider.
Kvalifikasjon: Utvalgt kontrollør nr. 40 2474

A Forandret form og armering		Date	15.4.87	G.J.	Kontor
VEKSTORRET I MØRE OG RØMSDAL FYLKE		Dato	24.3.1987		
PARSEL A I HULVÅGEN BRU		Tegn	G.J.		
HULVÅGEN BRU		Kontor		Arbeidsgiver	
PILLAR AKSE NR. 4				Hensvald	
FORM- OG ARMERINGSTEGNING				1:50, 1:20	
JOHS. HOLT A.S.				Tegning nr. 8655/40A	
RESURSE INGENIØR- FIRMETUNING				1:1 001 42 30 00	

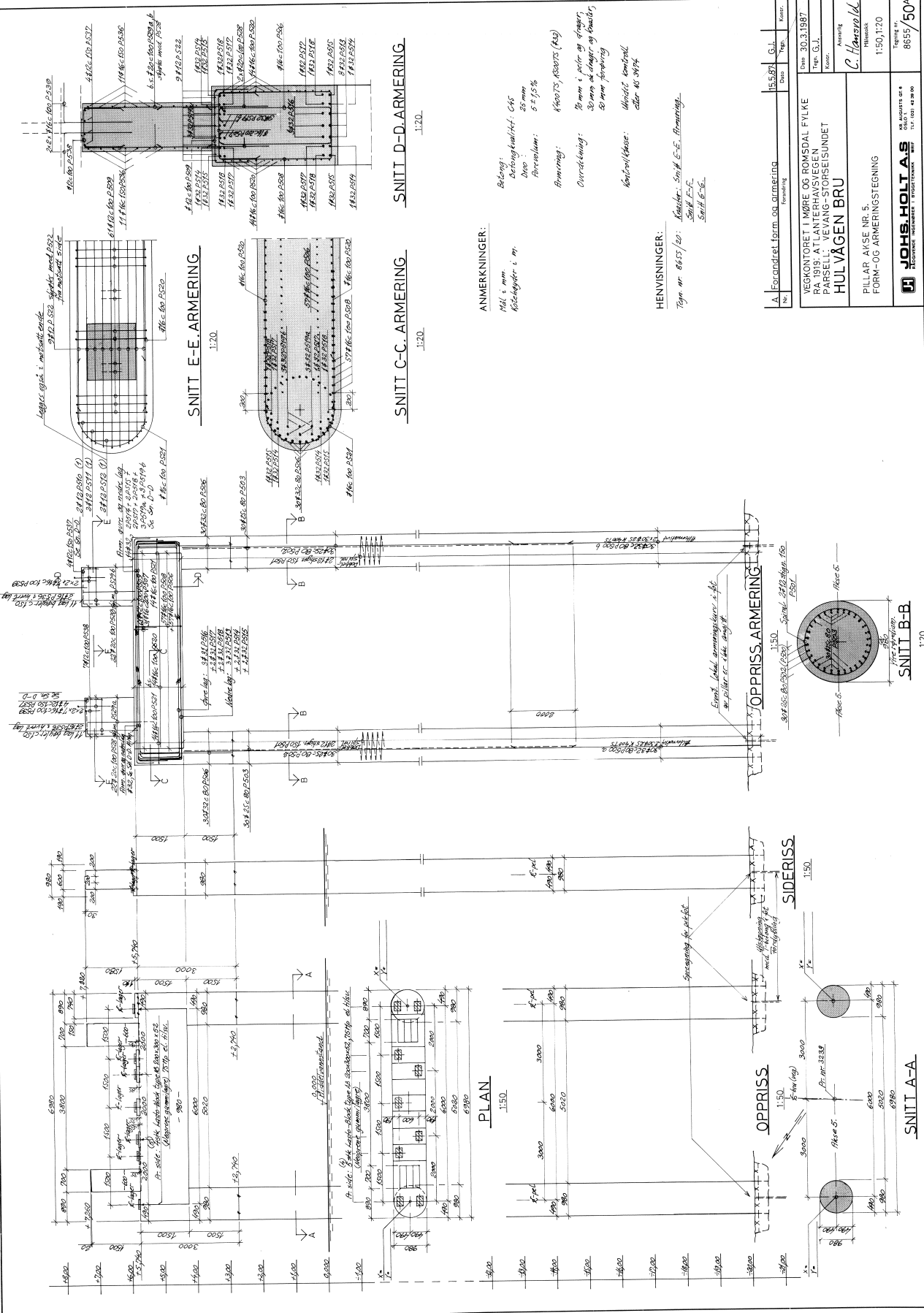
OPPRISS ARMERING
1:50

SIDERISS
1:50

OPPRISS
1:50

SNITT B-B ARMERING
1:20

SNITT E-E ARMERING
1:20



SNITT D-D-ARMERING

1:20

SNITT C-C-ARMERING

1:20

SNITT E-E-ARMERING

1:20

ANMERKNINGER:

- 1. Hø. i mm.
- 2. Betongkvalitet: C15
- 3. Decc: 25 mm
- 4. Armerings: 8 x 125
- 5. Armering: 4000 x 3000 (A3)
- 6. Overdekning: 70 mm i alle retninger, 30 mm ut langs og innover 80 mm forover
- 7. Kontrollklasse: Mindst 5000 eller 40 000

HENVISNINGER:

Tegnr nr 8655/20. **Arbeider: Snitt E-E, Armering- Snitt E-E, Snitt C-C, Snitt D-D.**

A. Forandret form og armering	15.5.97	G.I.	Korr.
	Dato	Tegn.	
Basis 30.3.1987			
Tegn. G.I.			
Korr.			
Arbeider			
C. Hansvold			
Pluss			
1:50, 1:20			
Tegning nr			
8655/50			

VEGKONTORET I MØRE OG ROMSDAL FYLKE
RA 1918: ATLANTERHANSVEGEN
PARSELL, VEIVANG-STORSEIUNDET
HULVÅGEN BRU

PILLAR AKSE NR. 5.
FORM- OG ARMERINGSTEGNING



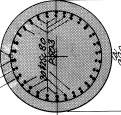
15. AUGUST 1987
710 020 12 000

OPPRISS-ARMERING

1:30

SNITT B-B

1:20



PLAN

1:50

OPPRISS

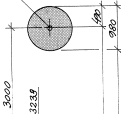
1:50

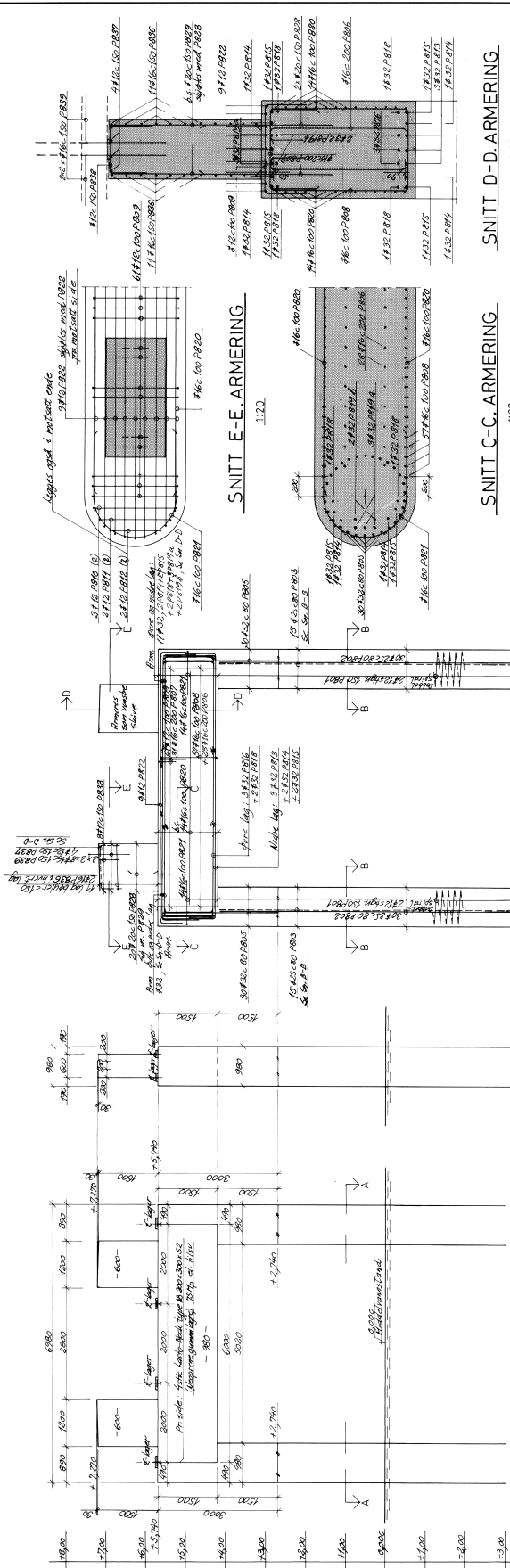
SIDERISS

1:50

SNITT A-A

1:50





ANMERKNINGER:

Arb. i mm.
Arbeidsdybde 1 m.

ARMERING:
Arbets, 3000/15 (412)

SPRØKKELING:
2 mm i pæler og vinger
30 mm ved støping
50 mm forbyring

KONTROLLER:
Målest. kontroll
dtr.-nr. 3874

HENVISNINGER:

VEKONTORET I MØRE OG ROMSDAL FYLKE
RA 1919 AT LANTERHAVSVÆGEN
PARSELL: VE VANG-STORSEIUNDET
HULVÅGEN BRU

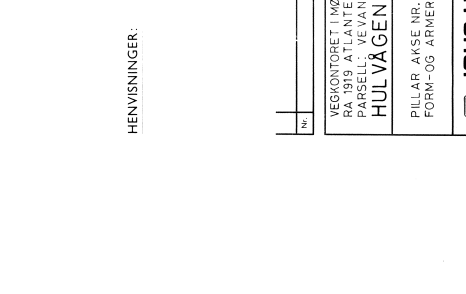
PILLAR, AVASE NR. 8
FORM- OG ARMERINGSTEGNING

No.	Formering	Dato	Tegn.	Kontor
Utgitt av: JOHNS. HOLT & S Tømrere, møbelsnekker og arkitekter Postboks 110, 1500, Tvedestrand				
Tegningsnr.: 8655/80 Skala: 1:50, 1:20				

PLAN
1:150

SNITT A-A
1:150

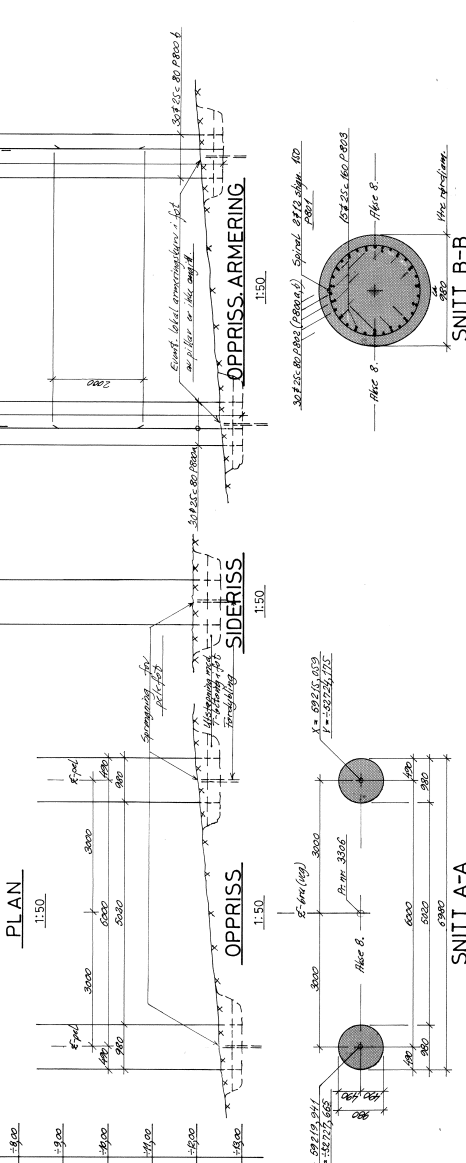
SNITT B-B
1:20

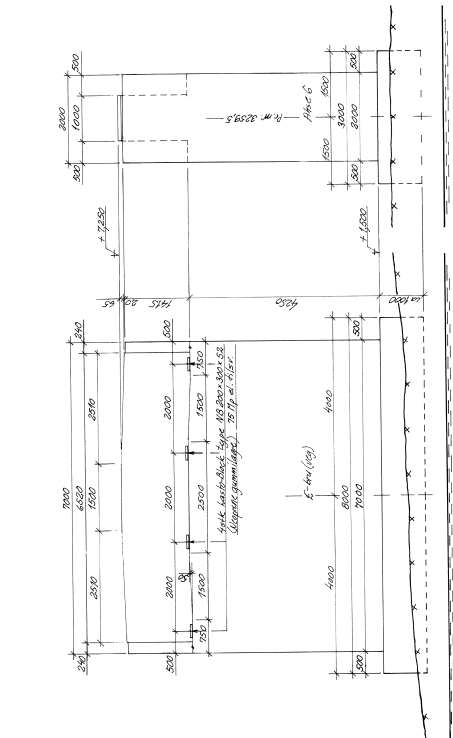


OPPISS-ARMERING
1:150

SNITT A-A
1:150

SNITT B-B
1:20

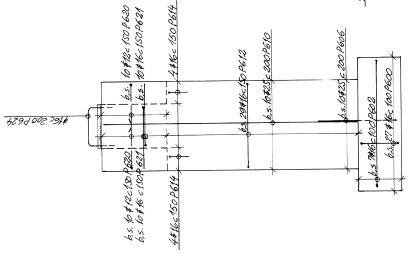
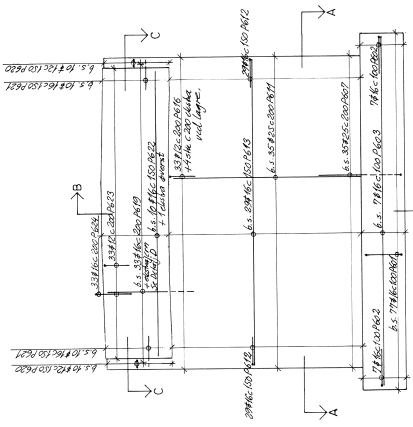




OPPRISS
1:50

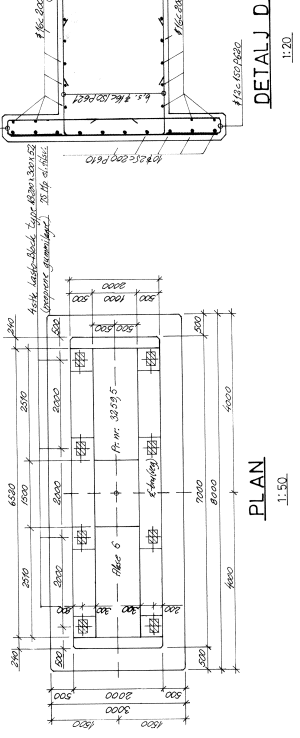
SIDERISS
1:50

OPPRISS ARMERING
1:50



SIDERISS ARMERING
1:50

SNITT B-B
1:50



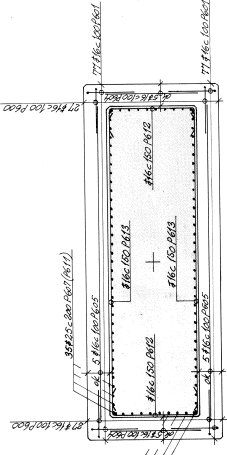
PLAN
1:50

DETALJ D
1:20

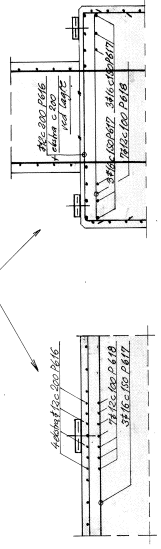
ANMERKNINGER:

- Betong: C35 med L6
- Støppestyringsdybde: 20 mm
- Armering: K60275
- Overdekning: 80 mm i fundamentet, 30 mm forøvrigt
- Kantstøbt løse: 100 mm forøvrigt eller 100 mm

HENVISNINGER:




SNITT A-A ARMERING
1:50



SNITT F-F
1:20

SNITT E-E
1:20

Nr.	Dato	Tegn.	Kontor.
Formering			
Dato 11.2.1987			
Tegn. G.J.			
Kontor.			
Anvendt			
Målestok			
1:50, 1:20			
Tegning nr.			
8655/60			
VEKONTORET I MØRE OG ROMSDAL FYLKE RA 1919 ATLANTERHAVNSVEGEN PARSELL: VEIVANG-STORSEISUNDET HULVÅGEN BRU			
SKJÆRPILLAR AKSE NR. 6 FORM- OG ARMERINGSTEGNING			
 JØRGEN HOLT AS 1100 SANDNESVEI 10 4015 SANDNES			
NS 840015 01 8 17 121 42 28 00			

Appendix B

Effective beam stiffness

In this appendix, effective moduli of elasticity reduced for creep is calculated in accordance with Appendix B of EC2. The resulting effective beam stiffness is included in the formula for the secondary moment from prestressing, presented in Section 6.6.2, and calculated in Appendix C in accordance with Section 7.3.

Calculations of stiffnesses in accordance with EC2 Appendix B

Material properties for the NIB beam:

$$f_{cm} := 53 \quad \text{MPa}$$

$$E_{cm} := 36000 \quad \text{MPa}$$

EC2 Table 3.1

Dimensions (mm)

Split the cross section vertically in five where the width properties change, numbered from bottom to top. This gives (using average widths):

$$h_1 := 270 \quad b_1 := 300$$

$$h_2 := 100 \quad b_2 := \frac{300 + 100}{2} = 200$$

$$h_3 := 920 \quad b_3 := 100$$

$$h_4 := 70 \quad b_4 := \frac{100 + 500}{2} = 300$$

$$h_5 := 75 \quad b_5 := 500$$

$$h := h_1 + h_2 + h_3 + h_4 + h_5 = 1435$$

Areas (mm²)

$$A_{c1} := b_1 \cdot h_1 = 81000$$

$$A_{c2} := b_2 \cdot h_2 = 20000$$

$$A_{c3} := b_3 \cdot h_3 = 92000$$

$$A_{c4} := b_4 \cdot h_4 = 21000$$

$$A_{c5} := b_5 \cdot h_5 = 37500$$

$$A_c := A_{c1} + A_{c2} + A_{c3} + A_{c4} + A_{c5} = 251500$$

Centre of gravity concrete (from lower edge) (mm)

$$z_{c1} := \frac{h_1}{2} = 135$$

$$z_{c2} := \frac{1}{2} \cdot \left(\frac{h_2}{3} + \frac{h_2}{2} \right) + h_1 = 311.7$$

$$z_{c3} := \frac{h_3}{2} + h_2 + h_1 = 830$$

$$z_{c4} := h - h_5 - \left(\frac{2}{3} \frac{h_4}{3} + \frac{1}{3} \frac{h_4}{2} \right) = 1332.8$$

$$z_{c5} := h - \frac{h_5}{2} = 1397.5$$

$$z_{tot} := \frac{A_{c1} \cdot z_{c1} + A_{c2} \cdot z_{c2} + A_{c3} \cdot z_{c3} + A_{c4} \cdot z_{c4} + A_{c5} \cdot z_{c5}}{A_c} = 691.5$$

Second moment of areas (mm⁴)

$$I_{z1} := \frac{1}{12} \cdot b_1 \cdot h_1^3 + b_1 \cdot h_1 \cdot (z_{c1} - z_{tot})^2 = 25.581 \times 10^9$$

$$I_{z2a} := \frac{1}{12} \cdot 100 \cdot 100^3 + 100 \cdot 100 \cdot \left(h_1 + \frac{h_2}{2} - z_{tot} \right)^2 = 1.389 \times 10^9$$

$$I_{z2b} := 2 \cdot \left[\frac{1}{36} \cdot 100 \cdot 100^3 + \frac{100 \cdot 100}{2} \cdot \left(h_1 + \frac{h_2}{3} - z_{tot} \right)^2 \right] = 1.513 \times 10^9$$

$$I_{z3} := \frac{1}{12} \cdot b_3 \cdot h_3^3 + b_3 \cdot h_3 \cdot (z_{c3} - z_{tot})^2 = 8.253 \times 10^9$$

$$I_{z4a} := \frac{1}{12} \cdot 100 \cdot 70^3 + 100 \cdot 70 \cdot \left(h - h_5 - \frac{h_4}{2} - z_{tot} \right)^2 = 2.812 \times 10^9$$

$$I_{z4b} := 2 \cdot \left[\frac{1}{36} \cdot 200 \cdot 70^3 + \frac{200 \cdot 70}{2} \cdot \left(h - h_5 - \frac{h_4}{3} - z_{tot} \right)^2 \right] = 5.83 \times 10^9$$

$$I_{z5} := \frac{1}{12} \cdot b_5 \cdot h_5^3 + b_5 \cdot h_5 \cdot (z_{c5} - z_{tot})^2 = 1.871 \times 10^{10}$$

$$I_z := I_{z1} + I_{z2a} + I_{z2b} + I_{z3} + I_{z4a} + I_{z4b} + I_{z5} = 64.084 \times 10^9$$

Concrete age at time of loading t_0

Loading occurs after $t_0 = 3$ days or $t_0 = 28$ days

Concrete age at time of consideration t

Consideration occurs after $t = 28$ days or $t = 36500$ days (1 year)

Relative humidity in ambient environment

$$RH := 70 \%$$

Creep calculations in accordance with EC2 Appendix B

Choose to use the whole circumference of the beam as perimeter of the member in contact with the atmosphere. This will be the case for the first 28 days, and using this for the whole time period (up to 100 years) will result in a conservative solution.

$$u := 2 \left[h_1 + \sqrt{\left(\frac{b_2}{2}\right)^2 + h_2^2} + h_3 + \sqrt{\left(\frac{2}{3} \cdot b_4\right)^2 + h_4^2} + h_5 \right] + b_1 + b_5 = 4036.6 \quad \text{mm}$$

$$h_0 := \frac{2 \cdot A_c}{u} = 124.6 \quad \text{mm}$$

$$\alpha_1 := \left(\frac{35}{f_{cm}}\right)^{0.7} = 0.748$$

$$\alpha_2 := \left(\frac{35}{f_{cm}}\right)^{0.2} = 0.920$$

$$\alpha_3 := \left(\frac{35}{f_{cm}}\right)^{0.5} = 0.813$$

$$\varphi_{RH} := \left(1 + \frac{1 - \frac{RH}{100}}{0.1 \cdot \sqrt[3]{h_0}} \cdot \alpha_1 \right) \cdot \alpha_2 = 1.334$$

$$\beta(f_{cm}) := \frac{16.8}{\sqrt{f_{cm}}} \quad \beta(f_{cm}) = 2.308$$

$$\beta_H := \min \left[1.5 \cdot \left[1 + (0.012 \cdot RH)^{18} \right] \cdot h_0 + 250 \cdot \alpha_3, 1500 \cdot \alpha_3 \right] = 398.176$$

The following expressions vary with varying t_0 and t

$$\beta(t_0) := \frac{1}{0.1 + t_0^{0.20}}$$

$$\beta(3) = 0.743 \quad \beta(28) = 0.488$$

$$\varphi_0(t_0) := \varphi_{RH} \cdot \beta(f_{cm}) \cdot \beta(t_0)$$

$$\varphi_0(3) = 2.287 \quad \varphi_0(28) = 1.503$$

$$\beta_c(t, t_0) := \left(\frac{t - t_0}{\beta_H + t - t_0} \right)^{0.3}$$

$$\beta_c(28, 3) = 0.428 \quad \beta_c(36500, 3) = 0.997 \quad \beta_c(36500, 28) = 0.997$$

The creep coefficients become

$$\varphi(t, t_0) := \varphi_0(t_0) \cdot \beta_c(t, t_0)$$

$$\varphi(28, 3) = 0.979 \quad \varphi(36500, 3) = 2.28 \quad \varphi(28, 36500) = 0.373$$

Effective moduli of elasticity become

$$EI_{\text{beam}}(t, t_0) := \frac{E_{cm} \cdot I_z}{1 + \varphi(t, t_0)} \quad \text{Nmm}^2 \quad \text{EC2 7.4.3 (5)}$$

$$EI_{\text{beam}}(28, 3) = 1.166 \times 10^{15} \quad \text{Nmm}^2$$

$$EI_{\text{beam}}(36500, 3) = 7.034 \times 10^{14} \quad \text{Nmm}^2$$

$$EI_{\text{beam}}(36500, 28) = 9.233 \times 10^{14} \quad \text{Nmm}^2$$

In the expression for secondary moment (calculated in the appendix regarding design loads from prestressing) the stiffnesses are inserted with unit kNm² instead of Nmm². This corresponds to:

$$EI_{\text{beam.28.3}} := \frac{EI_{\text{beam}}(28, 3)}{10^9} = 1.2 \times 10^6 \quad \text{kNm}^2$$

$$EI_{\text{beam.36500.3}} := \frac{EI_{\text{beam}}(36500, 3)}{10^9} = 703.4 \times 10^3 \quad \text{kNm}^2$$

$$EI_{\text{beam.36500.28}} := \frac{EI_{\text{beam}}(36500, 28)}{10^9} = 923.3 \times 10^3 \quad \text{kNm}^2$$

Appendix C

Loads from prestressing

In this appendix the loads from prestressing are calculated. The effective beam stiffness calculated in Appendix B are included in order to be able to establish the secondary moment from prestressing.

Calculations of design loads from prestressing

Material properties:

Load and reduction factors

$\gamma_{D.fav} := 0.9$	Favourable and unfavourable load factors
$\gamma_{D.unfav} := 1.1$	for prestressing force
$\alpha' := 0.85$	Simplified reduction factor for shear calculations

Prestressing forces in UK and OK

$$F_{P0.uk} := 134 \text{ kN}$$

$$F_{P0.ok} := 126 \text{ kN}$$

Dimensions (mm)

Concrete beam

Split the cross section vertically in five where the width properties change, numbered from bottom to top. This gives (using average widths):

$$\begin{aligned} h_1 &:= 270 & b_1 &:= 300 \\ h_2 &:= 100 & b_2 &:= \frac{300 + 100}{2} = 200 \\ h_3 &:= 920 & b_3 &:= 100 \\ h_4 &:= 70 & b_4 &:= \frac{100 + 500}{2} = 300 \\ h_5 &:= 75 & b_5 &:= 500 \end{aligned}$$

$$h := h_1 + h_2 + h_3 + h_4 + h_5 = 1435$$

Prestressing steel height (from lower edge)

$$\begin{aligned} h_{gr1} &:= 70 & h_{gr4} &:= 190 \\ h_{gr2} &:= 110 & h_{gr5} &:= 230 \\ h_{gr3} &:= 150 & h_{gr6} &:= 1435 - 30 = 1405 \end{aligned}$$

Areas (mm²)

Concrete cross sectional area

$$A_{c1} := b_1 \cdot h_1 = 81000$$

$$A_{c2} := b_2 \cdot h_2 = 20000$$

$$A_{c3} := b_3 \cdot h_3 = 92000$$

$$A_{c4} := b_4 \cdot h_4 = 21000$$

$$A_{c5} := b_5 \cdot h_5 = 37500$$

$$A_c := A_{c1} + A_{c2} + A_{c3} + A_{c4} + A_{c5} = 251500$$

Prestressing steel

$$A_{p.\text{strand}} := 100$$

$$A_{p1} := 5 \cdot A_{p.\text{strand}} = 500$$

$$A_{p2} := 5 \cdot A_{p.\text{strand}} = 500$$

$$A_{p3} := 5 \cdot A_{p.\text{strand}} = 500$$

$$A_{p4} := 5 \cdot A_{p.\text{strand}} = 500$$

$$A_{p5} := 2 \cdot A_{p.\text{strand}} = 200$$

$$A_{p6} := 4 \cdot A_{p.\text{strand}} = 400$$

Centre of gravity concrete (from lower edge) (mm)

$$z_{c1} := \frac{h_1}{2} = 135$$

$$z_{c2} := \left(\frac{1}{2} \frac{h_2}{3} + \frac{1}{2} \frac{h_2}{2} \right) + h_1 = 311.7$$

$$z_{c3} := \frac{h_3}{2} + h_2 + h_1 = 830$$

$$z_{c4} := h - h_5 - \left(\frac{2}{3} \frac{h_4}{3} + \frac{1}{3} \frac{h_4}{2} \right) = 1332.8$$

$$z_{c5} := h - \frac{h_5}{2} = 1397.5$$

$$z_{tot} := \frac{A_{c1} \cdot z_{c1} + A_{c2} \cdot z_{c2} + A_{c3} \cdot z_{c3} + A_{c4} \cdot z_{c4} + A_{c5} \cdot z_{c5}}{A_c} = 691.5$$

Centre of gravity prestressing steel (from lower edge) (mm)

$$A_{p.uk} := A_{p1} + A_{p2} + A_{p3} + A_{p4} + A_{p5}$$

$$h_{p.uk} := \frac{h_{gr1} \cdot A_{p1} + h_{gr2} \cdot A_{p2} + h_{gr3} \cdot A_{p3} + h_{gr4} \cdot A_{p4} + h_{gr5} \cdot A_{p5}}{A_{p.uk}} = 139.1$$

$$A_{p.ok} := A_{p6}$$

$$h_{p.ok} := h_{gr6} = 1405$$

$$h_p := \frac{h_{p.uk} \cdot A_{p.uk} + h_{p.ok} \cdot A_{p.ok}}{A_{p.ok} + A_{p.uk}} = 333.8$$

$$A_p := A_{p.ok} + A_{p.uk} = 2600 \quad \text{mm}^2$$

Eccentricity (mm)

$$e_{mm} := z_{tot} - h_p = 357.7 \quad e := \frac{e_{mm}}{1000} = 0.3577$$

Characteristic prestressing force (axial load)

$$F_{p0} := \frac{A_{p.uk}}{A_{p.strand}} \cdot F_{P0.uk} + \frac{A_{p.ok}}{A_{p.strand}} \cdot F_{P0.ok} = 3452 \quad \text{kN}$$

Reduced with approximate loss factor α'

$$F'_{p0} := \alpha' \cdot F_{p0} = 2934 \quad \text{kN}$$

Characteristic primary moment

$$M_0 := F'_{p0} \cdot e = 1050 \quad \text{kNm}$$

Design axial load

$$N_{Ed} := \gamma_D \cdot F'_{p0} = \gamma_D \cdot \alpha' \cdot F_{p0}$$

$$N_{Ed.fav} := \gamma_{D.fav} \cdot F'_{p0} = 2641 \quad \text{kN}$$

$$N_{Ed.unfav} := \gamma_{D.unfav} \cdot F'_{p0} = 3228 \quad \text{kN}$$

Design primary moment

$$M_0 := N_{Ed} \cdot e$$

$$M_{0.fav} := N_{Ed.fav} \cdot e = 945 \quad \text{kNm}$$

$$M_{0.unfav} := N_{Ed.unfav} \cdot e = 1155 \quad \text{kNm}$$

Secondary prestressing moment

$$M_{sec} := \left(-\frac{M_0}{EI_{beam.36500.3}} + \frac{M_0}{EI_{beam.28.3}} \right) \cdot EI_{beam.36500.28}$$

The following stiffnesses are calculated in the previous appendix:

$$EI_{beam.28.3} := 1.2 \cdot 10^6 \quad \text{kNm}$$

$$EI_{beam.36500.3} := 703.4 \cdot 10^3 \quad \text{kNm}$$

$$EI_{beam.36500.28} := 923.3 \cdot 10^3 \quad \text{kNm}$$

Indirect load effects from prestressing have load coefficient $\gamma_D = 1.0$. The secondary moment is therefore calculated using the characteristic primary moment M_0 . This gives:

$$M_{\text{sec}} := \left(-\frac{M_0}{EI_{\text{beam.36500.3}}} + \frac{M_0}{EI_{\text{beam.28.3}}} \right) \cdot EI_{\text{beam.36500.28}} = -570 \text{ kNm}$$

Design total moment

$$M_{\text{tot}} := M_0 + M_{\text{sec}} = 479.4 \text{ kNm}$$

Appendix D

Cross sectional properties

In this appendix various cross sectional properties are established for capacity calculations according to NS 3473:1977.

Concrete properties that are presented involve material properties that are included in the diagonal tension capacity and compressive shear capacity formulas according to NS 3473:1977. Furthermore cross sectional dimensions are given for both the regular cross section and the strengthened web cross section (occurring near the beam ends), and cross sectional areas, centres of gravity, first moment of area and second moments of area are established for both cross sections.

Reinforcement properties that are presented involve material properties that are included in the capacity formulas stated above. Furthermore reinforcement areas are given for longitudinal reinforcement (regular and prestressed) and for shear reinforcement. For the longitudinal reinforcement the placement in the cross section, centre of gravity, effective cross sectional depths and distances between the tension and compression reinforcement's centre of gravity is established. Coating of certain prestressing strands is taken into account, and the properties are therefore established for various regions x from the beam end.

Calculations of various cross sectional properties to be used for capacity calculations according to NS 3473:1977 (and EC2)

x: Distance from critical beam end

Concrete

Material properties in accordance with NS 3473:1977

Design concrete compressive strength f_c :

$$f_c := \frac{f_{cn}}{\gamma_m} \quad (4.3.2)$$

$$f_{cn} := 28\text{MPa} \quad \text{for C55 concrete with characteristic cube strength } f_{ck} = 55 \text{ MPa.} \quad (\text{Tab 4.4.1})$$

$$\gamma_m := 1.25 \quad \text{for concrete projects executed under extended or normal control} \quad (4.3.3)$$

$$f_c := \frac{f_{cn}}{\gamma_m} = 22.4 \cdot \text{MPa}$$

Design concrete shear strength f_v :

$$f_v := \frac{f_{vn}}{\gamma_m} \quad (4.3.2)$$

$$f_{vn} := 0.7\text{MPa} \quad \text{for C55 concrete with characteristic cube strength } f_{ck} = 55 \text{ MPa.} \quad (\text{Tab 4.4.1})$$

$$f_v := \frac{f_{vn}}{\gamma_m} = 0.6 \cdot \text{MPa}$$

Dimensions (mm)

Regular NIB beam section

Split the cross section vertically in five where the width properties change, numbered from bottom to top. This gives (using average widths):

$$h_1 := 270 \quad b_1 := 300$$

$$h_2 := 100 \quad b_2 := \frac{300 + 100}{2} = 200$$

$$h_3 := 920 \quad b_3 := 100$$

$$h_4 := 70 \quad b_4 := \frac{100 + 500}{2} = 300$$

$$h_5 := 75 \quad b_5 := 500$$

$$h_{\text{beam}} := h_1 + h_2 + h_3 + h_4 + h_5 = 1435$$

Voute section (for $x < 1425$ mm)

Split the cross section vertically in three where the width properties change, numbered from bottom to top. This gives (using average widths):

$$h_{v1} := h_1 + h_2 + h_3 = 1290 \quad b_{v1} := b_1 = 300$$

$$h_{v2} := h_4 = 70 \quad b_{v2} := \frac{300 + 500}{2} = 400$$

$$h_{v3} := h_5 = 75 \quad b_{v3} := b_5 = 500$$

Deck

$$t_{\text{deck}} := 250$$

$$b_{\text{deck}} := 2000$$

Total cross sectional height of composite beam

$$h_{\text{tot}} := h_{\text{beam}} + t_{\text{deck}} = 1685$$

Cross sectional area of composite concrete beam (beam + deck) (mm²)

Area of deck

$$A_{\text{c.deck}} := t_{\text{deck}} \cdot b_{\text{deck}} = 500000$$

Regular NIB beam composite section

$$A_{c1} := b_1 \cdot h_1 = 81000$$

$$A_{c2} := b_2 \cdot h_2 = 20000$$

$$A_{c3} := b_3 \cdot h_3 = 92000$$

$$A_{c4} := b_4 \cdot h_4 = 21000$$

$$A_{c5} := b_5 \cdot h_5 = 37500$$

$$A_c := A_{c1} + A_{c2} + A_{c3} + A_{c4} + A_{c5} + A_{c.deck} = 751500$$

Voute composite section ($x < 1425$ mm)

$$A_{cv1} := h_{v1} \cdot b_{v1} = 387000$$

$$A_{cv2} := h_{v2} \cdot b_{v2} = 28000$$

$$A_{cv3} := h_{v3} \cdot b_{v3} = 37500$$

$$A_{c.voute} := A_{cv1} + A_{cv2} + A_{cv3} + A_{c.deck} = 952500$$

Centre of gravity concrete (from lower edge) for composite beam (mm)

Distance from lower edge to centre of gravity for deck

$$z_{cdeck} := h_{beam} + \frac{t_{deck}}{2} = 1560$$

Regular NIB beam composite section

$$z_{c1} := \frac{h_1}{2} = 135$$

$$z_{c2} := \frac{1}{2} \cdot \left(\frac{h_2}{3} + \frac{h_2}{2} \right) + h_1 = 311.7$$

$$z_{c3} := \frac{h_3}{2} + h_2 + h_1 = 830$$

$$z_{c4} := h_{beam} - h_5 - \left(\frac{2}{3} \frac{h_4}{3} + \frac{1}{3} \frac{h_4}{2} \right) = 1332.8$$

$$z_{c5} := h_{beam} - \frac{h_5}{2} = 1397.5$$

$$z_{ctot} := \frac{A_{c1} \cdot z_{c1} + A_{c2} \cdot z_{c2} + A_{c3} \cdot z_{c3} + A_{c4} \cdot z_{c4} + A_{c5} \cdot z_{c5} + A_{c.deck} \cdot z_{cdeck}}{A_c} = 1269.4$$

Voute composite section ($x < 1425$ mm)

$$z_{cv1} := \frac{h_{v1}}{2}$$

$$z_{cv2} := h_{v1} + \left(\frac{1}{4} \cdot \frac{h_{v2}}{3} + \frac{3}{4} \cdot \frac{h_{v2}}{2} \right) = 1322.1$$

$$z_{cv3} := h_{\text{beam}} - \frac{h_{v3}}{2} = 1397.5$$

$$z_{cvtot} := \frac{A_{cv1} \cdot z_{cv1} + A_{cv2} \cdot z_{cv2} + A_{cv3} \cdot z_{cv3} + A_{c.deck} \cdot z_{cdeck}}{A_{c.voute}} = 1174.8$$

Second moment of areas (mm⁴)

Regular NIB beam composite section

$$I_{z1} := \frac{1}{12} \cdot b_1 \cdot h_1^3 + b_1 \cdot h_1 \cdot (z_{c1} - z_{ctot})^2 = 104.72 \times 10^9$$

$$I_{z2a} := \frac{1}{12} \cdot 100 \cdot 100^3 + 100 \cdot 100 \cdot \left(h_1 + \frac{h_2}{2} - z_{ctot} \right)^2 = 9 \times 10^9$$

$$I_{z2b} := 2 \cdot \left[\frac{1}{36} \cdot 100 \cdot 100^3 + \frac{100 \cdot 100}{2} \cdot \left(h_1 + \frac{h_2}{3} - z_{ctot} \right)^2 \right] = 9.3 \times 10^9$$

$$I_{z3} := \frac{1}{12} \cdot b_3 \cdot h_3^3 + b_3 \cdot h_3 \cdot (z_{c3} - z_{ctot})^2 = 24.2 \times 10^9$$

$$I_{z4a} := \frac{1}{12} \cdot 100 \cdot 70^3 + 100 \cdot 70 \cdot \left(h_{\text{beam}} - h_5 - \frac{h_4}{2} - z_{ctot} \right)^2 = 24.5 \times 10^6$$

$$I_{z4b} := 2 \cdot \left[\frac{1}{36} \cdot 200 \cdot 70^3 + \frac{200 \cdot 70}{2} \cdot \left(h_{\text{beam}} - h_5 - \frac{h_4}{3} - z_{ctot} \right)^2 \right] = 67.2 \times 10^6$$

$$I_{z5} := \frac{1}{12} \cdot b_5 \cdot h_5^3 + b_5 \cdot h_5 \cdot (z_{c5} - z_{ctot})^2 = 633.3 \times 10^6$$

$$I_{zdeck} := \frac{1}{12} \cdot b_{\text{deck}} \cdot t_{\text{deck}}^3 + b_{\text{deck}} \cdot t_{\text{deck}} \cdot (z_{cdeck} - z_{ctot})^2 = 44.8 \times 10^9$$

$$I_{z.tot} := I_{z1} + I_{z2a} + I_{z2b} + I_{z3} + I_{z4a} + I_{z4b} + I_{z5} + I_{zdeck} = 192.893 \times 10^9$$

Voute composite section ($x < 1425$ mm)

$$I_{zv1} := \frac{1}{12} \cdot b_{v1} \cdot h_{v1}^3 + b_{v1} \cdot h_{v1} \cdot (z_{cv1} - z_{cvtot})^2 = 162.312 \times 10^9$$

$$I_{zv2a} := \frac{1}{12} \cdot 300 \cdot h_{v2}^3 + 300 \cdot h_{v2} \cdot \left(h_{v1} + \frac{h_{v2}}{2} - z_{cvtot} \right)^2 = 482.054 \times 10^6$$

$$I_{zv2b} := 2 \left[\frac{1}{36} \cdot 100 \cdot h_{v2}^3 + \frac{100 \cdot h_{v2}}{2} \cdot \left(h_{v1} + \frac{2}{3} h_{v2} - z_{cvtot} \right)^2 \right] = 185.21 \times 10^6$$

$$I_{zv3} := \frac{1}{12} \cdot b_{v3} \cdot h_{v3}^3 + b_{v3} \cdot h_{v3} \cdot (z_{cv3} - z_{cvtot})^2 = 1.877 \times 10^9$$

$$I_{zvdeck} := \frac{1}{12} \cdot b_{deck} \cdot t_{deck}^3 + b_{deck} \cdot t_{deck} \cdot (z_{cdeck} - z_{cvtot})^2 = 76.776 \times 10^9$$

$$I_{zv.tot} := I_{zv1} + I_{zv2a} + I_{zv2b} + I_{zv3} + I_{zvdeck} = 241.632 \times 10^9$$

First moment of areas about the centroidal axis (centre of gravity for the concrete cross section) (mm³)

Regular NIB beam composite section

$$S_1 := b_1 \cdot h_1 \cdot (z_{c1} - z_{ctot}) = -91.883 \times 10^6$$

$$S_2 := b_2 \cdot h_2 \cdot (z_{c2} - z_{ctot}) = -19.2 \times 10^6$$

$$S_{3'} := b_3 \cdot (z_{ctot} - h_1 - h_2) \cdot \frac{h_1 + h_2 - z_{ctot}}{2} = -40.4 \times 10^6$$

$$S_{3''} := b_3 \cdot (h_1 + h_2 + h_3 - z_{ctot}) \cdot \frac{h_1 + h_2 + h_3 - z_{ctot}}{2} = 21303.6$$

$$S_4 := b_4 \cdot h_4 \cdot (z_{c4} - z_{ctot}) = 1.3 \times 10^6$$

$$S_5 := b_5 \cdot h_5 \cdot (z_{c5} - z_{ctot}) = 4.8 \times 10^6$$

$$S_{deck} := b_{deck} \cdot t_{deck} \cdot (z_{cdeck} - z_{ctot}) = 145.3 \times 10^6$$

$$S_{tot.upper} := S_{3''} + S_4 + S_5 + S_{deck} = 151.479 \times 10^6$$

$$S_{tot.lower} := S_1 + S_2 + S_{3'} = -151.479 \times 10^6 \quad (\text{control})$$

Voute composite section (x < 1425 mm)

$$S_{v1'} := b_{v1} \cdot z_{cvtot} \cdot \frac{(0 - z_{cvtot})}{2} = -207.039 \times 10^6$$

$$S_{v1''} := b_{v1} \cdot (h_{v1} - z_{cvtot}) \cdot \frac{h_{v1} - z_{cvtot}}{2} = 1.989 \times 10^6$$

$$S_{v2} := b_{v2} \cdot h_{v2} \cdot (z_{cv2} - z_{cvtot}) = 4.123 \times 10^6$$

$$S_{v3} := b_{v3} \cdot h_{v3} \cdot (z_{cv3} - z_{cvtot}) = 8.3 \times 10^6$$

$$S_{vdeck} := b_{deck} \cdot t_{deck} \cdot (z_{cdeck} - z_{cvtot}) = 192.578 \times 10^6$$

$$S_{vtot.upper} := S_{v1''} + S_{v2} + S_{v3} + S_{vdeck} = 207.039 \times 10^6$$

$$S_{vtot.lower} := S_{v1'} = -207.039 \times 10^6 \quad (\text{control})$$

Reinforcement

Material properties

Material coefficient

$$\gamma_m := 1.25 \quad (4.3.3)$$

Prestressing steel

The prestressing steel is of type St. 1700/1900.

$$f_{y.p} := 1700 \text{ MPa}$$

$$f_{s.p} := \frac{f_{y.p}}{\gamma_m} = 1360 \cdot \text{MPa}$$

Regular reinforcement

In the NIB beam reinforcement P11 of type K400Ts is placed in the lower edge (UK) and reinforcement P10 of type K500Ts is placed in the upper edge (OK).

$$f_{y.K400Ts} := 400 \text{ MPa}$$

$$f_{y.K500Ts} := 500 \text{ MPa}$$

$$f_{s.K400Ts} := \frac{f_{y.K400Ts}}{\gamma_m} = 320 \cdot \text{MPa}$$

$$f_{s.K500Ts} := \frac{f_{y.K500Ts}}{\gamma_m} = 400 \cdot \text{MPa}$$

In the bridge deck reinforcement ($\varnothing 16$ c250 mm) of type Ks500 is placed in the

lower edge (UK) and reinforcement (Ø12 c150 mm) of type Ks400 is placed in the upper edge (OK).

$$f_{y.Ks500} := 500 \text{ MPa}$$

$$f_{y.Ks400} := 400 \text{ MPa}$$

$$f_{s.Ks500} := \frac{f_{y.Ks500}}{\gamma_m} = 400 \cdot \text{MPa}$$

$$f_{s.Ks400} := \frac{f_{y.Ks400}}{\gamma_m} = 320 \cdot \text{MPa}$$

Shear reinforcement

Stirrups denoted P1 of steel quality K400Ts (given above) reaches vertically through the NIB beam and up into the bridge deck.

Dimensions (mm)

Prestressing steel height (from lower edge)

$$h_{p.gr1} := 70 \quad h_{p.gr4} := 190$$

$$h_{p.gr2} := 110 \quad h_{p.gr5} := 230$$

$$h_{p.gr3} := 150 \quad h_{p.gr6} := 1435 - 30 = 1405$$

Regular steel height (from lower edge)

$$\frac{1}{2} \text{in} = 12.7 \cdot \text{mm}$$

$$h_{gr1} := 40 + \frac{8}{2} = 44$$

2 Ø8 - P11 in production drawing

$$h_{gr2} := 1435 - 30 - \frac{12.7}{2} - 6 - \frac{16}{2} = 1384.7$$

2 Ø16 - P10 in production drawing

$$h_{gr3} := 1435 + 40 + 16 + \frac{16}{2} = 1499$$

Ø16 c250 mm, UK in bridge deck

$$h_{gr4} := 1435 + 250 - 40 - 12 - \frac{12}{2} = 1627$$

Ø12 c150 mm, OK in bridge deck

Reinforcement areas (mm²)

Prestressing steel

$$A_{p.strand} := 100$$

$$A_{p1} := 5 \cdot A_{p.strand} = 500$$

$$A_{p2} := 5 \cdot A_{p.strand} = 500$$

$$A_{p3} := 5 \cdot A_{p.strand} = 500$$

$$A_{p4} := 5 \cdot A_{p.strand} = 500$$

$$A_{p5} := 2 \cdot A_{p.strand} = 200$$

$$A_{p6} := 4 \cdot A_{p.strand} = 400$$

These reinforcement amounts are valid for the largest part of the composite beam. In the beam ends there are exceptions: A_{p3} has one strand with cover over 2000 mm, and A_{p4} has two strands with cover over 4000 mm and one strand with cover over 7000 mm from each beam end. This gives reduced reinforcement amounts $A_{p.i.x.y}$ between lengths x and y from the beam ends:

$$A_{p3.0.2000} := 4 \cdot A_{p.strand} = 400$$

$$A_{p4.0.4000} := 2 \cdot A_{p.strand} = 200$$

$$A_{p4.4000.7000} := 4 \cdot A_{p.strand} = 400$$

Regular longitudinal steel

$$A_{s11} := 2 \cdot \pi \cdot \frac{8^2}{4} = 100.5 \quad 2 \text{ } \varnothing 8 - \text{P11 in production drawing}$$

$$A_{s12} := 2 \cdot \pi \cdot \frac{16^2}{4} = 402.1 \quad 2 \text{ } \varnothing 16 - \text{P10 in production drawing}$$

$$A_{s13} := \frac{2000}{250} \cdot \pi \cdot \frac{16^2}{4} = 1608.5 \quad \varnothing 16 \text{ c}250 \text{ mm, UK in bridge deck}$$

$$A_{s14} := \frac{2000}{150} \cdot \pi \cdot \frac{12^2}{4} = 1508 \quad \varnothing 12 \text{ c}150 \text{ mm, OK in bridge deck}$$

In addition there are 5 $\varnothing 8$ (P9) reinforcement bars of steel quality K500Ts along the web of the NIB beam as seen from the production drawings by Vestlandske Spennbetong AS. These are ignored in all capacity calculations for simplicity.

$$A_{s1.tot} := A_{s11} + A_{s12} + A_{s13} + A_{s14} = 3619.1$$

Shear reinforcement

Stirrups of diameter 12 mm are placed double with varying central distance over the length of the beam. The central distance for the various regions is:

0 - 1800 mm: 100 mm 5800 - 9500 mm: 200 mm

1800 - 5800 mm: 150 mm 9500 - midspan: 300 mm

The shear reinforcement areas divided by the central distance for the various regions become

$$A_{sv.0.1800} := 2 \cdot \pi \cdot \frac{12^2}{4} \cdot \frac{1}{100} = 2.262$$

$$A_{sv.1800.5800} := 2 \cdot \pi \cdot \frac{12^2}{4} \cdot \frac{1}{150} = 1.508$$

$$A_{sv.5800.9500} := 2 \cdot \pi \cdot \frac{12^2}{4} \cdot \frac{1}{200} = 1.131$$

$$A_{sv.9500.midspan} := 2 \cdot \pi \cdot \frac{12^2}{4} \cdot \frac{1}{300} = 0.754$$

Effective cross sectional depths d (mm)

Distance from the tensile reinforcement's centreline to the compressive zone edge

$$d_i := \frac{f_{pd} \cdot A_p \cdot d_p + \sum f_{sd} \cdot A_s \cdot d_s}{f_{pd} \cdot A_p + \sum f_{sd} \cdot A_s}$$

Tension in upper edge (OK)

$$d_{ok} := \frac{f_{s.p} \cdot A_{p6} \cdot h_{p.gr6} + f_{s.K500Ts} \cdot A_{s12} \cdot h_{gr2} \dots + f_{s.Ks500} \cdot A_{s13} \cdot h_{gr3} + f_{s.Ks400} \cdot A_{s14} \cdot h_{gr4}}{f_{s.p} \cdot A_{p6} + f_{s.K500Ts} \cdot A_{s12} + f_{s.Ks500} \cdot A_{s13} + f_{s.Ks400} \cdot A_{s14}} = 1494.8$$

Tension in lower edge (UK)

For $x < 2000$ mm (does not occur in practise)

$$A_{hp.0.2000} := A_{p1} \cdot (h_{tot} - h_{p.gr1}) + A_{p2} \cdot (h_{tot} - h_{p.gr2}) + A_{p3.0.2000} \cdot (h_{tot} - h_{p.gr3}) \dots + A_{p4.0.4000} \cdot (h_{tot} - h_{p.gr4}) + A_{p5} \cdot (h_{tot} - h_{p.gr5})$$

$$d_{uk.0.2000} := \frac{f_{s.p} \cdot A_{hp.0.2000} + f_{s.K400Ts} \cdot A_{s11} \cdot (h_{tot} - h_{gr1})}{f_{s.p} \cdot (A_{p1} + A_{p2} + A_{p3.0.2000} + A_{p4.0.4000} + A_{p5}) \dots + f_{s.K400Ts} \cdot A_{s11}} = 1556.1$$

For $x = 2000$ to $x = 4000$ mm (does not occur in practise)

$$A_{hp.2000.4000} := A_{p1} \cdot (h_{tot} - h_{p.gr1}) + A_{p2} \cdot (h_{tot} - h_{p.gr2}) + A_{p3} \cdot (h_{tot} - h_{p.gr3}) \dots + A_{p4.0.4000} \cdot (h_{tot} - h_{p.gr4}) + A_{p5} \cdot (h_{tot} - h_{p.gr5})$$

$$d_{uk.2000.4000} := \frac{f_{s,p} \cdot Ah_{p.2000.4000} + f_{s,K400Ts} \cdot A_{s11} \cdot (h_{tot} - h_{gr1})}{f_{s,p} \cdot (A_{p1} + A_{p2} + A_{p3} + A_{p4.0.4000} + A_{p5}) + f_{s,K400Ts} \cdot A_{s11}} = 1555$$

For $x = 4000$ to $x = 7000$ mm

$$Ah_{p.4000.7000} := A_{p1} \cdot (h_{tot} - h_{p.gr1}) + A_{p2} \cdot (h_{tot} - h_{p.gr2}) + A_{p3} \cdot (h_{tot} - h_{p.gr3}) \dots \\ + A_{p4.4000.7000} \cdot (h_{tot} - h_{p.gr4}) + A_{p5} \cdot (h_{tot} - h_{p.gr5})$$

$$d_{uk.4000.7000} := \frac{f_{s,p} \cdot Ah_{p.4000.7000} + f_{s,K400Ts} \cdot A_{s11} \cdot (h_{tot} - h_{gr1})}{f_{s,p} \cdot (A_{p1} + A_{p2} + A_{p3} + A_{p4.4000.7000} + A_{p5}) \dots \\ + f_{s,K400Ts} \cdot A_{s11}} = 1549.4$$

For $x > 7000$ mm

$$Ah_p := A_{p1} \cdot (h_{tot} - h_{p.gr1}) + A_{p2} \cdot (h_{tot} - h_{p.gr2}) + A_{p3} \cdot (h_{tot} - h_{p.gr3}) \dots \\ + A_{p4} \cdot (h_{tot} - h_{p.gr4}) + A_{p5} \cdot (h_{tot} - h_{p.gr5})$$

$$d_{uk} := \frac{f_{s,p} \cdot Ah_p + f_{s,K400Ts} \cdot A_{s11} \cdot (h_{tot} - h_{gr1})}{f_{s,p} \cdot (A_{p1} + A_{p2} + A_{p3} + A_{p4} + A_{p5}) + f_{s,K400Ts} \cdot A_{s11}} = 1546.9$$

Distance between the tension and compression reinforcement's centre of gravity h' (mm)

$$a_{ok} := h_{tot} - d_{ok}$$

$$a_{uk} := h_{tot} - d_{uk}$$

$$h' := h_{tot} - a_{ok} - a_{uk} = d_{ok} + d_{uk} - h_{tot}$$

For $x < 2000$ mm

$$h'_{0.2000} := d_{ok} + d_{uk.0.2000} - h_{tot} = 1365.9$$

For $x = 2000$ to $x = 4000$ mm

$$h'_{2000.4000} := d_{ok} + d_{uk.2000.4000} - h_{tot} = 1364.8$$

For $x = 4000$ to $x = 7000$ mm

$$h'_{4000.7000} := d_{ok} + d_{uk.4000.7000} - h_{tot} = 1359.1$$

For $x > 7000$ mm

$$h' := d_{ok} + d_{uk} - h_{tot} = 1356.7$$

Appendix E

Capacity control in accordance with EC2

In this appendix the diagonal tension capacity and compressive shear capacity is performed in accordance with EC2. The calculations performed here are taken in use in Section 9.3.

In order for the EC2 calculations to be consistent and thorough, material properties and material coefficients are taken from EC2. The basis for the calculations (design loads, effective width of the bridge deck in the composite beam, etc.) will however remain unchanged from the NS 3473:1977 calculations.

Calculations of shear capacity in accordance with EC2 Section 6.2.1-6.2.3

EC2 Section 6.2.1(8) states that control of the diagonal tension capacity $V_{Rd,c}$ or $V_{Rd,s}$ can be performed at a distance d from the edge of the support. It has been assumed that the outer edge of the support is placed 50 mm from the beam end, and that the rubber bearing that constitutes the support has an extent of 200 mm in the longitudinal direction of the beam. This means that the middle of the support is placed 150 mm from the beam end, and that the inner edge of the support is placed 250 mm from the beam end.

The effective depth d of the cross section varies as can be seen in previous appendix. It can be chosen to use the value for $d = 1546.9$ mm, and control the shear capacity at a distance 1550 mm from the edge of the support, i.e. a distance $x = 1550 + 250 = 1800$ mm from the beam end and a distance $y = 1550 + 100 = 1650$ mm from the middle of the support. This d corresponds with the effective depth of the composite beam that is valid in the majority of the beam ($d_{uk} = 1546.9$ mm). It has been chosen to use this value instead of $d_{ok} = 1494.8$ mm which is valid for the considered region because the larger d allows for the diagonal tension capacity to be controlled in the section which is critical according to NS 3473:1977.

The shear capacity of the composite beam without shear reinforcement:

For a prestressed single span member without shear reinforcement the shear resistance for regions that are uncracked in bending is:

$$V_{Rd,c} := \frac{I \cdot b_w}{S} \cdot \sqrt{(f_{ctd})^2 + \alpha_1 \cdot \sigma_{cp} \cdot f_{ctd}} \quad (6.4)$$

Second moment of area I :

$$I := 192893000000 \quad \text{mm}^4$$

First moment of area S :

$$S := 151500000 \quad \text{mm}^3$$

Web width b :

$$b_w := 100 \quad \text{mm}$$

Design tensile strength f_{ctd} :

$$\alpha_{ct} := 0.85 \quad \text{NA 3.1.6(2)P}$$

Partial safety factor for concrete:

$$\gamma_c := 1.5 \quad \text{NA 2.4.2.4}$$

Characteristic axial tensile strength of concrete $f_{ctk,0.0.05}$:

$$f_{ctk,0.0.05} := 2.7 \text{ MPa} \quad \text{Table 3.1}$$

Design axial tensile strength of concrete f_{ctd} :

$$f_{ctd} := \frac{\alpha_{ct} \cdot f_{ctk,0.0.05}}{\gamma_c} = 1.53 \text{ MPa} \quad (3.16)$$

Furthermore the factor α_f is to be established. First we find the coefficient β_{cc} which depends on the age of the concrete t :

Assume the cement is of strength class N (normal):

$$s := 0.25 \quad 3.1.2 (6)$$

$$\beta_{cc}(t) := e^{s \cdot \left[1 - \left(\frac{28}{t} \right)^{\frac{1}{2}} \right]} \quad (3.2)$$

$$\beta_{cc}(3) = 0.6$$

Tensile strength with time $f_{ctm}(t)$:

Mean value of axial tensile strength of concrete:

$$f_{ctm} := 3.8 \text{ MPa} \quad \text{Table 3.1}$$

For $t < 28$ days:

$$\alpha := 1$$

$$f_{ctm}(t) := \left(\beta_{cc}(t) \right)^\alpha \cdot f_{ctm} \quad (3.4)$$

$$f_{ctm}(3) = 2.3 \text{ MPa}$$

Design tensile value of strength at time of release $f_{ctd}(t)$:

$$f_{ctd.}(t) := \frac{\alpha_{ct} \cdot 0.7 \cdot f_{ctm.}(t)}{\gamma_c} \quad 8.10.2.2(1)$$

$$f_{ctd.}(3) = 0.9 \quad \text{MPa}$$

The prestress is assumed to be transferred to the concrete at the release of the strands by a constant bond stress f_{bpt} :

For strands with 3 or 7 wires and not assuming good bond:

$$\eta_{p1} := 3.2 \quad 8.10.2.2(1)$$

$$\eta_1 := 0.7$$

$$f_{bpt} := \eta_{p1} \cdot \eta_1 \cdot f_{ctd.}(3) = 2.02 \quad \text{MPa} \quad (8.15)$$

The basic value of the transmission length l_{pt} :

Assume sudden release (conservative choice)

$$\alpha_1 := 1.25 \quad 8.10.2.2(2)$$

For strands with circular cross section:

$$\alpha_2 := 0.19 \quad 8.10.2.2(2)$$

Nominal diameter of the strand:

$$\phi := \frac{1}{2} \text{ in} \quad \text{i.e.} \quad \phi := 12.7 \quad \text{mm}$$

Tendon stress just after release:

Force in jack at prestressing of strands in lower edge

$$F_{pmax} := 139 \quad \text{kN}$$

Area of one prestressing strand

$$A_{p.strand} := 100 \quad \text{mm}^2$$

Assume that tendon stress just after release is approximately

$$\sigma_{pm0} := 0.95 \cdot \frac{F_{pmax} \cdot 1000}{A_{p.strand}} = 1320.5 \quad \text{MPa}$$

$$l_{pt} := \frac{\alpha_1 \cdot \alpha_2 \cdot \phi \cdot \sigma_{pm0}}{f_{bpt}} = 1971.8 \quad \text{mm} \quad (8.16)$$

Design value of the transmission length l_{pt2} (will be the less favourable for shear):

$$l_{pt2} := 1.2 \cdot l_{pt} = 2366.2 \text{ mm} \quad (8.18)$$

Finally we have:

$l_x := 1800 \text{ mm}$ because we consider a section $x = 1800 \text{ mm}$ from the beam end, and simplify by assuming that all strands begin their transmission length at the beam end

$$\alpha_1 := \min\left(\frac{l_x}{l_{pt2}}, 1.0\right) = 0.761 \quad 6.2.2(2)$$

Concrete compressive stress σ_{cp} at the centroidal axis due to prestressing:

Concrete cross sectional area A_c :

$$A_c := 751500 \text{ mm}^2$$

Axial load N_{Ed} in the section 1650 mm from the middle of the support (the coating of certain strands is neglected here):

$$N_{Ed} := 3228 \text{ kN}$$

$$\sigma_{cp} := \frac{N_{Ed} \cdot 1000}{A_c} = 4.3 \text{ MPa} \quad 6.2.2(2)$$

For a prestressed single span member without shear reinforcement the shear resistance for regions that are uncracked in bending is:

$$V_{Rd,c} := \frac{I \cdot b_w}{S} \cdot \sqrt{(f_{ctd})^2 + \alpha_1 \sigma_{cp} \cdot f_{ctd}} = 344952.7 \text{ N, i.e. } 345 \text{ kN.}$$

Considering a section 1650 mm from the middle of the support the design shear load is $V_{Ed} = 533 \text{ kN}$. The shear capacity without shear reinforcement is hence not sufficient.

For structural members without shear reinforcement the capacity with regard to compressive shear failure is given as

$$V_{Rd,max,c} := 0.5 \cdot b_w \cdot d \cdot \nu \cdot f_{cd} \quad (6.5)$$

A C55 concrete has a characteristic compressive cylinder strength of

$$f_{ck} := 45 \text{ MPa}$$

Table 3

The design compressive strength is then given as

$$\alpha_{cc} := 0.85$$

NA 3.1.6(2)P

$$f_{cd} := \alpha_{cc} \cdot \frac{f_{ck}}{\gamma_c} = 25.5 \text{ MPa} \quad (3.15)$$

ν is a strength reduction factor for concrete cracked in shear

$$\nu := 0.6 \cdot \left(1 - \frac{f_{ck}}{250} \right) = 0.492 \quad \text{NA.6.2.2(6)}$$

With effective beam height $d_{uk} := 1546.9 \text{ mm}$ we get the compressive shear capacity:

$$V_{Rd,max,c} := 0.5 \cdot b_w \cdot d_{uk} \cdot \nu \cdot f_{cd} = 970370.4 \text{ N, i.e. } 970 \text{ kN.}$$

Comparing this with the design shear load at the support, $V_{Ed} = 609 \text{ kN}$, it is evident that the compressive shear capacity is sufficient. However, as discovered above the diagonal tension capacity is not sufficient, and shear reinforcement is therefore necessary for the shear capacity of the beam to be sufficient.

The shear capacity of the composite beam with shear reinforcement:

The NIB beams are shear reinforced. The diagonal tension capacity when including shear reinforcement is calculated by the formula

$$V_{Rd,s} := \frac{A_{sw}}{s} \cdot z \cdot f_{ywd} \cdot \cot(\theta) \quad (6.8)$$

When Equation (6.10) is taken into use for calculations of shear compressive capacity, as will be the case here, f_{ywd} should be reduced to $0.8 f_{yk}$.

In the considered section the shear reinforcement A_{sw} consists of stirrups P2, with diameter 12 mm, central distance 150 mm and steel quality K400Ts.

$$A_{sw,P2} := \pi \cdot \frac{12^2}{4} = 113.1 \text{ mm}^2$$

$$s_{p2} := 150 \text{ mm}$$

$f_{y,K400Ts} := 400 \text{ MPa}$ as the characteristic yield strength of the steel

Inner lever arm z , approximated to $0.9 d_{uk}$ (simplified approximation, should be calculated properly when the cross section is exposed to axial load):

$$z := 0.9 \cdot d_{uk} = 1392.2 \text{ mm} \quad 6.2.3(1)$$

Firstly, assume that the angle θ between the concrete compression strut and the beam axis perpendicular to the shear force is 45 degrees. This will be in accordance with NS 3473:1977, where it is assumed that all cracks occur 45 degrees from the system axis, i.e. principal compressive and tensile directions are assumed to lie 45 degrees from the system axis. In radians this corresponds to

$$\theta := \frac{\pi}{4} \quad \text{giving} \quad \cot(\theta) = 1$$

The diagonal tension capacity will then be

$$V_{Rd,s} := \frac{A_{sw,P2}}{s_{P2}} 0.8 f_{y,K400Ts} \cdot z \cdot \cot(\theta) = 335904.5 \text{ N} \quad \text{i.e. } 336 \text{ kN.}$$

At the section 1650 mm from the middle of the support the design shear load is $V_{Ed} = 533 \text{ kN}$. The diagonal tension capacity with shear reinforcement is therefore not sufficient.

If, instead, the angle $\theta = 26.6$ degrees is chosen the shear reinforcement can be utilized to a maximum in accordance with Manual N400. In radians this corresponds to

$$\theta := 26.6 \text{ deg} = 0.464 \quad \text{giving} \quad \cot(\theta) = 2$$

The diagonal tension capacity will then be

$$V_{Rd,s2} := \frac{A_{sw,P2}}{s_{P2}} 0.8 f_{y,K400Ts} \cdot z \cdot \cot(\theta) = 670785.817 \text{ N} \quad \text{i.e. } 671 \text{ kN.}$$

With the design shear load of $V_{Ed} = 533 \text{ kN}$ at the section 1650 mm from the middle of the support it is clear that the diagonal tension capacity with shear reinforcement is more than sufficient. EC2 provides the opportunity to change the crack angle even further, with $\cot(\theta) = 2.5$. This shows that the EC2 formulas provide a possibility to utilize the shear reinforcement in a much better way than NS 3473:1977.

The compressive shear capacity is given for structural members with shear reinforcement as

$$V_{Rd,max,s} := \frac{\alpha_{cw} \cdot b_w \cdot z \cdot \nu_1 \cdot f_{cd}}{\cot(\theta) + \tan(\theta)} \quad (6.9)$$

$$\nu_1 := \nu = 0.492 \quad \text{NA.6.2.3}$$

For structures with prestressing α_{cw} is decided depending on the ratio σ_{cp}/f_{cd} . σ_{cp} can be calculated at a minimum distance from the support of $0.5d \cdot \cot\theta = 0.5d \cdot 2 = d$. Here the axial load is $N_{Ed} = 3228$ kN, equal to at the section 1650 mm from the support (coating neglected). Including the transmission of prestress this gives:

$$l_{x2} := d_{uk} = 1546.9 \quad \text{mm}$$

$$\sigma_{cp2} := \frac{l_{x2}}{l_{pt2}} \cdot \frac{N_{Ed} \cdot 1000}{A_c} = 2.808 \quad \text{MPa}$$

$$\frac{\sigma_{cp2}}{f_{cd}} = 0.11$$

which gives (for $0 < \sigma_{cp} < 0.25 f_{cd}$):

$$\alpha_{cw} := 1 + \frac{\sigma_{cp2}}{f_{cd}} = 1.11 \quad (\text{NA.6.11.aN})$$

Using $\theta = 26.6$ degrees as for the diagonal tension capacity the compressive shear capacity becomes

$$V_{Rd,max,s} := \frac{\alpha_{cw} \cdot b_w \cdot z \cdot \nu_1 \cdot f_{cd}}{\cot(\theta) + \tan(\theta)} = 776314.1 \quad \text{N, i.e. 776 kN}$$

Compared with the design shear load of $V_{Ed} = 609$ kN at the support it is evident that the compressive shear capacity is sufficient.

Appendix F

Design shear resistance at interface between beam and deck

In this appendix the design shear resistance at the interface between the NIB beam and the bridge deck is calculated. This is compared with the design shear stresses acting in the interface in Section 9.5.

Calculation of design shear resistance at the interface between the NIB beam and bridge deck in accordance with EC2 Section 6.2.5

Design shear resistance at the interface:

$$v_{Rd} := c \cdot f_{ctd} + \rho \cdot f_{yd} \cdot \mu \leq 0.5 \nu \cdot f_{cd} \quad (6.2.5)$$

Assuming smooth surfaces:

$$c := 0.20 \quad \mu := 0.6$$

Assuming that the bridge deck (C35) corresponds with a concrete quality of B25:

Design tensile strength f_{ctd} :

$$\alpha_{ct} := 0.85 \quad \text{NA 3.1.6(2)P}$$

Partial safety factor for concrete:

$$\gamma_c := 1.5 \quad \text{NA 2.4.2.4}$$

Characteristic axial tensile strength of concrete $f_{ctk,0,0.05}$:

$$f_{ctk,0,0.05} := 1.8 \text{MPa} \quad \text{Table 3.1}$$

Design axial tensile strength of concrete f_{ctd} :

$$f_{ctd} := \frac{\alpha_{ct} \cdot f_{ctk,0,0.05}}{\gamma_c} = 1.02 \cdot \text{MPa} \quad (3.16)$$

Compressive cylinder strength f_{ck} :

$$f_{ck} := 25 \text{MPa} \quad \text{Table 3}$$

Design compressive strength f_{cd} :

$$\alpha_{cc} := 0.85 \quad \text{NA 3.1.6(2)P}$$

$$f_{cd} := \alpha_{cc} \cdot \frac{f_{ck}}{\gamma_c} = 14.2 \cdot \text{MPa} \quad (3.15)$$

The ratio ρ is given as

$$\rho := \frac{A_s}{A_i} \quad 6.2.5(1)$$

The area of one stirrup (with diameter 12 mm) is

$$A_s := \frac{\pi \cdot 12^2}{4} = 113.1 \text{ mm}^2$$

The production figures of the NIB beams shows that 13 stirrups are placed over 770 mm at the beam end. This results in a central distance

$$s := \frac{770}{12} = 64.2 \text{ mm}$$

With width at the top of the top flange of

$$b := 500 \text{ mm}$$

the area of the joint becomes

$$A_i := b \cdot s = 32083.3 \text{ mm}^2$$

Finally ρ becomes

$$\rho := \frac{A_s}{A_i} = 3.525 \times 10^{-3}$$

With a steel quality of K400Ts the design yield strength of the reinforcement is:

$$f_{y.K400Ts} := 400 \text{ MPa}$$

$$\gamma_s := 1.15$$

Tabell NA.2.1N

$$f_{yd} := \frac{f_{y.K400Ts}}{\gamma_s} = 348 \cdot \text{MPa}$$

Figur 3.8

ν is a strength reduction factor for concrete cracked in shear

$$\nu := 0.6 \cdot \left(1 - \frac{f_{ck}}{250 \text{ MPa}} \right) = 0.54$$

NA.6.2.2(6)

Finally the design shear resistance at the interface v_{Rdi} can be found:

$$v_{Rd} := c \cdot f_{ctd} + \rho \cdot f_{yd} \cdot \mu$$

$$v_{Rd.max} := 0.5 \nu \cdot f_{cd}$$

$$v_{Rd} = 0.940 \cdot \text{MPa}$$

$$v_{Rd.\max} = 3.825 \cdot \text{MPa}$$

I.e. the design shear resistance is decided by v_{Rdi} , and we have

$$v_{Rd} = 0.940 \cdot \text{MPa}$$